FATIGUE AND FRACTURE OF CEMENT MORTARS CONTAINING FLY ASH

Peter Clement Taylor

Thesis presented for the Degree of

DOCTOR OF PHILOSOPHY

in the Department of Civil Engineering

UNIVERSITY OF CAPE TOWN

August 1995

DOCTORAL DEGREES BOARD
Room 218, Bremner Building
Private Bag,
7700 RONDEBOSCH
South Africa

Fax: (021) 650-2138/3726
Tel: (021) 650-2155

Internet Address:
reajmh@bremner.uct.ac.za

Please complete and return to the Doctoral Degrees Board, University of Cape Town, when submitting your thesis for examination

PhD THESIS TITLE: FATIGUE AND FRACTURE OF CEMENT MORTARS CONTAINING FLY ASH

I hereby

(a) grant the University of Cape Town free licence to reproduce the above thesis in whole or in part, for the purpose of research;

(b) declare that:

(i) the above thesis is my own unaided work, both in concept and execution, and that apart from the normal guidance from my supervisor, I have received no assistance except as stated below:

None

(ii) except as stated below, neither the substance nor any part of the above thesis has been submitted in the past, or is being, or is to be submitted for a degree in the University or any other university.

None

The thesis has been presented by me for examination for the degree of PhD.

SIGNED: Signed by candidate

P C Taylor

DATE: 24 August 1995

PROCS\Declare.doc

ABSTRACT

FATIGUE AND FRACTURE OF CEMENT MORTARS
CONTAINING FLY ASH

Peter Clement Taylor

Department of Civil Engineering, University of Cape Town

August 1995

The aim of the work described in this thesis was two-fold; to investigate the effects of fly ash on the fatigue resistance of cement mortars when included as a partial cement replacement, and to seek to improve the understanding of cyclic fatigue crack growth mechanisms in cementitious materials.

Mortar mixes were prepared with similar compressive cube strengths using a range of three fly ash contents from 0% to 25% (by mass of cement). Samples prepared using these mixes were tested in a double torsion facility under cyclic loading, and the rates of crack growth measured and recorded. These crack velocities were plotted against the applied stress intensities on log-log scales in so called V-K diagrams.

An advantage of using the double torsion system was that the applied stress intensity was constant for constant load conditions and changing crack length, unlike many other configurations. However, the amount of scatter inherent in the system, and in testing cementitious materials, is large. This has meant that comparison between sets of data has had to be carried out on the basis of comparing the positions of clouds of data, rather than comparing the slopes of best fit lines.

Another advantage of the DT system is that some of the parameters pertaining to the test can be changed whilst the test is in progress. This means that the effects of changing, say, load amplitude or cyclic frequency can be observed on the same specimen. Parameters that were considered in the test matrix included the following: fly ash content, sample age, cyclic frequency and amplitude, maximum applied stress intensity, relative humidity and temperature of the environment, drying preparation of the sample and the type of fluid in which the samples were tested. The relative effects of all of these variables were compared in a series of V-K plots and trends were noted.

It was apparent that the influence of the presence of fly ash was dependent on the age at which tests were conducted. At early ages the fly ash was found to increase fatigue resistance and toughness, whilst at greater ages the fatigue resistance of the mixes containing fly ash were slightly less resistant to fatigue crack growth. This was thought to be due to the spherical shape of the fly ash

particles resulting in a blunting effect on cracks. The relative size of the particles at these ages are similar to other flaws in the matrix (eg capillary pores). At greater ages the continued hydration of the cement reduces the average size of flaws in the matrix, but not all of the larger fly ages particles take part in the reaction. Electron microscopy indicated that the bond between the gel and the large fly ash particles was poor, resulting in their effectively acting as flaws that were now large in relation to other flaws in the matrix, thus reducing toughness and fatigue resistance.

In all of the tests there appeared to be a reasonable correlation between sample toughness and fatigue resistance, which is consistent with a crack growth mechanism controlled by some form of environmentally assisted cracking (EAC) described by the V-K model. This is in contrast to the inverse relation observed in metals in which crack growth is governed by a non-linear plasticity mechanism described by the Paris relationship.

The results of tests carried out in a variety of environments and over a range of load cases also pointed to an EAC mechanism dominating, yet there was a slight Paris type influence apparent. Another indication of the EAC mechanism dominating was the agreement between the measured relationship between static and cyclic fatigue crack growth rates, and a theoretical relationship for such a mechanism proposed by Evans and Fuller.

Some models to describe the mechanisms of crack growth in cementitious materials have been proposed. The first approach was to consider the mechanisms at an extreme microscopic level, where it has been proposed that a number of mechanism may be acting including: EAC, brittle shear failure, creep, slippage and wedging. The relative dominance of each mechanism is governed by the condition prevailing at the element being considered. At a slightly larger dimensional scale, these localised mechanisms would combine to become apparent in experimental results as two overall mechanisms, namely EAC and another called here pseudo-plasticity (PP). PP may be considered to be a result of all of the micro level mechanisms acting together that manifests as a form of non-linear plasticity behaviour.

The proposed model incorporating EAC and PP helps to explain the observed behaviour of EAC dominance but with a portion of plasticity being apparent. Further work is required in order to be able to quantify the relative effects of the different mechanisms for a variety of environmental and loading states.

ACKNOWLEDGEMENTS

I am indebted to a large number of people for their assistance, advice and support in preparing this thesis.

Firstly, I must thank my wife for not knowing what she was letting herself in for at the beginning.

Materials were supplied, free of charge, by Ash Resources (Pty) Ltd, Anglo-Alpha Limited and van Zyl Sand (Pty) Ltd, whilst Reinhold Amtsbüchler of Blue Circle Cement was of great assistance in preparing the mix designs, for all of which I am very grateful.

Funding was provided for the experimental phase of this work by National Research Programme for Waste Management - Mineral Wastes (Pulverised Fuel Fly Ash), CSIR.

The laboratory staff at the Departments of Civil Engineering at the Universities of the Witwatersrand and Cape Town provided help in preparing, storing and testing specimens, building and maintaining equipment and cleaning up afterwards.

The academic staff in the same departments, in particular Prof M Alexander, were of invaluable assistance in being available to advise, correct and discuss all aspects of this work. In particular my supervisors, Professors R Tait and M de Kock, put in a lot of time in helping to set up the project and seeing to its completion.

My employers, the Portland Cement Institute were very supportive in letting me take the time to prepare this document. I am indebted to Dr Graham Grieve and Dr Brian Addis for their gentle pressure and encouragement, and for allowing me to use the resources of the Institute. The library staff, Gill Goldstein, Hanlie Steyn, Ansie Martinek and Karin Scott were superb at finding obscure references, and at checking that my references were in a consistent form. Judith Forster gave a lot of her expertise in preparing the final layout of the thesis.

A final, special, vote of thanks is due to my brother for pushing me into starting this thesis. Thanks Bruce.

TABLE OF CONTENTS

LIST OF TABLES

LIST OF FIGURES

CHAPTER ONE - INTRODUCTION

1.1 Motivation

Concrete has been a building material of significant importance for many generations, and has not lost its market dominance over the years. The production of cement is a high technology activity, but satisfactory concrete can often be made by semi-skilled personnel using cement with local aggregates and rule-of-thumb mix proportions. Conversely, cement can also be used in very high technology applications such as "high performance concretes" where compressive strengths of 85 - 100 MPa are reliably being produced for building sites.

Despite the high energy consumption in cement manufacture, the total energy requirement to make a cubic metre of concrete is much lower than any other structural material. This makes it very attractive in an age of energy conservation and efforts to reduce environmental damage to the planet. The use of waste materials such as fly ash to modify the properties of concrete at the same time as reducing the proliferation of potential pollutants also adds desirability to the use of concrete in structures.

Considerable work has been reported [1.1 - 1.10] on the effects of fly ash when used as a partial cement replacement in concrete. Whole conferences [1.11 - 1.15] have been organised around fly ash, particularly on its effects on the potential durability of concrete.

On the other hand, durability is a subject that has largely been ignored in the past, but is becoming more and more important as large sums of money are being spent on concrete repair.[1.16] This has been partially due to changes in the composition of portland cement with time, with one of the major changes being the tendency to yield higher early strengths. This has lead to lower cement contents in concrete, and in turn to massive durability problems world wide.

A topic that is not durability related in the traditional sense, but certainly connected with structural serviceability, is that of fatigue. By fatigue is meant the accumulation of damage in a structure due to cyclic or constant application of loads that are less than the ultimate short term strength of the material.

Fatigue is becoming increasingly important because economic and aesthetic pressures have promoted the use of increasingly slender structural sections, which in turn have been facilitated by the development of technologies able to meet such requirements. However, the more slender the section, the greater the relative effect of (cyclic) live load compared with dead load, and the greater the flexibility of the structure. All of these contribute to an increased risk of fatigue damage to cyclically loaded structures such as bridges as well as the burgeoning number of offshore structures.[1.17 - 1.19]

This trend has accentuated the need for design codes that take cognizance of fatigue, and some such codes have been proposed.[1.20 - 1.22] Most of these are based on empirical methods or relatively simple test methods, but few of them approach the topic from a fundamental mechanistic point of view. Academics have addressed the subject of fatigue in the past, but with little impact on design code philosophies. In addition, very little work has been reported in which the effects of fly ash on fatigue or fracture toughness of concrete have been investigated.

One of the techniques or disciplines available to assist in evaluating the fatigue and crack growth behaviour of materials is that of fracture mechanics. Fracture mechanics is presently a fashionable topic for concrete, despite the questions raised about the validity of linear elastic approaches and the insensitivity of concrete to notch size. A number of models have been proposed to describe the fracture behaviour of cementitious materials, some concepts of which can be used in the investigation of fatigue.

This study has used fracture mechanics techniques to observe the effects of fly ash as a partial cement replacement on fatigue and fracture behaviour of cement mortars, along with the effects of local environmental changes. These investigations would contribute to building the knowledge base, and in increasing understanding of the subject of fatigue mechanisms of cementitious materials.

1.2 Scope

This thesis describes how samples, made from three different mortar mixes, each containing different amounts of fly ash, were subjected to various fatigue loading regimes in a variety of environments. The loading regimes included variation of load amplitude and frequency, while the environmental parameters included sample drying, relative humidity, temperature and immersion in water or alcohol.

The samples tested were in the form of 225 x 75 x 8-mm plates which were subjected to double torsion loading whilst crack growth rates were monitored and recorded.

The results from the different sets of tests have been compared, and on the basis of these, models have been proposed to describe the mechanisms of fatigue crack growth. The proposed mechanisms have been separated on the basis of magnitude. At the microstructurally localised level several mechanisms can occur, but they cannot be directly observed or separated. At a slightly greater magnitude, the "process zone" level, the microstructural mechanisms are investigated and appropriate conclusions drawn.

1.3 Thesis outline

This section gives a brief outline of the contents of each of the following chapters.

The next two chapters comprise of a literature survey, where a broad review has been carried out because little work has been reported on the direct topic of this thesis. Chapter 2 covers the chemical and physical properties of cementitious materials including the effects of fly ash as relevant to this study. This is followed in Chapter 3 by a more specific look at fracture mechanics, its application to cementitious materials and in particular, its use in fatigue related research.

Chapter 4 is a mixed literature and experimental overview chapter, specifically looking at the experimental technique used in the study, that of double torsion. A brief review of the test method is followed by a description of the experimental confirmation of the validity of the approach to the materials and samples tested in this study. Some limitations in terms of specimen dimensions and setting up tolerances were also established as described in this chapter.

Chapter 5 is a description of the experimental work carried out, including the materials and the reasons for their selection, the mix proportions and the other variables in the test matrix. The results given in Chapters 6 and 7, are separated into the effects of loading type variables such as load amplitude and frequency, and the material type variables such as fly ash content and environment.

Chapter 8 is another mixed chapter with a literature review of the application of scanning electron microscopy to the subject, followed by a description of the work and findings of the microscopy carried out in this study.

The results and some relevant literature are discussed in Chapter 9 in which models are proposed to describe and explain the observed behaviour of cementitious materials subjected to static and cyclic fatigue loading. The whole is then summarised into a conclusion chapter, including recommendations for future work and ideas for future consideration. The thesis is closed with comments on the application of the findings to everyday engineering practice.

CHAPTER TWO - MATERIALS REVIEW

2.1 Introduction

It is not unusual[2.1, 2.2] for authors of texts on cement and concrete to refer to "concretes" manufactured by the Romans, particularly those structures that survive to the present day and provide excellent examples of great durability. These structures, however, were not built using portland cement, but rather natural hydraulic cements.[2.1]

Since Joseph Aspdin registered his patent for portland cement,[2.1] many structures have been built using this material, most of which have reached or surpassed their intended lifetimes. Portland cement is a blend of shale, clay and limestone that, when finely milled and heated, produces a hydraulic cement.[2.3] This material, when mixed with water will harden and increase in strength with time in an irreversible reaction.[2.4] Portland cements have evolved with time, particularly with respect to their strength behaviour at early ages.[2.1] This has largely been due to a demand from the construction industry for concrete that would be strong enough to be self supporting at ever earlier ages. Consequently, the early days of research and specification writing emphasized the need for strength.[2.5]

This in turn has resulted in a period when strong concretes with relatively little cement in them were failing, not for lack of strength, but for lack of durability[2.6]. Durability has since become the topic of extensive research,[2.7] seeking to use the modern cements as economically as possible and still to produce durable concrete.

Durability can be defined as the ability to survive the environment and load conditions into which the concrete is placed for the desired lifetime. Lack of durability may be due to the passage of aggressive agents which attack embedded steel (such as chlorides[2.8]), or those that attack the matrix of the concrete itself (such as acids[2.9]). Alternatively, lack of durability may be due to

slow chemical reactions occurring within the concrete such as alkali silica reaction.[2.10] Finally, a lack of durability may be regarded as the inability to carry the loads without excessive deformation or failure under service loads with time, caused by mechanisms such as creep, shrinkage or fatigue. It is this last topic (ie fatigue) that is the subject of this study, with particular emphasis on the effect of fly ash, a material often added to enhance durability of a concrete from the point of view of chemical attack.

Fly ash, a waste product from modern coal fired power stations, has been found to have a number of beneficial affects on concrete when used as a partial cement replacement.[2.11] These benefits include the reduction in the heat of hydration,[2.12] an improved workability[2.13] and an improvement in potential durability.[2.14]

The intrinsic physical and chemical properties of hardened cement paste (HCP) and fly ash within HCP, along with the reported changes in concrete properties due to the addition of fly ash, are discussed in this Chapter.

No mention has been made in this Chapter concerning fatigue as a failure mechanism in cementitious materials, the causes behind it or the effects of fly ash on fatigue performance. This is because the topic is discussed in detail in Chapter 3.

2.2 Portland cement

Portland cement is an artificially produced hydraulic cement product made by crushing selected raw materials and heating them together to approximately 1 450 °C in order to create new chemical compounds. These compounds will hydrate with water in an irreversible reaction, that is slow, exothermic and continues in the presence of water. The products of this hydration cause the mix to change from a plastic to a solid phase that continues to gain strength with time, as long as water is available to drive the hydration process.[2.3, 2.4]

In the manufacture of portland cement, great effort is made to limit the variability of the final product. This rigorous control is carried out in order that designers and those building with the material have a product that is predictable and consistent, and therefore economic and safe. Cement manufacture is a multibillion rand industry, with capacity available in South Africa to produce approximately one third of a tonne of cement per person per year.

It is a material that is known to be "abuser friendly"; anyone can obtain a bag of cement at a store and use it to produce a mortar, plaster or concrete and so build with it. However the technology behind the efficient and reliable use of cement is extremely complex. This will be illustrated in the following sections covering, in broad outline, the chemistry of hydration, the physical forms of HCP and the mechanisms of failure of paste and mortar.

2.2.1 Chemistry

The chemistry of the hydration of portland cement is a very complex study and the topic of continued high level research over many years.[2.15 - 2.29] This short section presents only a brief summary of the commonly accepted features of the hydration process which are relevant to this study. The section has been written to cover the materials and their basic chemistry, with a view to leading on to their physical characteristics and so their effects on the behaviour of mortars under mechanical loading and chemical attack.

The raw materials of concrete are cement, water and aggregate. The reaction of aggregates will not be considered in this section because siliceous aggregates were used in the experimental work, and it is considered that such materials do not influence the hydration reaction.[2.30]

The composition of a typical portland cement sample into its chemical oxides is given in Table 2.1. The predominant oxides are calcium oxide (CaO), silica (SiO_2), alumina (Al_2O_3) and iron oxide (Fe_2O_3). These are normally abbreviated in cement chemistry terms to C, S, A, and F respectively and will be used as

such in this section.[2.16] (Note that this notation has nothing to do with carbon, sulphur, arsenic or fluorine.)

Table 2.1: Chemical composition of a typical portland cement sample[2.17]

Oxide	% content by mass	Oxide	% content by mass
CaO	64,3	MgO	2,1
SiO_2	22,8	Na_2O	0,4
Al_2O_3	4,2	Mn_2O_3	0,2
Fe_2O_3	3,8	LOI	1,1
SO_3	1,7		

The sulphate in cement is normally added as calcium sulphate ($CaSO_4$), also known as gypsum in the impure state, which is added to the clinker at the time of grinding.[2.16] This acts as a regulator to the initial rate of hydration as described below. Other materials occurring in cement are described at the end of this section.

Portland cement is generally accepted[2.16, 2.17, 2.19, 2.25 - 2.27] to comprise of four main compounds, which are crystalline combinations of the four oxides described above:

- tricalcium silicate, C_3S or 3 $CaO.SiO_2$, known as alite in the impure form,
- dicalcium silicate, ß-C_2S or 2 $CaO.SiO_2$, known as belite in the impure form,
- tricalcium aluminate, C_3A or 3 $CaO.Al_2O_3$,

- tetra calcium alumino ferrite, C_4AF or 4 $CaO.Al_2O_3.Fe_2O_3$, known as ferrite.

The relative proportions of these materials are affected by the composition of the raw materials but typical ranges in portland cement are:[2.2, 2.18]

C_2S 25 - 30%

C_3S 45 - 70%

C_3A 5 - 12%

C_4AF 5 - 12%.

These proportions are not normally measured, but rather calculated using equations presented by Bogue[2.24] from the proportions of the individual oxides. These equations are not precise but do provide a basis for monitoring and understanding the behaviour of a cement.

The chemical reactions of portland cement as it hydrates, presented in a drastically simplified manner, are given for each compound below.[2.16] The final ratios of calcium, silica, alumina and sulphate vary throughout the hardened cement paste (HCP) and the equations given are general approximations.

(i) C_3S - Alite

$$3(3CaO.SiO_2) + 6H_2O = 3CaO.2SiO_2.3H_20 + 3CaOH_2$$

The reaction of tricalcium silicate with water produces a calcium silicate hydrate (CSH) that is known as tobermorite gel. The name is misleading because despite the gel's similarity to tobermorite it is, in fact, something different.[2.19] This gel is responsible for most of the attractive characteristics of hardened cement paste (HCP) including strength and stiffness.[2.18] The by product is calcium hydroxide which is blocky, flaky, and a source of weakness in the HCP as discussed in Section 2.2.2.

(ii) C_2S - Belite

$$2(2CaO.SiO_2) + 4H_2O = 3CaO.2SiO_2.3H_20 + CaOH_2$$

The calcium silicate hydrate is a similar gel to that arising from the hydration of C_3S, whilst the amount of calcium hydroxide produced is less. Hydration rates are slower, which from a construction point of view is less desirable and therefore the amount of C_2S is often minimised in cement manufacture.

(iii) C_3A with $CaSO_4$

$$3CaO.Al_2O_3 + 3CaSO_4 + 32H_2O = 3CaO.Al_2O_3.3CaSO_4.32H_2O$$

$$3CaO.Al_2O_3.3CaSO_4.32H_2O + 2(3CaO.Al_2O_3) + 4H_2O = 3(CaO.Al_2O_3.CaSO_4.12H_2O)$$

The rate of hydration of C_3A is regulated by the presence of gypsum by mechanisms that are still debated.[2.18] Simply put, the reaction is in two stages, the second starting when all the locally available sulphate has been consumed in the first stage. The calcium-sulpho-aluminate formed in the first stage is known as ettringite and has the form of thin rods and is known as AFt, whilst the monosulphate hydrate from the second phase is found in thin hexagonal plates and is known as AFm.[2.21, 2.28] When both the stages given above are complete, then the remainder of the C_3A (if any) hydrates very rapidly as described below.

(iv) C_3A with $Ca(OH)_2$

$$3CaO.Al_2O_3 + Ca(OH)_2 + 12H2O = 4CaO.Al_2O_3.13H_2O$$

In the absence of sufficient gypsum in the clinker the above reaction occurs, leading to flash set and the generation of large amounts of heat. However, C_3A

is not excluded from cement as its presence is necessary in the manufacturing process to act as a flux and thus lower the temperature at which C_3S is formed.[2.31] Additionally, alumina is almost always present in the raw materials, which would make it difficult or expensive to exclude.

(v) C_4AF

$$4CaO.Al_2O_3.Fe_2O_3 + 4Ca(OH)_2 + 22H2O = 4CaO.Al_2O_3.13H_2O + 4CaO.Fe_2O_3.13H_2O$$

This is a slow reaction producing a material known as hydrogarnet that contributes little to the final characteristics of the HCP.

Each compound has a different rate of hydration, and these rates and the products formed are affected by the presence or absence of the others, thus making the study of this topic extremely complex.[2.22] Their respective hydration rates, expressed in a strength-time graph derived by Bogue, are shown in Figure 2.1 taken from an old but still often quoted text book by H F W Taylor.[2.26]

Alite has the fastest strength gain and has the greatest ultimate strength, followed by belite with similar ultimate strengths. The other compounds do not contribute significantly to the strength. These conclusions have since been revised in work reported by Beaudoin and Ramachandran,[2.23] indicating that the C_4AF has the greatest strength at early ages, but is superseded by the C_3S and C_2S in time (Figure 2.2).

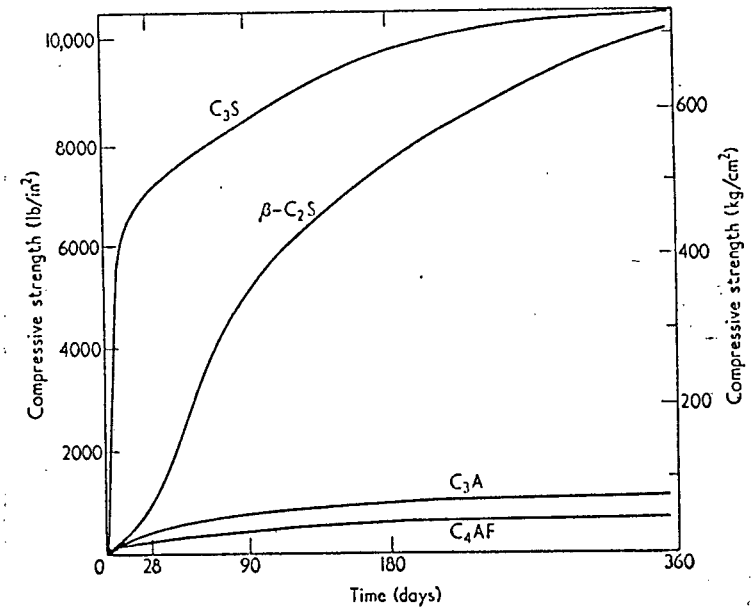

Figure 2.1: Curves of compressive strengths against curing time for the pure phases of cement[2.26]

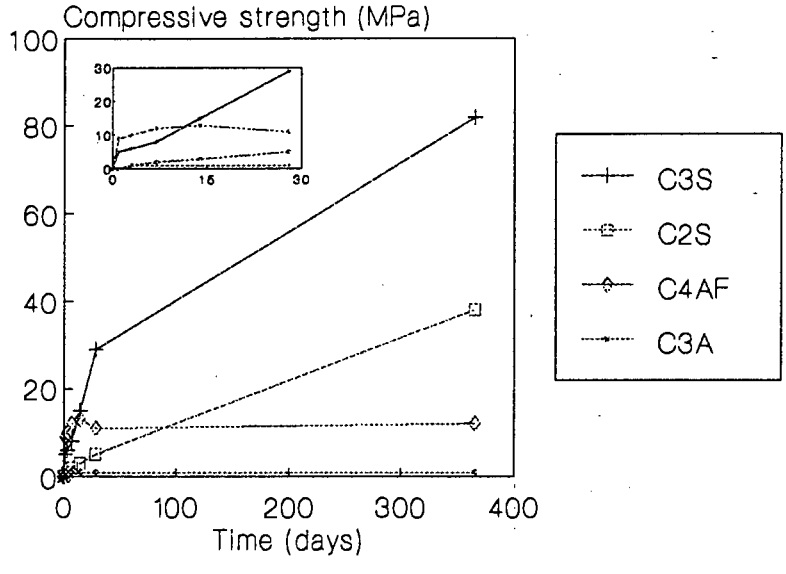

Figure 2.2: Revised curves of compressive strengths against curing time for the pure phases.[2.23]

The combined compounds hydrate in a process that goes through several phases, the study of which is also beyond the scope of this study. A simplified summary of this process has been described in five phases by Skalny and others as follows:[2.18, 2.22, 2.27, 2.29]

(i) initial or pre-induction: this occurs in the first few minutes and involves the leaching of large amounts of calcium and small amounts of silicate into solution. Combinations of A and S form a surface layer or membrane around grains. Large amounts of heat are released.

(ii) induction or dormant: slow dissolution of calcium, with reactions slowed by the membrane, with little heat formation, for the period from 20 minutes to 3 hours after starting.

(iii) acceleration: precipitation of calcium hydroxide which ruptures the membrane, and fibrous growth occurs as well as ettringite formation along with some heat formation from 3 hours to 24 hours.

(iv) deceleration: CSH is formed from the contact of calcium and silicate rich solutions from each side of the damaged membrane. CSH is in the form of thin foils which entwine and curl, and contributes significantly to strength.

(v) diffusion: reaction continues, governed by availability of materials by diffusion through hydrate products.

From an engineering point of view not all of these phases are noticed, except when things go wrong such as flash set or severe retardation. The stages that may be observed are the dormant period, allowing a useful time for handling and placing the concrete, and the setting and hardening of phases (iii) to (v).

Other compounds that occur in portland cement include carbon dioxide, water, magnesium oxide and trace contaminants.[2.16]

Carbon dioxide (CO_2) has little significant effect, except on hardening rates if present in excess. The amount of CO_2 is determined along with the free water as the loss-on-ignition, or the percentage reduction in mass on heating to 1 000°C. The water is present as a result of the tendency of cement to be hygroscopic as well as due to the practice of cooling clinker by water sprays.

Magnesium oxide is frequently present in the raw materials of cement, and will result in unsoundness or expansion if in excess of 5% by mass. This is due to its very slow hydration and consequent expansion in the presence of water.

Alkalis remaining from the raw materials or from the fuel used to heat the clinker, do not effect cement hydration. However they may react over a long period of time with water and certain stressed silica aggregates, if present, resulting in an increased volume of gel causing expansion and cracking of the concrete.[2.32]

The next section covers the physical microstructure of the HCP formed by the chemical reactions summarised above.

2.2.2 Structure and microstructure

The microstructure of paste, mortar and concrete is another topic that has occupied the attention of many high level studies over the years. Diamond[2.25] provided an excellent review in 1976 in which he made the point that the topic should be addressed at three levels:

- the atomic level (nm),
- the particle level (μm),
- the micromorphic level (10-100 μm).

Pastes may be considered to be comprised of the following elements:

- CSH gel,
- calcium hydroxide crystals,
- ettringite and calcium aluminate monosulphate hydrate,
- unhydrated clinker,
- contaminants,
- gel pores,
- capillaries,

whilst mortars and concretes also contain:

- aggregates (fine and coarse),
- interfacial zones.

Atomic level

At the atomic level, the CSH gel is estimated to comprise approximately 70% of a fully hardened cement paste and is in the form of a poorly crystalline, quasi-amorphous or amorphous phase that is extremely varied and difficult to describe and categorise fully.[2.19, 2.25]

The calcium hydroxide, ettringite with calcium aluminate monosulphate hydrate, and clinker are estimated to account for approximately 20%, 7% and 3% respectively of a fully hardened cement paste.[2.25] These are either fully crystalline or with small proportions of glassy, lesser crystalline phases.[2.33]

Particle level

At the particle level the CSH gel is found in a variety of forms that have been described by Diamond[2.25] as:

- Type I - spines, rod shapes or aciculae. These have near parallel sides, with branches at the outer tip; some but not all are hollow, and they are flexible.

- Type II - reticular network or interlocking structure. These are elongated particles with a similar cross section to Type I but branch frequently, interlock and combine to form a 3-dimensional mesh.

- Type III - nondescript, equant grains. These are small flattened particles that combine to form a massive structure.

- Type IV - inner product formed inside boundaries of the original grain and the membrane.

Type I is dominant in immature paste with Type II appearing occasionally. Type III tends to become dominant at greater maturity whilst Type IV is rare. With increasing age all the types, along with the other products merge into a nondescript, massive form.[2.25]

The presence of "inner product" was later questioned by Barnes[2.34] in a paper describing the observation of so-called "Hadley grains". These are particles where a shell of hydration product has formed around an original cement grain that has subsequently dissipated leaving a void, a smaller cement grain or low density material.[2.21, 2.28, 2.34] Increasing temperature during early curing has been shown to result in thicker shells and larger pores (colloquially known as coarser grains) which leads to a reduction in strength.[2.35, 2.36]

Jennings and Pratt[2.22] showed that both Type I and II forms were derived from the interlocking and combination of thin foils of CSH formed early in the hydration process. The type formed was related to the density of the foils.

The different microstructural types found in HCP are best summarised in the Table 2.2 from Pratt and Jennings.[2.18, 2.21]

Calcium hydroxide is initially seen as planar hexagonal crystals that combine eventually into a massive structure enmeshed with the CSH. Ettringite forms

long narrow rods with no branching, whilst the calcium aluminate monosulphate hydrates are thin hexagonal plates.[2.21, 2.25, 2.28, 2.37]

Micromorphic

At the next level up (micromorphic), HCP is seen as an intimate combination of all of the above intertwined. At mature ages, it becomes difficult to separate the separate entities from the solid ground mass.[2.25]

Table 2.2: Physical products of hydration

Classification	Morphology
Type E	Gelatinous coating on particles approaching AFt composition
Type I (CSH)	Fibres
Type II (CSH)	Reticular network as seen on fracture surfaces
Type III (CSH)	Small irregular grains as seen on fracture surfaces or interlayered partly crumpled sheets as seen in transmission
Type IV (CSH)	Dimpled (<0,1 μm) dense "inner" product
Hadley Grain	Hollow shell
Spherulites	Spherical
AFt	Rods and tubes
AFm	Plates

In mortars the interfacial zone between the aggregate and the paste is typified by weak crystalline structures predominantly containing calcium hydroxide and ettringite.[2.33] This is a relatively new field of study that only attracted attention after the experimental work of the present study was complete. It is now generally accepted that the interface is a source of weakness in mortar or concrete[2.21, 2.33, 2.38, 2.39] and this is a topic for a large amount of future research.

Pores in HCP and mortars are formed by several mechanisms and are roughly classified according to their source and size, although there is some overlap between the classes.

Gel pores are the smallest pores and are contained in the gel as a result of the form of the gel. The number of gel pores therefore increases with increasing gel volume. They are dimensionally small, from 2 nm up to approximately 50 nm and their shape is a topic of debate.[2.21] They often contain water which may not be removable as it is a monolayer on the surface of the pores.

Capillary pores are normally accepted as being part of original water filled space that has not been filled with hydration product. They can be as small as the largest gel pores, from 50 nm, and upwards. The number of capillary pores decreases with continued hydration. If their volume fraction is greater than 0,1 then it is probable that they are interconnected. The amount of capillary pores in a paste can be adjusted by the use of a lower cement/water ratio or by the addition of fine filler materials such as microsilica.

Hadley grains also contribute to the porosity of an HCP in that if they occur, the volume between the skin and the grain is empty. They can be relatively large, up to 50 μm across.[2.21]

Air voids are the largest voids, normally with dimensions in the order of mm. They are normally spherical and can often be interconnected. Their presence is controlled by the water content of the mix, degree of compaction and the possible use of chemical admixtures to expel or entrain them.

This section has presented a brief physical overview of the structures within hardened cement paste and mortar, from the nanometre scale up to the millimetre scale. The chemical and physical characteristics are used in the next section in a description of the mechanisms by which a paste or mortar fails under static compressive or tensile forces or under certain chemical attack.

2.2.3 Failure mechanisms of hardened portland cement

Having described the structure of HCP and mortar, this section covers their mechanisms of failure, with particular reference to mechanical loading although some chemical attack is also touched on. Once again, this topic is enormous and not yet fully understood.[2.40] This review describes the broad concepts, particularly as they relate to this study.

The most important aspect of HCP and mortar, to those modelling their behaviour, is that most models are based on the assumption that the material is homogenous and isotropic, which is not true, whether considered at a micro or a macro scale. It should be noted that most of the discussion above has been at the particle or micrometer scale, whilst in this section it is at the millimetre scale.

Porosity

It was recognised at an early stage that the strength of an HCP, mortar or concrete was related to porosity, with increasing porosity leading to decreasing strength.[2.19, 2.41, 2.42] For instance, Figure 2.3 shows that the line plotting strength versus pore volume can be projected back to an ultimate theoretical strength of about 500 MPa for zero porosity.[2.23]

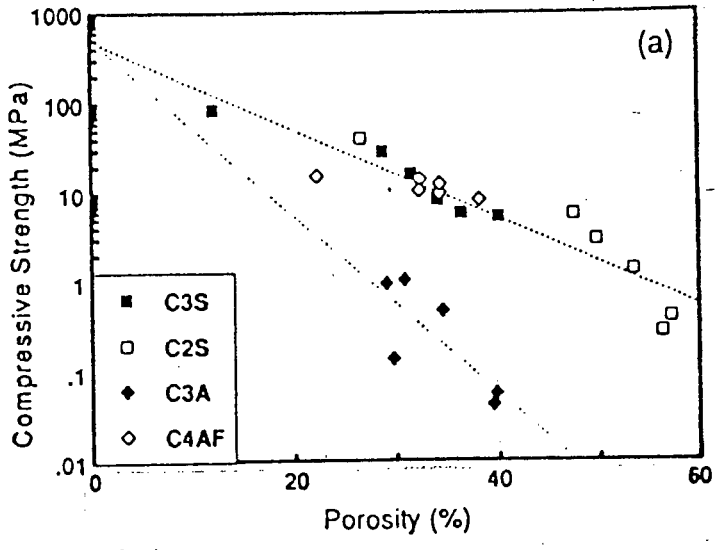

Figure 2.3: Compressive strength of the phases of HCP versus porosity[2.23]

The difficulty in following up this concept arises from the measurement of porosity. This is because of the size and form of some of the pores, for instance gel pores, makes them impossible to measure directly. This means that different experimental methods yield different results, making comparisons difficult.[2.41]

The extent, size, shape and properties of different flaws all affect the strength and behaviour of a material[2.43] although it has been reported that pores less than 10 nm do not materially effect the strength of an HCP.[2.42]

HCP and mortar, as already indicated, contain a variety of flaws, from the very small gel pores up to air bubbles, crystals of $Ca(OH)_2$ with planes of weakness, the transition zone between aggregate and paste as well as Hadley grains.[2.44, 2.45]

Fracture mechanics

Fracture mechanics, the study of cracked and flawed materials under stress has lead to a better understanding of the mechanisms behind the effect of flaws and this is covered in more detail in Section 3.3.[2.46]

Microcracks

It is generally accepted that unloaded HCP, and to a lesser extent mortar, contains a number of "submicrocracks" or "microcracks" which are present as result of the hydration process, most likely due to shrinkage of the paste as it is allowed to dry out.[2,40, 2.47, 2.48]

On loading, these microcracks tend to increase in size and become orientated in the direction of the application of compressive force or perpendicular to applied tensile force.[2.40, 2.46, 2.48] Their effect is negligible with stresses up to about 30% of the ultimate strength of the material, which is reflected in a linear elastic behaviour, constant modulus of elasticity and a straight line on the stress strain curve (Figure 2.4).[2.46, 2.49, 2.50] This point is also thought to be related to the so called fatigue limit (Section 3.2). At about the same load microcracking becomes apparent in the interfacial zones.[2.47, 2.51]

As the stress (or strain, or more particularly strain gradient[2.52, 2.53]) is increased beyond about 50% of ultimate, some of the microcracks and bond cracks coalesce to form a few larger cracks.[2.49] These cracks tend to be in the direction perpendicular to the principal tensile stress.[2.40, 2.46, 2.47, 2.50, 2.51, 2.53]

Cracks in mortar tend to form more readily than in paste, an indication that the aggregate may be acting as a stress raiser.[2.40, 2.48] It has also been noted that the presence of microcracks is more critical as cement/water ratio (or strength) increases.[2.40]

The tips of these cracks are indistinct, but rather appear as zones of microcracking, sometimes known as the process zone. This zone may have the

effect of shielding the cracks from the applied stresses (and stress intensity).[2.51, 2.54, 2.55] The presence of a process zone also makes it difficult to define a formal crack length, a concept necessary for linear elastic fracture mechanics to be applied.[2.46, 2.56] The size and shape of the process zone is dependent on the loading configuration, as well as the method of observation and type of materials tested, although it is has been reported as approximately 1 to 6 mm in extent.[2.57, 2.58]

The coalescence is made apparent in the stress strain plot becoming curved, eventually reaching a peak at failure load as shown in Figure 2.4.[2.49]

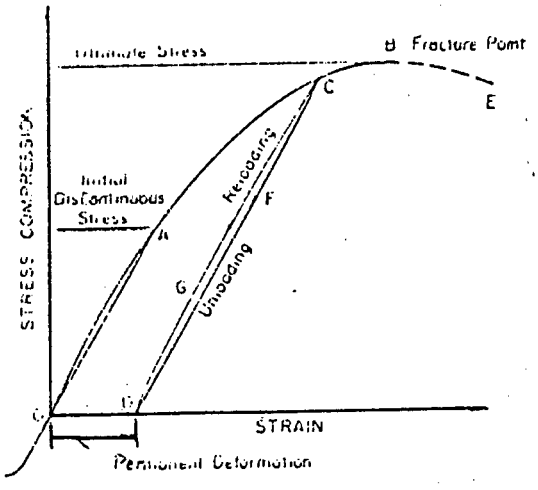

Figure 2.4: Typical stress strain curve for plain concrete[2.49]

Damage mechanics

The subject of damage mechanics, where changes in mechanical behaviour are modelled by relatively large scale non-linear approximations rather than microstructural elements, is beginning to be applied to cementitious systems.[2.51]

If a sufficiently stiff testing machine is used, it is possible to record a descending branch in the stress strain curve, where there is increasing strain and still some stress carrying capacity.[2.49, 2.59] The shape of this curve is

dependent on specimen configuration, test equipment and materials used and there does not seem to be a unique curve for a given paste.[2.58] However this effect is being used in non-linear fracture mechanics studies. This tendency is apparently not related to microcracking, but is more likely due to the tendency of cracks to jump or be discontinuous.[2.40]

The concept of a process zone also makes discussion on the basis of strain difficult, as the shorter the gauge length, the higher the strains that are recorded.[2.58] It is often more meaningful to refer to crack opening displacement (COD), the width of a crack at its "tip", which can be calculated from other measurements. This COD is typically in the range from 1 μm[2.57] to 24 μm[2.58] for mortar and paste. On this basis it is considered by some that spherical bubbles bigger than this can act as crack blunters and slow crack growth.[2.57]

Cracks in HCP and mortar are not straight, but will always be tortuous and may be discontinuous.[2.60] The route taken depends on the strength of the paste, the strength of the bond, the strength and shape of the aggregate and the rate of loading.[2.45, 2.61, 2.62] In immature pastes the preferential route is around particles, at or near the interface.[2.63] As the paste gets stronger it may be energetically preferable for the crack to go through the particles.[2.28] At high strain rates the cracks get straighter, particularly in moist samples, even if they have to go through stronger or tougher materials.[2.45, 2.64, 2.65] It was proposed by Rossi[2.64] that this is due to the presence of menisci of water between particles, the so called "Stefan" effect. The surface tension of the water tends to resist the separation of the particles, thus increasing toughness and promoting straighter cracks.

It has been shown that cracks are not fractal in form, but rather unique in pattern for each type of morphology that they pass through, and this pattern is not repeated with increasing magnification.[2.62]

It is known that the strength or load required to propagate a crack is dependent on the presence of water or moisture.[2.49, 2.54, 2.60, 2.65] It is thought by some that this is related to a type of stress assisted corrosion attack of bonds.[2.46, 2.66]

Chemistry

The present study is predominantly concerned with physical rather than chemical effects. However, it is necessary to cover briefly some aspects of chemical attack of HCP and mortar, in particular those involving water soluble materials.[2.9]

Most of the products of hydration contain calcium in some form and it is the attack or by removal of this element that dominates the following discussion.[2.9, 2.67]

Soft waters have the tendency to leach calcium out of the paste at high rates, leading to rapid deterioration of a concrete. Similarly, acids also tend to attack the calcium in the HCP leading to damage.[2.9]

Salts such as magnesium and sulphate can react with ions in the HCP, often resulting in changes in volume of the paste and so leading to swelling, internal stressing and damage to the structure.[2.9]

Alkali silica reaction is a special case of this, with alkalis from the cement or aggregates reacting with water and stressed alkalis to form a gel that is greater in volume with the consequent stressing and cracking.[2.10, 2.68]

Other salts such as chlorides may be non-deleteriously bound to the gel, or transmitted through the paste leading to potential problems with other embedded items such as reinforcing steel. The permeability of the mortar or concrete, or its resistance to transmission of such salts is therefore critical to its durability.[2.33, 2.69, 2.70]

This completes the description of cement, its hydration and behaviour as HCP. The next section provides a similar coverage of fly ash and its pozzolanic reaction in HCP.

2.3 Fly ash

Ash is one of the waste products from the combustion of low grade pulverized coal in thermal power stations. The coal delivered from the mine is milled to approximately 50 μm in diameter and blown into the furnace.[2.71] After combustion, approximately 80% of the residue is released as so called "fly ash" and the remainder as bottom ash[2.72] which together are known as pulverised fuel ash (PFA). For the remainder of this thesis the term "fly ash" will be used as opposed to PFA, and will be presumed to be the product of the combustion of pulverised coal, as opposed to any other fuel.

Fly ash is comprised of particles in the range of approximately 0,1 μm to 100 μm in diameter.[2.73] These particles are often spherical as a result of their being melted in the furnace, and are composed of mineral oxides that vary with the source of the coal. After being fired the particles are carried by the flue gasses out of the furnace where they are separated from the gasses, normally by means of electrostatic precipitators.[2.74] Ash disposal is a major problem to the operators of power stations and this has lead to various research initiatives into possible uses of the material.

It was acknowledged[2.75] as early as 1937 that fly ash was pozzolanic (see Section 2.3.2) but only in the fifties was work commenced in earnest on using fly ash in concrete both in the UK[2.76] and America.[2.77] Initially fly ash was used for producing lightweight aggregates and mass concrete, later it was introduced for highway construction and more recently for structural concrete.[2.76 - 2.78] Usage in the UK was boosted in the seventies by the formation of the company Pozzolanic (Pty) Ltd which actively marketed a consistent material. This was further assisted by aggressive marketing by the Central Electricity Generating Board (CEGB) and the introduction of standards and specifications, to the point

where at present 45% of the ash produced in the UK is commercially utilised.[2.79]

It is interesting to note that in countries where land is at a premium the usage of ash is relatively high (West Germany 85%, Israel 60%)[2.80] while in countries with more open spaces the usage is relatively low (USA 15%, RSA 5%).[2.81] This would indicate that it is the disposal of ash that is a problem as opposed to the need for its benefits that motivates its imaginative use.

Pulverised Fuel (PF) was first utilised in South Africa in the thirties but limited means of ash extraction in the chimney resulted in ash being blown into the atmosphere with a resultant pollution problem, thus making the use of PF unpopular. It was only in the sixties that ESKOM began using PF boilers with efficient precipitators thus producing large quantities of ash. At present approximately 14 million tons of ash are produced annually by ESKOM[2.82] although most of the fly ash marketed in South Africa for use in concrete is currently obtained only from Matla and Lethabo Power Stations.

Research into the properties of South African fly ash was only started in the early sixties with disappointing results due to the inconsistency of the material.[2.83] Awareness and research was boosted by a Symposium in 1979 in Pretoria[2.84] followed by considerable work by the National Building Research Institute[2.85] on characterizing the behaviour of South African fly ashes. An International Conference "ASH: A Valuable Resource" in 1987 in Pretoria[2.11] provided a forum for the dissemination of the present state of knowledge as well as focusing publicity on the practical uses of fly ash in South Africa.

Due to the fact that most of the fly ash commercially available in South Africa comes from only two sources, with little difference in quality between the two, the characterisation of their quality, as well as mix design procedures is not a great source of problems. For this reason these aspects have only been lightly touched on in this section, whilst emphasis has been placed on the effects that

fly ash has on concrete, particularly from the point of view of failure mechanisms.

2.3.1 Chemistry and microstructure

The chemical composition of a fly ash is dependent on the minerals with which the coal is embedded, which will vary from mine to mine as well from country to country.[2.80, 2.86 - 2.88] This means that generalised statements about the chemical or physical attributes of ashes must be considered as very broad. Nonetheless the chemical composition of a selection of ashes worldwide given in Table 2.3 indicates that fly ash is normally comprised of the oxides of various minerals. These are predominantly silica and alumina as well as smaller portions of iron and calcium oxides together with traces of potassium, magnesium, sodium and sulphur oxides. There is also normally present a portion of unburnt carbon, a measure of which is given by the loss-on-ignition (LOI). (Note that LOI includes not only carbon but other volatile materials such as waters of crystallisation.)

Table 2.3: Summary of chemical compositions of some fly ashes worldwide

	RSA [2.89]	USA Class F [2.90]	USA Class C [2.91]	Germany [2.92]	UK [2.93]	China [2.12]
SiO_2	38,2	47,0	45,8	46,3	48,7	50,5
Al_2O_3	28,3	17,7	22,3	25,5	27,8	29,8
Fe_2O_3	5,2	25,3	7,4	-	9,2	8,2
CaO	14,4	2,1	19,0	-	3,0	3,3
MgO	4,0	1,0	5,0	-	1,9	1,2
SO_3	1,0	0,3	1,6	0,8	0,9	0,5
K_2O	0,8	2,3	0,3	2,7	} 5,1	1,0
Na_2O	0,5	0,7	0,2	0,7		0,7
LOI	2,9	2,4	0,2	3,1	3,9	5,7

The calcium oxide (lime) content has a large effect on the behaviour of fly ash in concrete in that it affects the soundness of the concrete (or the expansion due to the reaction of free lime).[2.94] The magnesium also affects the soundness and is limited by BS 3892 to 4% by mass. In West Germany a maximum of 8% by mass of calcium oxide (or 4% if 1,5% is free lime).[2.95] In America, ashes are classified into two classes; high calcium (Class C, CaO >10%) and low calcium (Class F).[2.96, 2.97]

In South Africa the policy is not to limit the amount of calcium oxide or magnesium oxide but to monitor and limit the unsoundness caused by both compounds.[2.83, 2.98] It should be noted that South African fly ashes have a low silica content and a moderately high calcium oxide content.

The presence of lime in the fly ash may also cause it to behave marginally as an hydraulic cement as well as a pozzolan.[2.83, 2.86] This would mean that such an ash would deteriorate in the presence of moisture.[2.77]

The other component that has a marked affect on fly ash in concrete is that of LOI which is limited to a maximum of 7% in the British Standard, BS 3892[2.99], 5% in DIN 1045[2.100] and 2,5% in SABS 1491.[2.98] This is because the carbon tends to form into larger particles and so reduce fineness and increase water requirement.[2.101] The presence of carbon also reduces the pozzolanicity of the fly ash.[2.78, 2.93, 2.101 - 2.104]

It should be noted that the fly ash from any single power station is generally more consistent in composition and quality than the cement from a single factory.[2.78] This is because the source of the material is from one mine and the operating conditions of the furnace are normally kept constant in order to maintain efficiency.

The sulphate and alkali contents are also limited in several specifications in order to minimise the adverse affects that these materials may have on the final concrete.[2.98 - 2.100]

The chemical compounds described above are formed into a number of mineral phases, predominantly quartz, mullite, hematite and magnetite as well as amorphous components appearing as glassy spheres.[2.105] The amorphous component is predominant in terms of volume, whilst the others appear as cryptocrystalline components in the glass or as irregular grains and sometimes as mantles on the spheres.[2.105]

The physical characteristics of fly ash may be described by three variables: fineness, particle shape and phase; of which the most influential is fineness.

Fly ash particles size, normally in the range 0,1 μm to 100 μm, can be expressed by various means. The most practical is the percentage retained on a 45 μm sieve;[2.93, 2.99, 2.102, 2.103] although the specific surface given in m^2/kg,[2.93] or a plot of cumulative mass against grain size[2.78, 2.92, 2.104, 2.106] have been used.

The fineness of a fly ash is governed by its source, the fineness of the pulverised coal before it is burnt, the operating conditions of the furnace and also by the means of ash collection and classification. For example a finely ground coal produces a finer ash than a coarse ground coal while a very hot furnace will generally produce a finer ash than a cooler one. Fly ash collected from the last plate of a series of precipitators is generally finer than that collected from the first plate.[2.83, 2.95]

With increasing fineness of the fly ash there is a reduction in water requirement (or an improvement in workability) for concrete containing fly ash, which leads to higher strengths due to a lower cement:water ratio for the same workability.[2.102, 2.107] Increasing fineness also results in an increase in the Pozzolanic Activity Index (see Section 2.3.2).

It has been suggested that fineness is the most suitable single parameter with which to classify ashes physically.[2.78, 2.97, 2.102] However it has also been suggested[2.93, 2.108] that a useful measure of the water reducing ability of a fly ash is the product of the LOI and the percentage retained on the 45 μm sieve. The higher the value of this number the smaller the influence on the workability. A copy of the relevant table is reproduced as Table 2.4.

Table 2.4: Classification of fly ash on the basis of water reducing ability[2.109]

Fineness* x LOI	Observations
< 50	Large water reductions
50 - 100	Moderate water reductions
100 - 150	Small water reductions
> 150	No water reduction, unsuitable

*(retained on 45μm sieve)

It has been noted by Diamond that due to the method of formation of the fly ash particles, no two particles may necessarily be similar in chemical or physical form. This means that microstructural studies of the behaviour and influence of fly ash in cementitious materials must take the different forms into account.[2.110]

Fly ash particles are predominantly spherical in shape as a result of their molten formation. This is generally believed to explain the improved workability of concretes containing fly ash. These spheres may be solid (Fig 2.5), hollow (cenospheres), or hollow and containing smaller spheres (plerospheres). Other common particle shapes are rounded (but not spherical), a limited number of angular crystalline particles, and broken spheres.[2.86, 2.110, 2.111] There are also amorphously shaped particles which are normally relics of the combustion process.[2.105, 2.112]

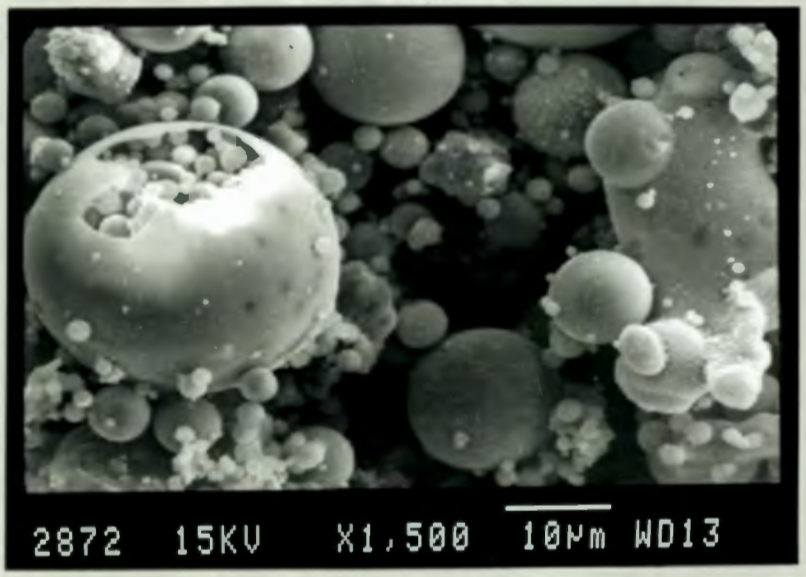

Figure 2.5: Micrograph of fly ash particles

The shapes of the ash particles are directly related to their constituent phases; the predominant phase is glassy[2.87, 2.112] which constitutes the spheroidal particles. The other phase is crystalline which often comprises small crystals embedded in the larger glassy spheres.[2.86] The glassy phase is considered the

more reactive whilst the crystals tend to be more stable and inert.[2.86, 2.92, 2.94, 2.110] However a glass phase content within the limits of 63 - 75% has been shown not to effect markedly mechanical behaviour[2.87], and one Indian fly ash has been shown to be insensitive to the presence of cenospheres in terms of its reactivity.[2.113]

It has been reported by Swamy[2.88] that good concrete can even be made using ashes that fall outside the limits of current standards. It is critical, however, that the ash does not vary with time.

2.3.2 Fly ash as a pozzolan

A pozzolan is defined an aluminous and/or silicious material which, when finely divided, chemically reacts with calcium hydroxide (lime) and water to form cementitious compounds.[2.97]

Fly ash was recognised as a pozzolan in the thirties but the first attempt to quantify this characteristic was only made in the mid fifties when the concept of the Pozzolanic Activity Index (PAI) was introduced.[2.107] This index has become an accepted means of characterising an ash and is defined as the ratio of the 28 day strengths of a mortar mix containing a proportion of ash over a mix without ash; both mixes having the same workability. The percentage of fly ash used varies from specification to specification.[2.99, 2.114] The PAI provides a reasonable indication of the strength behaviour of the ash where a high PAI is normally associated with a high reactivity.[2.115] Modifications to the PAI have also been proposed where the water/binder ratio is kept constant; or a measure is made of the strength of a cube at seven days; or cubes are made with fly ash and lime.[2.102, 2.116 - 2.118]

The reactivity is primarily affected by the fineness and the loss-on-ignition of the ash as described in Section 2.3.1,[2.78, 2.102] with increasing fineness and decreasing LOI leading to increased pozzolanic activity. A finer ash has a greater surface area available for reaction, whilst the carbon interferes

chemically and slows the reaction.[2.101, 2.109] Increasing soluble silica content has also been shown to increase reactivity, probably due to the increased availability of silica for reaction.[2.119] The difference in reactivity between ash that has been blended with cement, or interground, depends on the fineness of the original ash. Fine ashes are not affected whilst coarse ashes will improve in reactivity if interground.[2.120]

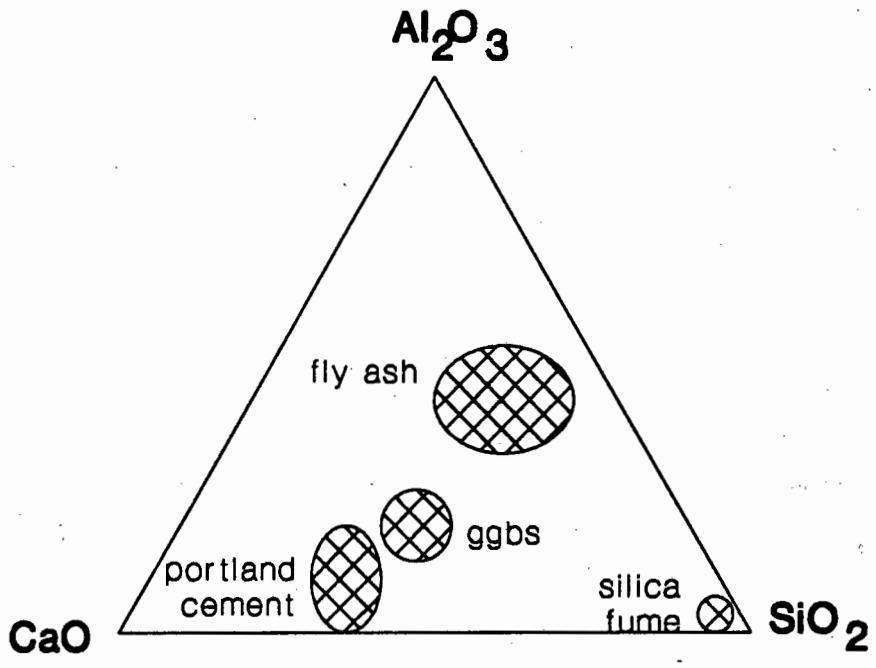

Figure 2.6: Ternary phase diagram showing compositions of portland cement and some cement extenders

As can seen from Figure 2.6, the primary difference in composition between a portland cement and a typical fly ash is the calcium oxide content. However, a by-product from the cement hydration reaction is calcium hydroxide, which is then available to react with the fly ash and so form a type of calcium silicate hydrate.[2.86, 2.121, 2.122] The presence of sulphates has also been shown to accelerate the rate of the pozzolanic reaction.[2.121, 2.123] This reaction is expedited by the form (glassy, often hollow spheres), and size of the fly ash particles being of the same magnitude as the cement grains. It has been shown that the reaction consumes CaO. This leads to the conclusion that the optimum

amount of fly ash (on a purely chemical basis) seems to be about 30% by mass before all the available $Ca(OH)_2$ is used up.[2.122, 2.124]

The hydration of the fly ash is dependent on the availability of $Ca(OH)_2$, both in terms of the amount of lime generated and the amount of contact between the two materials. At an early stage the ash appears to act predominantly as an inert filler and by providing nucleation sites, although it has been shown to interfere with the hydration rates of the cement compounds.[2.86, 2.122, 2.125] Generally, no pozzolanic reaction occurs for at least 7 days,[2.122, 2.126] probably due to the early formation of a layer of porous hydrate around the fly ash particles that inhibits access of reagents to each other. Work by Dhir, and others, has shown that overall, there is an early reaction of a limited number of particles, increasing to approximately 50% reaction by six months, and reaching 60 - 80% reacting at 2 years.[2.112, 2.127] The effects of the unreacted particles on the physical behaviour of the paste is discussed in Section 2.3.5.

The following section gives a summary of the influence of fly ash on plastic concrete and mortar.

2.3.3 Effects of fly ash on plastic concrete

The addition of fly ash to concrete has many different effects on the concrete's behaviour, some beneficial and others deleterious. These effects are looked at in the following sections. This section covers the characteristics of freshly mixed or "plastic" concrete whilst the next deals with hardened concrete. In order to limit the bounds of this survey no consideration has been given to the effects of chemical additives such as superplasticisers in the discussion.

It is generally accepted[2.13, 2.75, 2.83, 2.112, 2.128 - 2.130] that the workability of a concrete is improved if part of the cement or fine aggregate is replaced with a reasonable quality fly ash.

Rather than quantify a change in workability due to a change in ash content or quality, the reduction in water content required to produce the same slump is more often measured.[2.78, 2.89, 2.95]

The improvement in workability is affected by the following:

- amount of ash in the mix; up to a limit, the more ash there is the better the workability.[2.108]

- the fineness of the ash; the finer the ash the greater the workability; in fact a coarse ash can decrease the workability of a mix.[2.108, 2.131]

- if a coarse ash has been ground to increase fineness the improvement in workability is less marked.[2.108]

- the LOI: a high carbon content decreases workability due to water being absorbed by the carbon grains.[2.101, 2.108]

A rule of thumb for South African fly ashes is that an approximate water reduction of 10 ℓ/m^3 is obtained for each 15% fly ash in the cementitious fraction.[2.13] It has also been noted that the improvement is visually deceptive, a fly ash mix will appear to be sticky until energy is put into it, when the improved workability becomes discernible as a tendency to flow more easily.[2.132]

The reasons for the changes in workability are varied. It is probably largely due to the spherical particles acting as ball bearings.[2.92, 2.131, 2.133] This effect is reduced when fly ash is ground, although there is still a net improvement in workability with the use of fly ash.[2.75, 2.112] It has also been proposed that the reduced water requirement is because of the different zeta potentials between the ash and cement particles causing the deflocculation of the cement grain

flocs.[2.92, 2.94, 2.108, 2.133] This results in water that is entrapped in the flocs being released as well as making mixing of the effectively smaller grains, easier.

It is generally well accepted that the rate of bleeding is reduced by the addition of fly ash.[2.13, 2.129] The smaller particles of fly ash result in slower sedimentation rates and reduced bleeding. However the longer setting times mean that this advantage may be lost because the total amount of bleed water is similar to that of a mix without ash.

Both the initial and final setting times of fly ash concrete are greater than those of OPC concrete. The finer the ash and the lower the carbon content the less the effect on a given mix; whilst increasing amounts of ash delay the setting to a greater extent. For South African ashes a 15% replacement mix will have the initial set delayed by approximately 30 - 60 minutes and the final set is generally retarded more than the initial set.[2.13, 2.78, 2.95] The cause of the delay is attributed to the presence of alkaline sulphates on the surface of the ash particles which retard the normally rapid hydration of the C_3A.[2.108]

2.3.4 Effects of fly ash on hardened concrete

Strength gain in a fly ash concrete is initially slower than for OPC concrete, but continues for a longer period as shown in Figure 2.7. The result of this is that with time a fly ash mix will be stronger than an OPC concrete with the same strength at a given age.[2.107, 2.109, 2.129, 2.134 - 2.136]

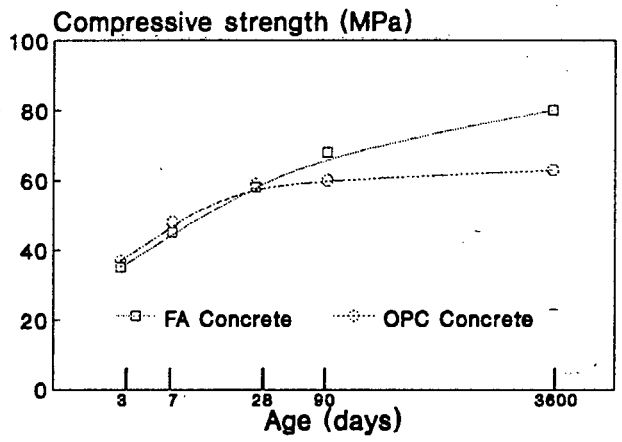

Figure 2.7: Compressive strength development of OPC and fly ash concrete[2.136]

The extent of this effect is controlled by a number of factors, not least the amount of fly ash in the mix. For mixes with 15% or less fly ash, there is little discernible difference between OPC and fly ash concrete. Strength is also dependent on the quality of the ash (ie LOI and fineness) although tests on some 25 year old concrete made using sub-standard ash (by present day standards) have shown that the concrete was satisfactory.[2.76]

The mechanism of the effect of fly ash on strength gain is two fold. Initially it acts as a fine filler and provides nucleation sites for hydration to initiate. With time, as reaction of the fly ash commences with the $Ca(OH)_2$, CSH gel is then formed which contributes to the strength.[2.112, 2.129, 2.137, 2.138]

This can only take place if sufficient water is available to promote hydration when the fly ash begins to react, thus necessitating curing of the concrete for this period. If water is not available then the fly ash will not hydrate, effectively reducing the amount of binder in the mix, thus explaining the often reported sensitivity of fly ash concrete to poor curing.[2.88, 2.109, 2.124, 2.139 - 2.141]

This sensitivity is not globally accepted in the literature, as it has been reported that fly ash concrete is equally as sensitive, or less sensitive than OPC

concrete to poor curing.[2.83, 2.135, 2.142 - 2.145] There is, however, agreement that enhanced curing has more of a beneficial effect on fly ash concrete than OPC concrete.[2.128, 2.135, 2.140, 2.144]

The modulus of elasticity of fly ash mixes is related to the strength of the concrete and it reported that similar strength concretes with and without fly ash have similar elastic moduli.[2.109, 2.129, 2.139, 2.146]

Permeability is often used as a measure of the durability of a concrete.[2.129] The consensus of research worldwide is that the permeability at 28 days of concretes of the same strength is less in fly ash mixes.[2.14, 2.134, 2.136, 2.147, 2.148] It has also been indicated that the permeability of older fly ash concretes was less than at 28 days; the slow pozzolanic reaction resulting in continued hydration, thus filling voids and reducing permeability.[2.129]

The sensitivity of fly ash concrete to carbonation is another unsettled issue. It would appear that initial carbonation rates are higher in fly ash concrete due to the reduced amount of $Ca(OH)_2$ to neutralize carbon dioxide entering the concrete.[2.109, 2.134, 2.149] The better impermeability, however, later slows the carbonation rate, meaning that in the long term the overall amount of carbonation appears to be similar for OPC and fly ash concretes.[2.134, 2.150 - 2.152]

Sulphate resistance of fly ash concrete is generally greater than that of OPC concrete.[2.93, 2.94, 2.129, 2.153] This is due to the reduced permeability of the concrete, the dilution of C_3A content as well as reaction of the calcium hydroxide with the fly ash.[2.78, 2.147]

It is also generally reported that fly ash concrete has a greater ability to slow the movement of chlorides, both due to its impermeability as well as to some form of chemical binding. This has the effect of improving the protection of embedded steel reinforcement.[2.109, 2.115, 2.134, 2.136]

The drying shrinkage of fly ash concrete is equal to, or more often, less than OPC concretes of similar strength. This is probably due to the lower water content of a mix with the same workability.[2.109, 2.143, 2.146, 2.153, 2.154]

There are conflicting opinions concerning creep. There are reports of increased creep (particularly in high percentage fly ash mixes);[2.129] "no change"[2.95, 2.129] and decreased creep.[2.83, 2.109, 2.146, 2.153] The variation in reported results is probably due to differences in water and paste contents, strengths and fly ash contents.

One of the most beneficial attributes of fly ash concrete is its resistance to alkali aggregate reaction (AAR). Resistance to AAR increases with increasing amounts of fly ash, above a minimum threshold of approximately 30% by mass of cement. The mechanism by which fly ash reduces the AAR reaction is reported to be a combination of the dilution of available alkalis in the mix as well as the chemical binding of some alkalis.[2.107, 2.129, 2.134, 2.136, 2.147, 2.155 - 2.157]

Another beneficial and commonly exploited attribute of fly ash is its tendency to reduce the heat of hydration.[2.12, 2.13, 2.75] This is also apparently due to the slower rate of reaction as well as the interfering effect of the LOI.

All of the above clearly shows the generally beneficial effects obtained by using fly ash as a pozzolanic addition or replacement in concrete. The next section covers the mechanisms by which the mechanical behaviour of fly ash concrete is changed due to the presence of another type of particle in the already complex microstructure of HCP, mortar and concrete.

2.3.5 Failure mechanisms of cementitious materials containing fly ash

This section provides a brief review of reported mechanisms of failure of fly ash concretes and mortars where they differ from OPC mixes, under mechanical loading.

It has been stated by several authors[2.90, 2.112, 2.127, 2.135, 2.158] that only a proportion of fly ash particles are hydrated even after several months, or years, in structural grade fly ash concretes. This means that the others provide another source of flaws, albeit small, as discussed in Section 2.2.3.

These flaws are often seen in SEM micrographs,[2.121] although it may questioned whether these visible flaws are as a result of the preparation of the sample for examination, or inherent.

Even those particles that do react appear to form a weak layer of calcium hydroxide[2.111, 2.122, 2.158] or acicular CSH[2.90] around their surfaces. The effect of these was illustrated by Montgomery and Diamond in micrographs clearly showing the path of cracks around and through cenospheres.[2.111]

Additionally, if such an unreacted sphere is also a hollow cenosphere, the effective size of the flaw may be increased, although it is apparent that the wall of a cenosphere is generally thick and strong enough to modify the path of a crack. This modification tends to cause a crack, which is going around the outside of the sphere, to branch. This was interpreted by Montgomery as indicating that crack paths were caused to be more tortuous, thus absorbing more energy and so increasing the toughness of the matrix.[2.111]

This conclusion was not confirmed by Brooks and Sikharulidze who indicated that OPC and OPC/fly ash mixes of similar strengths also had similar fracture energies.[2.159] It would be reasonable to state, however, that the effect of flaws present as a result of fly ash in a matrix may be masked by larger flaws caused by other mechanisms.

This is illustrated by the reports of decreased $Ca(OH)_2$ orientation, and amount in the interfacial zone with aggregates.[2.138, 2.160] Thus despite formation of a small amount of lime around a fly ash particle, the lime in the much larger

aggregate interfacial zone is reduced, giving an overall beneficial effect as the size of the flaws is reduced.

Thus on a relatively large scale fly ash appears to improve microstructure due to its pozzolanic effects. However on a much smaller scale, its presence results in an increase in the number of flaws, the effect of which may masked by the presence of other, larger flaws in the paste or mortar.

CHAPTER THREE - FATIGUE REVIEW

3.1 Introduction

3.1.1 General

Fatigue, in the engineering or materials science context, is the phenomenon whereby a material undergoes permanent and progressive change in mechanical properties due to the growth of cracks or damage when it is subjected to cyclic loads which are lower than the ultimate strength.[3.1, 3.2] This means that structures or components subjected to repetitive loads are liable to fail after a certain period despite the fact that each applied load is less than the ultimate strength of the unit.

The consequences of such failures can be, and have been, disastrous, from the Comet aircraft in the fifties to the potential failure of oil rigs subjected to tidal or wave action.[3.3, 3.4] It is therefore critically important that this failure mechanism be understood so that designers of engineering structures can make allowance for it, or strive to design so that its effect is minimised. The mechanisms of fatigue crack growth for metals are reasonably well understood and codes and practices are available for structural steel design.[3.5] However for cementitious materials, despite investigation since the turn of the century,[3.6] there is as yet no fundamental clarity. Methods of design are available,[3.7 - 3.9] but they are largely empirical, and possibly based on assumptions that are not strictly valid.[3.10]

The conventional method of describing fatigue behaviour for most materials is by means of the S-N or Wohler Curve,[3.1, 3.10 - 3.13] an example of which is shown in Figure 3.1 for aluminium. This curve plots the number of cycles to failure of a material (on a log scale), against the maximum stress applied (normally expressed as a percentage of the ultimate stress,[3.14 - 3.16] and also often on a log scale). It can be seen for example, that such a material can sustain only a few hundred cycles under a high stress of 80-90% of ultimate, but several million cycles at the 40-50% stress level.

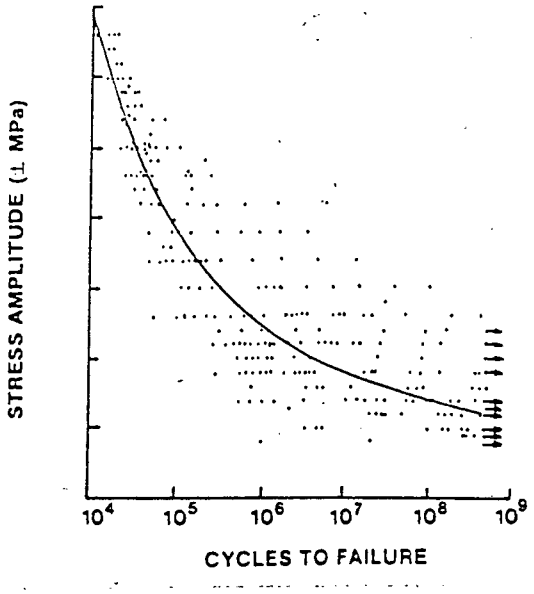

Figure 3.1: An S-N curve for aluminium alloy [3.13]

There are, for all materials, two distinct phases in the development of cracks under fatigue, the first is the initiation of the crack, which is predominantly dependent on the presence and size of existing flaws in the material. The second is the growth of the crack to a size that is critical to the integrity of the component. The rate of crack growth is largely dependent on the magnitude (cyclic amplitude and peak stress) of loading, and to a lesser extent frequency, environmental conditions, waveform and the type of material. These curves do not differentiate between the time, (or strictly, number of cycles) taken for initiation and that for growth. This leads to a large amount of inherent scatter when plotting experimental data, because the initiation stage can vary from a negligible to a considerable percentage of the lifetime.

Due to the large amount of scatter in the experimental results the S-N curve is frequently presented with bands of probability as shown in Figure 3.2.[3.17] This means that the designer in choosing the desired lifetime of his structure, can take into account an acceptable probability of failure when reading off the maximum permissible stress level to be used in his design.[3.2, 3.7, 3.18]

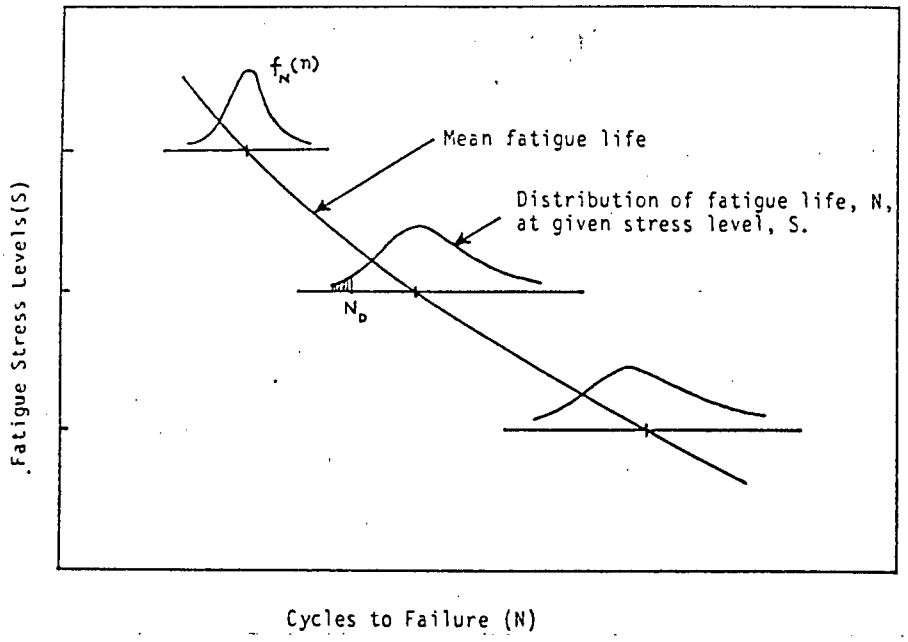

Figure 3.2: An S-N curve for concrete showing bands of probability[3.17]

Some materials exhibit a fatigue limit, characterised by the flattening off of the S-N curve, implying that below a given maximum stress level, fatigue damage does not accumulate within the material.[3.2, 3.19] Materials such as concrete are frequently reported as not exhibiting this fatigue limit, ie damage is incurred, albeit slowly, at all stress levels. There is a practical difficulty in confirming this as the time required to observe such slow damage accumulation becomes excessively high. Because of this, some define a "fatigue strength" of such materials as the cyclic stress applied which results in a specified number of cycles (normally one or ten million) before failure.[3.20]

The fatigue strength of most materials is affected by the amplitude of the applied cyclic stress wave. This is often allowed for by stating the stress (R) ratio (the ratio of minimum to maximum applied stress) pertaining to the S-N curve or by presenting a family of curves for a number of stress ratios (Figure 3.3).

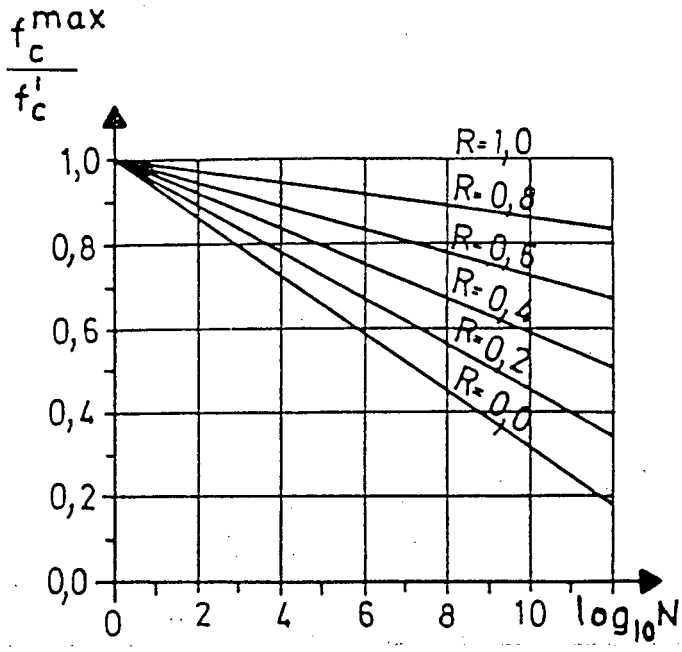

Figure 3.3: Families of S-N curves for different stress ratios (R) [3.21]

The mechanism of fatigue crack propagation in metals is one of plastic deformation of the crack tip leading to crack extension with each cycle.[3.22] This means that the growth rate per unit cycle is independent of frequency. It also means that it is the amplitude of the cycle, rather the than the magnitude of the maximum stress, that is critical.

The methods given above are the traditional methods of describing the fatigue behaviour of materials, particularly metals. An alternative means of description is to use the fracture mechanics parameter of stress intensity (K), plotted against the rate of crack growth (V) in the so-called "V-K diagram" for brittle materials, or the "Paris equation" approach [3.23, 3.24] for metals (da/dn vs ΔK).[3.25] This topic is covered in more detail in Section 3.3 and Chapter 4.

The following section summarises reported research on the fatigue of cementitious materials, particularly from a point of view that does not include fracture mechanics, as this is considered later in a section on its own.

3.1.2 Fatigue of cementitious materials

Despite research reports dating back as far as 1903/7 as reported by van Ornum [3.26], the mechanisms of fatigue of cementitious materials are still not well understood. Most design codes[3.2, 3.7, 3.27] are based on the S-N curve, the Goodman Diagram and Miner's Rule, all of which are covered in this section.

The type of concrete structures that need to be designed for fatigue include concrete road pavements,[3.28, 3.29] bridges, [3.30, 3.31] and structures exposed to marine tidal action such as off-shore platforms[3.32] and sea walls. Some examples of reported failures include a post-tensioned slab due to loads from changing ambient conditions,[3.33] dolosse,[3.34] and numerous bridge decks.[3.27]

Whilst most concrete structures include reinforcing, this review has been limited to plain concretes because the experimental work in the research was carried out on mortars only, as discussed in Chapter 5.

Numerous methods have been used to try to measure and describe the accumulation of damage in concrete (see Section 3.2.1). The research has indicated that the relationship between cyclic loading and damage is extremely complex and dependent on a large number of variables. These include:

- the loading cycle; including amplitude, maximum or peak load in the cycle,[3.17, 3.35] load or stress ratio,[3.15, 3.36] profile of the loading wave, and frequency or elapsed time aspects;[3.36, 3.37]

- loading history; ie the magnitude and sequence of previously applied cycles,[3.16, 3.35, 3.38, 3.39] or rest periods;[3.40]

- environmental conditions; including moisture content and temperature of the material,[3.16, 3.41 - 3.44] and presence of aggressive chemicals;[3.20, 3.45, 3.46]

- type of binder;[3.1, 3.42]
- sample size.[3.47, 3.48]

An alternative graphical method to the S-N curve of presenting the fatigue life of a material is the so called "Goodman diagram" (Figure 3.4).[3.2, 3.7] This plot gives the range of maximum and minimum stresses for a given number of cycles to failure. The model takes into account both the magnitude of the cycle peak as well as the amplitude of the cycle. This is unusual as most fatigue models only consider the peak or the cyclic amplitude, not both. The graph is often presented with different lines provided for different numbers of cycles, clearly showing that if a higher amplitude or peak stress is to be applied, the number of cycles that can be carried is reduced. The curves are normally derived from experimental compression or tension testing of prisms, in which the number of cycles to failure under a given cyclic load are counted.

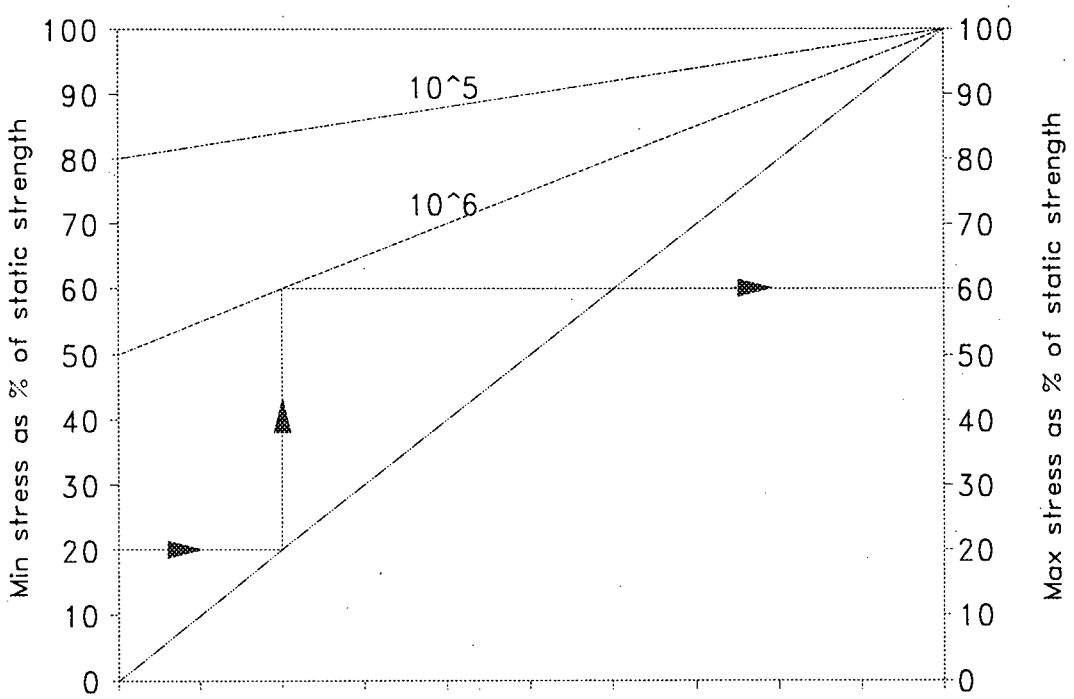

Figure 3.4: Goodman diagram

The process of fatigue failure appears to be the progressive growth of cracks and microcracks that are initiated in flaws.[3.2, 3.49] Some of these coalesce to form larger cracks that grow in dimension until the structure is overstressed, leading to failure.[3.50] This would help to explain the reported sigmoidal or "S" shape of the curve of the damage accumulation (Figure 3.5).[3.19, 3.27, 3.51 - 3.53] The first zone is the initiation of crack growth, whilst the linear portion is the zone of steadily accumulating damage as microcracking cracks increase and crack bridging decreases,[3.22] and the final acceleration is the agglomeration of a number of small cracks into a few major cracks that lead to failure. [3.10, 3.54, 3.55]

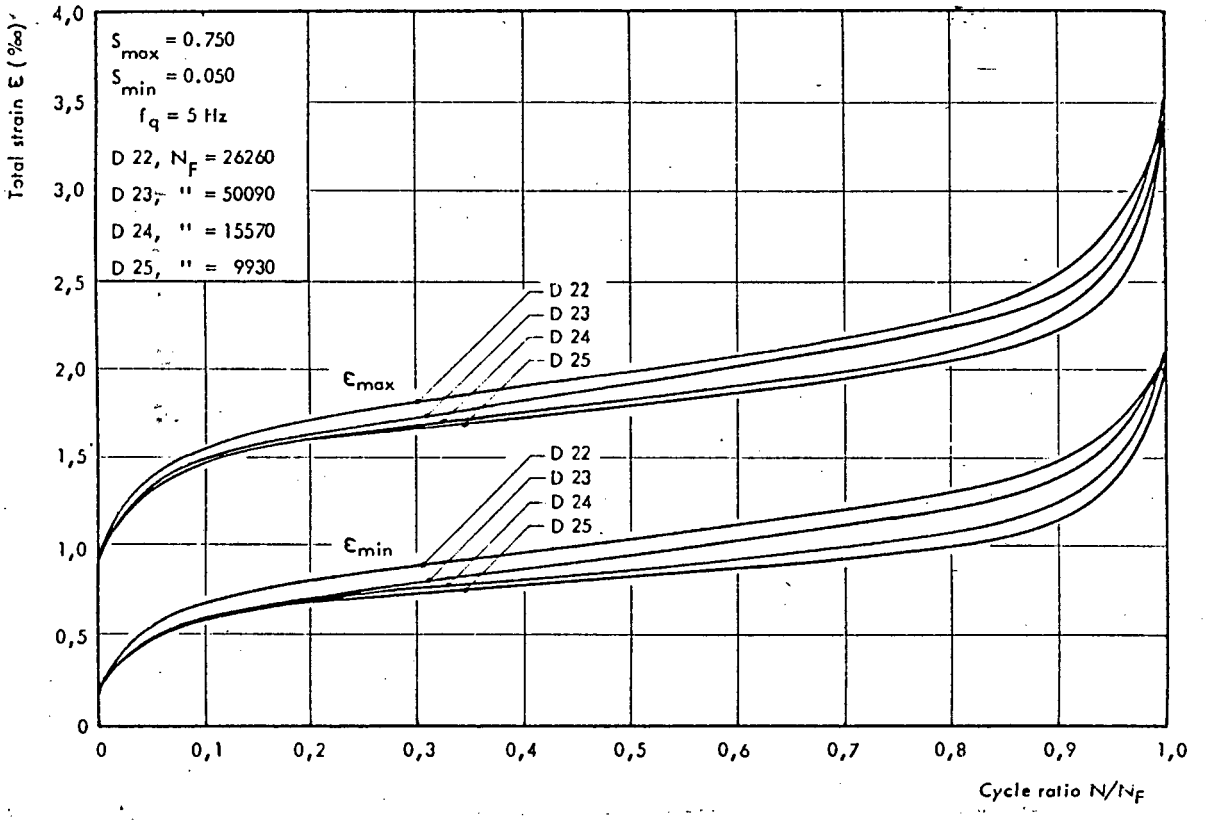

Figure 3.5: Typical S-shape curve of fatigue damage accumulation [3.19]

It is also often reported that the rate of growth is subject to a lot of scatter, even within a single sample. This can be explained by the existence of local

zones with varying strength due to the heterogenous nature of concrete or mortar.[3.56]

The presence and growth of a zone of microcracking of appreciable size, known as the process zone, that would absorb large amounts of loaded energy by elastic deformation helps to explain the reported hysteresis in the stress strain curve as a number of other reported effects (see Section 3.2).[3.51, 3.57]

Fatigue hardening, or the increase in static strength of samples subjected to low amplitude cyclic loading, has also been reported.[3.44, 3.58] It is thought to be due to the hydration of previously unhydrated cement grains freshly exposed by the microcracking caused by the fatigue loading.[3.44, 3.58]

It has been reported[3.10, 3.40] that for cementitious materials the rate of crack growth is largely a function of time rather than the number of cycles irrespective of loading frequency, (particularly at high stress levels). It has also been reported that it is the maximum stress[3.17, 3.38], or stress ratio[3.21] (or stress intensity, see Section 3.3.3) rather than cyclic stress amplitude that governs the rate of crack growth. However, some influence of amplitude is still observed.[3.56] Such a maximum stress approach would also indicate a transportation or chemical process mechanism, consistent with a form of environmentally assisted cracking (EAC). This is opposed to a plasticity controlled elongation mechanism of conventional metal fatigue. An EAC mechanism would validate the use of the V-K diagram as opposed to the Paris equation approach in describing fatigue behaviour.[3.25, 3.56, 3.59]

Variations in the magnitude of loading cycles, ie variable R ratio, is often handled by means of the Miner hypothesis[3.60 - 3.63] as used in many specifications. There are, however, some that query the validity of the approach.[3.2, 3.19, 3.35, 3.39] This topic is discussed further in the following sections along with the reported effects and mechanisms.

3.2 Fatigue mechanisms and cementitious materials

3.2.1 Measurement

Damage incurred in a concrete over a period of time may arise as a result of two forms of fatigue. Static fatigue is the imposition of a constant load on a structure or sample that is lower than the short term strength of the material that still results in damage and possible failure as a function of elapsed time. Cyclic fatigue is the accumulation of damage with the application of cyclic loads that are also less than the short term strength.

Measurement of the damage incurred in a sample of concrete subjected to cyclic or static fatigue loading is difficult to carry out directly. However there are a number of indirect approaches that have been reported.

The most common[3.22, 3.52, 3.64 - 3.68] is to count the number of cycles to failure of samples under various loading configurations, often for load cycles of constant amplitude. The results are normally expressed in the form of S-N or Wohler curves as described in the previous section. The general shape of these curves are similar, irrespective of the mode of loading.[3.27] The experimental results tend to exhibit a large amount of scatter, apparently largely due to the inherent scatter in measuring the strength of the specimens when normalising the vertical axis.[3.19, 3.67]

In order to accommodate variable amplitudes or frequencies, reference is often made to the Palmgren-Miner hypothesis.[3.60 - 3.63] This states that the amount of damage incurred can be expressed as a fraction of the number of applied cycles divided by the total number of cycles that can be carried at that loading level. When the sum of the fractions for the differing loading conditions reaches one, failure nominally occurs.

$$M = \sum_{i=1}^{k} \left(\frac{N_i}{N_{Fi}}\right) = 1.0 \quad \ldots\ldots\ldots\ldots\ldots\ldots\ldots\ldots\ldots\ldots\ldots\ldots \quad (3.1)$$

Where

N_i = number of cycles applied at stress level i

N_{Fi} = number of cycles to failure at stress level i[3.19]

Although it is widely used, this approach is not accepted as valid by all authors.[3.2, 3.19, 3.35, 3.39]

The equation 3.1 has been refined by van Leeuwen[3.63] to allow for the non-linear fatigue behaviour of concrete by using a log relationship.

Other methods have been used to measure the amount of damage more directly. Examples include:

- measuring the change in secant modulus of the concrete with increasing number of cycles,[3.19, 3.51]
- the change (or hysteresis) in the shape of stress strain curve[3.19, 3.66, 3.67]
- recording acoustic emission[3.10, 3.19]
- measuring the change in ultra sonic pulse transit time (UPTT).[3.10, 3.19, 3.69]
- counting the number of cycles to failure of:
  - compression prisms,[3.64, 3.65]
  - beams in flexure,[3.66]
  - direct tension prisms,[3.52, 3.67]
  - compact tension specimens;[3.22]
- surface crack mapping.[3.70, 3.71]

Another approach is to use the double torsion (DT) test configuration which forms a (nominal) single crack, the length and growth rate of which can be

directly observed as discussed in Chapter 4.[3.10, 3.72 - 3.75] In this case, crack growth rates may be directly related to damage development rates.

Measuring the crack length in tensile tests of other specimen shapes (eg compact tension) has also been attempted,[3.68] but unlike the DT approach, such specimen configurations have an increasing, not constant, stress intensity. Therefore the cracks tend to accelerate rapidly as they progress, which can make observation difficult or even impossible.

Environment, loading details, and other variables all have their own effects which are discussed in the following sections.

3.2.2 Effect of frequency and loading rate

It is generally acknowledged that an increased loading strain rate leads to an increased strength of a concrete being recorded.[3.47, 3.76 - 3.79] This is more apparent in wet than dry concretes,[3.77, 3.80, 3.81] and in weak rather than strong concretes.[3.81]

Concretes fatigued at high frequencies are effectively subjected to high strain rates. Thus, for evaluation, the stresses (normalised as a proportion of the now higher ultimate strength) are consequently lower - leading to an increase in the number of cycles that can be carried. This agrees with reported results, particularly for high stress levels.[3.9, 3.36, 3.37, 3.82] However, at lower stress levels and frequencies this is not always observed.[3.47]

However, there is a strong influence of time. That is, a tenfold increase in frequency does not give a tenfold increase in the number of cycles to failure, therefore a shorter life measured on the basis of time. This was acknowledged by Hsu in his derivation of an equation for predicting fatigue life that included both time and number of cycles.[3.36] It is necessary to try to separate the different effects of high loading rate at high frequency from the time

dependence of the failure mechanism. The scatter in such results [3.36] can cover two orders of magnitude, therefore it is difficult to be explicit, but the influence of time is real.

There are some reports relating creep or secondary creep with fatigue (Figure 3.6) [3.67, 3.79, 3.83, 3.84] where there is a "strong interaction".[3.63] Some researchers have attempted to separate the two effects by monitoring the developing microcracking, but it is possible that at this level creep and fatigue involve the same mechanism with the microcracking simply not being visible. The topic of creep is discussed further in Section 3.2.5.

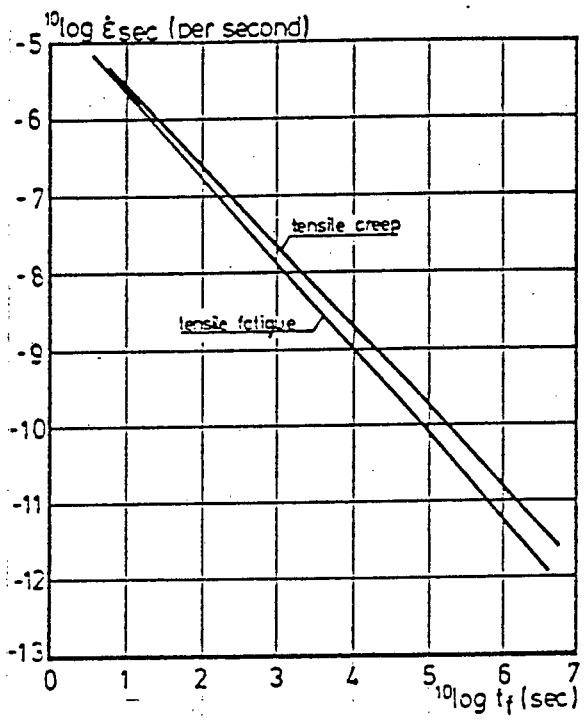

Figure 3.6: Comparison of strain rate vs time to failure of tensile creep and fatigue [3.67]

The influences of the presence of moisture, and the function of time on fatigue crack behaviour indicate that the mechanism of failure possibly involves some form of stress corrosion cracking. This is discussed further in Section 3.3.3.

3.2.3 Effect of amplitude, load ratio and loading history

The effect of cyclic load amplitude on the fatigue behaviour of concrete is described by authors in a variety of ways, which makes direct comparison difficult.

As shown in Figure 3.7, a change in amplitude may be described on the basis of four basic variables:

- stress amplitude,
- maximum stress,
- mean stress,
- R ratio (defined as minimum stress/maximum stress).

Many authors (particularly those used to working with metals) use the last as a point of comparison, deriving relationships or families of curves with R as a variable (Figure 3.3).[3.21, 3.27, 3.36]

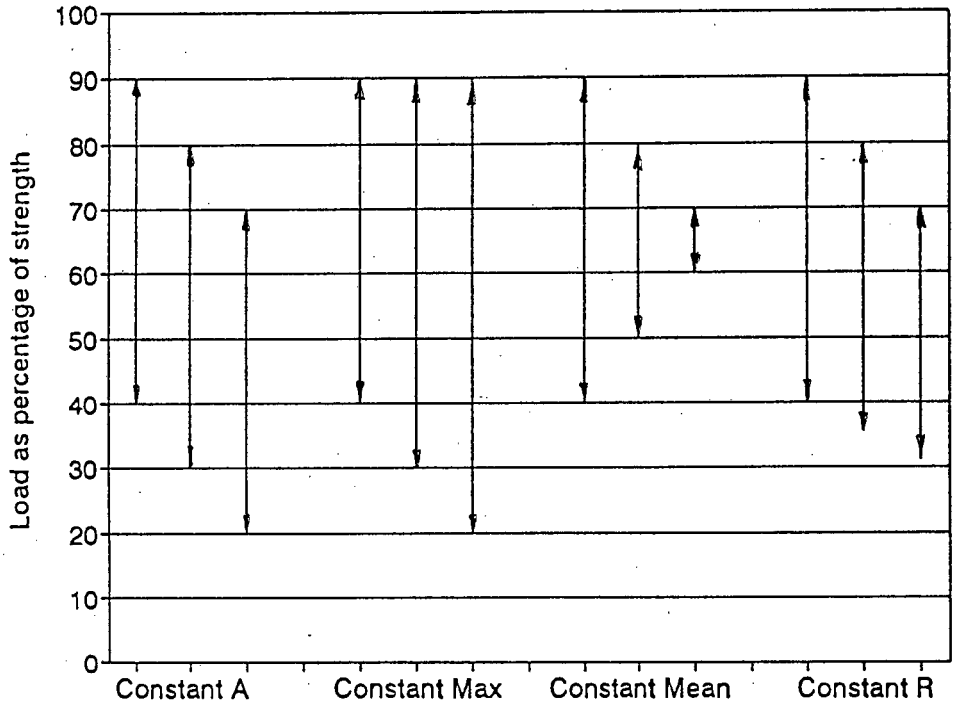

Figure 3.7: Describing changes in amplitude

However, as shown in Figure 3.7, a change in R is in effect a change in amplitude and maximum and mean stresses and a single R value does not uniquely define the characteristics of the load cycle applied. In order to avoid ambiguity, the approach used in the remainder of this study has been to describe both maximum stress intensity and amplitude.

As discussed in Section 3.3.3, the basic difference between the Paris equation for metals,

$$\frac{da}{dn} = C\Delta K^{m} \qquad (3.2)$$

and the V-K relationship for brittle materials,

$$V = AK^{n} \qquad (3.3)$$

is that in the first the amplitude of the loading cycle is critical, whilst in the latter, the magnitude of the maximum or peak load is critical. In the following discussion, changes have been described by a change in one parameter, (amplitude or maximum load) in order to be able to evaluate the applicability of either of the two equations above.[3.25, 3.56]

As can be seen from Figure 3.3, an increase in R (reducing amplitude) will lead to a greater number of cycles that can be carried at a given peak load.[3.56, 3.85] This indicates that there is an effect of both amplitude (Paris) and peak load (V-K).

It is interesting to note one of the conclusions drawn by Holmen[3.19], that "variable amplitude loading seems to be more damaging than predicted by the Palmgren Miner hypothesis. This is due to sequence effects present by variable loading". This is as a result of testing using variable amplitudes in each cycle

rather than batches of constant amplitude. His view is contradicted by Siemes[3.8] who considers that the Miner approach is "remarkably good for describing the cumulative damage due variable amplitude loadings".

Work carried out by Ruimin et al [3.54] showed that fatigue damage due to blocks of differing amplitude could be related to measurement of maximum strain in compression prisms.

The application of blocks of cycles of different amplitude has been shown to affect the fatigue life of samples in laboratory tests, albeit with trends reported in opposite directions. Oh and Kim[3.35] concluded that increasing load amplitude leads to damage with a Miner number greater than one, and vice versa with decreasing load amplitude. This is consistent with Petkovic et al[3.16] who reported that low loads applied initially lead to a greater number of cycles that can be carried. Tait[3.10] has quoted two sets of results, one that shows a behaviour similar to that above, and another that is in the opposite direction as shown in Figure 3.8.

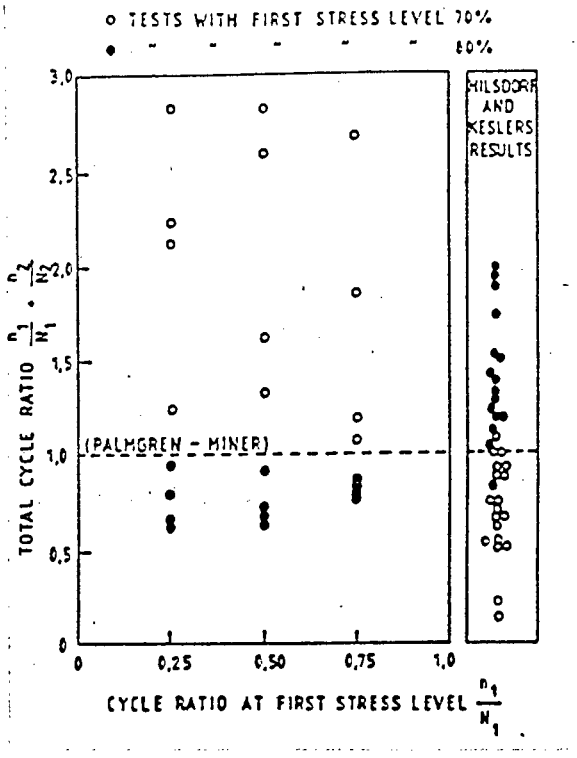

Figure 3.8: Two sets of data showing opposite trends as a result applying similar loading histories [3.10]

The cause of these trends have not been commented on, but may have been due to the rate of damage accumulation being lower under lower loads, or due to some other effect.

These apparent contradictions lend weight to the contention that there are many variables that contribute to fatigue, and to try and apply strict numerical relationships to the topic of fatigue without qualification is ambitious at best.

Static fatigue, as defined earlier, still results in long term failure of structures under sustained loading, even with no cyclic amplitude. Examples of this are shown in Figure 3.9[3.86] and the subject is discussed further in Chapter 9.

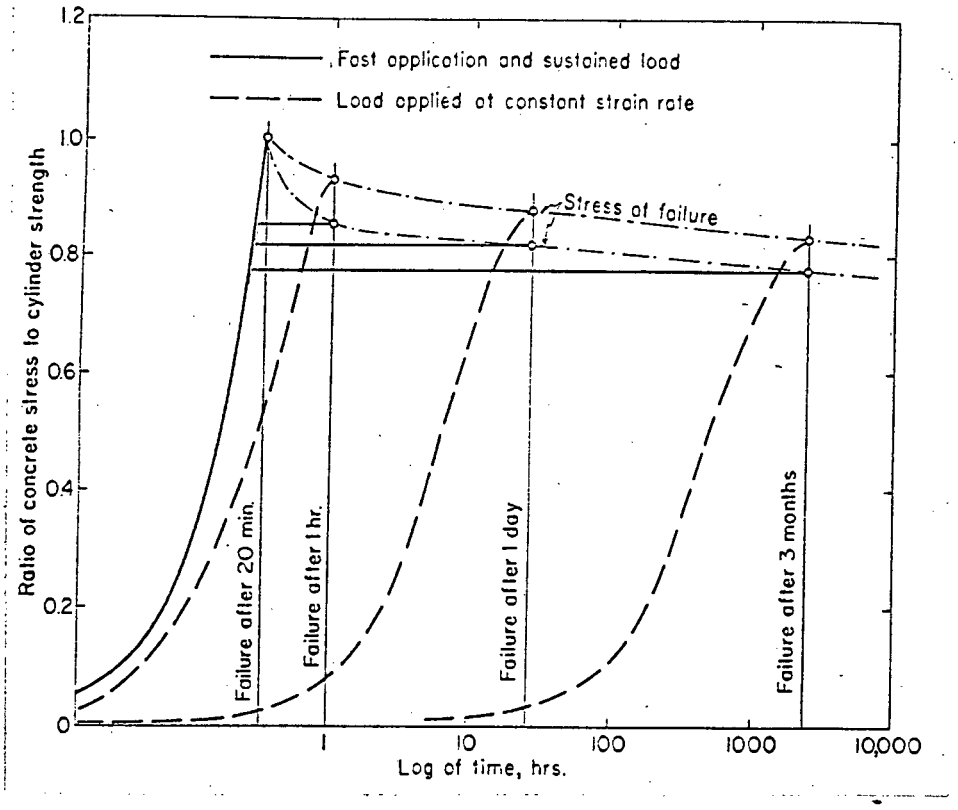

Figure 3.9: Influence of type of loading on ultimate strength [3.86]

The next section covers the effects of the environment.

3.2.4 Effect of environment

The bulk of the papers on the effect of environment on fatigue strength described work carried out using static fatigue tests on compression prisms, beams under bending loads or double torsion specimens. In this context, "environment" is considered to involve temperature effects,[3.87, 3.88] the presence of water[3.16, 3.20, 3.27, 3.42, 3.43, 3.45, 3.89] (measured as relative humidity) or the immersion of the sample in a liquid.[3.10, 3.90, 3.91]

It is generally reported that the wetter a concrete is, the earlier the failure under static or cyclic fatigue loading.[3.16, 3.20, 3.27, 3.42, 3.43, 3.45, 3.89] This is presumed to be due to the attack of stressed concrete microstructure of (possibly) silicate bonds by hydroxyl ions, or additionally by the wedging of the cracks by water.[3.20, 3.87]

This is borne out by the markedly increased resistance to static fatigue of beams loaded under vacuum.[3.43]

Tait and Garrett[3.92] employed double torsion tests in the measurement of V-K curves (see Chapter 4) under static and cyclic loading, and showed that with increased relative humidity, the crack growth rate was faster. The results also indicated that the mechanism of crack propagation under static and cyclic loadings was essentially the same, ie possibly that of hydroxyl ion attack. This means that the difference in crack growth rates between static and cyclic loading is a function of integrated time and stress, as predicted by Evans and Fuller [3.59] in the equation:

$$\frac{da}{dN} = \lambda \, g \, A \, K_{Ia}^{n}$$

. . . . . (3.4)

Where: da/dN is the crack growth per cycle as calculated from a measured static crack growth rate,

λ = period of each cycle,

g = correction factor (See Appendix B),

A and n = materials properties (see Section 3.3.3)

K_{Ia} = **Average** cyclic stress intensity.

This can be manipulated (See Appendix B) to read:

$$V_c = \frac{V_s \, g}{(1 + \zeta)^n}$$

. . . . . (3.5)

Where V_c = calculated crack velocity due to cyclic loading (for K_{max})

V_s = measured crack velocity due to static loading

g = correction factor (Appendix B)

$\zeta = K_{amplitude} / K_{average}$

This contention needs to be balanced with the effect of fatigue hardening, which is probably due to hydration of freshly exposed grains,[3.58] which in effect increases fatigue lifetime. This effect has, however, only been observed at low fatigue stress levels.[3.89]

Retesting of loaded and healed compression prisms by Abdel-Jawad et al[3.93] resulted in failure in the old cracks indicating that even if autogenous healing occurs, the healed cracks still act as flaws or stress raisers under loading.

The greater sensitivity of wet concrete to loading rate than dry [3.78] has been described as being due to the Stefan effect.[3.80] This effect considers the surface tension of water, in contact with two faces close together, resisting the forces separating the faces (Figure 3.10).[3.81]

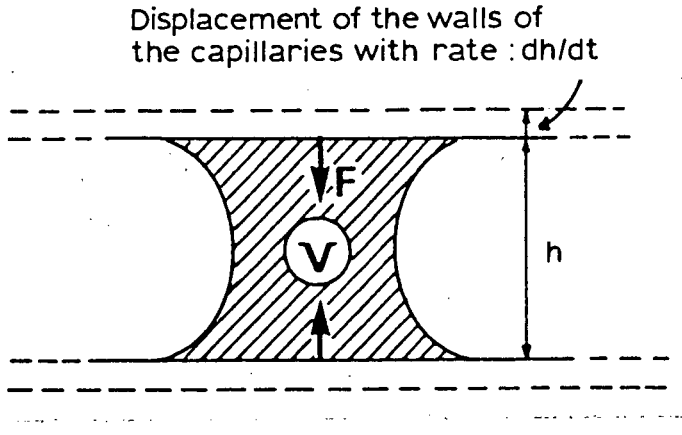

Figure 3.10: Stefan effect inside the pores of concrete [3.81]

It was reported by Barrick and Krokosky [3.87] that temperature has an inverse effect from that expected, in that increasing temperature reduces the damage incurred by fatigue loading. This was more marked in wet than dry specimens. They thought that this was due to the reducing solubility of $Ca(OH)_2$ with increasing temperature, thus reducing the availability of hydroxyl ions to attack

the stressed bonds (Fig 3.11).[3.20, 3.87, 3.94] However, they employed somewhat questionable statistics in that they discarded a lot of their data if fatigue occurred "too quickly".[3.87]

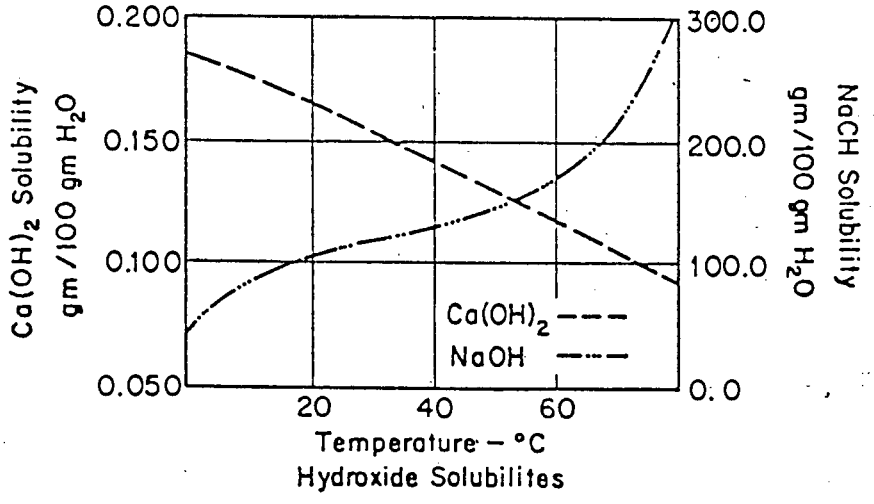

Figure 3.11: Solubilities of hydroxides with temperature [3.94]

This contrasts with the report that fracture energy decreases with increasing temperature,[3.88] which is again more marked in wet concretes. This was explained as being due to a reduced activation energy. Fracture energy has also been reported to decrease with increasing humidity[3.95] (Fracture energy is the energy input required to create new surfaces within a body, and is discussed further in Section 3.3.1.) In a similar manner, increased stressing of Si-O-Ca-O-Si bonds leads to lower activation energy for chemical attack and subsequent cracking.[3.96]

In summary, the extent of fatigue damage appears to be affected by the environment due to a combination of:

- stressed silica-oxide bonds being more susceptible to corrosive attack than unstressed bonds,

- liquids that will chemically attack such bonds must be present in sufficient quantities for sufficient time; (transport effects),

- increasing temperature appears to have an influence in that the activation energy to propagate cracks is lowered. There is also a report that hydroxyl ion solubilities may have a part to play.

- some influence of wedging is also indicated, the extent of which has not been quantified.

The next section discusses the implications of the above findings from the point of view of the mechanisms of fatigue damage of cementitious materials.

3.2.5 Failure mechanisms

A summary of the failure mechanisms of concrete under static or cyclic fatigue is presented in this section.

It is generally acknowledged that hardened concrete that has not been loaded contains a number of different types of flaws, including shrinkage cracks, air bubbles and interfaces between the different constituents.[3.29, 3.43, 3.70, 3.97] A study by Hansen[3.97] could not detect shrinkage cracks by optical microscopy, although it is possible that the magnification was too low or preparation of the concrete had allowed shrinkage to occur without incurring visible cracking. As discussed in Chapter 8, some cracking has been observed in samples that have not been loaded when studied in an electron microscope.

Crack initiation and propagation can occur at any of the numerous flaws in a typical concrete. The process involved is still not fully resolved but it is likely that general load increases cause large local increases in stresses at the tips of flaws and cracks. The bonds of such tips become highly stressed and hence more susceptible to attack (for example by water). The effect of having both moisture and local stress at crack tips is that the additional energy required to

overcome the activation energy for cracking is reduced and may even be sufficient to overcome the activation energy. This will result in crack growth in a number of locations.[3.43] Hansen[3.97] has noted that as loads were increased, microcracks tended to coalesce into continuous cracks that eventually led to failure.

In the case of prisms loaded in compression,[3.70] cracks were reported as tending to grow along the aggregate interfaces, perpendicular to the (tensile) principal stresses (ie parallel to the direction of the compressive load). When the surface of the aggregate changed direction, the cracks were then observed to branch off into the paste and maintain their original approximate direction. The specimens were thus broken up into a number of columns that subsequently failed in buckling. The release of stored strain energy also resulted in more damage.[3.70, 3.97]

Cracks in concrete or hardened cement paste are seldom straight and continuous, even at the microscale level. They tend to be straighter in high strength concrete where failure occurs through the aggregate as well as through the paste and interfaces. Bentur and Mindess[3.98] also noted that cracks often went around rounded particles.

Schlangen stated that crack jumping (or as he called it, bridging) leads to toughening in the scale 5 μm - 25 mm, where the maximum size of such bridging is affected by aggregate size. The falling branch of stress-strain curves was described as being related to this bridging effect. The interface bond strength is also critical where low bond strength leads to more jumping and bridging, and therefore more so-called "ductility". [3.99]

Bridging of the cracks by aggregate particles would also contribute to the toughening of the concrete, which is large in relation to the energy absorbed by the process zone.[3.22]

Fatigue crack growth and creep are thought to be related by Suter[3.100] and Cornelissen[3.101] who have proposed that the rate of secondary creep gives a measure of the damage within a concrete including that due to fatigue loading. Bazant and Gettu[3.102] have reported that there is a strong interaction between fracture and creep in concrete. In tests where strong load relaxation was observed in samples maintained at constant crack mouth opening displacement (CMOD) in the post peak regime, the relaxation was attributed to creep as well as time dependant crack growth (EAC). The phenomenon of creep is normally attributable to the movement of water at the gel pore and small capillary pore level under the action of applied loads, or relative movement of particles.[3.103] This would imply that samples that have been dried are less subject to the former mechanism.[3.69]

The broad outlines of the different mechanisms of static and cyclic fatigue crack growth and in concrete as described above may be summarised as:

- crack propagation by chemical attack of stressed fibres, particularly those subject to stress concentrations such as at the tips of existing flaws,

- creep, or the movement of particles due to water movement or particle movement at gel pore level,

- brittle cleavage type fracture,

- non-linear "plasticity" mechanisms.

This discussion has largely excluded the concepts presented by the discipline of fracture mechanics. The next section briefly covers fracture mechanics as a subject, its application to concrete and its relevance to the study of fatigue of concrete.

3.3 Fracture mechanics

3.3.1 Fracture mechanics theory

Fracture mechanics has been defined as the branch of applied mechanics that deals with the behaviour of cracked bodies under load.[3.104] This section gives a broad definition and outline to the topic, the next considers its application to cementitious materials, and the following the application of fracture mechanics to cementitious materials under cyclic loading.

The bulk strength of materials (σ_c) is normally found to be substantially lower than the theoretical value by a factor of 10 to 100.[3.105] This is due to the presence of flaws or cracks in most materials which cause concentrations of stress, which are locally higher than σ_c, thus propagating the crack. Flaws on the surface of a body have been shown to contribute more to this effect than those within a body.

In the early 1920's, Griffith [3.106] undertook some elegant experimental fracture research on glass since he realised that the fracture stress was approximately two orders of magnitude less than the theoretical value for complete separation of two sides of a crack. Using glass slides as specimens, he found that the product of fracture strength and square root of the crack length was effectively constant. He used an energy balance argument given below to provide a theoretical background to these observations.

For a stressed brittle material, the stored strain energy **per unit volume** (U) is

$$U = \sigma^2/2E' \qquad (3.6)$$

where σ is the applied principal stress and E' = the young's modulus E in plane stress, or $E' = E/(1-\upsilon^2)$ in plane strain. If a through-thickness crack were to develop in a semi infinite sheet of such material with surface energy γ (in J/m^2), then stored strain energy would be released immediately above and below the crack region as the crack surface cannot sustain a stress normal to its surface.

For unit thickness material, the strain energy released is simply the energy per unit volume multiplied by the volume per unit thickness. Griffith [3.106] was able to show that this relaxed area was equivalent to the value $2\pi a^2$ for a crack length of 2a. Hence

$$U = -\frac{\sigma}{2E'} \times 2\pi a^2 = \frac{-\sigma^2 \pi a^2}{E'} \quad \ldots\ldots\ldots\ldots\ldots\ldots\ldots\ldots\ldots\ldots \quad (3.7)$$

This released strain energy goes into the creation of the new surfaces (crack surfaces need energy just like surface tension in fluids) which for a crack length of 2a and unit thickness gives a surface energy requirement (S) of

$$S = 4a\gamma \quad \ldots\ldots\ldots\ldots\ldots\ldots\ldots\ldots\ldots\ldots\ldots\ldots\ldots\ldots \quad (3.8)$$

One can now write a total energy (W) balance equation for the crack as follows:

$$W = 4a\gamma - \frac{\sigma^2 \pi a^2}{E'} \quad \ldots\ldots\ldots\ldots\ldots\ldots\ldots\ldots\ldots\ldots\ldots\ldots \quad (3.9)$$

This is represented on a schematic energy vs crack length plot as shown in Figure 3.12.

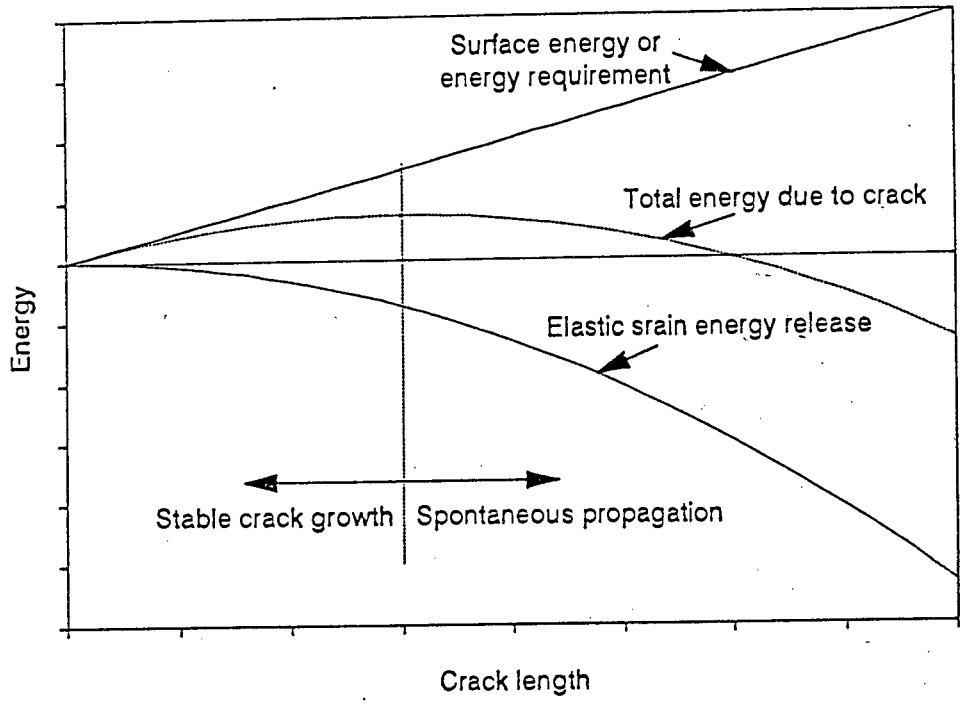

Figure 3.12: Energy balance as crack extends in brittle material [3.69]

The stability of the crack in the material can now be assessed from an energy release rate approach. Up to the vertical line in Figure 3.12 the energy release is less than the energy demand for new cracks to form, hence the crack is stable. Beyond the "maximum" the converse is true, there is more energy supplied from the released strain energy field than is required by the new crack surfaces, therefore the crack becomes unstable and accelerates, leading to catastrophic failure. This maximum can be found by differentiating the total energy term W with respect to crack length a, and setting to zero as is standard calculus procedure.

$$\frac{dW}{da} = 4\gamma - \frac{\sigma^2 \pi 2a}{E'} = 0 \quad \ldots\ldots\ldots\ldots\ldots\ldots\ldots\ldots\ldots\ldots\ldots\ldots\ldots\ldots \quad (3.10)$$

Therefore at the point of unstable fracture

$$\sigma_f = \sqrt{\frac{E2\gamma}{\pi a_c}} \quad \ldots\ldots \quad (3.11)$$

or

$$\sigma_f\sqrt{\pi a_c} = \sqrt{2\gamma E} = \text{a constant} \quad \ldots\ldots \quad (3.12)$$

where σ_f is the fracture stress and a_c is the critical crack length. This provides a theoretical justification for Griffith's experimental observations that $\sigma\sqrt{a}$ was constant.

The term 2γ = dU/da is known as the strain energy release rate G, also occasionally known as the crack resistance. Note that the rate is with respect to crack length and not time).

The term $\sigma\sqrt{(\pi a)}$ is also known as the stress intensity K, (ie $K = \sigma\sqrt{(\pi a)}$) and is a convenient parameter since it can be superimposed and added as a vector in much the same way as stress is used. K provides a measure of the toughness, or ability to resist crack propogation, of a material.

When discussing fracture mechanics parameters, it is necessary to separate the three loading modes with respect to cracks, ie opening, in-plane and anti-plane shear known as I, II and III as shown in Figure 3.13.

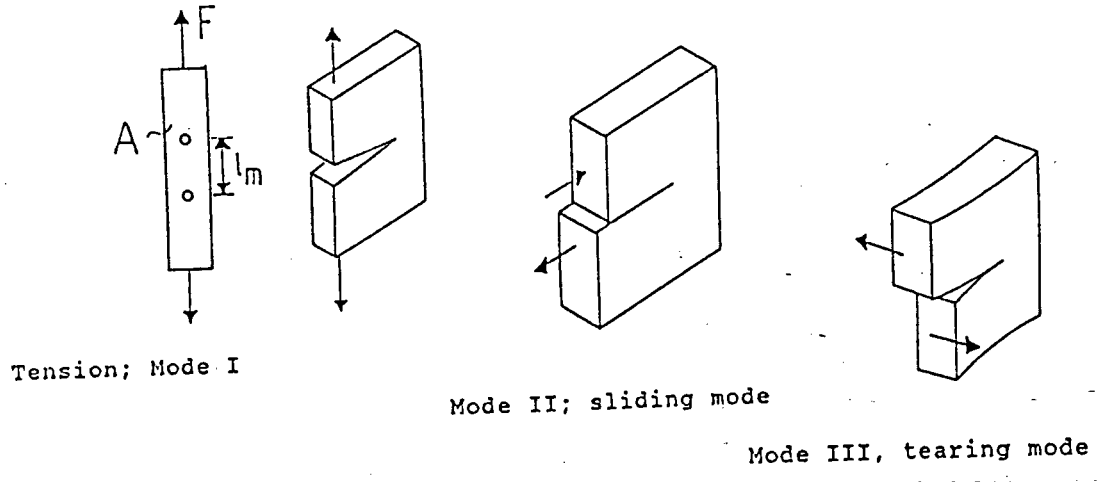

Figure 3.13: Fracture mechanics failure modes [3.107]

It is also practical to incorporate a so called compliance function Y in the formulation

$$K = Y\sigma\sqrt{(\pi a)} \quad \ldots\ldots\ldots\ldots\ldots\ldots\ldots\ldots\ldots\ldots\ldots\ldots\ldots\ldots\ldots\ldots \quad (3.13)$$

which is related to the geometry of the loaded structure and the shape of the flaw under consideration.

This stress intensity term K must be distinguished from the stress concentration factor (SCF) parameter k_t. This parameter may be regarded purely as a geometrical factor which refers to the enhancement of stress due to local macro geometry effects, ie

$$k_t = \sigma_{max}/\sigma_{min} \quad \ldots\ldots\ldots\ldots\ldots\ldots\ldots\ldots\ldots\ldots\ldots\ldots\ldots\ldots\ldots\ldots \quad (3.14)$$

where σ_{max} is the maximum stress experienced near a crack tip and σ_{min} is the average stress remote from the flaw.

K_{IC}, the critical stress intensity is the fracture toughness of the material, and is a measure of its ability to resist cracking. The relationship between K and G (for plane strain conditions) is given by

$$K = \sqrt{(EG)} \quad \quad (3.15)$$

All of the above discussion is limited to linear elastic fracture mechanics (LEFM), based on assumptions of homogeneity and elasticity. This concept and K parameter is practically useful for a number of engineering materials,[3.108 - 3.111] in the limitation that the plastic zone ahead of a crack tip is less than a/15.[3.69] However, materials that display a large amount of plastic deformation, and those that contain zones of crack bridging, microcracking or a number of discontinuous cracks, are outside the bounds of the assumptions for LEFM.

Such materials can be accommodated in fields such as elastic-plastic fracture mechanics (EPFM), which utilise terms such as the J-integral or crack tip opening displacement (CTOD) to characterise the toughness of a material.[3.112] The J-integral is broadly related to the area under the stress strain curve (including the descending branch for concrete) and under elastic conditions is equivalent to the strain energy release rate G discussed above.

Alternatively, an approach known as the R curve, a plot of toughness index (K,G, CTOD or J), plotted against crack length (a) (Figure 3.14) provides a means of evaluating the probability of cracking in a given body by comparing a characteristic material R curve of toughness against the energy supply curve (ie the release of stored strain energy U). The system is stable up to the tangent between the two graphs, but unstable cracking occurs beyond this point.[3.69, 3.113]

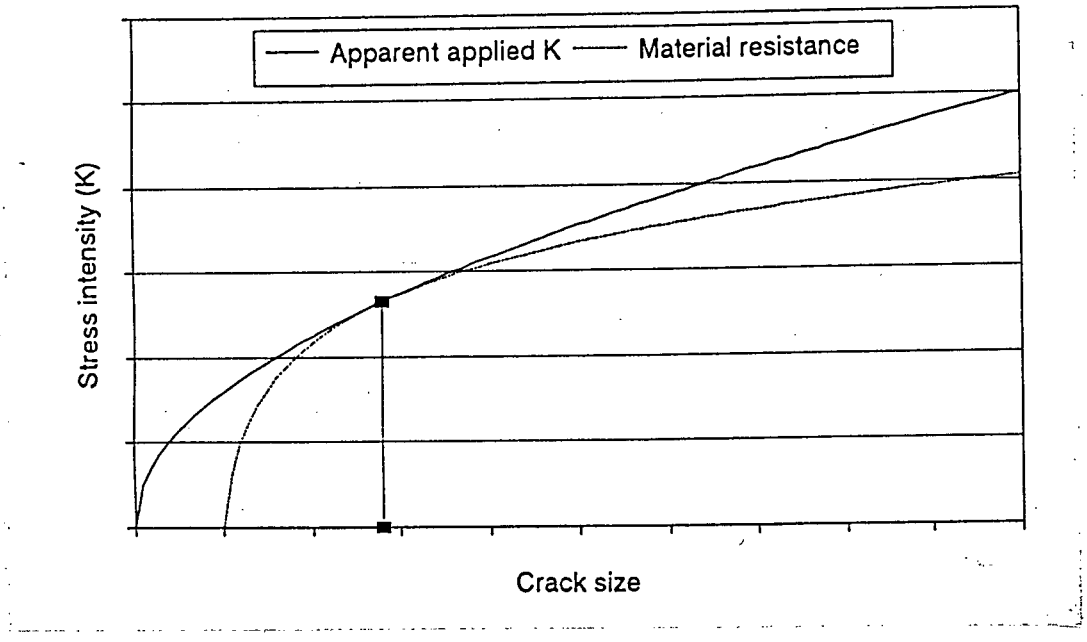

Figure 3.14: Typical R-curve showing point of instability at tangent of energy supply curve and material toughness curve[3.113]

The next section continues the discussion with particular reference to cement based materials.

3.3.2 Fracture mechanics and cementitious materials

Linear elastic fracture mechanics (LEFM) as described above is based on a number of assumptions, including the homogeneity and linear elasticity of the material concerned as well as the extent to which it can be considered as isotropic.[3.69] Few of these assumptions are valid for cementitious materials, and in particular, concretes. This is due to the nature of concrete, a material made up of a number of phases that are not homogenously mixed, even at a macro scale. Indeed, some of the phases do not comply with these assumptions in their own right.

The application of fracture mechanics to concrete is a topic that is still the study, at very high level, of a large number of people as well as a topic leading to a certain amount of contentious debate.[3.114 - 3.121]

A review by Mindess in 1983[3.121] concluded that the question of the applicability of fracture mechanics to cementitious materials had not been answered. Since that time a number of increasingly sophisticated models have been proposed and refined,[3.115] but it would appear that the question has still not been settled conclusively. Design of concrete structures using fracture mechanics is still in the hands of the theoreticians,[3.119, 3.122] not practising engineers.

Some of the models referred to include the fictitious crack model by Hillerborg[3.123] the crack band model of Bazant[3.117, 3.124] and the two parameter model of Jenq and Shah.[3.125] R curves,[3.113, 3.116, 3.126 - 3.128] the J-integral[3.129] and damage (or continuum) mechanics[3.114, 3.130, 3.131] are also described as having varying degrees of success.

When concrete, mortar or paste is stressed, a crack is formed that is typically not straight, continuous, or singular.[3.132] In fact a zone of softening or microcracking is said to form in front of the visible crack tip[3.133 - 3.135] which contributes to the material's non-linearity.[3.116, 3.127] Determination of the size of the so called fracture process zone (FPZ) is another topic of much research and discussion.[3.136]

An effect of the process zone is the shielding of the crack tip or redistribution of strain (or strain gradient[3.71]) such that potentially critical flaws are not subjected to critical displacements and failure is delayed. This can also be considered from the view point that energy is absorbed in the creation of a large number of micro-cracks around the nominal crack tip as well as in crack bridging.[3.115, 3.137]

Therefore, energy introduced into a concrete by loading can be dissipated in three ways:

- creation of a new surface or surfaces,
- microcracking or process zone,
- and crack bridging behind the crack path.

LEFM describes the first type only, whilst Bazant's model covers the first two and the two parameter model addresses all three.[3.138]

Birchall [3.139] has shown (Figure 3.15) that pastes behave as predicted by Griffith down to maximum flaws of about 20 μm, the first form of energy dissipation. This is the basis of the manufacture of very high performance, or macro-defect-free mortars and pastes that have remarkably high tensile strengths as reported for example by Jennings and Birchall.[3.140, 3.141]

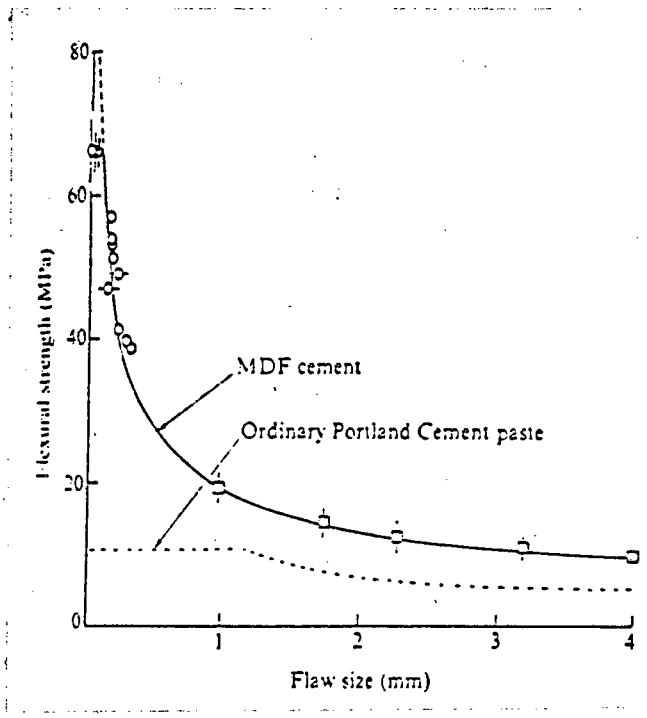

Figure 3.15: Flexural strength vs (artificial) flaw size [3.139]

Some of the flaws that affect fracture parameters are:[3.142]

- air bubbles due to poor compaction and due to entrainment,
- cracks in the coarse aggregate,
- interfaces with coarse and fine aggregate,
- CaOH crystals,
- capillary pores
- gel pores.

These range in size from the macro (mm) to the micro (μm). Additionally, there are cracks induced by shrinkage (which are said to be inherent) or due to loading, which range in size from the macro to the so-called process zone. These flaws may reduce toughness, or act as crack arrestors depending on their orientation with respect to the crack direction.[3.95, 3.143]

It is interesting to note the increase in fracture toughness of mortar impregnated with polymers, attributed to the improvement of the microtoughness by the polymer binding microflaws and suppressing microcracking.[3.144] This is probably related to crack bridging acting as an energy sink as described by Yu.[3.137]

LEFM is also largely based on the assumption that failure is predominantly in Mode 1 (Figure 3.13), as proposed by Schlangen,[3.145] although work on fracture modes 2 and 3 is continuing.[3.125, 3.146]

Despite all of these difficulties, it is possible to measure a fracture toughness (eg K_{IC}) of a concrete or mortar, using specimens with a suitable geometry.[3.116] The result appears to be dependent on the size of the sample, [3.147 - 3.150] and the rate of loading,[3.102, 3.113, 3.151] whilst for a concrete, samples would have to be very large before influences due to the process zone become small.[3.121, 3.147] Wolinski et al have reported that there were no distinctive relationships between fracture mechanics parameters and aggregate size.[3.152]

The parameter K_{IC} may be considered a reasonable means of assessing and comparing various similar concretes under similar loading conditions. It is this parameter that has been used in the experimental work of this study in fatigue testing as described in the next chapter.

The next section looks at the application of fracture mechanics parameters to the study of fatigue in cementitious materials.

3.3.3 Fracture mechanics, cementitious materials and fatigue

The validity of fracture mechanics, and particularly linear elastic fracture mechanics to failure in cementitious materials is still open to debate. However, the use of LEFM parameters such as K for comparative fatigue testing of samples of similar shape and size is accepted[3.110, 3.153 - 3.155] as being reasonable. If it is accepted that the driving mechanism of failure is fracture based rather than purely stress based, [3.121, 3.144] even if the modelling of it has not been resolved, then FM parameters can be used to monitor behaviour and used in seeking to understand mechanisms.[3.56, 3.153, 3.156]

The advantage of using these parameters is that it is possible to separate the initiation and growth phases of crack propagation,[3.55, 3.157] unlike the S-N curves. Additionally it is possible to get closer to an understanding of crack advance mechanisms, ie plasticity controlled (Paris[3.154]) or some form of stress enhanced attack (V-K[3.153]) as discussed in this section.

The mechanism of fatigue crack growth in metals is described as a plastic process where a zone of local plasticity is induced in front of the crack tip, into which the crack extends by localised shear and subsequent bulging with each cycle.[3.157 - 3.159] This is one of the models that leads to the well known striations visible in electron micrographs of fatigue crack surfaces of ductile materials such as aluminium alloys.[3.157] A plot of da/dN against ΔK on a log-log scale is given in Figure 3.16 which is typical for metals. In terms of lifetime, the predominant zone is that marked B in which there is a constant rate of crack growth when expressed as a function of stress intensity amplitude ΔK, on a log-log basis. This is described by the equation, known as the Paris relationship

$$da/dN = C\Delta K^m \quad \ldots\ldots\ldots\ldots\ldots\ldots\ldots\ldots\ldots\ldots\ldots\ldots\ldots\ldots\ldots\ldots \quad (3.16)$$

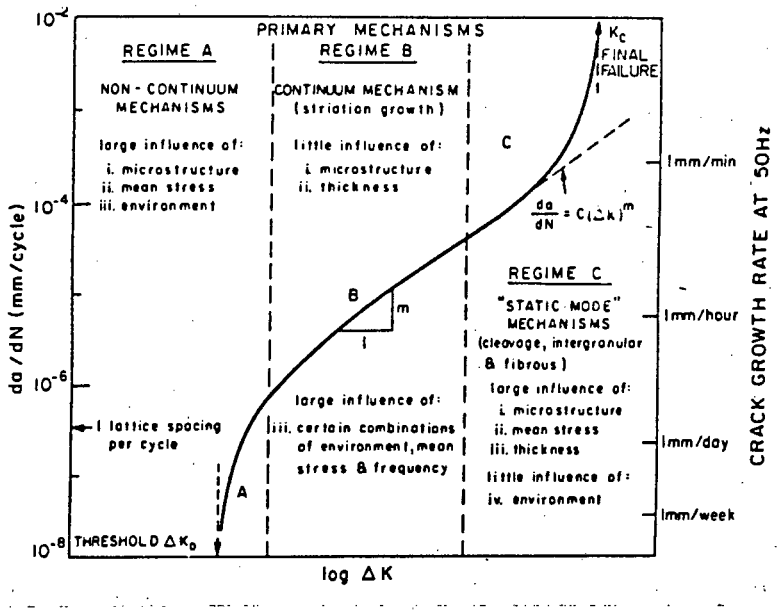

Figure 3.16: da/dN - ΔK curve for metals [3.160]

For such growth behaviour, it is the magnitude of the amplitude of the cyclic stress rather than the maximum stress which governs the rate of crack growth. This behaviour is typical of metals and alloys, with **m** usually in the range 2 to 4. Note that the rate of crack growth is expressed per unit cycle rather than per unit time, ie the frequency of cycling does not influence the crack growth rate (at least for the middle linear portion).

On the other hand the governing relationship for cyclic fatigue of brittle materials such as cementitious or ceramic based materials is rather different.[3.161] One representation is the V-K curve (Figure 3.17).[3.10, 3.153, 3.162, 3.163] The difference is in the crack advance mechanism where there is no substantial plastic zone (although there may be a process zone of microcracking), and the growth mechanism is rate dependent. Thus the parameters are da/dt rather than da/dN and K rather than ΔK. The maximum load K_{max} is the critical parameter, rather than the cyclic load amplitude ΔK. However this is not strictly true as there is an effect of the amplitude reflected in variations caused by changing the stress ratio R. Alternatively Baluch[3.25] has shown, in tests on

concretes, all at the same frequency, that the Paris approach was valid, but expressed ΔK as a relationship with the stress ratio R. Kim[3.163] has reported using a similar system with granite. It would seem that the truth for cementitious materials is some combination of the two relationships.

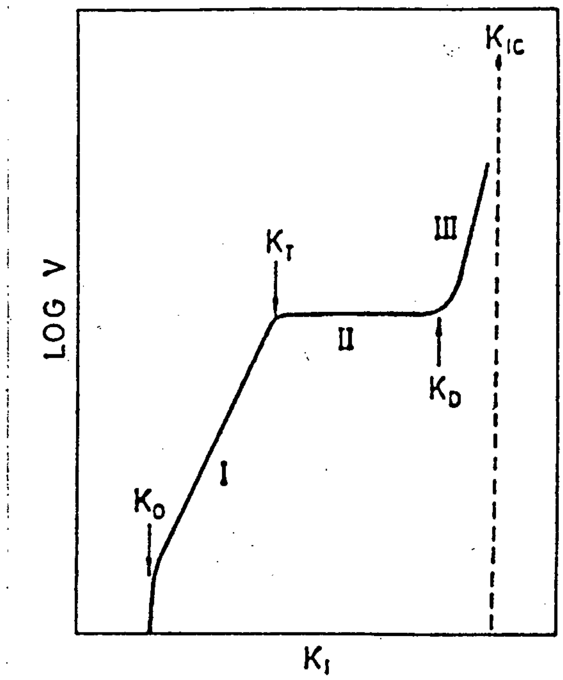

Figure 3.17: V-K Curve for concretes. [3.10]

The shape of the plot is somewhat different from that of the Paris approach, but the predominant characteristic is still that of constant rate with increasing K (marked I in Figure 3.17). This is expressed by the equation:

$$V = AK^n \quad (3.17)$$

where A and n may be considered as materials parameters and a measure of the static fatigue resistance properties of a material. The mechanism is thought to be reaction rate and transport dependent, where failure is by means of stressed fibres at the crack tip undergoing environmental attack and breaking, thus accounting for a strong time dependence. The plateau region marked II in

Figure 3.17 corresponds to a limiting velocity, constrained by the availability of aggressive species at the crack tip to cause corrosive attack, and thus is transport rate limited rather than stress limited.

Measurement of V-K behaviour is most easily carried out using specimens which have a geometry such that imposed loading results in a constant stress intensity (K), even as the crack length extends. Details of these types of configurations are given in the next chapter. If it is accepted that K is valid for a given specimen size and configuration, comparisons in fatigue effects due to changes in rate, environment or material are then possible. This can still be evaluated using specimens which do not exhibit constant K but measurement is more difficult.[3.153 - 3.155] The technique of comparing V-K behaviour as employed in this study, is described in the following chapter.

CHAPTER FOUR - THE DOUBLE TORSION TEST

4.1 Introduction

Determination of the V-K plot for brittle materials is most easily carried out using specimens which have a geometry such that imposed loading results in a constant stress intensity (K), even as the crack length changes.[4.1] A common test used for measuring fracture toughness of many materials is the single notch beam loaded in three point bending.[4.1, 4.2] However the stress intensity is not constant with crack length, making the determination of a V-K curve very difficult. A configuration which does exhibit constant K conditions, namely the double torsion test, is discussed in this chapter.

The available configurations include the tapered double cantilever beam (TDCB), constant moment (CM) and double torsion (DT) tests.[4.1, 4.3, 4.4] Their geometry is such that the imposed stress intensity at the crack tip is independent of the crack length, at least for a significant portion of the specimen length, [4.3, 4.5, 4.6] unlike most other configurations in which stress intensity typically increases with crack length. Thus it is possible to apply a known, constant, stress intensity (or stress intensity range) to a given specimen under controlled environmental conditions, and observe the crack growth rate. This makes it relatively easy to plot the V-K curve for the material in question under those conditions.

The biggest disadvantage of the TDCB is the shape of the specimen which requires considerable precise machining. This is a particular disadvantage in testing cementitious materials. The CM test has been described as more difficult than the DT to carry out.[4.1] The DT specimen is a simple configuration to prepare, although it is very sensitive to the accuracy of setting up in the testing machine as discussed later in this chapter.

The double torsion test was first reported by Outwater et al[4.6a] and used experimentally by Kies and Clarke.[4.6b] Since then it has been used

extensively for a number of brittle materials including polymers[4.7], ceramics[4.1,4.8], rock[4.9, 4.10], cementitious materials[4.4, 4.5, 4.11 - 4.15], tungsten carbide[4.16] and glass[4.17]. It has also been usefully employed for testing materials in aggressive environments.[4.18, 4.19]

The remainder of this chapter is used to describe the theory and analysis of the DT test including a literature review, the results of a modelling exercise carried out at University of Cape Town, as well as the results of testing carried out as part of this study. This testing was conducted in order to satisfy the writer that the technique did indeed yield constant K conditions for the specimens and the equipment used. Limits of acceptability of skewness, and the range of crack length, were also determined experimentally and are described here.

4.2 Description

The specimen used in the double torsion test consists of a flat plate, with approximate proportions of 1:10:30 for the depth, width and length respectively, as shown in Figure 4.1. A notch is cut from one end through the full depth for about one quarter of the length along the centre line.

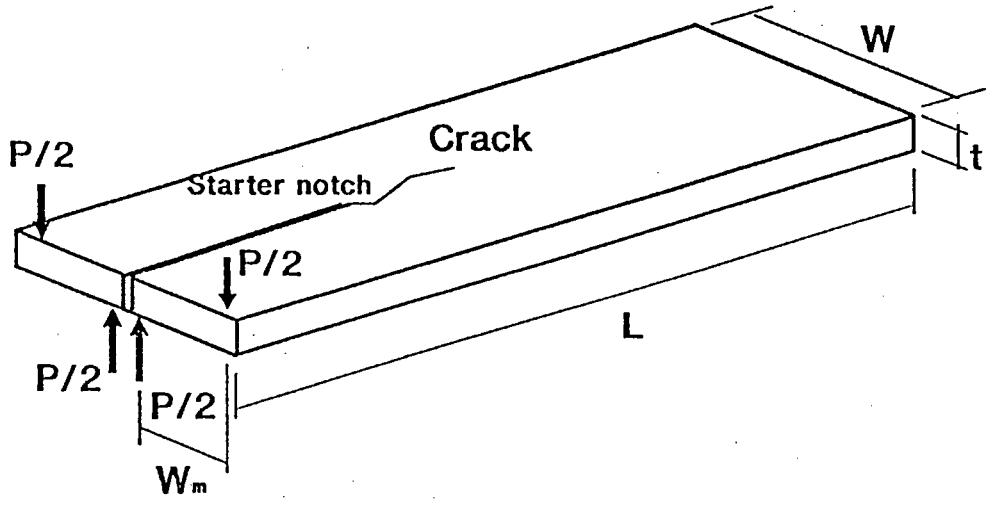

Figure 4.1: The double torsion test specimen

Grooves, approximately one tenth of the depth are sometimes formed by investigators into the top and/or bottom faces on the same line as the notch, for the full length of the specimen. Various groove profiles have been used, such as semi-circular, rectangular or triangular.[4.20, 4.21] The purpose of the groove is to try and force the crack created during loading to grow down the centre line. The validity and effect of grooves is discussed in the next section.

At the edge at which the notch is started, four point loading is applied as shown in Figure 4.1 such that each half-beam is effectively loaded in torsion in opposite directions, hence the name "double torsion". A crack tends to grow down the centre line of the specimen if the loads are applied perfectly symmetrically and square. The crack front profile in the longitudinal section of the crack is assumed to be square to the face, but is in fact a curve as shown in Figure 4.2. The effect of this on the theoretical validity of the test is discussed in the next section.

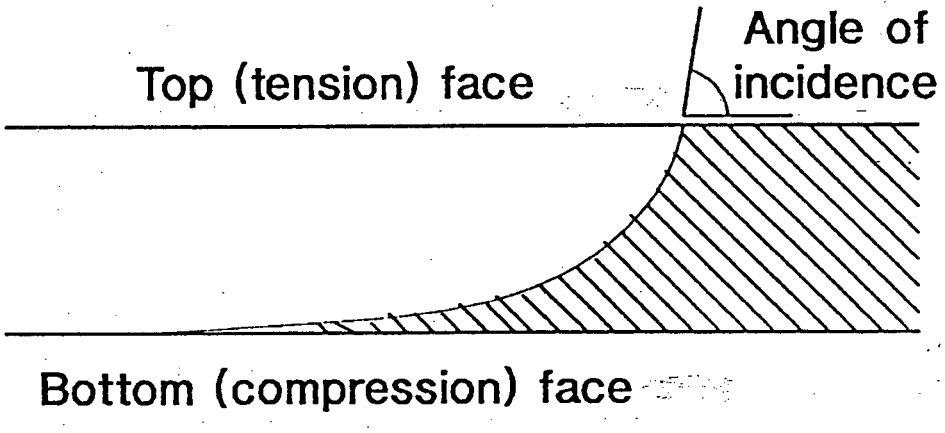

Figure 4.2: Profile of the crack front for a DT specimen

The stress intensity at the crack tip, for a constantly applied load, is constant as the crack grows for approximately the middle third to middle half of the length of the specimen.[4.3, 4.5, 4.16]

Plots of load or stress intensity vs crack length should therefore nominally be constant within these limits. This is useful in fatigue studies as the rate of crack growth for a given load cycle, material and environment should also be constant. It is also useful because it is possible to change one of these parameters, for instance cyclic load amplitude or frequency, and to observe the change in crack velocity as a result, on a single specimen. This helps to reduce the errors induced by testing multiple specimens which is useful because the scatter of results from the test tends to be large.[4.22] A typical a-N curve where the load has been increased several times is shown in Figure 4.3.

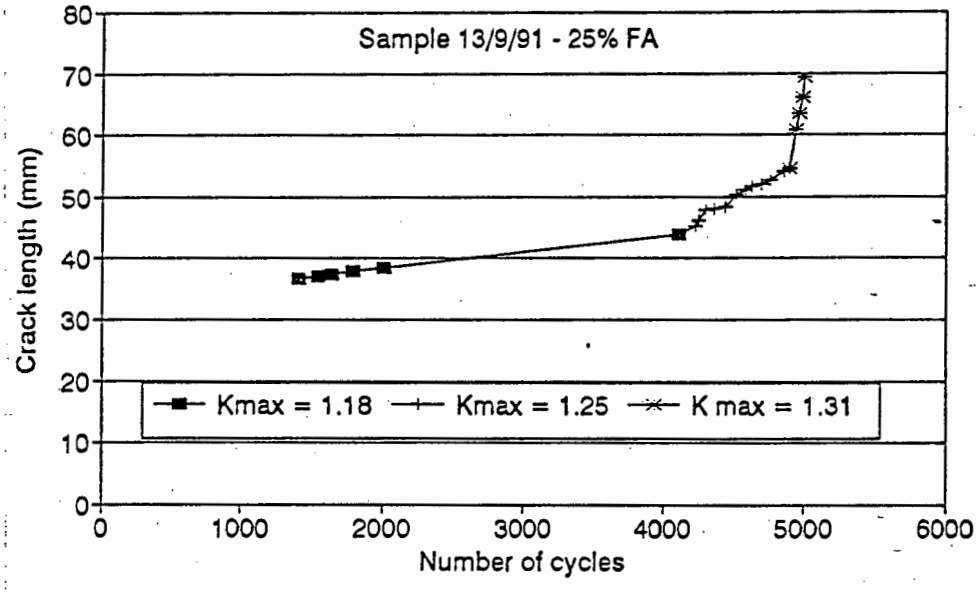

Figure 4.3: Effect on the a-N curve for a mortar of increasing maximum load (or K_{max})

The next section describes the limitations and some of the theory behind the test method and discusses the factors that affect its validity.

4.3 Discussion

The derivation of the equations for calculating stress intensity has been discussed extensively elsewhere [4.5, 4.6, 4.16, 4.21] and only major points will be covered here. The proof is given in reference 4.3 by Tait.[4.3, 4.5]

The relationship used in this thesis was based on plane stress (see Figure 4.1.):

$$K = PW_m \left(\frac{3(1+\nu)}{t^3 t_n W \Psi} \right)^{\frac{1}{2}} \quad \ldots\ldots\ldots\ldots\ldots\ldots\ldots\ldots\ldots\ldots\ldots\ldots \quad (4.1)$$

where
- P = the applied load
- W_m = distance between supports (moment arm)
- ν = Poissons ratio
- t = specimen thickness
- t_n = crack thickness (specimen thickness in the groove)
- W = specimen width
- Ψ = as given below

$$\Psi = \left(1 - \frac{5}{4}\frac{t}{W} \right) \quad \ldots\ldots\ldots\ldots\ldots\ldots\ldots\ldots\ldots\ldots\ldots\ldots \quad (4.2)$$

Points worth noting are the effects of specimen geometry and size, grooving, the crack face profile, mode of failure, the range of validity and sensitivity to setting up in the test machine. These are discussed individually below.

Specimen proportions and dimensions

A wide range of specimen proportions and sizes have been used in experimental work. Reported length to width ratios range from 2 to 12,7 with a value of 3 being the most popular and which has been validated against double cantilevered beam testing for several materials.[4.3] The width to thickness ratios reported have been in the range 3,33 to 50 with 8 to 12 being the most recommended.[4.3]

One effect of having a thick plate relative to the width is the overlap and potential interference of the adjacent bottom corners at the crack interface below the neutral axis of the two torsion beams. A correction factor for this effect has been proposed by Fuller.[4.6] Calculation of this correction factor for the specimen size used in this study showed an error of approximately 0,1% and it has therefore not been included.

The selection of the minimum specimen size is dependent on the grain size of the material being tested as the sample thickness should be at least 15 to 20 grain diameters. Fine grain ceramics and cement pastes have been tested in specimens as small as 20 mm long and 1 mm thick.[4.3, 4.23]

For metals and alloys where some local ductility occurs at the crack tip, there is a limiting requirement for the ratio of plastic zone size to specimen dimensions for valid plane strain linear elastic conditions. For the double torsion configuration this requirement for thickness reduces to:[4.16]

$$t > \left(\frac{K_{Ic}}{\sigma_y} \right)^2 \qquad (4.3)$$

The implication for concrete materials is that the minimum thickness of specimen would be approximately 100 - 200 mm. Hillerborg and Wittmann have however suggested that to measure K_{Ic} for concrete or paste, double torsion specimens 3 m or 200 mm long respectively would be necessary.[4.21, 4.24] This derives from a standard DT specimen of proportions 3:1:0,1 and typical strength and toughness values of paste and concrete.

The effect of side grooves

The use of grooves in the faces to channel the direction of the crack has previously been considered.[4.3, 4.6, 4.20] The conclusion drawn by Fuller [4.25] and Tait [4.3] is that careful control of specimen placing will improve the probability of a straight crack whilst avoiding the unknown effects of the stress concentrating effect of the groove on the stress intensities.[4.3] If a crack grows along the corner of an approximately rectangular groove, it is unclear what the stress intensity really is.[4.3] Both increased[4.25] and decreased[4.20] scatter due to the use of grooves have been reported.

Crack profile

The above DT analyses make the assumption that the crack profile in longitudinal cross section is square to the tensile face. However, in practice the

actual shape of the crack front is typically curved as shown in Figure 4.2. It is generally assumed that the profile remains constant as it propagates and hence the calculation of stress intensity may be assumed to be correct. For constant K the profile has been shown to be constant whilst the variation with changing K is marginal.[4.3, 4.16, 4.17]

Corrections to calculate the actual velocity from the observed velocity on the tension face due to the crack profile have been proposed depending on the angle between the crack front and the tensile surface. This is because the actual velocity is orthogonal to the crack front, which is not necessarily perpendicular to the tension face.[4.3, 4.16] In effect the stress intensity varies along the profile front and corrections to the measured tension face crack velocity can be made as a function of the sine of the angle of incidence θ. (Figure 4.2).

For this present study it was difficult to measure the crack front shape consistently, but was typically greater than 80°, for which the effect of the correction would be to reduce the observed velocity by approximately 1,5%. Because all of the work in this study has been carried out on specimens of the same dimensions and with similar materials, and was intended to be primarily based on **comparison** between samples, this error was felt to be acceptable and no correction has been applied.

Mode of failure

It is normally assumed [4.3, 4.6] that the mode of failure in the double torsion specimen is Type I (tensile crack opening) although this is open to question. There is an argument that there is a certain amount of Type III [4.16] (antiplane shear) but for most materials where K_{IIIc} is larger than K_{Ic} this may be ignored.[4.3, 4.6] Evans has shown by comparison with other techniques that the correlation based on this assumption is acceptable.[4.6]

Range of validity

The range of validity for constant K conditions has been variously reported as from 0,05L to 0,3L minimum and 0,47L to 0,85L maximum.[4.3, 4.6, 4.16] The range as calculated by Epstein[4.26] was approximately 0,33L to 0,72L and that determined experimentally as described in Section 4.4 was approximately 0,44L to 0,8L. The difference between Epstein's results and the observed may be explained by the crack profile. Epstein assumed a perpendicular profile while the real profile was a curve trailing behind the observed crack tip. This means that the "centre of gravity" of the crack must be somewhat behind the tip.

Specimen misalignment

Tait and Fry have reported[4.3] that it is possible to steer a crack that was going off course by rotating the specimen.[4.5, 4.16] This was checked by Epstein as part of an undergraduate project[4.26] in which the test was numerically modelled. The output showed that as a result of lateral misalignment: (a) the stress along the length of the sample was not changed (the stress intensity was not modelled) and (b) the principal stress field was skewed in the direction that cracks had been observed to move in experiments (Figure 4.4). Thus the modelling confirmed that it should be possible to steer a crack if action is taken early enough.

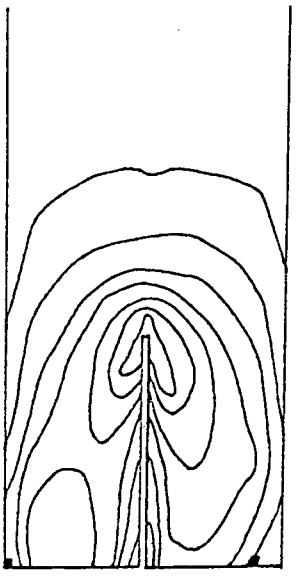

Sample moved to the right wrt
the loading points.
Stress field also skewed to the right.

Figure 4.4: Modelled effect of lateral misalignment on the principal stress field[4.26]

The other aspect checked by modelling[4.26] was the effect of misalignment of the loading points such that the top outer points were closer to the remote end of the specimen than the inner. The stresses were lower than the perfectly aligned model, again as observed experimentally in this study.

4.4 Experimental validation

In order to address the question of the validity of the assumption of constant stress intensity with increasing crack length for the materials and set-up used in this study, a number of experimental trials were carried out. A secondary intention was to evaluate the limits of validity of obtaining constant K in relation to the length and skewness of the crack.

The trials consisted of using specimens and the equipment as described in Chapter 5 in so called "ramp" tests. In these tests the samples were loaded at constantly increasing displacement (0,007 mm/s) with the machine in displacement control. The measured load was recorded (in volts) on a chart plotter against time or displacement. The signal was manually "spiked" when the crack was observed to cross marks on the specimen at regular intervals.

This provided a means of correlating the slope of the plot with the crack length as well as allowing the calculation of crack velocity. Ideally, according to theory above, the load should increase linearly to a maximum, remain constant for a period before dropping off again as the crack moved into, through and out of the zone of validity (Figure 4.5). Similarly the effects of deliberate misalignments in setting up the specimen were investigated.

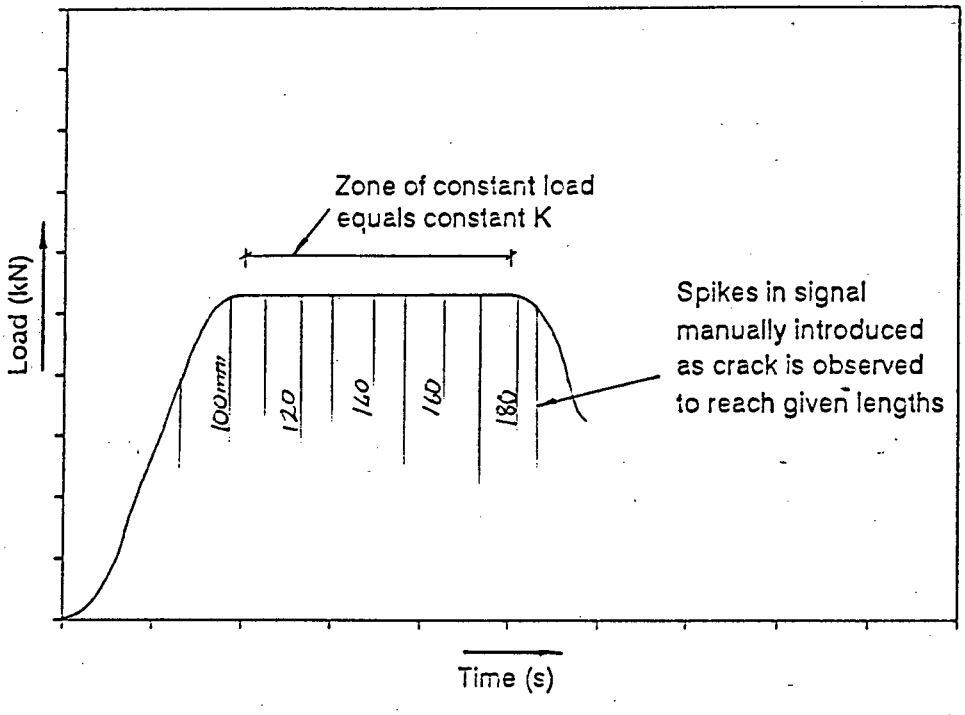

Figure 4.5: Ideal plot of load versus time for the double torsion ramp test

Typical plots of the various cases are shown in the following five figures. It can be seen that with good alignment, constant K conditions (or as shown in the plots, constant load independent of crack length) was observed in the range of crack length from 100 mm to 180 mm (0,44L to 0,8L) from the front face of the specimen (Figure 4.6). It should be noted that there is a relatively large amount of "noise", ie load variation, in the plateau region (Figure 4.7) which is not surprising considering the non-homogenous nature of mortar.

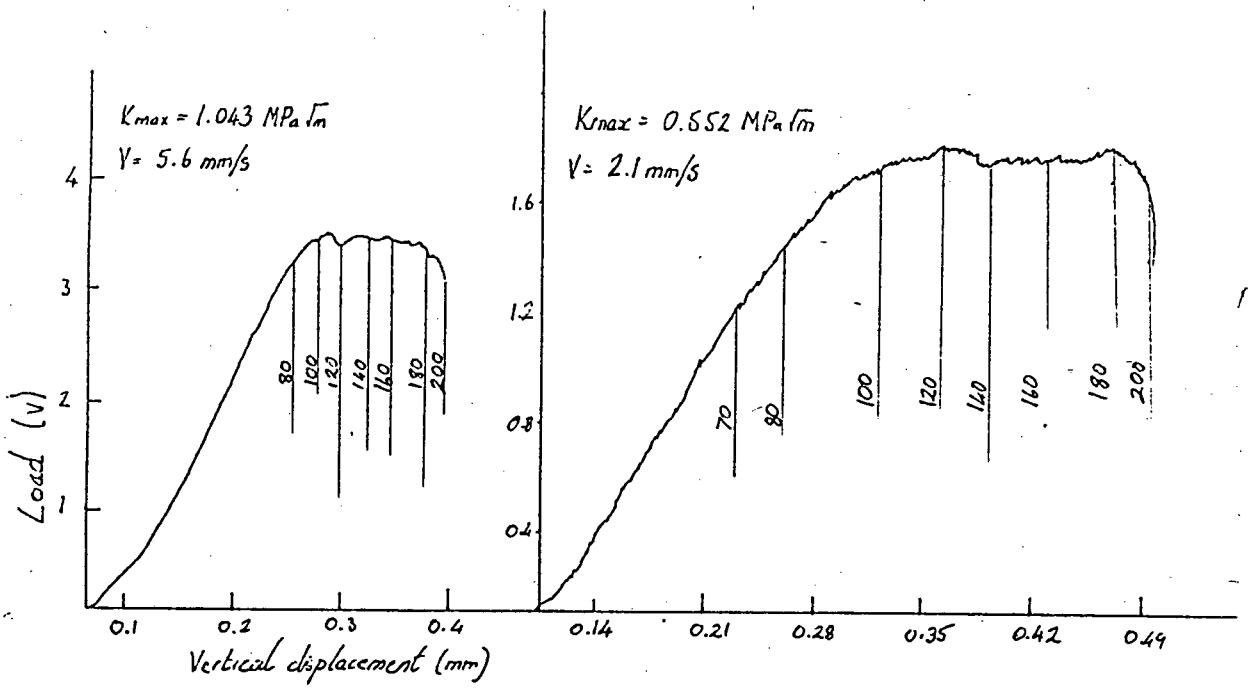

Figure 4.6: Typical load deflection plots for specimens that have been well set up

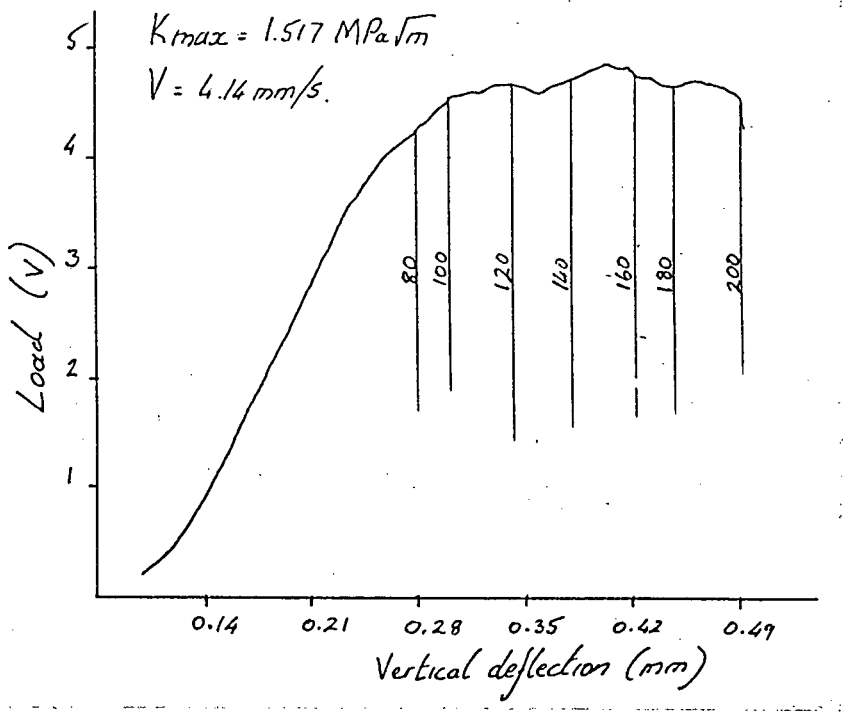

Figure 4.7: A typical load deflection plot showing the amount of noise that can occur

If the loading points were misaligned longitudinally by as little as 0,1 mm such that the upper/outer points were closer to the remote end of the specimen than the lower/inner, then the load increased as the crack grew along the specimen (Figure 4.8). Conversely if the upper loading points were closer to the notched end than the lower, thus causing the specimen to lift off the back supports, the load (or K) reached a maximum at a short crack length (80 mm) before decreasing steadily (Figure 4.9).

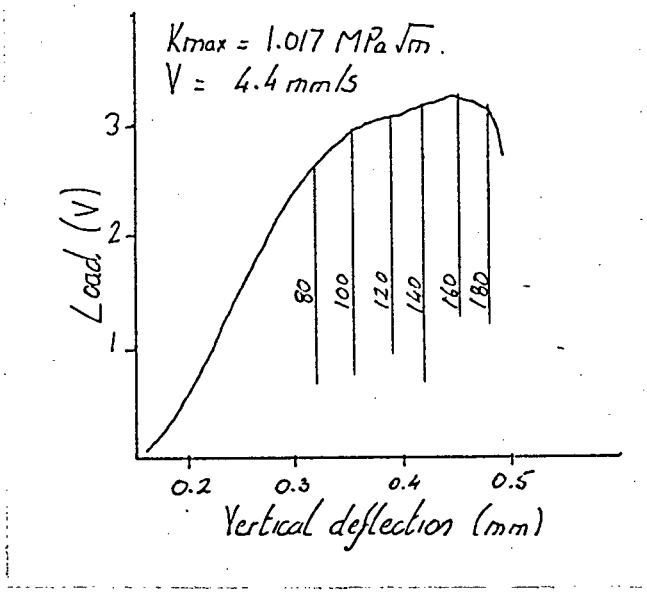

Figure 4.8: Typical load deflection plot where the upper load points were behind the lower

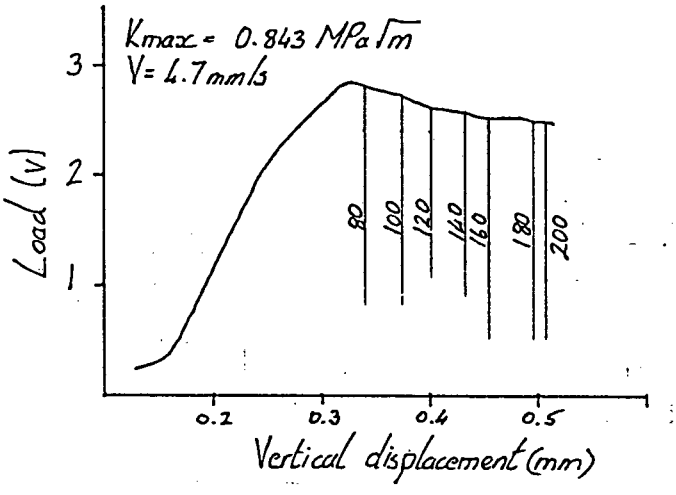

Figure 4.9: Typical load deflection plot where the upper load points were in front of the lower

If a crack was allowed to grow skew, then the load was seen to drop off when the lateral deviation was larger than approximately 10 mm from the centre line, as shown in Figure 4.10. This was also observed in fatigue loading where the

crack was seen to accelerate after moving more than 10 to 12 mm off the centre line.

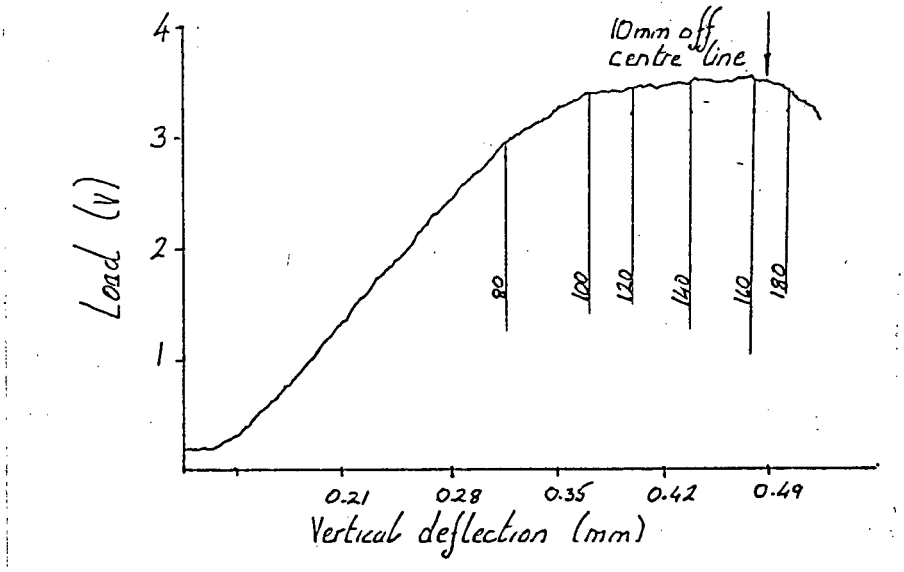

Figure 4.10: Typical load deflection plot showing the drop off in load as the crack grows more than 10 mm off the centre line

Some fatigue tests were also carried out in which attempts were made to steer the crack that was growing skew. In this case it was found that, to a limited extent, if the notched end of the sample was moved in the same direction that the crack was going skew, it could be straightened out.

4.5 Summary

This chapter has described the basis of the decision to use the double torsion test configuration in order to carry out fatigue studies of cement mortars.

Alternative "constant K" configurations have been discussed and evaluated. A brief literature review of the advantages, disadvantages and limitations of the double torsion test has been presented along with some results from a modelling exercise carried out with some input from the writer.

Finally, typical plots of load versus time, with the crack length marked, have been presented, based on experimental work carried out by the writer. These plots show that there is a zone in which constant stress intensity with increasing crack length is achieved for the materials, samples and equipment used for the remainder of the study. The effects of misalignment of the specimen on the machine have been demonstrated and approximate bounds of validity of the position of the crack tip on the specimen, for constant K, have been confirmed.

All of this has contributed to the writer being satisfied that the double torsion test was suitable for the work to be carried out in the remainder of the study as described in the following chapters.

CHAPTER FIVE - EXPERIMENTAL DETAILS

5.1 Introduction

The details of and reasons for using the double torsion system for the work carried out in this study have been described in the previous chapter. In this chapter details are given of the specific experimental procedures including the selection of materials, specimen preparation and a description of the equipment. A description of the execution and processing of the tests is given, along with the range of variables in the test programme.

5.2 Materials

The use of mortars was selected in order to minimise the number of materials (ie variables), and yet to have a material from which it was relatively easy to make consistent samples of a suitable size.

Cement paste was not chosen because of the potentially high risk of shrinkage cracking and the difficulty in obtaining repeatable test results. On the other hand, concrete was not suitable for use in small double torsion samples, because valid thickness criteria[5.1, 5.2] (as discussed in Section 4.3) could not be met in the testing machine.

The specimen size selection (225 x 75 x 8 mm) was based on the need to be able to make, handle and store a reasonably large number of them, as well as to make use of the equipment available in the laboratory. This also meant that the maximum size of aggregate that could be used was governed by the size of specimens (see Section 5.2.3).

It was felt that it was desirable to seek to understand the mechanisms of fatigue crack growth in mortars initially, with larger scale tests using concrete to follow, if possible, in future studies.

The following sections describe the materials that were used, along with the reasons for their selection.

5.2.1 Cement

The decision was initially made to work with samples of a fixed age of seven days for the bulk of the testing, in order to avoid the loss of time waiting for 28-day trial mixes. On this basis, a rapid hardening portland cement was selected.

The cement was obtained from a single batch from a local factory in order to minimise the variability inherent in cements from several batches. An analysis of it's composition was conducted at the beginning and the end of the work and the results are given in Table 5.1. It was a Type II cement containing a permissable non-deleterious inert material up to 5% by mass.

Table 5.1: Composition of cement and fly ash (as a percentage by mass) with physical properties

	RHPC at begining of programme	RHPC at end of programme	Fly ash
CaO	62,8	63,4	8,00
SiO_2	22,2	22,3	47,8
Al_2O_3	4,2	5,1	29,8
Fe_2O_3	2,7	3,0	3,96
MgO	2,2	2,9	2,2
SO_3	2,7	2,5	0,65
TiO_2	0,2		1,86
Mn_2O_3	0,3		
P_2O_5	0,2		1,18
Na_2O	0,06	0,05	0,6
K_2O	0,44	0,49	0,75
L.O.I.	0,8	0,7	0,92
Free lime	0,8		
Insoluble residue	0,3		
Specific surface	471	429	
Setting time initial	3:20	3:05	
Setting time final	4:00	3:45	
Expansion	0	0	
% passing 45µm sieve			92,2

The cement was supplied in 50 kg sacks and stored in airtight 200 ℓ drums in order to prevent deterioration with time. This appears to have been effective as the cube results did not drop over the duration of the project. It was found that cubes made using cement taken from a drum that had been open for some time did exhibit reduced strengths. When this occurred, the cement was discarded and a fresh drum opened.

5.2.2 Fly ash

The fly ash was obtained from a single batch from Matla Power Station, the only commercial source of fly ash at the time. As can be seen from the chemical composition (Table 5.1) it was neither a Class C nor a Class F material in that it contained a moderate amount of calcium. This fly ash was also stored dry in 200 ℓ airtight drums.

5.2.3 Sand

A plaster sand (nominally 100% passing the 1,18 mm sieve) was used in order to limit the maximum particle size to a small proportion of the specimen thickness. This was done to reduce the potential variability (eg interfacial zone effects) due to the presence of particles that were large with respect to the specimen minimum dimension. The sand was a red siliceous pit sand from Randfontein with a dust content and grading as given in the bold line in Figure 5.1.

After the project had been extended and moved to a laboratory in a different city, there was an insufficient supply of the original material. The dune sands available in Cape Town were predominantly single sized with a low dust content. In order to make up a similar material to the original, a dune sand was blended with a selected pit sand from a glass manufacturer and some granitic rock flour from an aggregate crushing plant. The grading achieved was similar (Figure 5.1) and there was no observable effect on the fatigue results (see Section 7.4). The mix designs were not modified but it was noticed that the

mortars made with the blended sand were less workable, probably due to greater fineness of the sub 75-μm fraction of the rock flour.

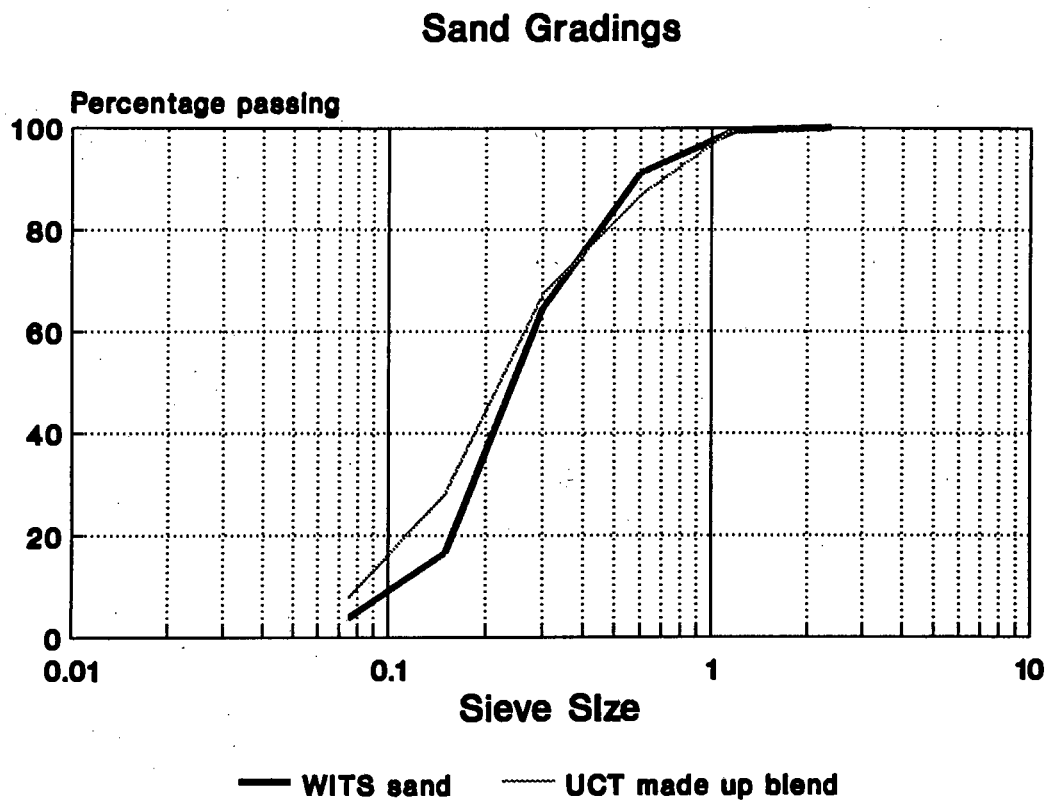

Figure 5.1: Grading curves of the sands used

5.2.4 Mix design

The aim of the mix design was to obtain similar compressive strengths at seven days using three different proportions of fly ash, namely 0, 15 and 25%. The other targets were to have similar workability as determined by using a flow table[5.3], and similar sand contents.

The target strength was set at approximately 40 MPa at seven days. This meant that the fly ash mixes would be expected to have higher compressive strengths than the OPC mix at greater ages, and this must be born in mind in the evaluation of the results at the other ages. This approach was based on the desire to follow practical engineering practice, that is to specify a strength at a given age with a given workability. The selected age was seven days because of the original short duration of the project.

The approach was to select a water:cementitious ratio (W/Cm) for each mix based on data collected by the local supplier of fly ash. The amount of sand in the mix giving the right workability was found by means of trial mixes conducted by the fly ash supplier's laboratory.

Two of the initial mixes were found to be too weak and their water:cement ratios were decreased. The mix proportions were not changed thereafter and are given in Table 5.2.

Table 5.2: Mix proportions per m^3 of mortar

	OPC (0% FA)	15% FA	25% FA
Cement (kg)	681	586	561
Fly ash (kg)	0	103	187
Sand (kg)	1145	1143	1078
Water (ℓ)	341	328	325
W/Cm	0,50	0,56	0,43
Aggregate/Cm	1,68	1,66	1,44

5.3 Specimen preparation

5.3.1 Mixing and moulding

Purpose made moulds were machined to the required sizes from sheets of clear perspex. The parts were numbered so that assembly was always in the same pattern. The original sheets were selected to be as flat as possible in order that the moulded specimens should also be dimensionally true. Each mould held a batch of fifteen specimens which were cast with the longest dimension vertical. The moulds were sized such that the top few millimetres of each specimen were cut off to remove mortar that was affected by bleeding.

The moulds were oiled using a release agent before assembly, and then clamped with steel plates to give rigidity during filling and vibrating.

The method of mixing the mortar was carried out as described below, and normally took place at mid morning. Batches were made in four litre lots, which was sufficient to fill the fifteen DT moulds and to make four cubes of fifty millimetres dimension, with a minimum of waste.

The dry ingredients were placed in a pan mixer and mixed for a few seconds before the water was added and mixed for one minute. When the work was being conducted at Wits University a flow test was then carried out. This was not possible at the University of Cape Town as there was no flow table available, but by this time the writer had gained enough experience to be able to guage the consistance by eye. The material was then remixed for thirty seconds and transferred to the moulds. The mould was clamped onto a running Vebe vibrator and was filled by means of a purpose made square funnel that just fitted into the mould. The time taken to fill the moulds varied because the fly ash mixes were stickier than the OPC mix, but was about five minutes. The moulds were then covered with plastic sheeting and left overnight.

Leakage sometimes occurred from the bottom of the moulds, but this was found to be preferable to having large air bubbles. The specimens were

prepared so that the areas of leakage were at the remote end from the load points. The leakage occured on the side corners of the samples, and thus was some distance away from the crack and so did not affect the final measured crack growth rates. Some tests were carried out on specimens that had been notched from the other (bottom) end to confirm whether the direction of casting had any measurable effect on crack growth rates. For the same reason, a set was prepared and tested in which the moulds were temporarily adapted so that the samples were cast on their sides.

5.3.2 Stripping and curing

The moulds were left under the plastic sheeting overnight, then stripped approximately 24 hours after filling. The specimens were marked with the date of casting, the percentage fly ash and a specimen number. They were then placed into a curing tank filled with lime saturated water controlled at 25°C. They were left in the tank (except for trimming) until removed for drying (where relevant) or testing.

The surface finish of the specimens was good as can be seen from Figure 5.2. The visible marks were due to the mould oil.

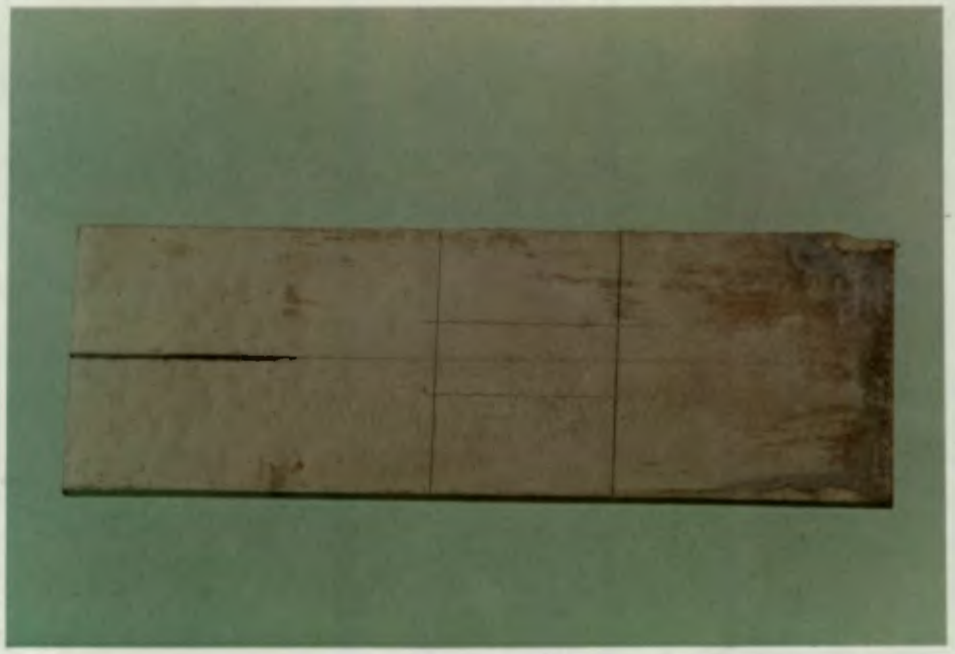

Figure 5.2: Photograph of a double torsion specimen

5.3.3 Trimming and notching

After four to seven days, the top 15 mm was cut off the specimens using a diamond tipped blade on a standard "Clipper" cutting table. They were then notched at the top end for approximately one third of the length on the centre line (Figure 5.2). It was critical that the notch was in the centre of the specimen and that it was straight and perpendicular.

After some difficulty with the notching process, a rig was made on a converted lathe that held the specimens straight and flat with respect to a dedicated 1,2 mm wide diamond blade. Centrality was ensured by turning the specimens over and cutting a second time. The notch length was generally 60 mm on the faces of the specimens.

The samples were then marked with a centre line and the bounds of validity of the position of the crack tip for fatigue specimens; or with lines at 20 mm intervals parallel to the short dimension for monotonic tests (Figure 5.3).

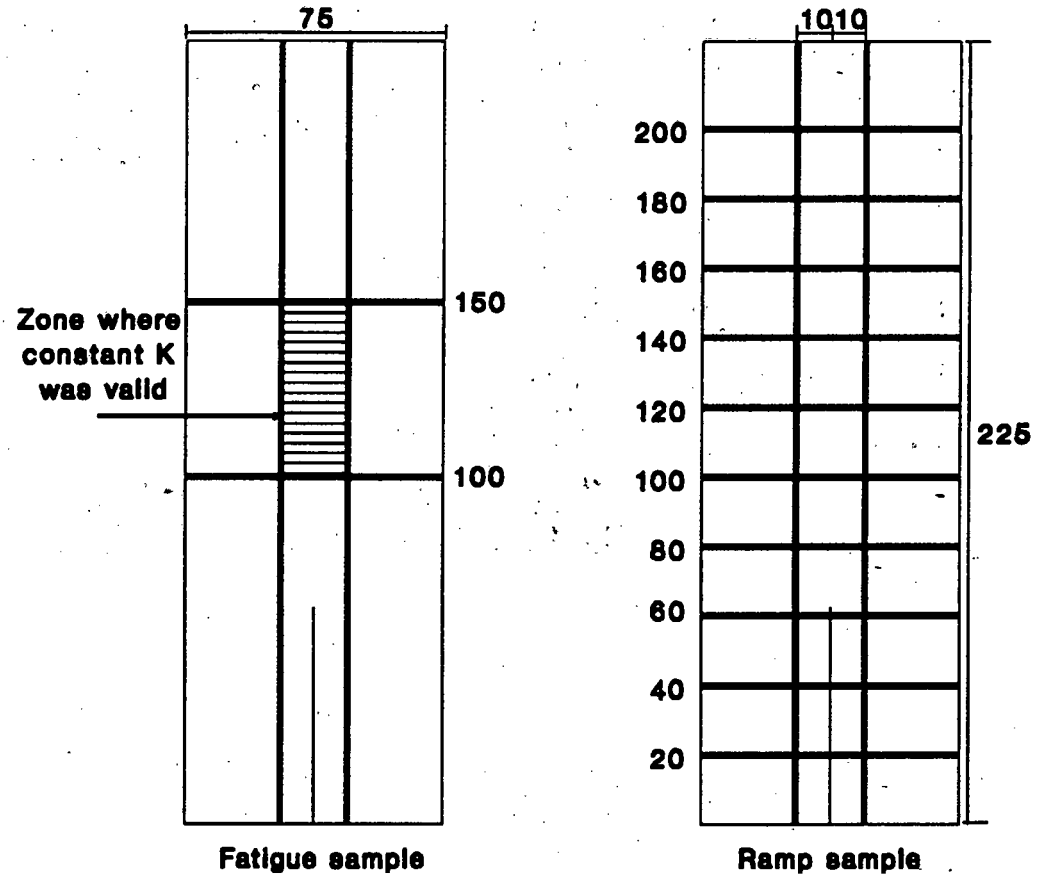

Figure 5.3: Markings placed on fatigue and ramp specimens

Some lime efflorescence was not uncommon which made observation of the crack tip difficult. This was normally polished off by rubbing two specimens together before measurement and testing.

5.3.4 Drying

Most of the tests were conducted on specimens that were wet. However, one of the variables in the test matrix was the drying of the specimens. Three methods were used:

- Specimens were air dried for seven days, and then placed in the environmental chamber for testing.

- Specimens were sealed for seven days in a plastic packet with silica gel and then placed in the environmental chamber.

- Specimens were air dried for 24 hours followed by 24 hours in an oven set at 100°C, then placed in the environmental chamber.

5.4 Equipment

5.4.1 ESH universal testing machine

All the fatigue, monotonic and ramp tests were conducted using an ESH servo-hydraulic machine (Figure 5.4). The machine comprised an hydraulic ram, mounted on the top platen, which was controlled by a servo-valve with a feed back system. The ram could be controlled with respect to the desired position (stroke control) or load (load control).

The machine had a maximum load capacity of 50 kN with a 10 kN load cell with ranges down to 1 kN attached for the present study. The machine was set on ranges such that a signal of 1 volt corresponded to 0,1 mm or 10 kN depending on the mode of control. The output of the machine was to 4 significant figures in volts, which corresponded to reliable readings to a lower limit of 1 N or 0,01 mm.

A ramp generator was used for monotonic (ramp) tests such that the rate of change of position of the ram was controlled at 0,007 mm/s. A signal generator with a range from 0,1 Hz to 10 MHz and sine wave output was used for the

fatigue tests in load control. The amplitude and mean level of the load cycles was controlled so that any desired loading cycle could be applied.

A peaks reading digital volt meter was used for precise monitoring of the cycling. This electronic device effectively removed the middle 99% of the wave signal displayed on an oscilloscope, so that the maximum and minimum values of the signal could be amplified on the oscilloscope and accurately monitored.

Any of the control signal parameters could be changed during a test, thus allowing direct observation of their effects on the crack growth rate in the specimen. A cycle counter was used to monitor the number of cycles applied to the specimens.

Figure 5.4: Photograph of the ESH testing machine

A chart recorder linked to the ESH was used to plot the load:deflection or load:time curves of some of the ramp tests. These plots were also marked by spiking the signal to the recorder by hand at selected crack lengths facilitating the direct calculation of crack velocities under ramp loading conditions.

Two different machines were used at the two different laboratories in which the work was carried out. They were of the same make and operation and both their load cells and amplifiers had been calibrated by the South African Bureau of Standards. The results from the two machines were therefore directly comparable. One test rig, as described in the next section, was used throughout the program.

5.4.2 Double torsion test rig

A purpose made, mild steel, test rig for double torsion testing had been made for a previous study on tungsten carbide and was suitable for this program.[5.4] It consisted of a base plate bolted to the bottom platen of the ESH. Two pedestals supported the specimens, with the front pedestal on the centre line of the ram. Load transfer was through the ball bearings mounted on the front pedestal whilst the support of the back pedestal was simply to hold the specimen level, particularly during setting up.

The supports were marked with centre lines to assist with the setting up, and also had side walls with setting screws to move and hold the specimens in place during setting up (Figure 5.5). The support at the rear consisted of a line support on the specimen centre line. The loads were applied by means of a clevis attached to the hydraulic ram through the load cell.

Figure 5.5: Photograph of the double torsion loading rig

This setup was limited in that more screw adjustments were needed to be able to move the rig in a controlled way when it was installed on the machine, and the specimens on the rig.

5.4.3 Crack length measurement

The crack length measurement was achieved using an Olympus microscope with 10X eyepiece and 1-15X zoom objective and 75 mm working distance, an attached cold light source, no polariser, a crosshair; all of which was supported on a sliding mounting arm on a heavy base (Figure 5.6).

Figure 5.6: Photograph of microscope system used for crack observation.

The procedure used was to centre the crosshair on the observed crack tip and to use a vernier calliper to measure distance between the stops on the sliding arm and support arm of the microscope. The readings were thus not absolute but relative, but a measured reading on a known point on a specimen gave the means of calculating the real crack length if necessary. However the difference in readings between two points was sufficient to calculate a change in crack length for growth rate measurements.

The arrangement was accurate to approximately 0,1 mm, which was as close as the actual crack tip could be judged. Further discussion about the observation of the crack tip is given in Section 5.5.3. The system was relatively cheap and satisfactory for this project. Any improvement in precision could only be obtained at much greater cost.

5.4.4 Environment chamber

For the tests conducted in a controlled environment, a perspex chamber with an aluminium base was built that fitted inside the loading frame. The entire test rig went inside the chamber along with a batch of specimens and a digital relative humidity/temperature meter. Access to the specimens and rig was by means of long sleeved rubber gloves, whilst the ram passed through rubber bellows.

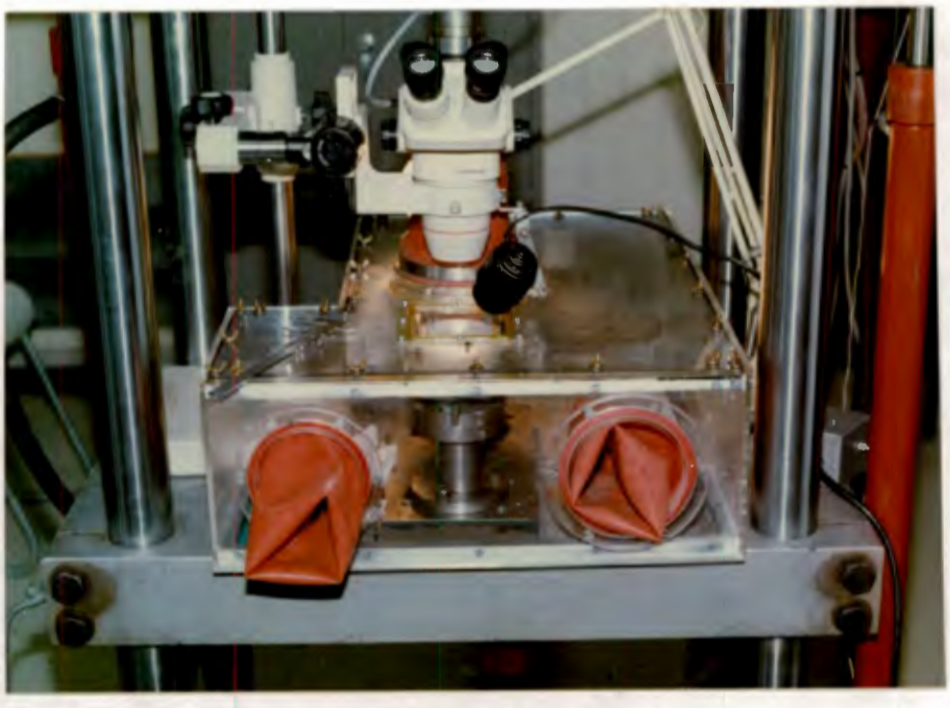

Figure 5.7: Photograph of environmental chamber

The top of the chamber was removable for initial setting up and for putting in specimens and equipment. The top was sealed with vaseline and held down by wing nuts. The system was not completely airtight, but the relative humidity was held within 5 percentage points over a period of one day. A suitable modification would be to provide an extra set of bellows so that glove movement does not cause pressure differentials in the tank.

A glass port was fixed into the top of the chamber over the specimen in order to facilitate observation of the crack tip. This tended to mist up at high humidities.

The humidity in the chamber was controlled by means of exposed saturated solutions of selected salt solutions or with silica gel.

5.4.5 Fluids tank

A perspex container on an aluminium base was built in order to be able to carry out tests within a variety of fluids. This was mounted on the pedestals just below the specimen supports. This tank was just wide enough to go around the rig with a 10 mm freeboard on three sides and an adjustable weir at the specimen's loaded end. The weir could be set such that the tank could be filled with a fluid to the level of the top of specimen. This meant that whilst the specimen was immersed, a localised area of the top surface at the crack tip was dry, facilitating observation of the crack.

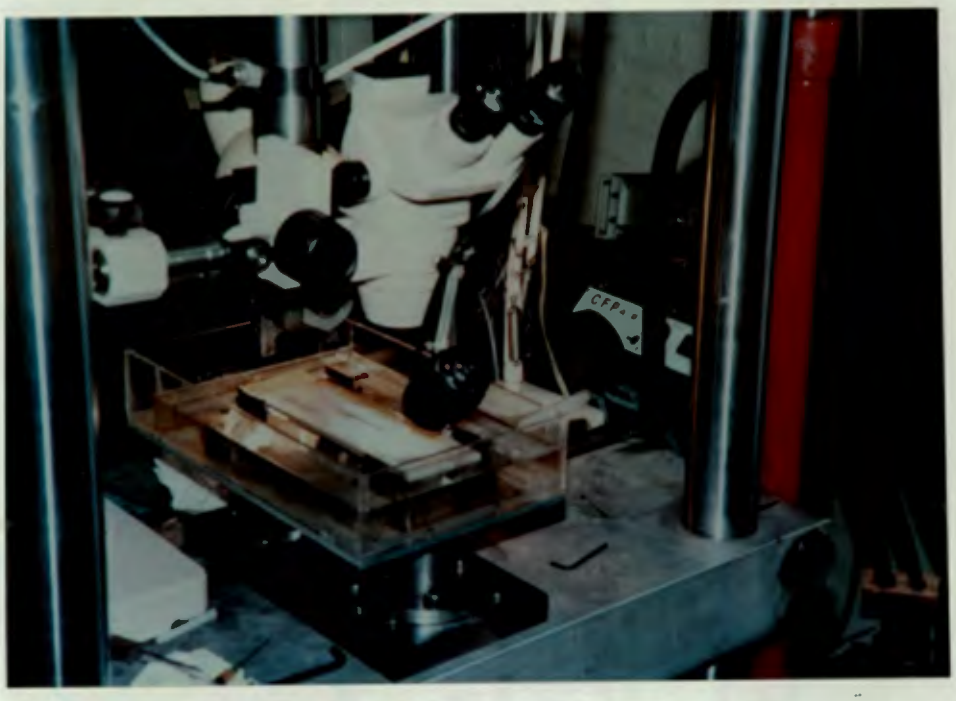

Figure 5.8: Photograph of fluids tank

The overflow was recirculated by a peristaltic pump with the inlet at the end of the tank remote from the weir. This was to ensure uniformity of the temperature, which was monitored using a thermometer placed just below the specimen.

The liquid used was stored in a container next to the machine, and temperature control devices were installed there when necessary. A difficulty was encountered with the use of ethyl alcohol which degraded the perspex; the tank lasted just long enough for the desired tests to be completed!

5.5 Test description

5.5.1 Setting up

The technique of setting up the rig and the specimen was critical because any misalignment resulted in skew cracks, thus invalidating the test. Tolerances of

less than a millimetre were necessary, and the following method was developed over some time having wasted many specimens.

The first step in setting up was to fix the height of the top platen with respect to the lower in order to prevent compression damage of the equipment (and load cell) if there was a loss of control resulting in the ram travelling to the end of its stroke.

If either of the perspex tanks were to be used, they were then placed in position before the test rig was bolted to the table. The lateral position of the rig was set by swinging the clevis which was attached below the load cell onto the ram, to the left and right whilst moving the rig. The rig was secured when the clevis just touched the uprights on the rig symmetrically on each side. The clevis was then rotated until preset marks lined up with the base. This process was repeated iteratively until everything was straight and square. The final adjustment was to check that the centre-line of the rig was below that of the ram lengthwise, again measured using the marks on the clevis and the rig. This could be adjusted a small amount by moving the rig within the play of the bolts, or else different sized spacer washers could be placed inside the clevis.

A check run was then conducted using a waste specimen to see if the crack ran straight under a ramped load. The position of the lower loading balls were moved in the same direction as the crack if the crack skewed to one side.

The specimen was set up by lining up its front (notched end) with the front of the rig whilst a vernier calliper was used to set its lateral position such that the notch was over the machine centre line.

5.5.2 Fatigue tests

From a batch of fifteen specimens, the first three would be ramped to provide a measure of the inherent "toughness" of the batch at the beginning of testing. The next ten specimens would be fatigued and the last two ramped again to

indicate if there was a change in the material over the period taken for testing. This was particularly relevant for the seven day tests as a batch could take a full day to test.

A fatigue specimen would then be loaded by ramping in stroke control mode until the crack was observed to be in the field of view of the microscope. The load taken to achieve this was also recorded and used as the basis for calculating the desired load amplitude as a percentage of the ultimate. The load was then reduced by fifty percent and machine control switched to load control. A cyclic load was then applied at the desired amplitude, frequency and maximum peak load. This was monitored and controlled using the peaks meter, amplitude measuring unit and oscilloscope as well as the digital output of the machine.

At regular intervals a record was made of the number of cycles elapsed, the crack length, the maximum load and amplitude, as well as any comments and observations. The crack length (a) and the number of cycles (N) was plotted on a computer as the test progressed using spreadsheet graphics. The slope of the line joining the data points gave the crack velocity (V), which in turn could be plotted against the maximum stress intensity (K). Periodically the test parameters would be changed, thus allowing direct observation of their effect on the rate of fatigue crack growth in the specimen as indicated by the change of slope of the a-N curve. The range and variety of parameters that were tested are described in Section 5.6 on test parameters.

On the basis of experience and experimentation, it was accepted that a crack within ten millimetres of the longitudinal centre line was considered to be valid and the test was continued whilst it stayed within that limit. This was confirmed as described in Section 4.4. A maximum length of one hundred and fifty millimetres from the front of the specimen was also accepted before the test was stopped and the specimen was ramped to check its ultimate strength.

5.5.3 Observation of the crack tip

The greatest difficulty in any given test, apart from the setting up, was the observation of the crack tip in order to measure the crack length. This was primarily because mortar does not have a crack tip, but rather a **zone** with a number of cracks decreasing in size, spreading out from the so called "crack tip" . Therefore if one noted a point as being the limit of cracking on a specimen, and then increased the magnification or introduced a fluid to the surface, a series of smaller cracks extending further could be observed, seemingly ad infinitum.

However, in the measurement of crack growth rate, the absolute position of the "crack tip" need not be known, but only the position of some point a constant distance behind it. Therefore if a given technique was used consistently in a given specimen by the same observer identifying a point at which the crack was opening a given constant amount, then velocities could be measured satisfactorily and reliably.

Techniques used to identify this fictitious crack tip point included:

- observation of small bubbles of fluid (water, oil or dye-penetrant) being pumped out of the crack having been introduced into the crack some distance behind the tip;

- pumping of air bubbles on a wet surface;

- observation of the colour change in the damp surface of a specimen as it cracked;

- the relative movement of the mortar on each side of a crack as the load was cycled.

The crack was often seen to jump in discrete steps of up to five mm, rather than incrementally. This made observation difficult as the crack could jump out

of the field of view of the microscope, thus the operator would be waiting for the crack to grow whilst it has already jumped and continued down the specimen. Alternatively the crack would split, causing it to slow down due to the increased energy required to drive two cracks instead of one, each with their own process zone.

For further discussion on these effects and their consequences reference should be made to the discussion in Chapter 9.

5.5.4 Ramp tests

The so called ramp tests involved the application of a constantly increasing downward displacement of the loading ram at a rate of 0,007 mm/s. This is the commonly accepted rate for fracture mechanics tests on other materials[5.5, 5.6] for these specimen sizes. Whilst this displacement was applied, a record could be kept of the load, deflection, time and crack length. A plot of load versus time or crack length should show an increasing characteristic up to a maximum and then a plateau of constant load as the crack grew under nominally constant load conditions until failure (see Figure 4.5) as described in Section 4.4. The tests were conducted to ascertain whether the DT specimen gave a constant stress intensity (K) along its length.

A simpler version of the test was also carried out on five specimens in every batch as well as at the beginning and end of each fatigue specimen to find the ultimate strength of each specimen/batch. Only the ultimate load was recorded from these tests.

5.6 Matrix of experimental variables

The factors that were varied during the course of the project were:

Percentage ash in the mix (%)	**0** 15 **25**
Specimen age at testing (days)	7 **28** 90 180 random
Cyclic load frequency (Hz)	0,1 **1** 5 10 20
Relative humidity of environment	0 10 50 100 **ambient**
Temperature (°C)	
(for underwater tests)	0 **20** 60
(in air)	**ambient**
Type of fluid environment	**air** water ethyl-alcohol
Cyclic amplitude	
(% of ultimate load)	50 to 95
Load ratio (maximum/minimum)	**0.1** 0.4 other
Specimen orientation	**normal**, up-side-down, side-ways-on
Maximum load (% of ultimate)	50 to 95
Type of sand	pit sand, blend
Drying preparation before test	air, silica-gel, oven dry, **none**

Not all possible combinations of the above variables were tested. A base set of those highlighted in **bold** above were selected, and then, in any given batch of specimens, one or two of the variables were changed within the ranges given.

The project was conducted in three phases. The first was to confirm that the stress intensity was constant over the specimen length using ramp tests as described in Section 4.4.

The second phase tested the effects of "mechanical" test parameters, ie specimen orientation, cyclic load amplitude and frequency. The third phase was to vary the "materials" changes including fly ash content, age, type of sand, specimen preparation, surrounding fluids, relative humidity and temperature.

Some ramp tests were also conducted on mini specimens mounted inside the SEM as described in Chapter 8.

5.7 Data processing

5.7.1 Crack length - number of cycles (a-N) curves

During the progress of a test, a record was kept of the number of cycles and the length of the crack, and these were plotted on computer (Figure 4.3). The slope of the line was the crack velocity for a given set of test parameters and applied stress intensity. A linear regression program was used to calculate the velocity from the line.

Whilst the line was straight in most cases there were occasions when the crack would slow down due to splitting or would decelerate and stop altogether. This would result in a curve rather than a straight line, making it difficult to read a so called constant velocity for "stable" test conditions. The reasons for this are discussed in the results section.

5.7.2 Crack velocity - stress intensity (V-K) Plots

The calculated velocities and applied stress intensities were recorded on a spreadsheet along with details of the test variables. The stress intensity values were then adjusted for the calibration of the load cell and plots of crack velocity (V) versus stress intensity (K) (as the maximum in the cycle) generated on a log-log scale. According to the literature [5.4, 5.7 - 5.10] the plot of data for a given set of variables should be a straight line on this scale. This means that the data can be represented by the equation:

$$V = AK^n \qquad 5.1$$

The data did indeed show this behaviour, albeit with the large amount of scatter typical of this test system.[5.7, 5.11] Comparison of the values of **A** and, particularly, **n** should provide a quantitative means of measuring the effect of changing conditions or materials on the fatigue behaviour of mortar. However

the scatter was large enough to prevent the significant evaluation of these parameters and for the purposes of this thesis only the relative position of the "clouds of data" for sets of parameters has been used as a basis of discussion. A cloud of data to the top left of a V-K plot implies that for a given applied load, the crack growth rate is higher and therefore considered to be "worse" than a cloud of data to the bottom right of the plot.

As has been described in Section 4.4, each specimen was non-homogenous, thus leading to relatively large scatter in the data.

This chapter has described in detail the materials, equipment and techniques used in the experimental work in the present study. The next chapter presents the results of the some one thousand eight hundred tests that were carried out.

CHAPTER SIX - RESULTS PART 1 - LOADING EFFECTS

6.1 Introduction

Results of the tests, carried out as described in the previous chapter, are presented in the next two chapters. This chapter covers the effects of "loading" type parameters such as the orientation of the specimens with respect to casting direction, cyclic frequency and amplitude. The next chapter presents the data from tests investigating the "materials" parameters such as composition of the samples, their preparation methods, age and the environment to which they were exposed.

Each parameter has been discussed in a separate section, in which the data has been presented in the form of V-K plots showing crack growth velocity in mm/s versus applied stress intensity in MPa$\sqrt{m}$, both on log scales. The same data is also presented in V-K_{rel} plots where the stress intensity figures for the horizontal axis have been normalised against the maximum stress intensity determined for each individual specimen. The validity and implications of this approach are discussed in Chapter 9.

The extent of the scatter is shown in Figure 6.1 for a typical, single, set of results on both V-K and V-K_{rel} plots. It can be seen that for a single K value, V varies by approximately 1,6 orders of magnitude, and for a K_{rel} value V varies approximately 1,7 orders of magnitude. This scatter is apparently normal for this type of test on mortars.[6.1, 6.2]

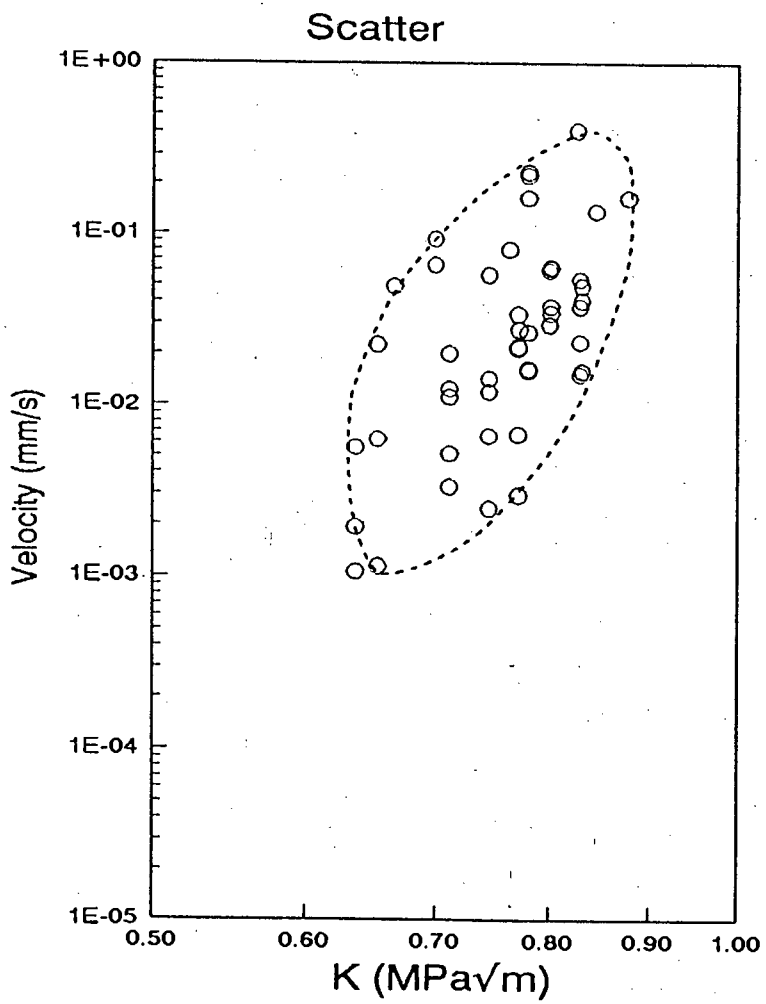

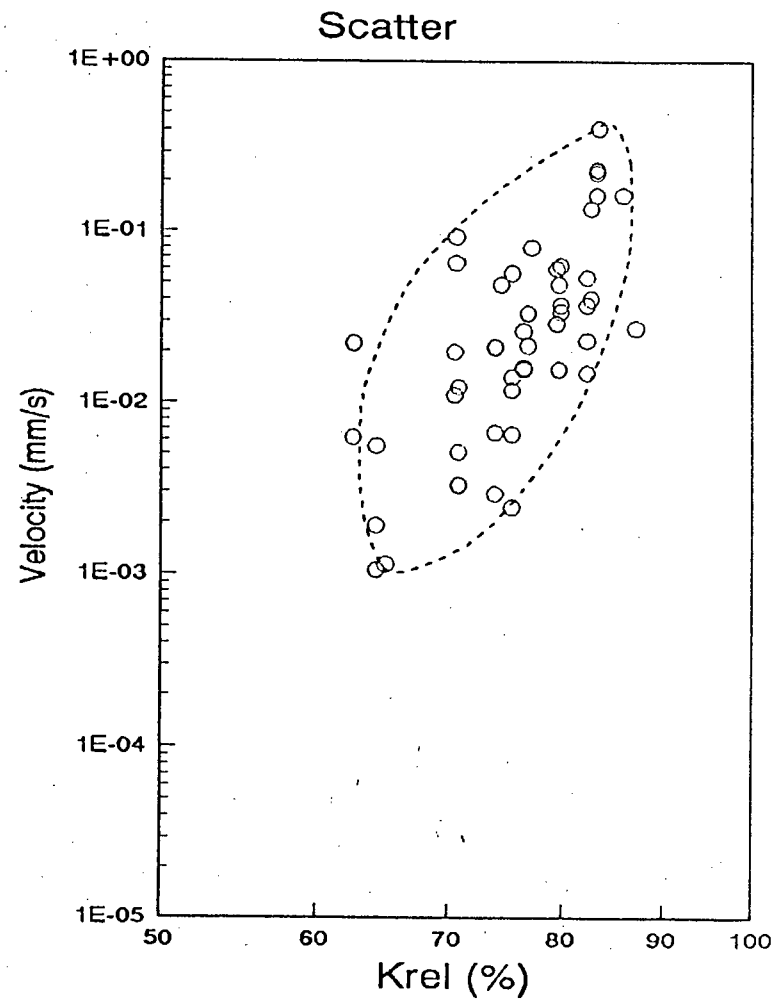

Figure 6.1: V-K and V-K_{rel} plots showing the extent of a scatter in a typical data set

6.2 Sample orientation and setting up

A limited number of tests were carried out in which crack growth direction was varied with respect to sample casting direction. As stated in Section 5.3.3 the standard orientation was to cut the starter notch from the end that had been at the top of the mould. This was in order to reduce the probability of the load points at the corners being applied onto the soft zones due to leakage from the mould.

However, it is possible that due to bleeding and gravitational effects, the mortar at the top of a sample was not the same as that at the bottom. To investigate this, one set of samples was prepared such that the starter notch was cut from the bottom end (called the up-side-down set). A set was also prepared in which a mould was modified and placed on its side so that the width of the sample was vertical (called the sideways set).

The samples were all made from mortar containing 25% fly ash. Standard fatigue testing was carried out using the base set of variables as shown in bold in Section 5.6. The effect of the casting orientation on the rate of crack growth is shown in Figure 6.2

The clouds of data appear to occupy the same area, indicating that there was no discernible difference in fatigue behaviour due to casting orientation. Additionally it indicates that the slowing and stopping discussed subsequently was not due to material variations related to casting orientation.

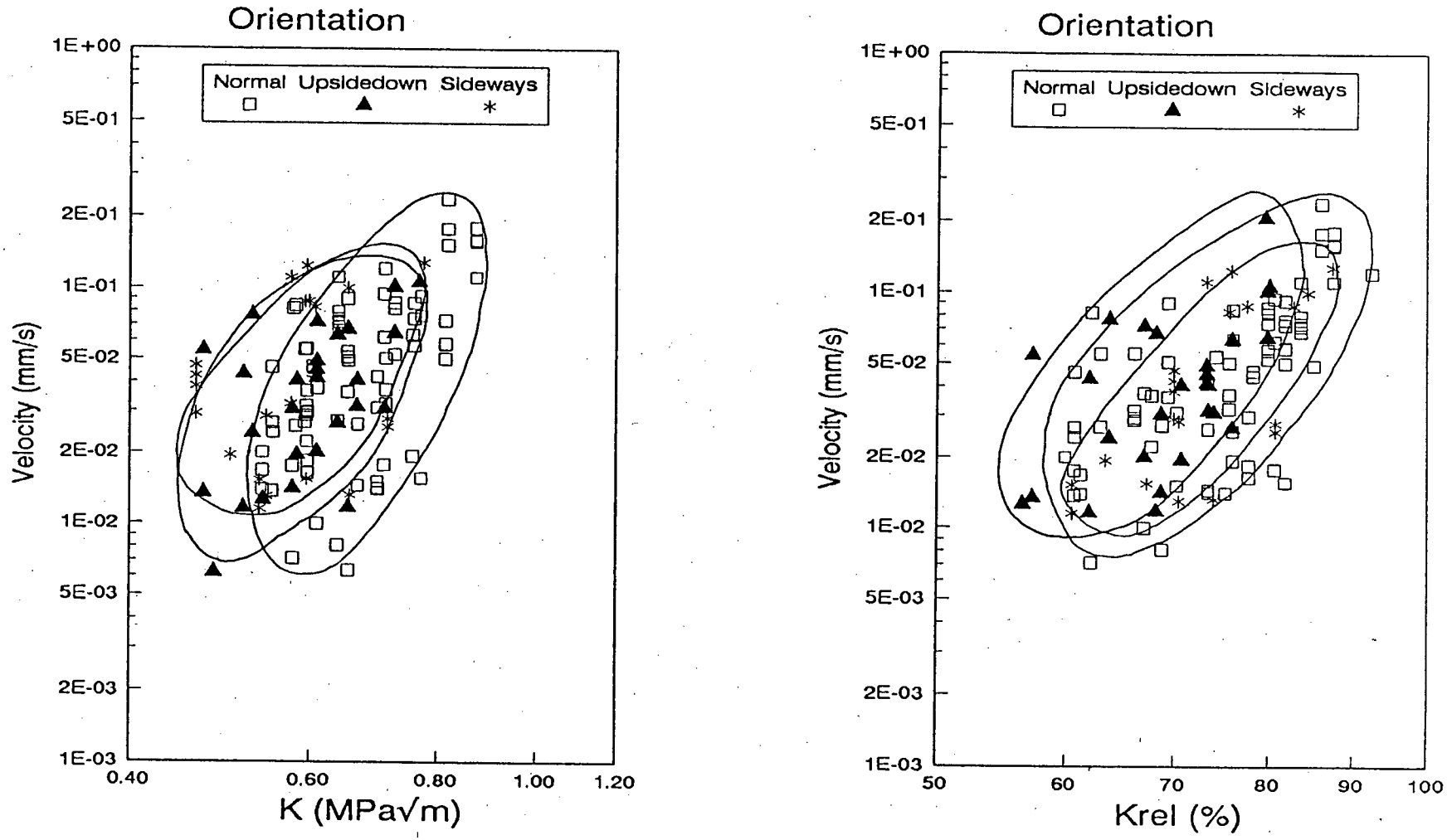

Figure 6.2: V-K and V-K_{rel} plots showing the effect of changing specimen casting orientation with respect to crack growth direction

Part of the motivation for this exercise was the observation in other tests that the crack was often seen to slow down and stop (Figure 6.3). This set was carried out to see if variation in material properties as a result of casting orientation was causing the slowing and stopping.

It was subsequently found that there was a small error in alignment between the loading points such that the upper points were closer to the back of the specimen than the lower. This resulted in a condition where the load (or stress intensity) was not constant along the length of the specimen, but increasing (see Section 4.4). Once this had been corrected, the problem was encountered less frequently.

6.3 Cyclic frequency

As stated in the literature review, it is generally accepted that the fatigue behaviour for cementitious materials is described by the V-K relationship between crack velocity and K_{max}, as opposed to the Paris relationship between da/dn and ΔK.[6.2, 6.3] The V-K relationship implies that there is a time dependency in the failure mechanism at the crack tip for cementitious materials. To assess this, a range of tests were carried out in which the cyclic frequency was varied from 0,1 Hz up to 20 Hz. The results are presented in the following figures. If a pure V-K mechanism is dominant then the clouds for the different frequencies should be inseparable on a V-K plot. However the same data presented on a da/dn-K plot should spread the clouds out with the high frequency data below that of the lower frequencies.

As can be seen from Figures 6.4 and 6.5, the V-K plot is as expected with little real difference between frequencies of 1 Hz to 20 Hz. However the 0,1 Hz band is significantly separated from the rest. The da/dn plot shows spread between all of the ranges. These indicate that the mechanism is not necessarily a pure "V-K" effect, particularly at the lowest frequency.

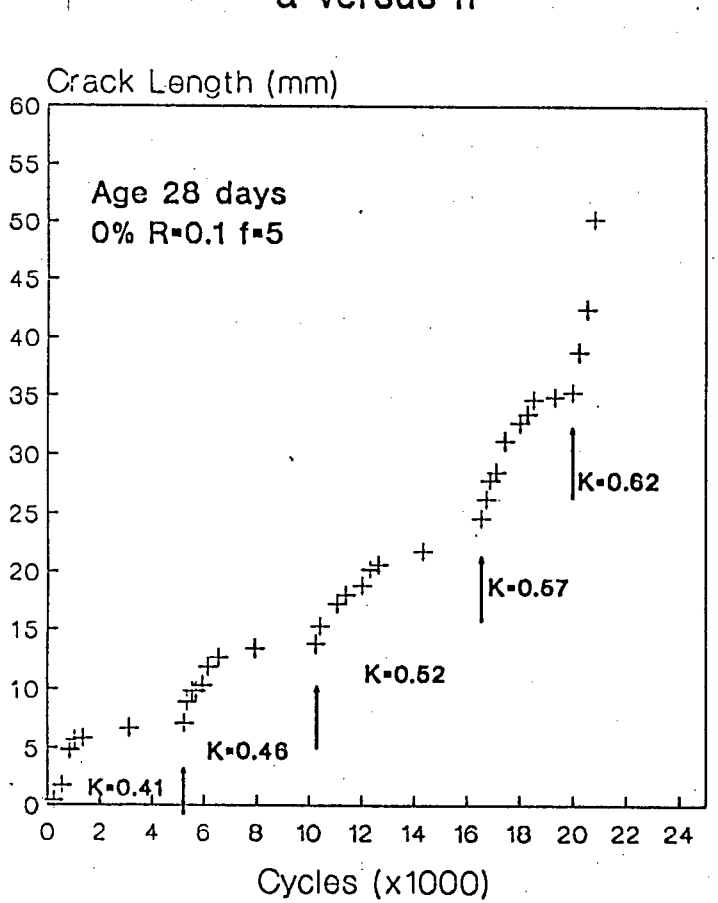

Figure 6.3: A-N plot showing a typical sample in which the crack slowed to a stop

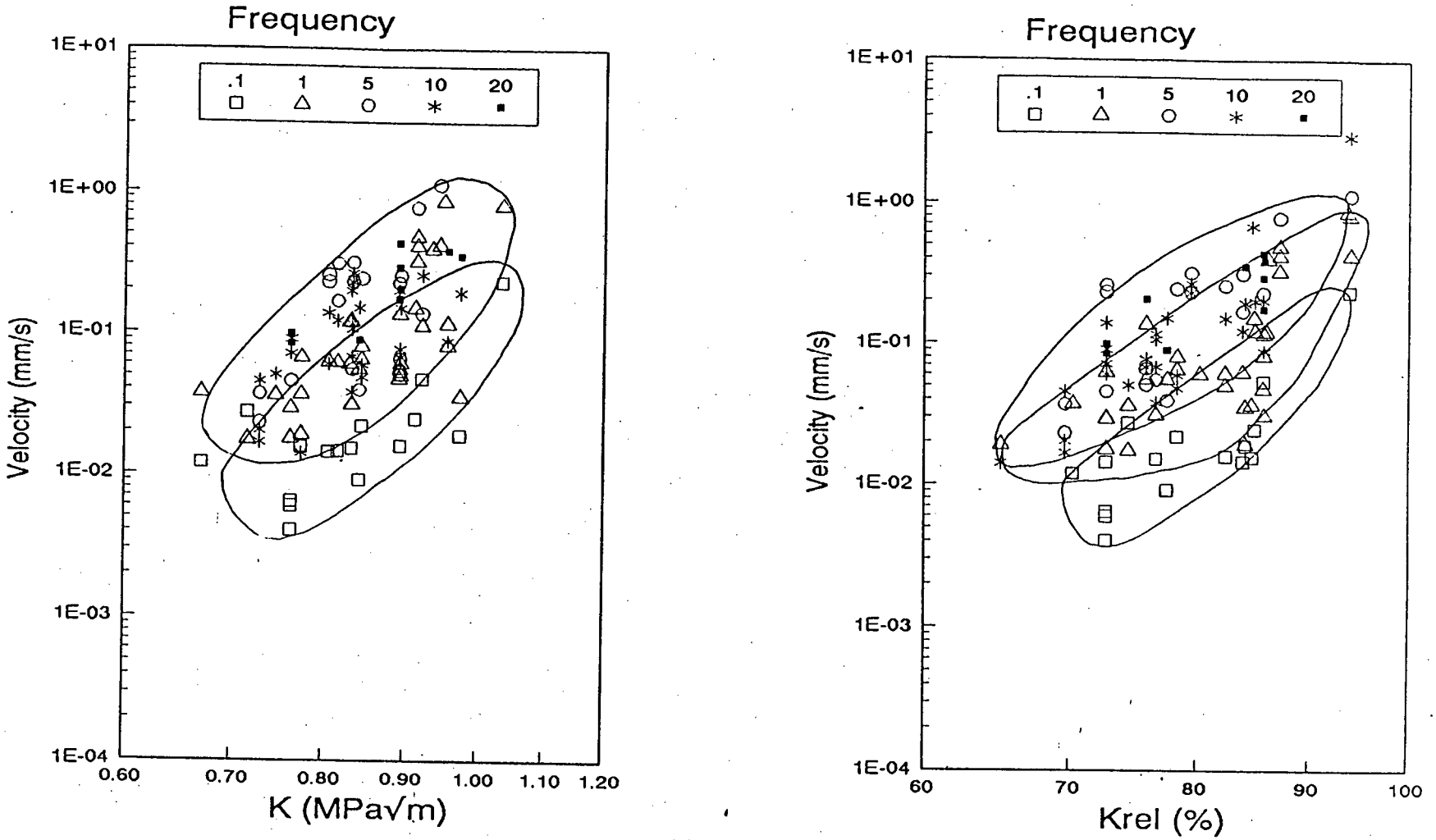

Figure 6.4: V-K and V-K_{rel} plots showing the effect of changing cyclic loading frequency with respect to crack growth rate per unit time

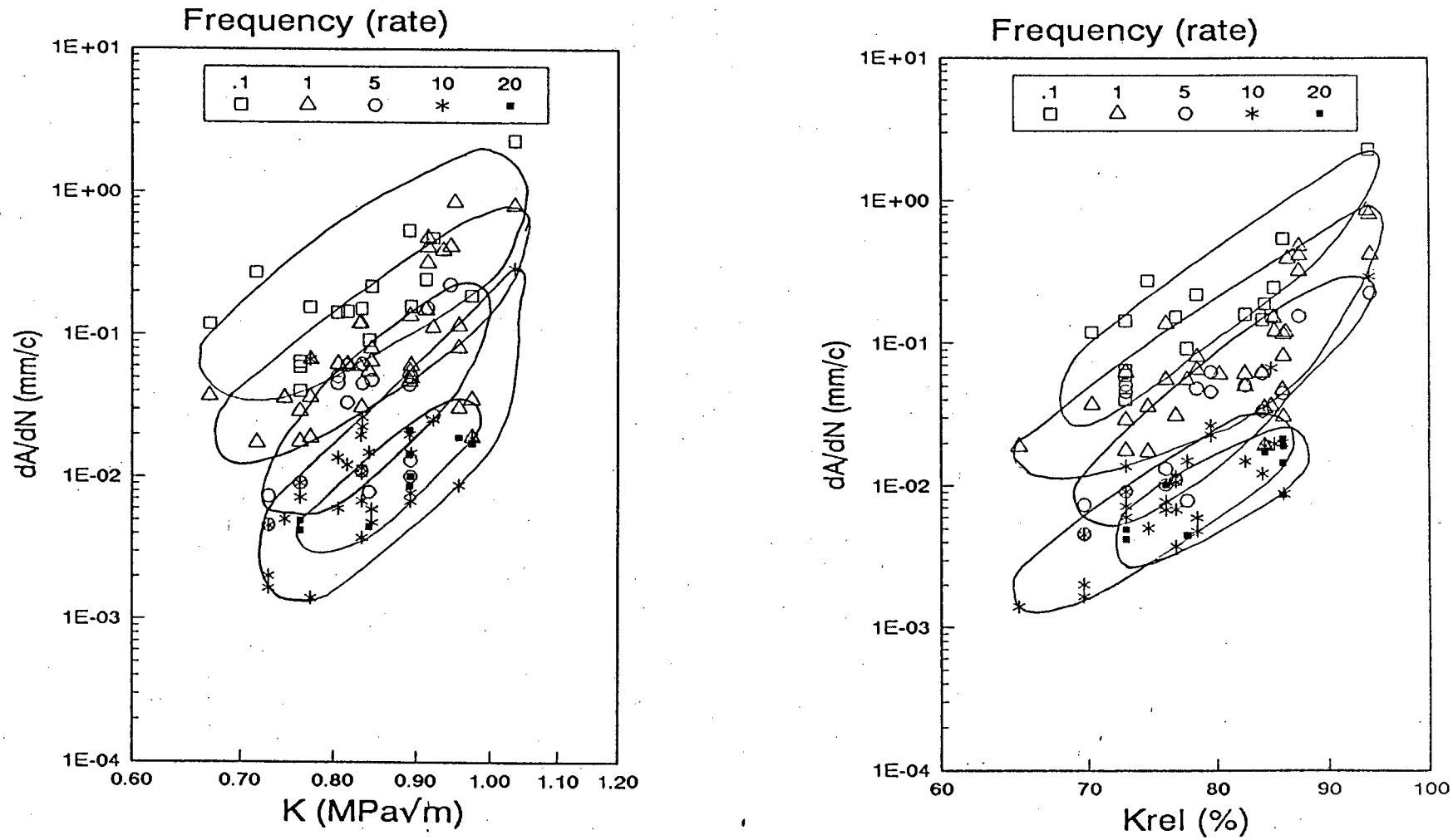

Figure 6.5: da/dn-K and da/dn-K_{rel} plots showing the effect of changing cyclic loading frequency with respect to crack growth rate per unit cycle

6.4 Load amplitude

The other half of the discussion regarding the applicability of the V-K or Paris relationships to cementitious materials is the effect of load amplitude. In metals the crack growth rate is largely governed by the amplitude of the cyclic stress intensity (ΔK), while in cementitious materials it is thought to be governed by K_{max}.[6.2, 6.3] This was assessed in a range of tests in which the amplitude and the K_{max} were varied. The results are presented in the following figures.

As discussed in the literature review, the means of expressing such investigations should be clearly defined. The use of the R ratio p_{min}/p_{max} does not adequately separate the variables and has not been used. The results have been presented as velocity versus K_{max} for families of amplitude (expressed as a percentage of the K_{Ipeak} of the cycle)(Figure 6.6). The same data has been presented in plots of velocity versus ΔK for families of K_{max} (Figure 6.7). It should be noted that these tests were conducted at a frequency of 1 Hz, therefore the vertical axis of Figure 6.7 may be considered to be a rate (da/dn) or a velocity (da/dt).

These plots also indicate that the material does not behave in a manner consistent with the pure V-K model, nor the pure Paris model.

The results have also been presented in the form of a Goodman diagram in Figure 6.8 where lines of similar crack velocity (ie a measure of lifetime) have been plotted against scales of K_{min} versus K_{max}. The results are similar in form to a typical Goodman diagram (such as Figure 3.4), thus indicating that, in principal, the Goodman diagram is valid.

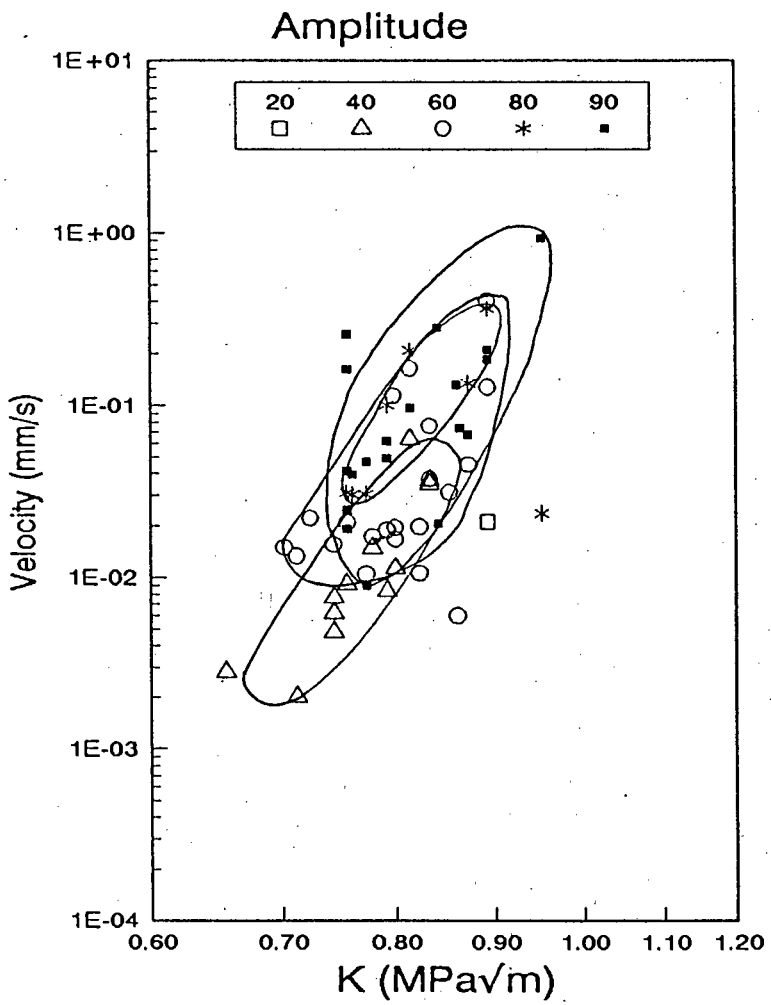

Figure 6.6: V-K plot for families of different amplitudes. The amplitudes have been expressed as percentages of K_{peak}

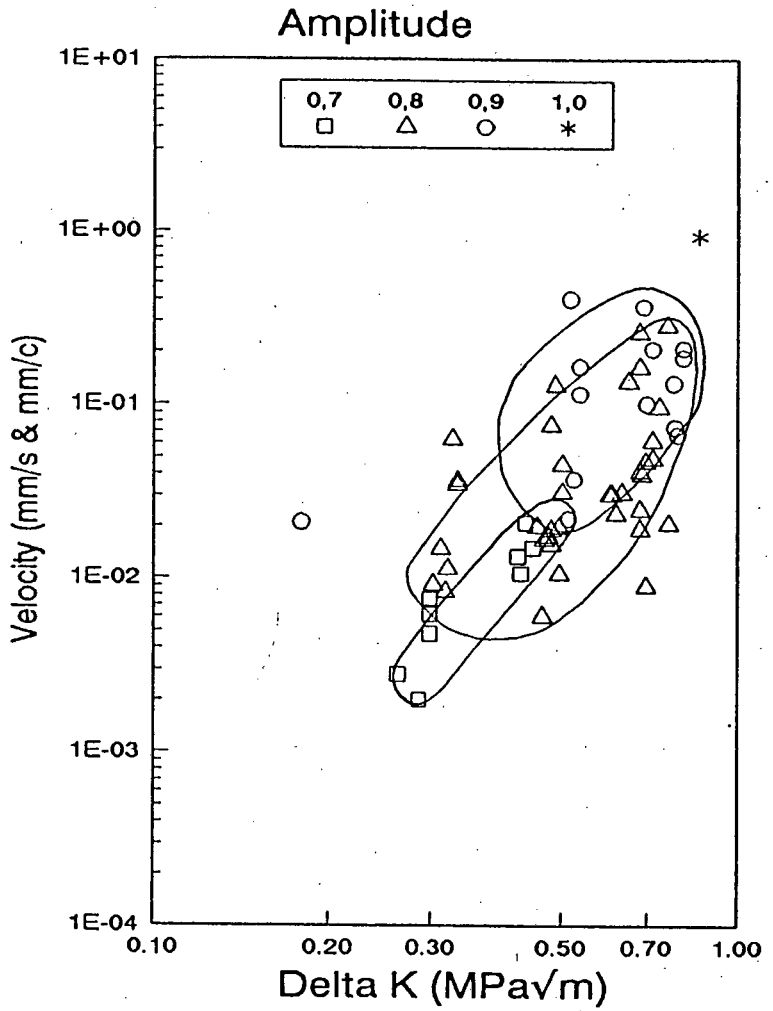

Figure 6.7: Paris type da/dn-ΔK plot for families of different K_{max} where K_{max} is given in MPa√m

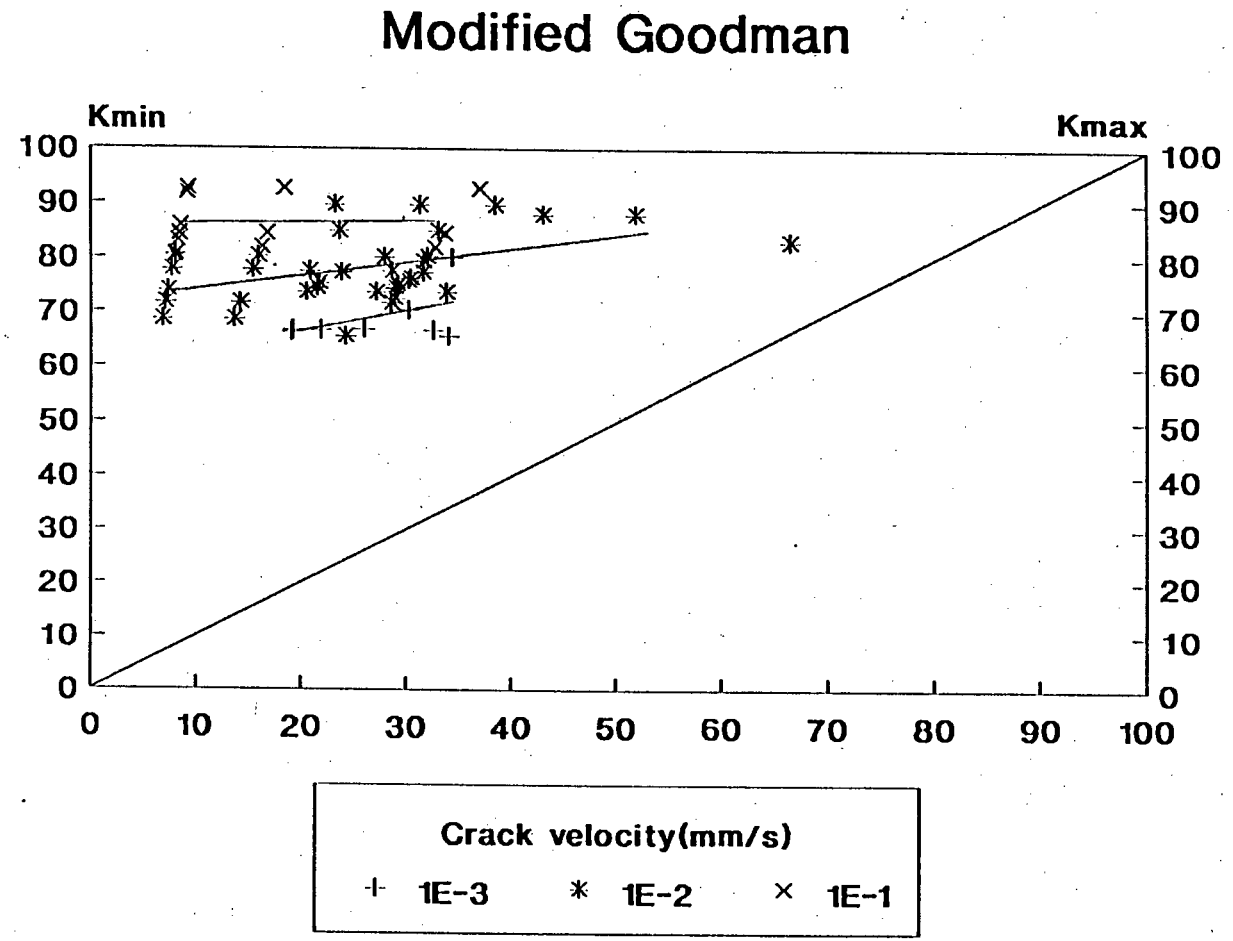

Figure 6.8: Amplitude results presented in the form of a Goodman diagram for families of similar crack velocity (in mm/s)

6.5 Loading history

One set of results has been presented in Figure 6.9 to indicate the effect of previous loading history on the fatigue crack growth rate. The set labelled "base" are the results for the initial cyclic loading condition on the samples. In the cases where the load, or K_{max} was then increased, the data points have been labelled "above" indicating that the loads for the points in question were at an applied stress intensity greater than previously applied. Conversely, where the loads were reduced the data points have been labelled as "below".

The plots show that there is no discernible effect due to the loading history. This is not surprising for the double torsion configuration where the stressed zones are relatively small with respect to the specimen size and the crack length. This means that the zone around the present crack tip has probably not been affected by previous loading due to the relative remoteness of the zone carrying the loads.

6.6 Ramp tests

As described in Section 4.4, the crack growth rate was determined during some of the ramp tests. In these tests, the position of the loading ram was monotonically changed at a constant rate, given in mm/s. The effect of the different loading rates on the crack velocity and the K_{max} is shown in Figure 6.10.

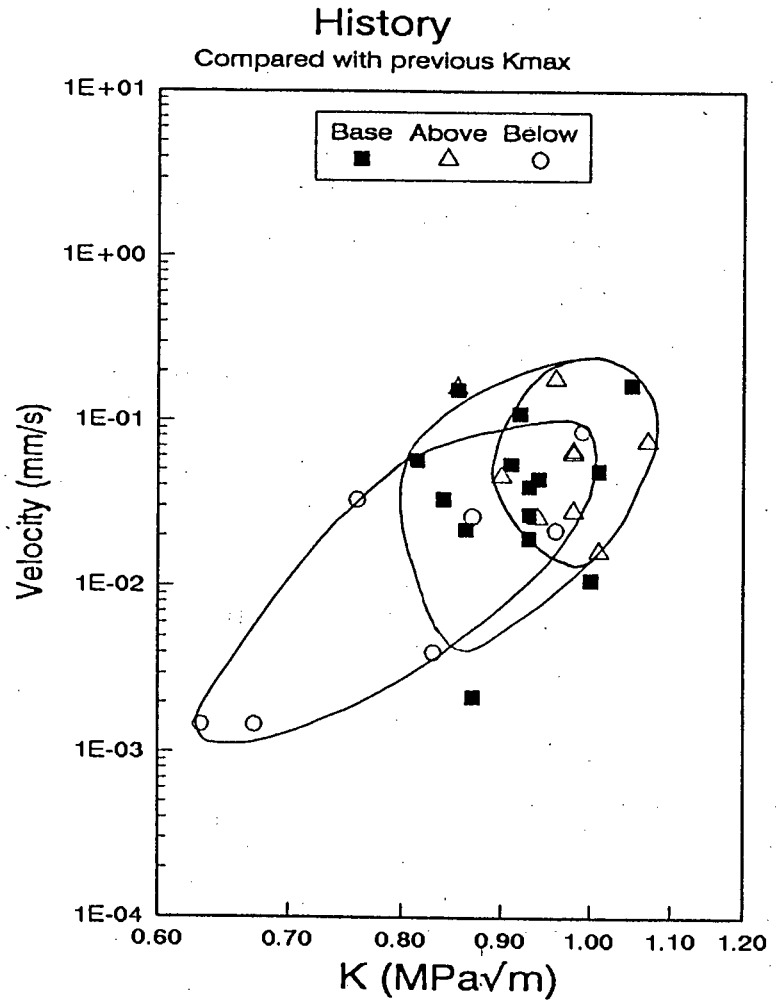

Figure 6.9: Plot showing the effect of loading history

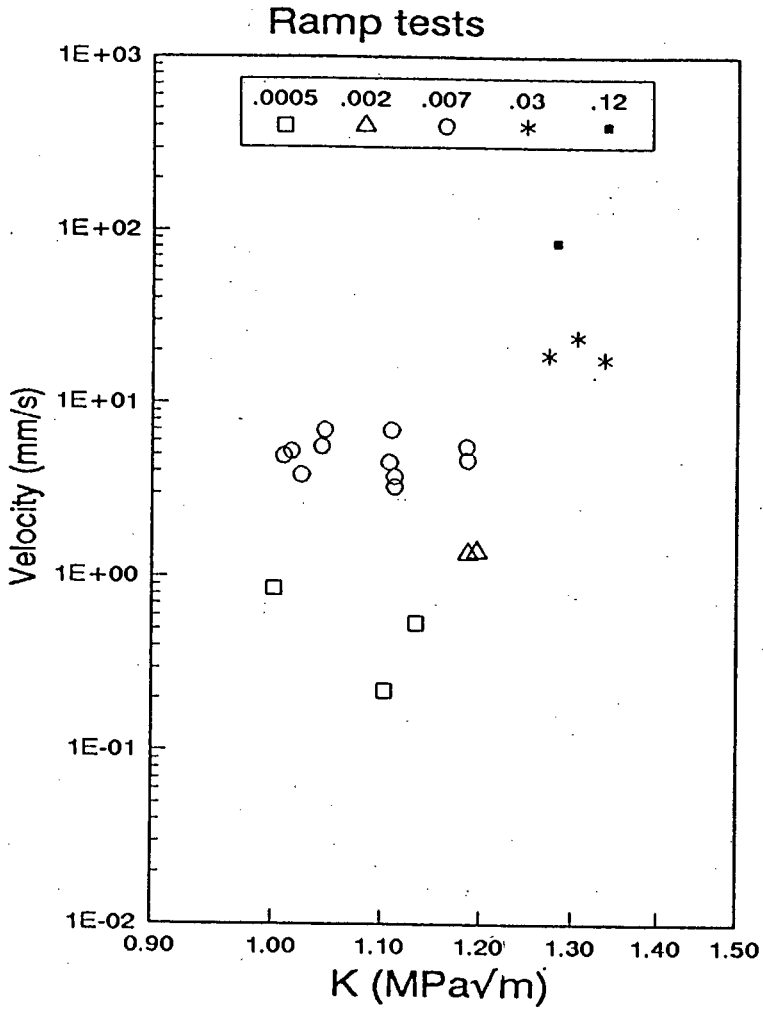

Figure 6.10: V-K plot for ramp tests at various vertical loading rates given in mm/s

6.7 Summary

The effects of various mechanical aspects of loading have been demonstrated in this chapter by means of several V-K plots for different loading parameters. They indicate that mortar does not behave in a manner consistent with the pure V-K model, nor the pure Paris model. In terms of age, the variation after 7 days is negligible, and if normalised against the maximum capacity of the material, the results for the 7 day old samples is similar to the older samples.

The following chapter presents similar plots showing the effects of material type variables.

CHAPTER SEVEN - RESULTS PART 2 - MATERIALS EFFECTS

7.1 Introduction

This chapter covers the effects of "materials" type parameters such as the composition of the samples, their preparation methods and the environment to which they were exposed. The intention behind these tests was to seek to understand better the mechanisms of fatigue crack growth by evaluating the effects of different materials parameters on fatigue crack growth rates.

As in the previous chapter, the results are given in the form of V-K and V-K_{rel} plots for various variables with each variable covered in a different section.

7.2 Specimen age

The compressive strengths of cubes from the three mixes are given in Figure 7.1. This shows the similarity in 7- and 28-day strengths of all the mixes, and the greater strengths of the fly ash mixes at greater ages.

The results of fatigue tests on the effects of specimen age are presented in Figures 7.2 to 7.4 in the form of V-K and V-K_{rel} plots for each of the three fly ash contents.

It is interesting to note that there is little apparent difference between the 28 day and older sets, but the 7 day sets show a higher crack velocity for the same stress intensity. This is true for all fly ash contents on the V-K plots, but disappears when the data is presented as V-K_{rel}.

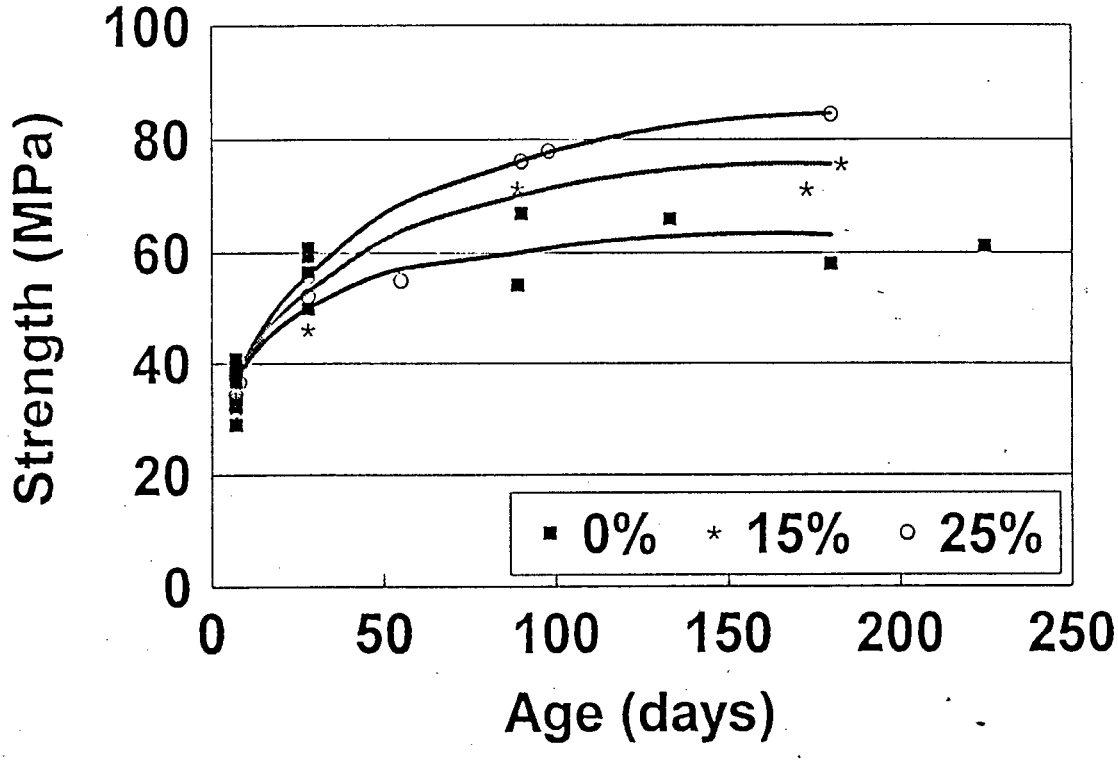

Figure 7.1: Plot of the compressive strength results at various ages of the mixes with their different fly ash contents

7.3 Fly ash content

The results presented in this section are based on the same data as those in the previous section, except that the plots are in given sets of similar age showing the effect of the fly ash content. Figures 7.5 to 7.8 are for ages 7, 28, 90 and 180 days respectively. At 7 and 28 days the OPC (0% fly ash) mix appears to have a similar crack velocity to that containing fly ash. However at greater ages the fly ash mix exhibits a faster (worse) crack velocity for the same applied stress intensity.

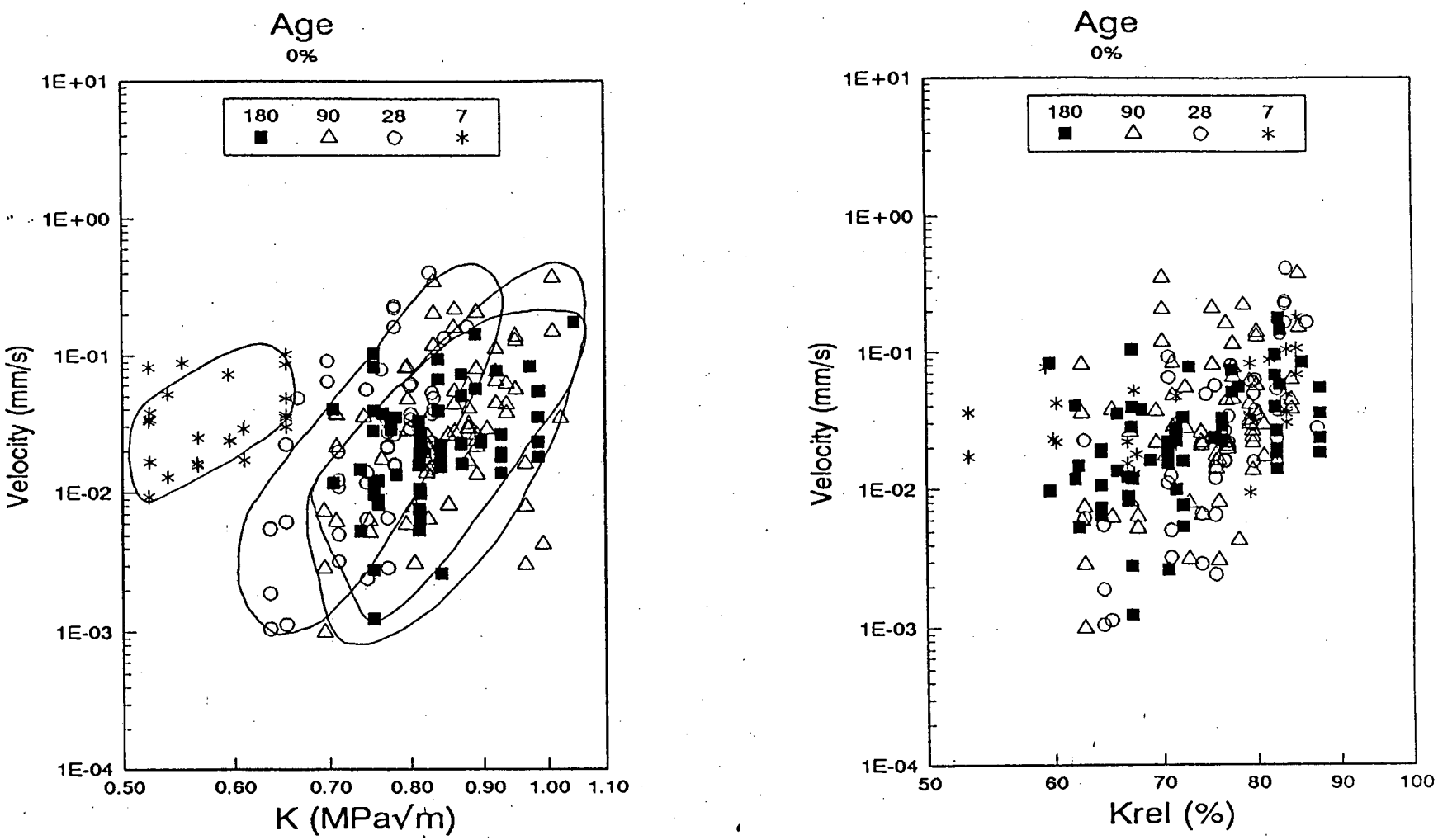

Figure 7.2: V-K and V-K_{rel} plots for 0% fly ash showing the effect of sample age (in days)

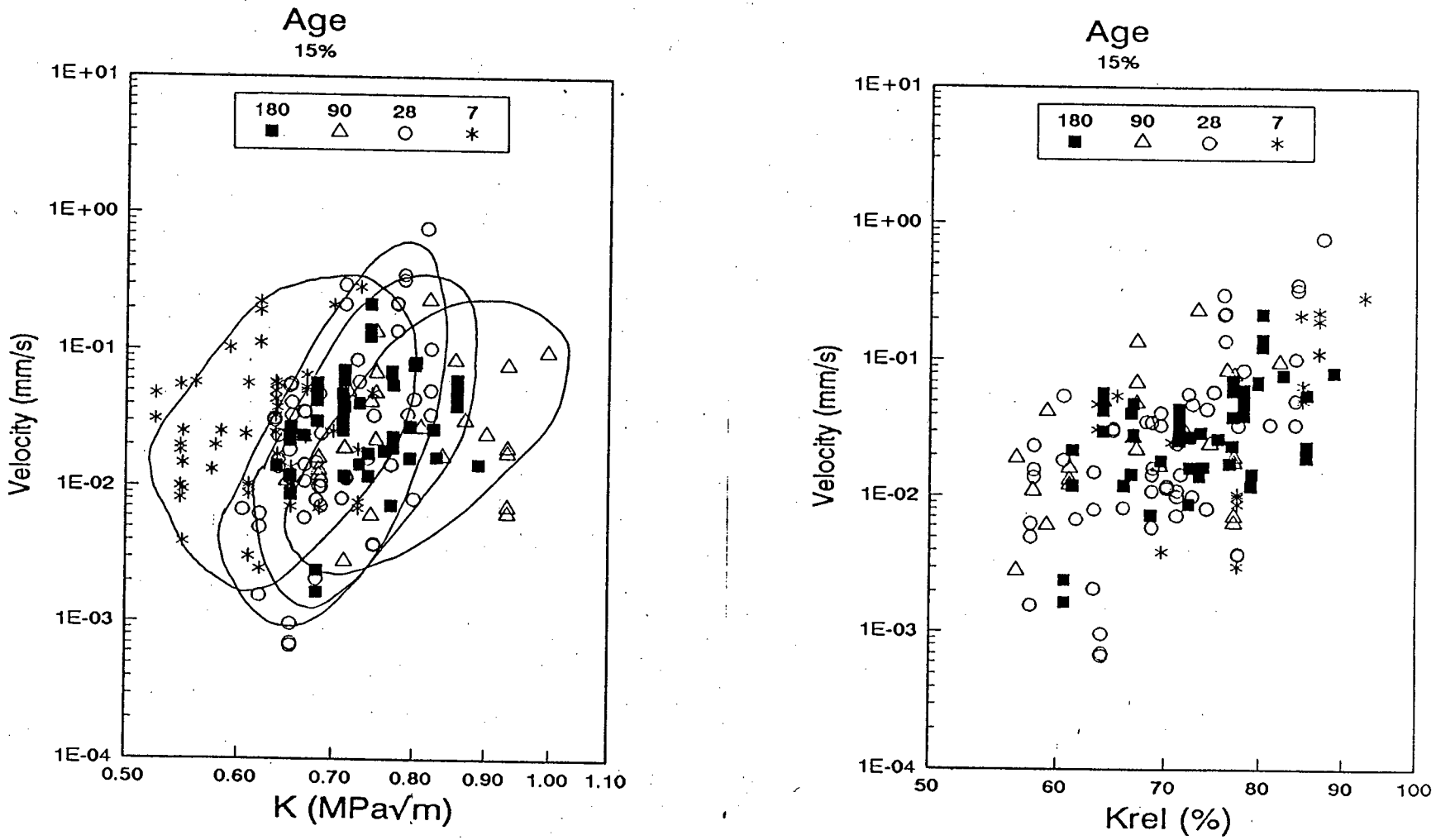

Figure 7.3: V-K and V-K_{rel} plots for 15% fly ash showing the effect of sample age (in days)

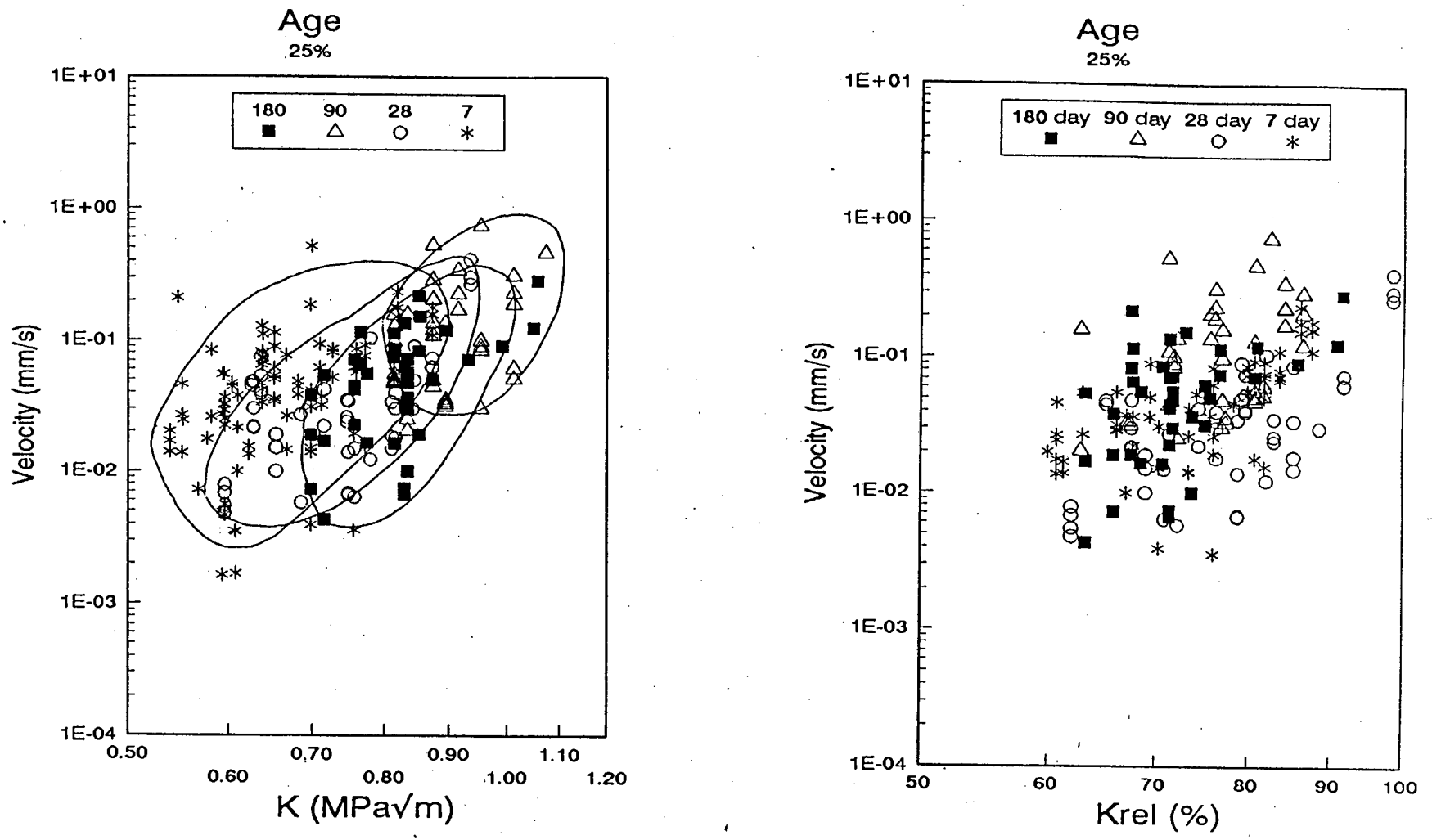

Figure 7.4: V-K and V-K_{rel} plots for 25% fly ash showing the effect of sample age (in days)

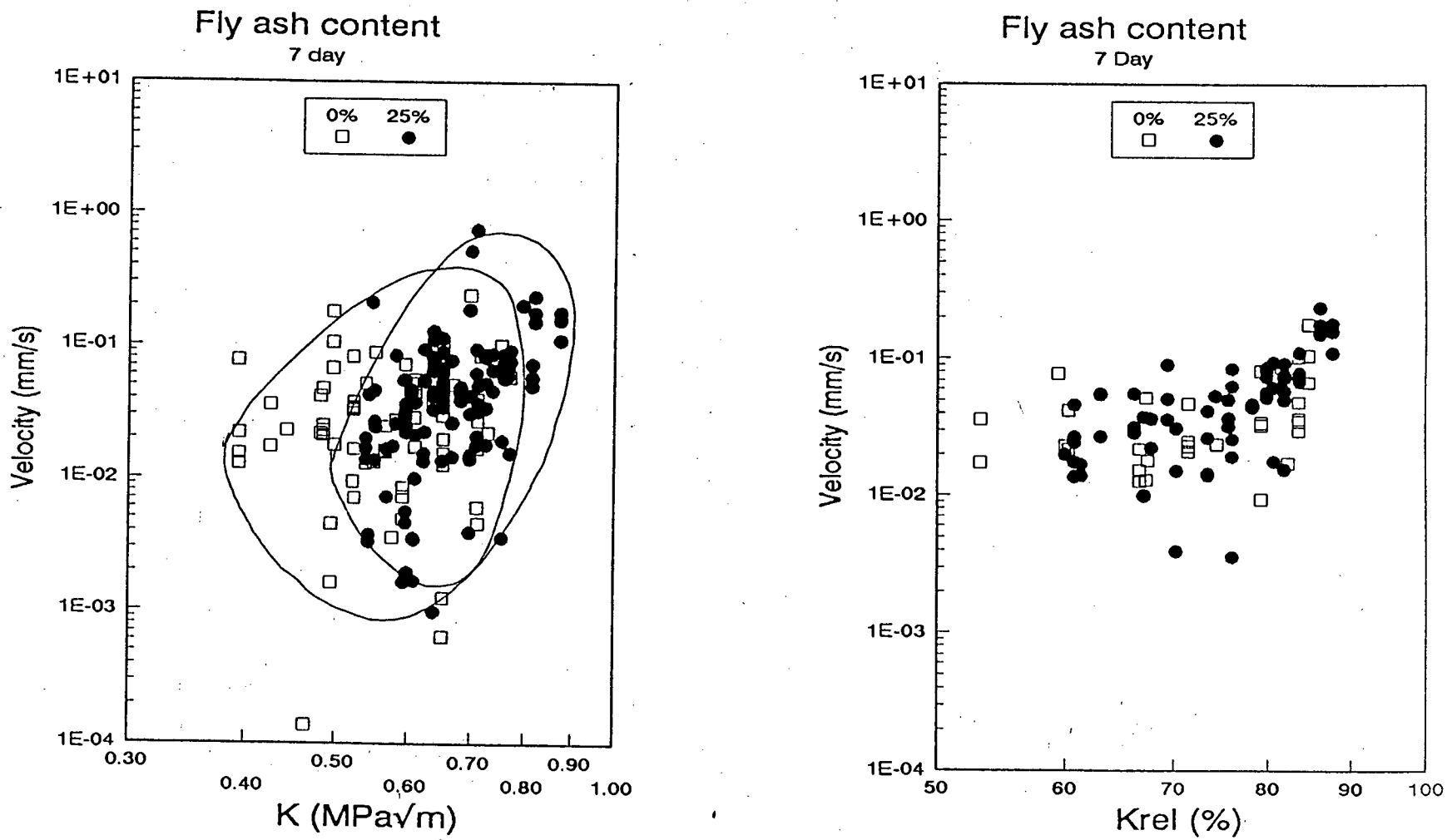

Figure 7.5: V-K and V-K_{rel} plots for 7 day old samples showing the effect of fly ash content

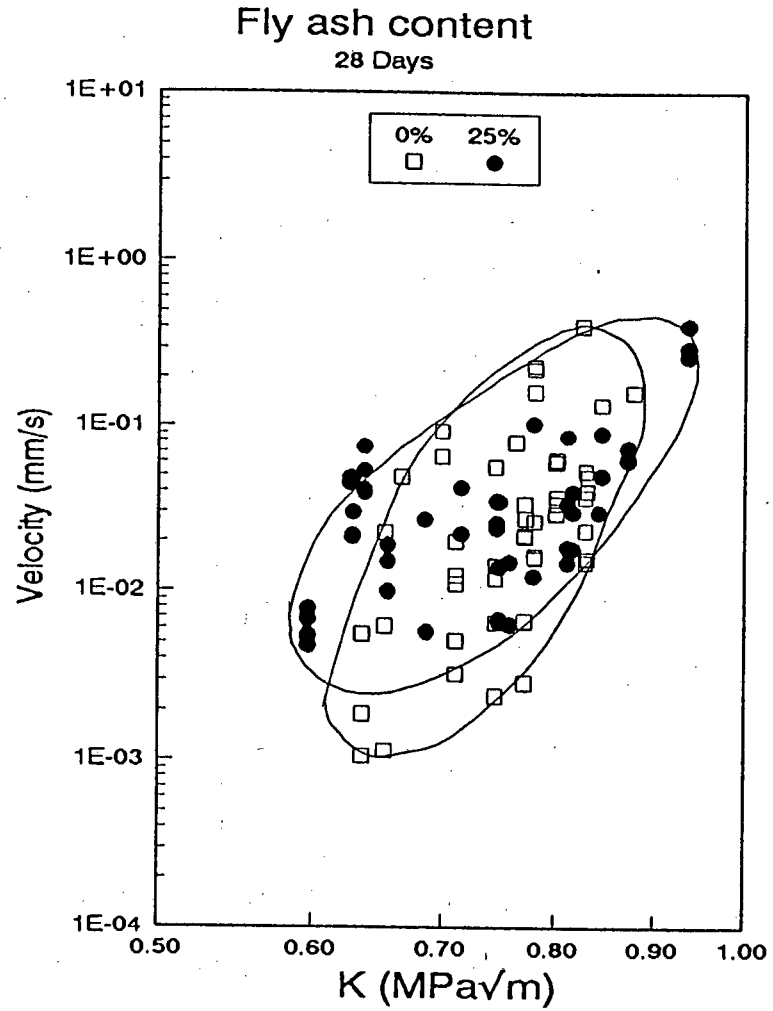

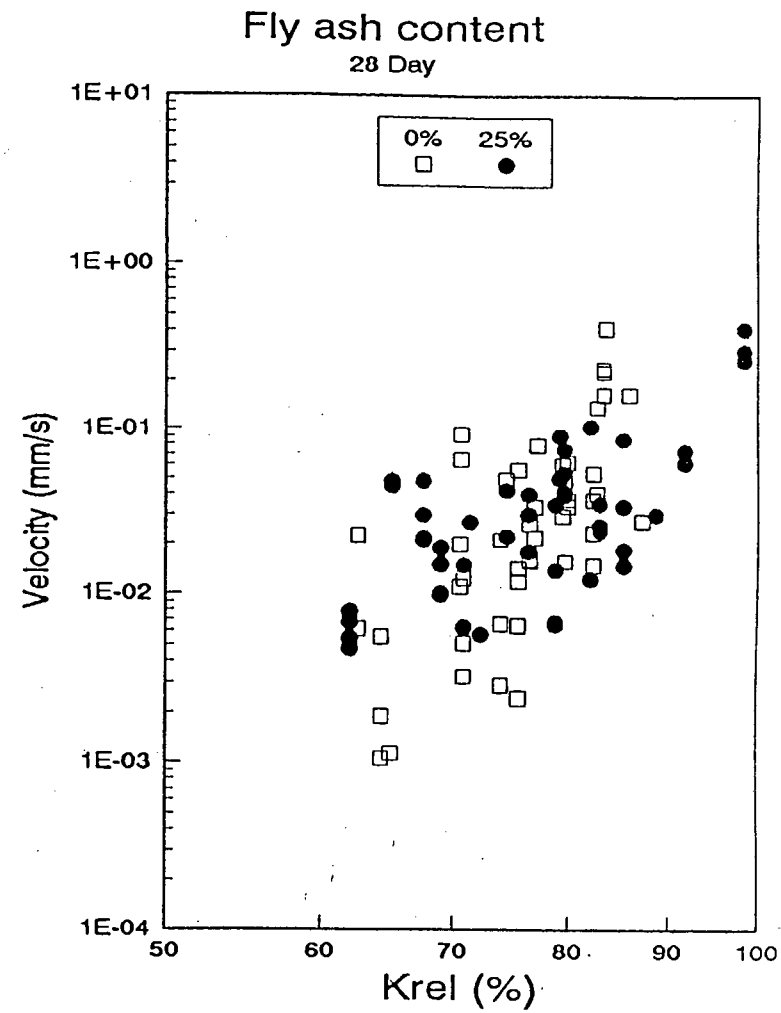

Figure 7.6: V-K and V-K_{rel} plots for 28 day old samples showing the effect of fly ash content

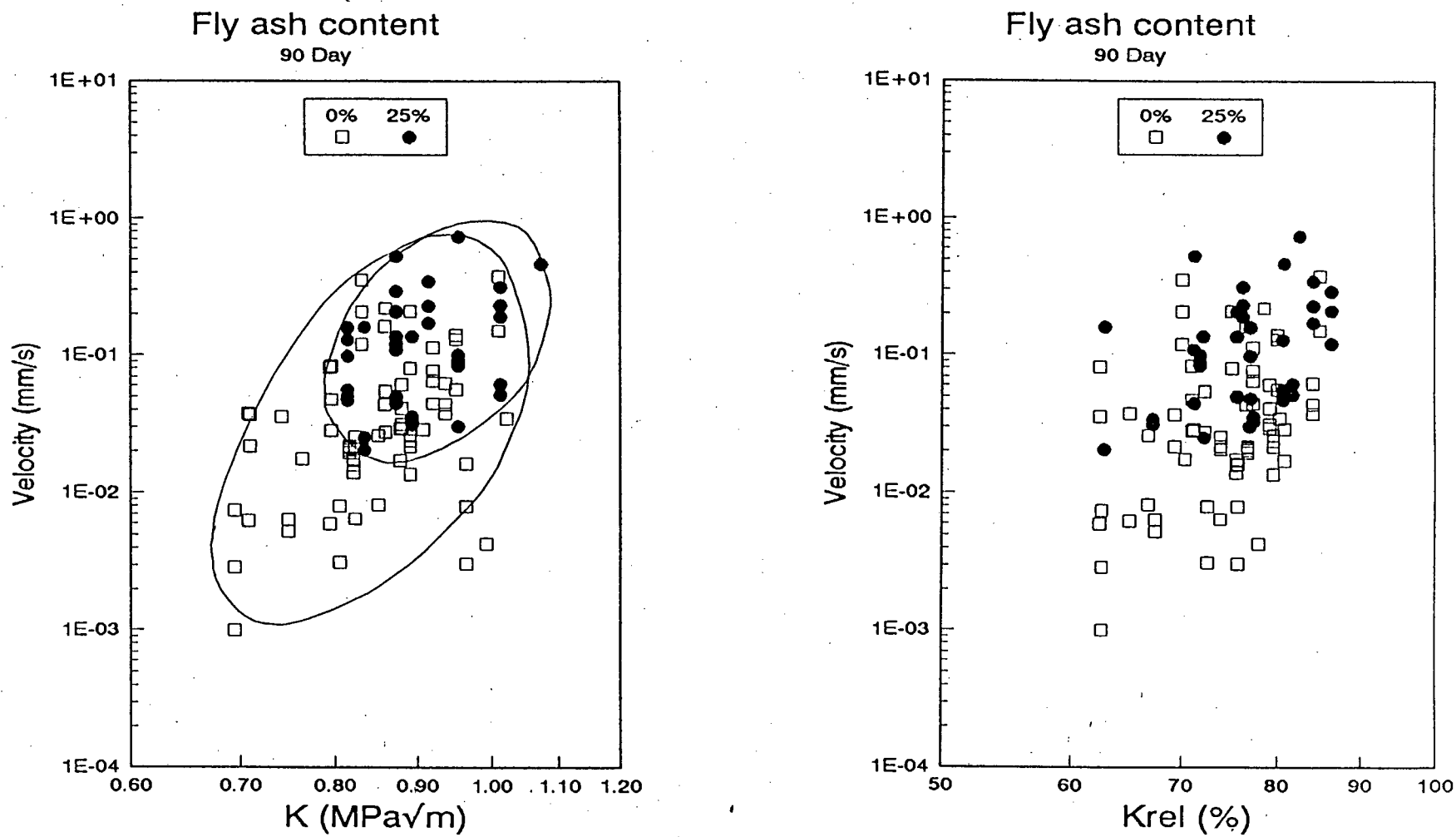

Figure 7.7: V-K and V-K_{rel} plots for 90 day old samples showing the effect of fly ash content

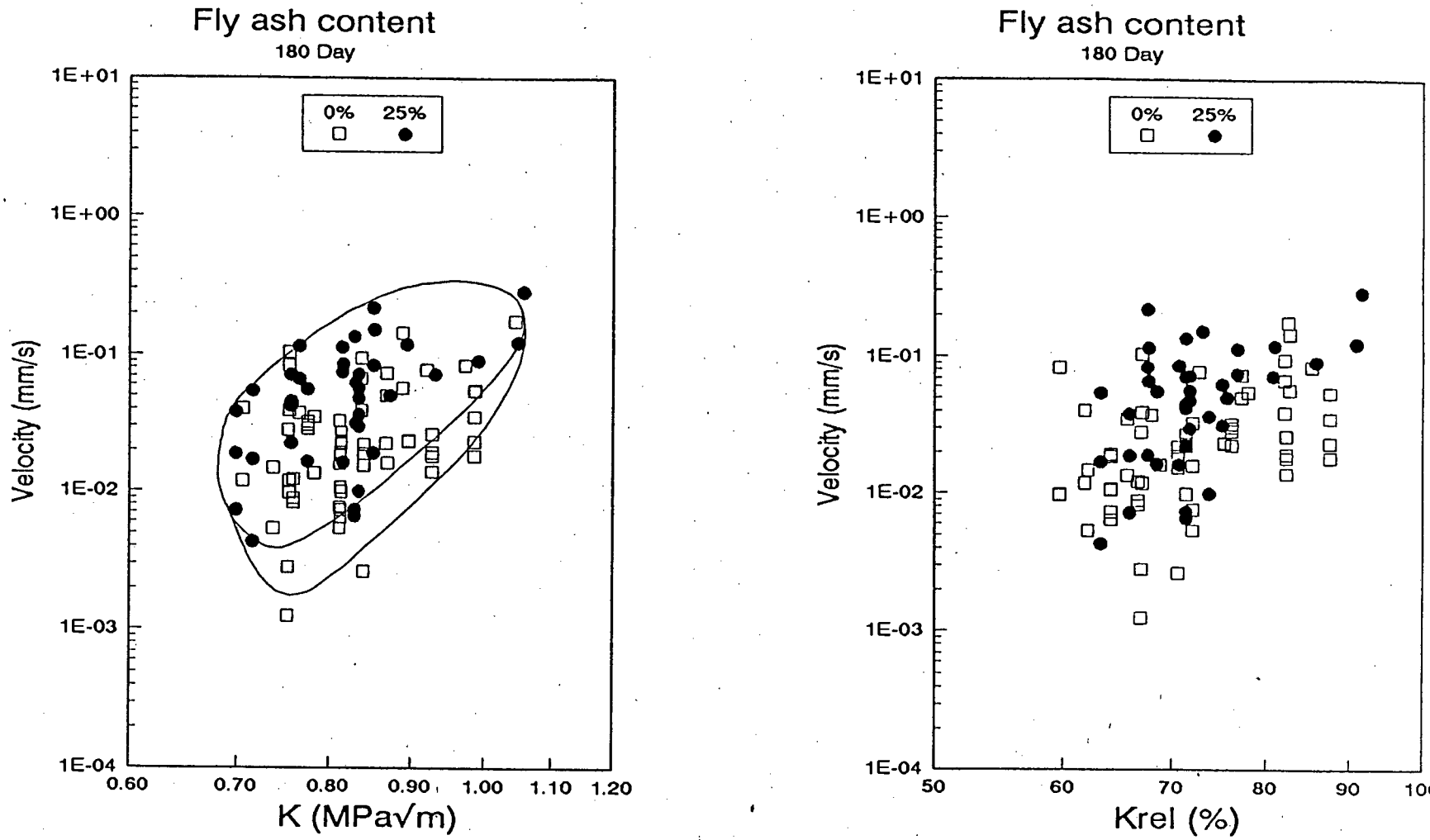

Figure 7.8: V-K and V-K_{rel} plots for 180 day old samples showing the effect of fly ash content

7.4 Sand type

During the course of this study the writer moved from Johannesburg to Cape Town. A supply of sand was transported to Cape Town that was initially thought to be sufficient for the remainder of the work. However, there was insufficient sand for the tests carried out in the last year of the project. The sand used in Johannesburg was a typical fine siliceous pit sand with a relatively high proportion of material passing the 75μm sieve, whilst those available in the Cape are predominantly wind blown dune sands that are single sized. It was therefore necessary to blend a dune sand with a pit sand and a portion of rock flour from a local crusher in order to achieve a similar grading.

A set of tests was carried out to observe whether the change in material had an observable effect on the V-K results. The results, given in Figure 7.9, show that there was no distinct effect, thus indicating that results from tests carried out before and after the change could be compared directly.

7.5 Relative humidity

A set of tests was carried out in which the relative humidity of the air in the environmental chamber was controlled by using trays of saturated salts, and monitored using a digital RH meter. The results of these tests are presented in Figures 7.10 to 7.12. Each figure is for a separate specimen preparation regime in which different means were used to dry the samples before testing.

The plots show that there was no distinct or unique trend in changing crack velocity with changing RH.

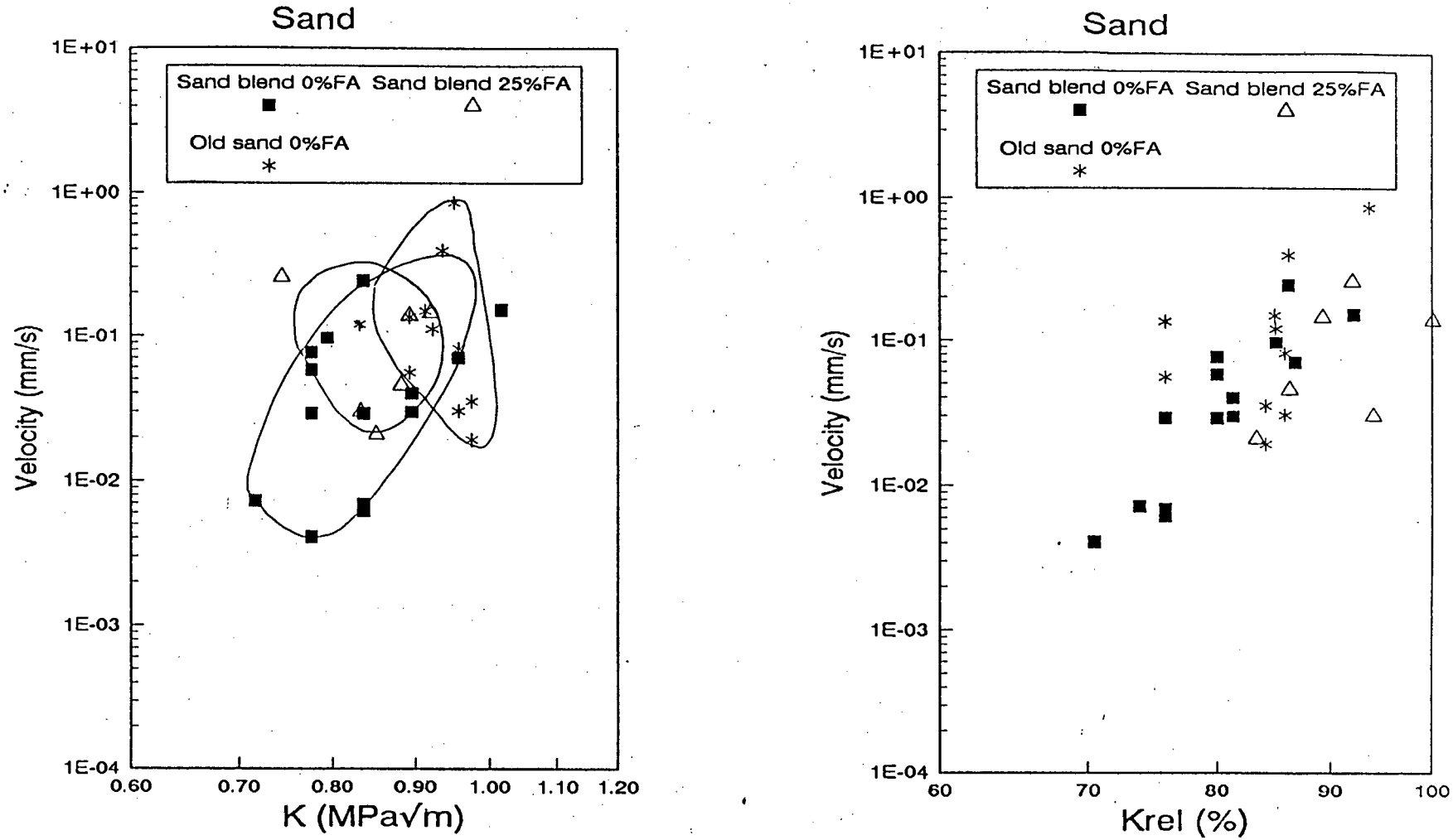

Figure 7.9: V-K and V-K_{rel} plots for different sand types

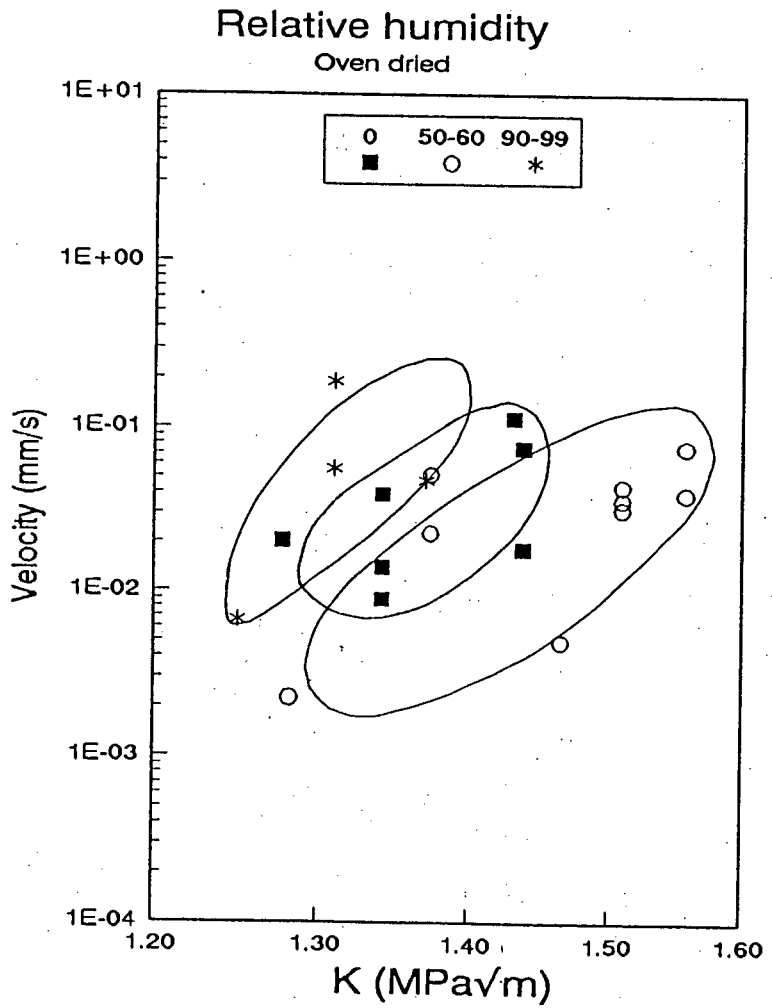

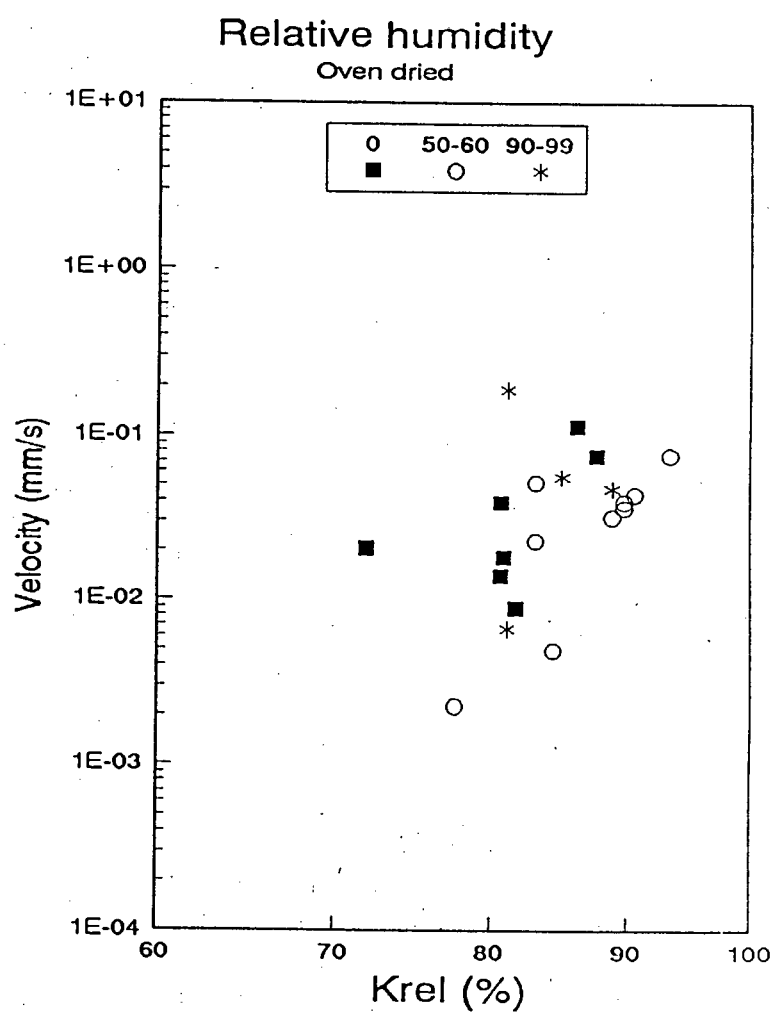

Figure 7.10: V-K and V-K_{rel} plots samples dried in an oven showing the effect of atmospheric RH

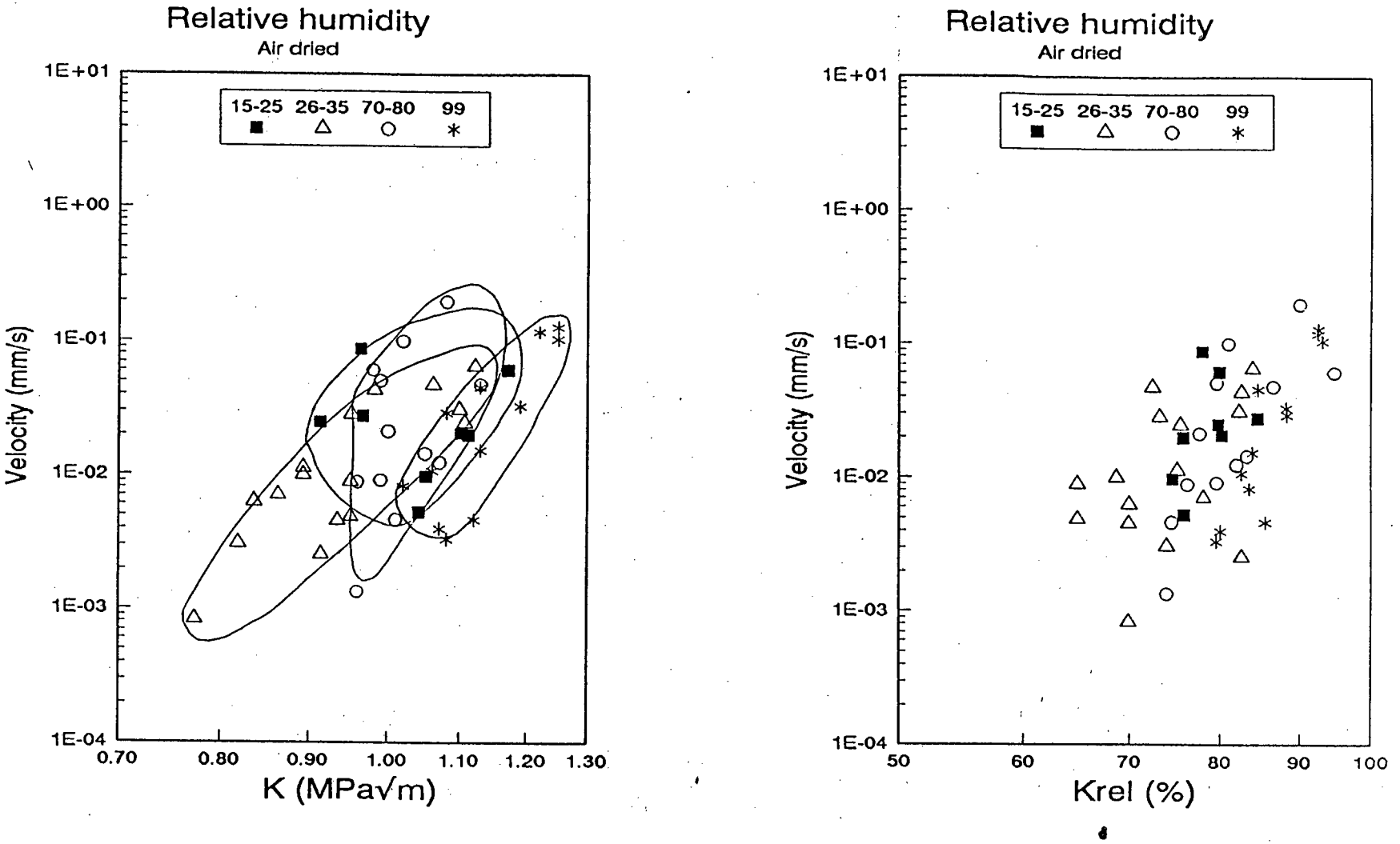

Figure 7.11: V-K and V-K_{rel} plots samples dried in air showing the effect of atmospheric RH

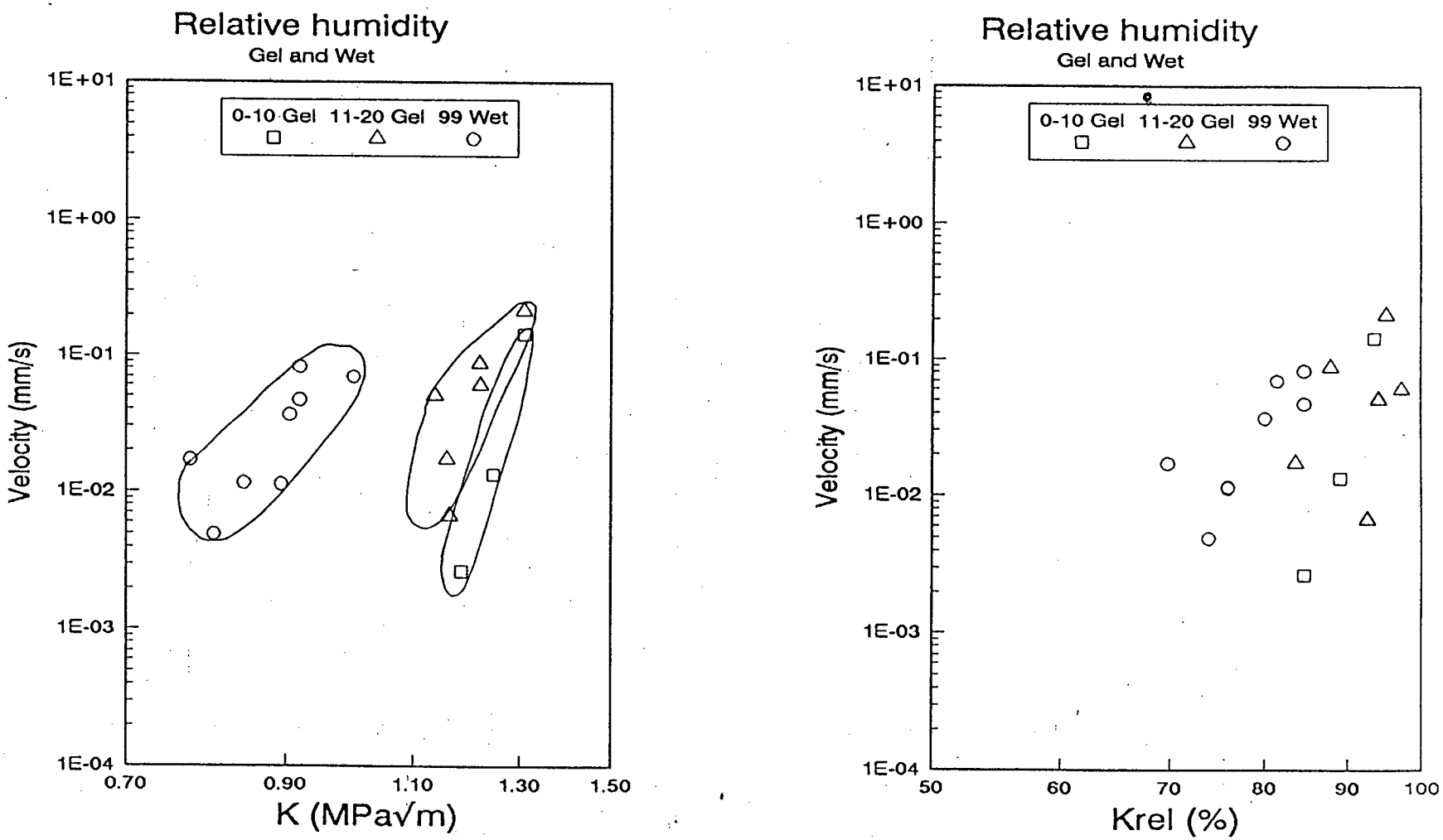

Figure 7.12: V-K and V-K_{rel} plots for samples dried over silica gel or not dried showing the effect of atmospheric RH

7.6 Sample preparation

The results in Figures 7.10 to 7.12 are repeated in Figures 7.13 and 7.14, but set out in order to show the effect of specimen drying methods for two different bands of environmental RH.

For the lower humidity set, the sets of data for the different drying systems all lie on the same line, albeit at different locations on the line with the air dried set exhibiting lower toughness. For the higher RH sets the data lies on different lines with the air dried set exhibiting the fastest crack resistance whilst the oven dried set were the slowest. As previously noted, these differences are not as apparent when the K axis is normalised.

7.7 Immersion in fluids

The final variable assessed in the programme was the effect of immersing the samples in different fluids at different temperatures. The results of this set are presented in Figures 7.15 and 7.16.

Figure 7.15 show samples tested in water at temperatures ranging from 4 to 60°C, plotted with a set that was tested in air with a relative humidity of 99%. The low temperature set shows a better crack resistance than the higher temperature set, while the 99% RH set was similar to the 4° set. These samples had not been dried.

Figure 7.16 shows the sets tested in alcohol at room temperature (air dried and oven dried) along with an air dried set tested in air at RH of 99%. The air dried alcohol samples show faster crack growth than the air dried wet set. This indicates that the alcohol was more aggressive to the mortar than water.

7.8 Summary

The results of tests assessing the effects of various materials parameters have been presented in this chapter.

The common thread in most of these results has been the apparent lack of variation when the results are presented with the stress intensity figures normalised against the K_{Ic} for each sample. The spread of the V-K sets is generally wider than that of the V-K_{rel} sets, the implications of which are discussed in Chapter 9.

Further to this, Figures 7.17 and 7.18 show the range of K_{Ic} figures measured for the samples containing different fly ash contents at different ages, and those tested under a range of preparation and environmental variables. These plots show the marked effect of these variables on the toughness of mortar.

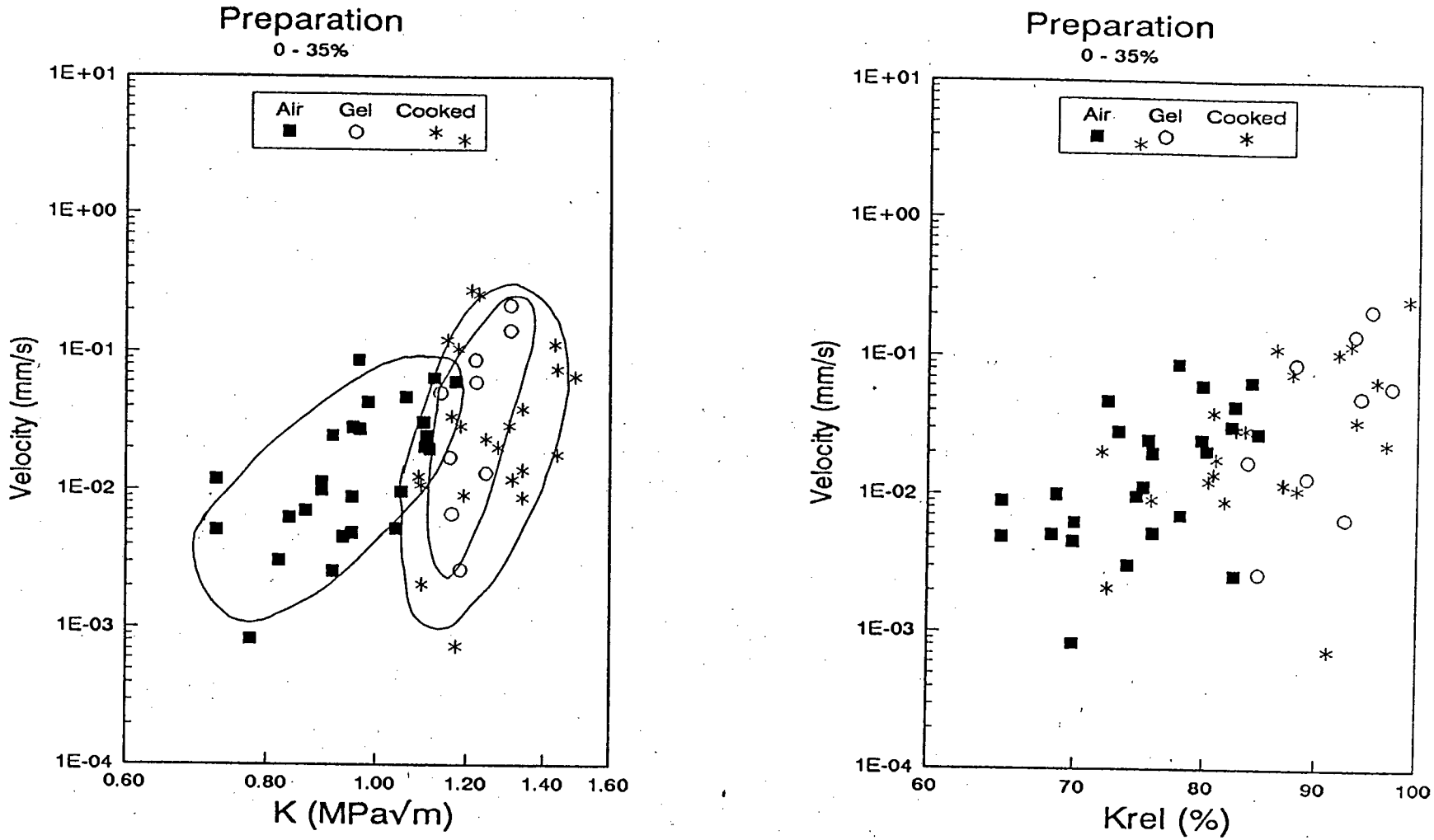

Figure 7.13: V-K and V-K_{rel} plots for samples tested in an RH range of 0 - 35% showing the effect of drying methods

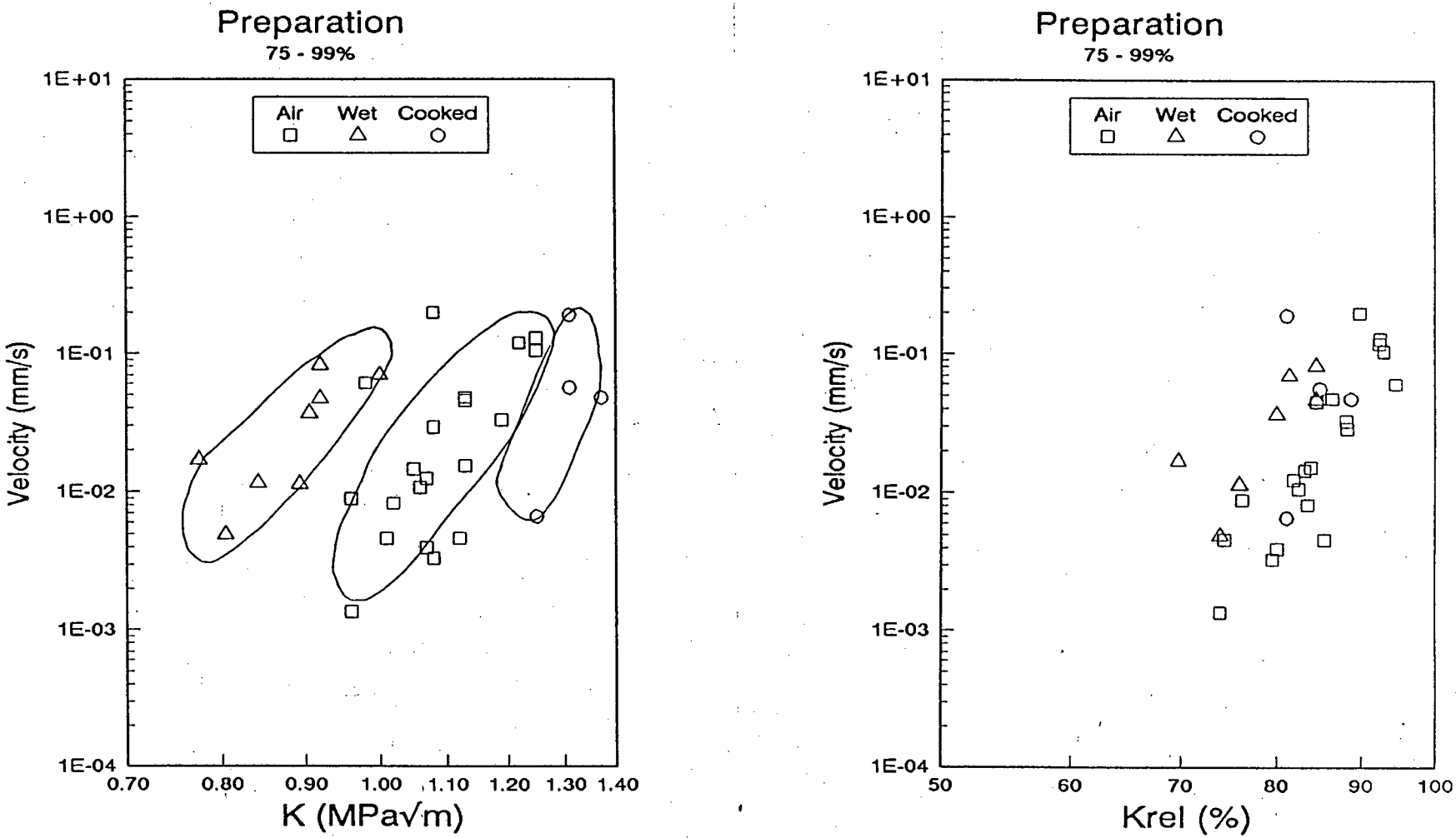

Figure 7.14: V-K and V-K_{rel} plots for samples tested in an RH range of 75 - 99% showing the effect of drying methods

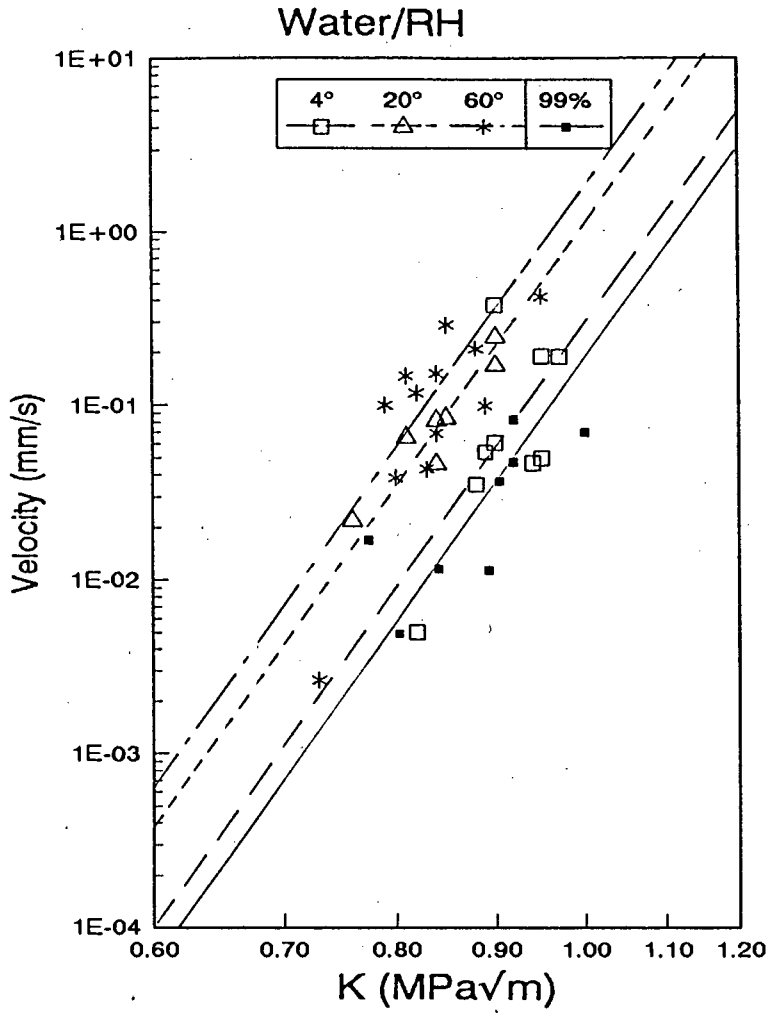

Figure 7.15: V-K plot for samples tested immersed in water at different temperatures (4 to 60°C), along with a set tested in air at RH 99%

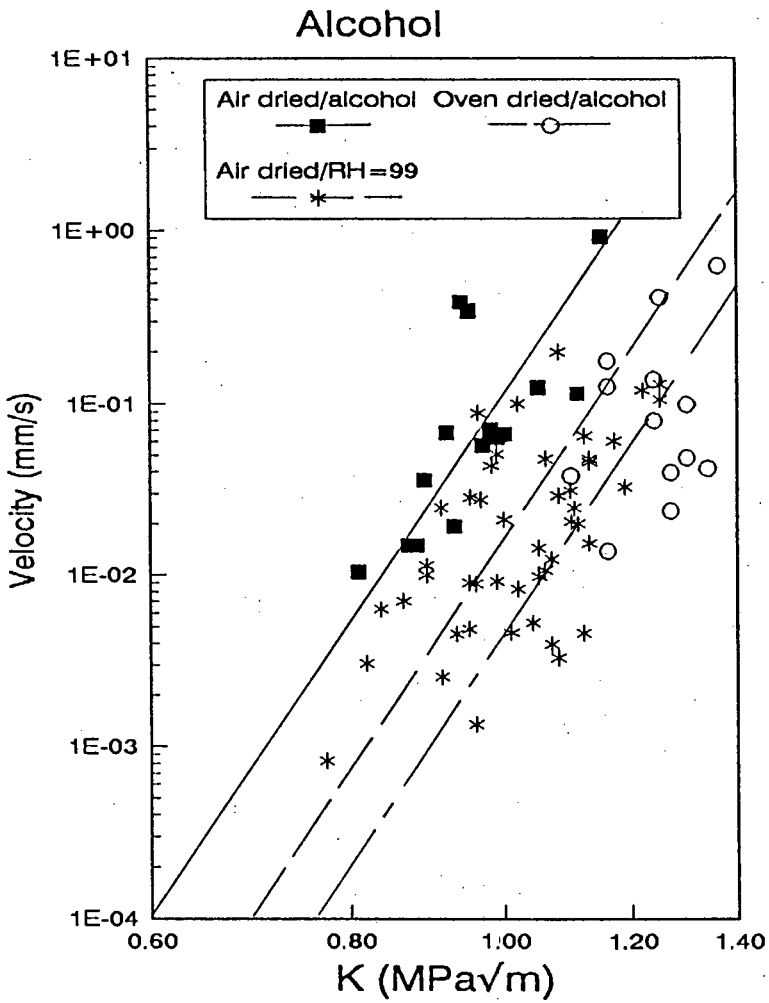

Figure 7.16: V-K plot for samples tested immersed in alcohol along with a set tested in air at RH 99%

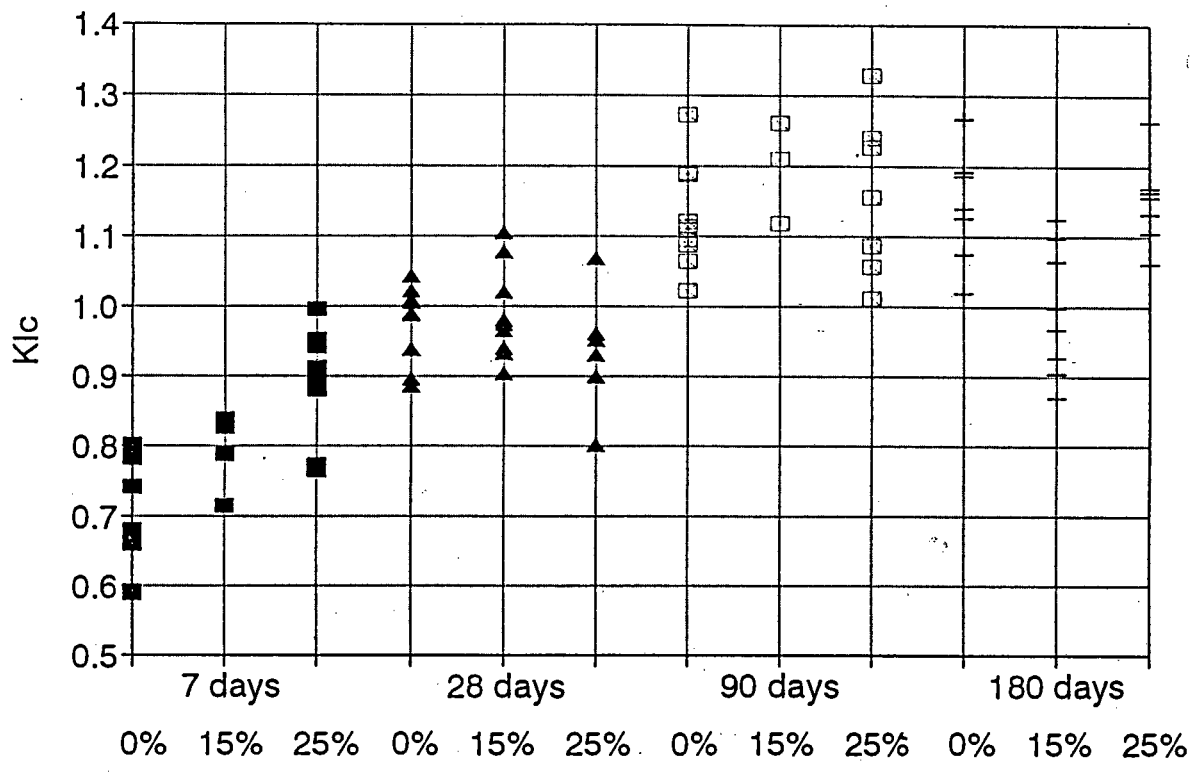

Figure 7.17: K_{Ic} values of samples with different fly ash contents tested at various ages

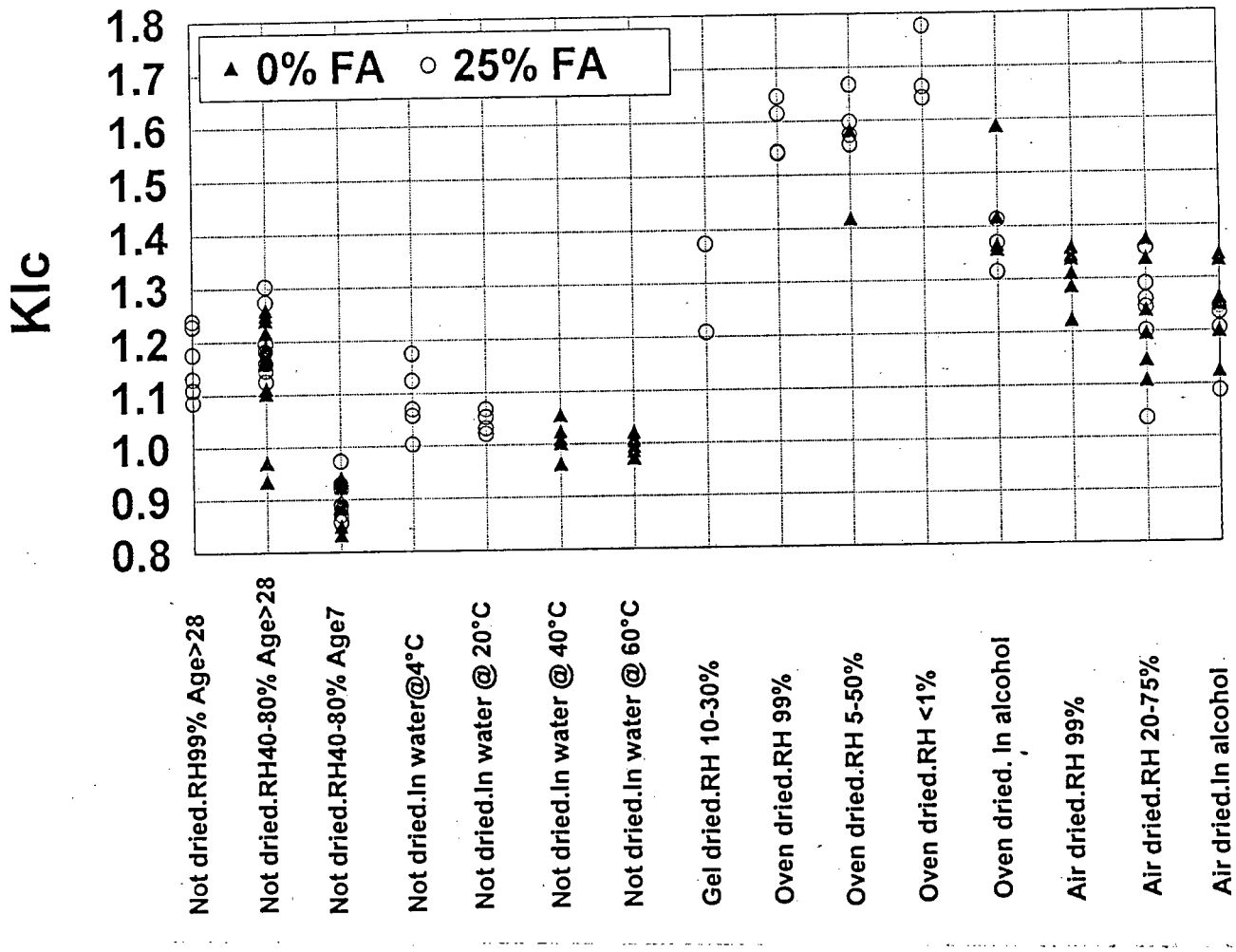

Figure 7.18: K_{Ic} values of samples tested under various environmental conditions

CHAPTER EIGHT - SCANNING ELECTRON MICROSCOPY

8.1 Introduction

An additional aspect to the work carried out in this project was a limited amount of scanning electron microscopy to try to observe the microstructural changes in the samples due to the different binders used, and how these affected physical properties as a function of continued hydration with time, and the loads applied.

This chapter presents a brief summary of some of the literature pertinent to the topic and a description of the work carried out. Notable points are identified in this chapter, whilst they are expanded in conjunction with the rest of the experimental observations in the discussion in Chapter 9.

8.2 Literature overview

Scanning electron and optical microscopes have long proved to be useful tools in the search to understand the microstructure and microstructural behaviour of materials containing portland cement.[8.1 - 8.6] Microscopy has assisted in improving understanding of hydration mechanisms as well as the forms of damage incurred in paste and the paste/aggregate interface under load. A selection of some of these findings are presented below.

Hardened cement paste

The process of cement hydration has been studied by several people using microscopy, including Jennings and Diamond.[8.5, 8.7]

Some of the notable features indicated by the published [8.5, 8.7, 8.8] micrographs include:

- The initial fibre like form of CSH gel forming radially out of the cement grains (type I) [8.1].

- The longer fibres which have branched and interlocked (type II).

- The almost featureless mass (type III) which is made up of rounded nodules fused together [8.5, 8.8]. It is not clear if the different types are developments, with time, from one to the other, although this would seem to be a reasonable supposition.

- The so-called Hadley grains with the potential flaw between the unhydrated particle (or later the dense (type IV) inner product) and the membrane, or simply hollow shells.[8.5, 8.7, 8.9]

- The increasing density of the HCP with time, with the associated reduction in the number and size of flaws.[8.5, 8.6]

- Hexagonal calcium hydroxide crystals, often interlayered with CSH gel.[8.1, 8.5]

- High concentrations of calcium hydroxide crystals and ettringite at the paste-aggregate interface, or debonding at the interface.[8.1, 8.4, 8.7]

The variation in the number of flaws and their sizes at various stages of hydration, as well as the structure of the CSH grains, will affect the toughness and the mechanical behaviour under load of the product. Some of the properties influenced include stiffness, damage accumulation and creep, as discussed in Section 9.3.

Fly ash

The reaction of fly ash particles within a hydrating cement paste have also been studied [8.3, 8.6, 8.9, 8.10] and the principal observations are summarised below.

There is little sign of the fly ash taking part in the chemical reactions at early ages, but only some light etching [8.9] or some deposition of duplex CSH gel on

the surface of the fly ash particles.[8.3] This film would have the effect of slowing or limiting the reaction of fly ash and appears to form a coating around the particles which debonds easily when loaded.[8.3, 8.9, 8.10] Even at reasonably high ages, it has been observed that there are some unreacted and only lightly etched fly ash particles as well as those that have reacted.[8.6, 8.9, 8.10]

Reacted and unreacted fly ash particles are often surrounded by, but not always bonded to, dense paste which includes a predominance of calcium hydroxide grains.[8.6, 8.9, 8.11, 8.12]

Ettringite fibres have been noted to develop within hollow fly ash particles,[8.12] which will have little effect on microcracking patterns but can be the subject of attractive micrographs (Figure 8.6).

Microcracking/toughness

The third part of the microstructural study of cementitious materials is the effect of loading on their microstructure. Some of the pertinent observations include:

- A zone of microcracking around the so-called crack tip can be observed. The size and orientation of these microcracks is dependant on the imposed stress field.[8.8, 8.13]

- The fracture plane is not strictly fractal in that it is not repeated at ever decreasing magnitudes.[8.2]

- The fracture plane of tougher mortars is smoother than that of less tough samples.[8.2]

- Cracks commonly branch,[8.4, 8.8] sometimes into two or more cracks that run parallel to each other, so absorbing energy and increasing toughness.

- Cracks are often not continuous, but appear to "jump".[8.13]

From optical microscopy it has also been shown that tensile cracks are not straight or continuous. Cracks have been reported [8.14] to go around aggregates in high strength concrete, but through them when loaded at a high strain rates. In similar concretes made with low-density aggregates, the cracks tended to go through the aggregate. This is probably a function of the ratio of aggregate to paste strengths. The shape of the aggregate was observed to cause an effect on crack patterns in that cracks were seen to go around rounded aggregate particles.[8.14]

In terms of the effect of fly ash on crack patterns, the most pertinent observation was that of Montgomery [8.11] that cracks tend to go round poorly bonded cenospheres, so causing branching and a probable increase in toughness. This is similar to the behaviour observed with rounded aggregate particles described above.

Summary

All of the above observations assist in building an explanation of the fracture behaviour of cementitious materials. The structure of hydrated cement paste, flaws within the gel and the apparent poor bond with fly ash particles all contribute to the fracture behaviour of a mortar or concrete. The fact that all of these properties change with time, mix proportions, curing and environment helps to contribute to the complexity of the issue. The implications of these properties are discussed in Chapter 9.

8.3 Experimental

In order to confirm the observations described above, some microscopy was carried out by the writer in two phases. The first phase was the imaging of a fly ash mix at various stages of reaction, and the second phase was double torsion testing within the SEM.

Fly ash

In this phase a sample of fly ash was glued to a mounting stub, gold-palladium coated and micrographed. Figure 8.1 shows a typical set of the types of particles in the sample including a plerosphere, several smooth glassy spheres and an amorphous particle.

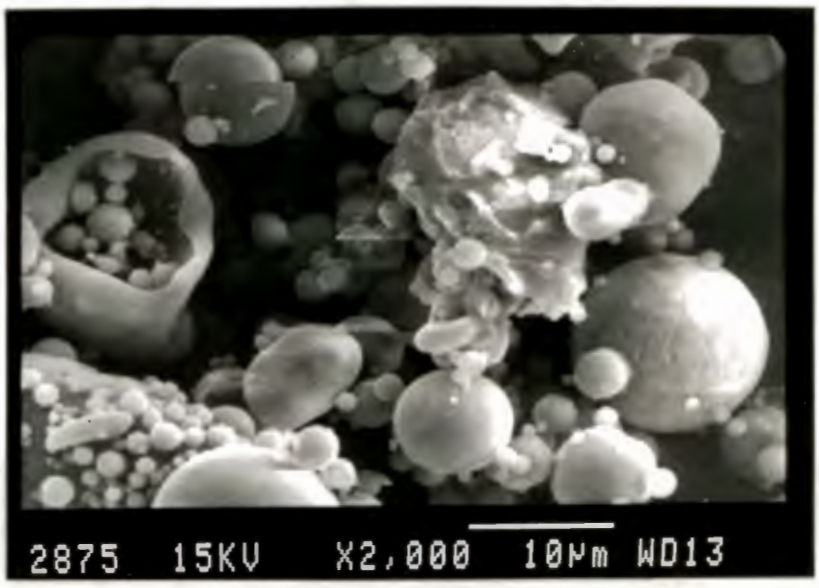

Figure 8.1: A typical view of the fly ash used in this study.

A one litre batch of the mix containing 25% fly ash as binder was then prepared and moulded in short lengths of 10-mm diameter plastic tubing. The samples were cured in water until tested. At the desired age, the samples were freeze dried by immersion in liquid nitrogen and exposure to vacuum. This was in order to remove free water and so stop the hydration process whilst minimising the amount of damage incurred in removing the water. They were then fractured, the fracture surface coated with gold-palladium and photographed in a Cambridge S180 scanning electron microscope.[8.6]

The micrographs (Figures 8.2 to 8.6) clearly show the development of hydration products, the increasing density of HCP and the increasing relative size of flaws induced by the fly ash compared with the rest of the paste.

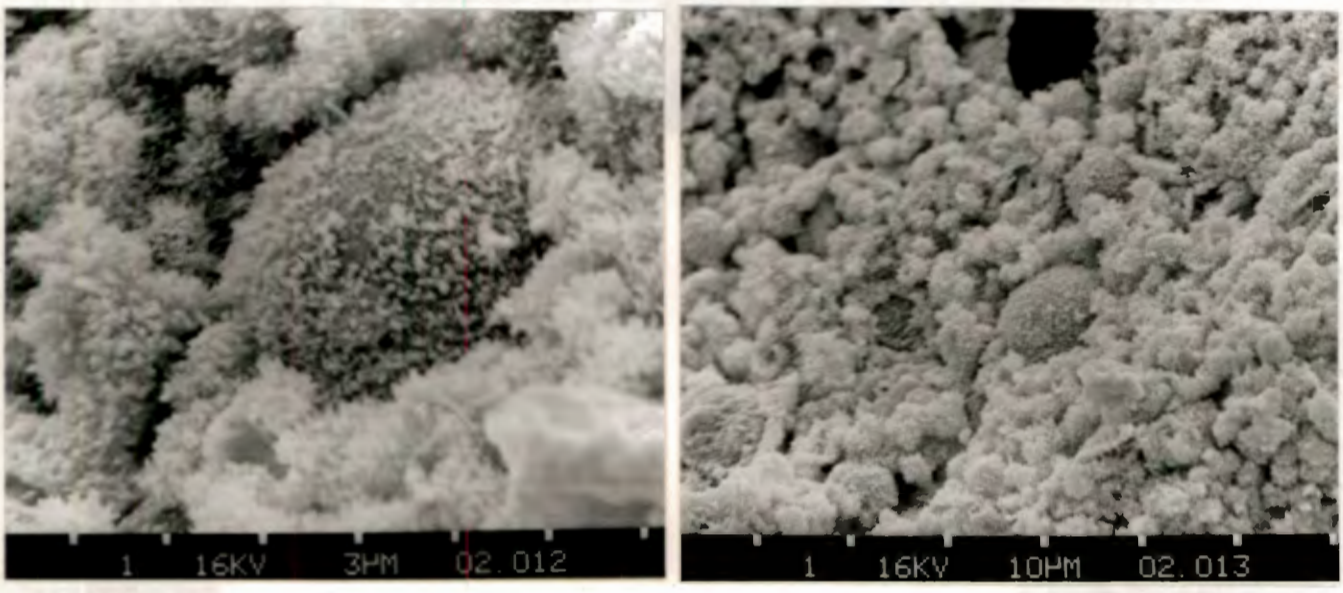

Figure 8.2: After 2 days of hydration the matrix is somewhat more dense and the hydration product on the particles surfaces is thicker

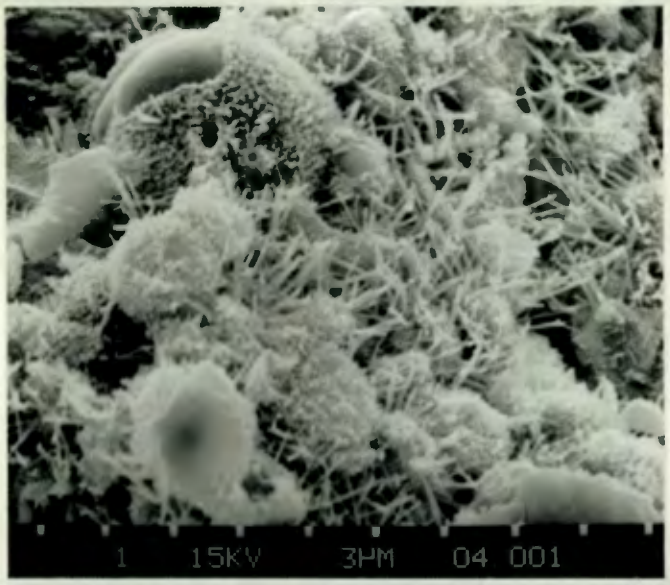

Figure 8.3: After 4 days of hydration long CSH fibres that are beginning to mesh together can be seen. The material on the large fly ash particle appears to have debonded cleanly, indicating that it was probably a deposit rather than a product of fly ash hydration

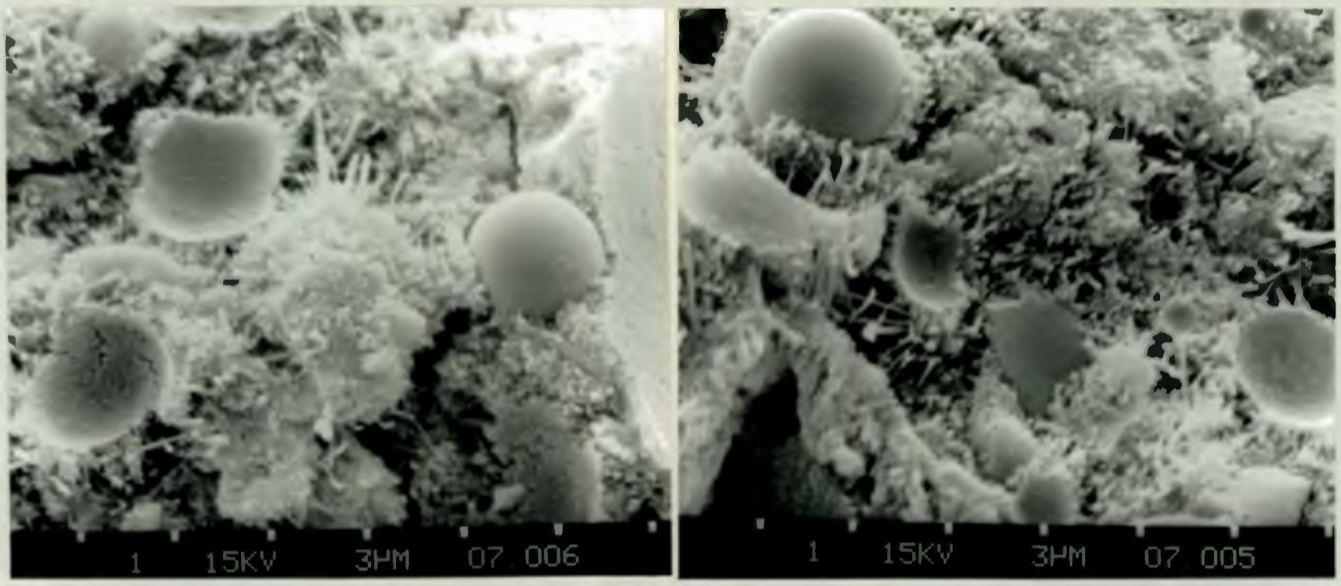

Figure 8.4: After 7 days of hydration the matrix is dense and relatively few individual gel fibres can be seen. The fly ash particle remaining in the sample appears to have debonded cleanly, although in the hollow where a particle has been removed there is evidence that some etching had occurred in the particle. The fibres that are visible appear to have been developing radially away from the fly ash particles

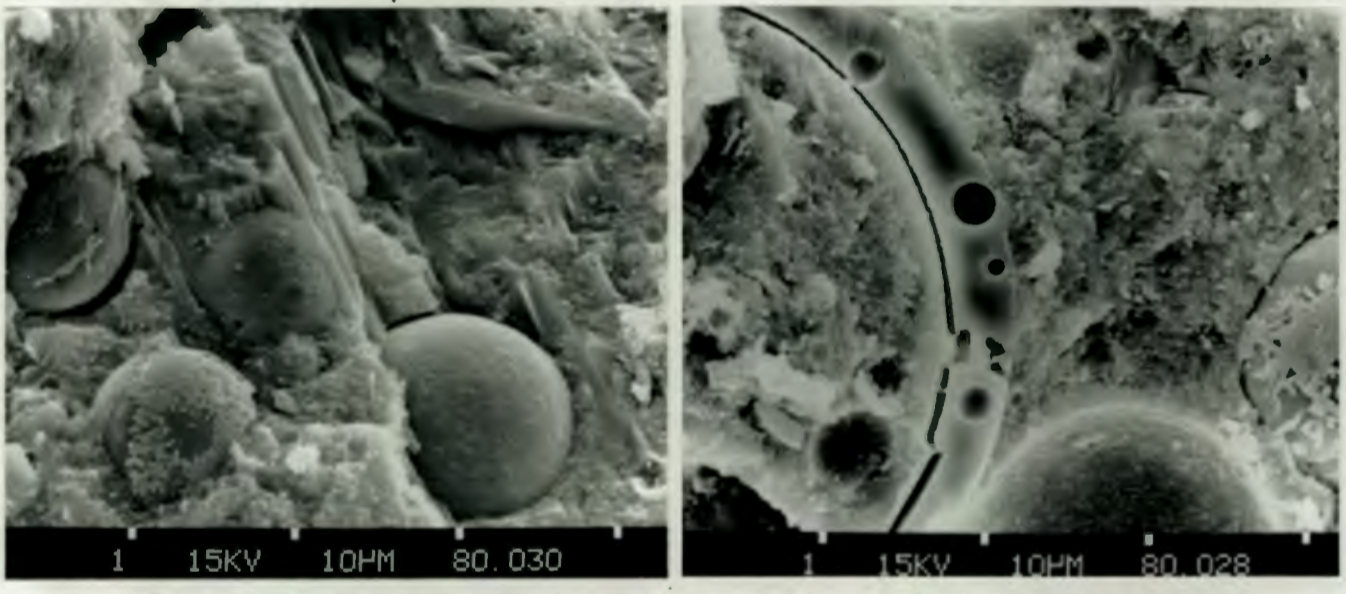

Figure 8.5: After 8 months the matrix is very dense with the fly ash particles firmly embedded within it. Calcium hydroxide crystals are clearly visible(b), as are signs of etching on the surfaces of the fly ash. The poor crack resistance of the product around the fly ash particles is shown by the debonding, which probably occurred when the sample was fractured

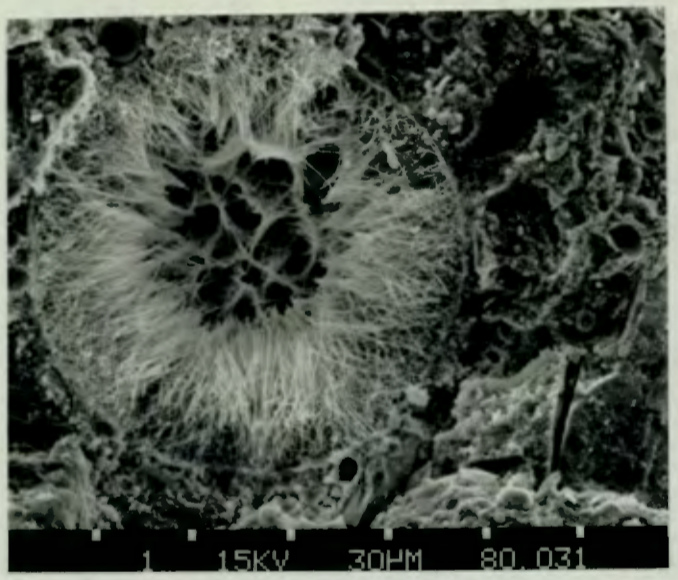

Figure 8.6: This micrograph shows a well bonded fly ash particle that has been split in two when the sample was fractured, with ettringite fibres that have developed within the hollow sphere

An overall impression gained from studying all of the micrographs was that the larger fly ash particles tended to be less reactive than the smaller. This is probably related to the different mineralogical composition of different sized particles.

In summary, with increasing time the HCP increases with density and the flaws within the gel reduce in size and number. Initially fly ash particles do not appear to react, although some hydration product is deposited on their surfaces. With time the smaller fly ash particles appear to be consumed or buried in the gel. The larger fly ash particles either do not react, or if they do react the reaction product does not bond well onto the original/remaining material. This means that the flaws introduced by the having the fly ash particles will probably play an increasing role in decreasing the toughness of the paste.

There are some well bonded larger fly ash particles, but not many. The presence of ettringite fibres within the particles similar to that described by Marusin [8.12] indicated that reaction of the fly ash had occurred.

Microcracking studies

A sample of the 25% fly ash mix was cast into a small block shaped like a bread loaf. This was cured for 28 days in water before being sliced using a fine geologist's diamond blade to form DT samples with dimensions 20x8x1. These were notched and polished in carborundum paste before being freeze dried as described above. The samples were then coated and kept in vacuum until tested.

The samples were tested in an in-situ DT rig built by Tait,[8.15] and loaded under increasing displacement control, whilst load versus deflection was plotted and the sample kept under observation and photographed (Figures 8.7 to 8.10).

These tests were not very successful from the point of view of double torsion testing. The cracks in all of the samples grew skew and constant stress intensity was not achieved. This also made photography difficult as it was impossible to assess which branch of the crack was going to be the predominant one.

The gel was very dense with no individual fibres or fly ash particles visible. One picture shows some small spherical particles, which may have been fly ash, adhering to the internal surface of an air bubble. It is possible that the individual structures and the fly ash particles were obscured or disguised in the polishing process.

A large amount of microcracking was observed, as well as crack splitting and jumping. There was also considerable debonding around the aggregates in the interfacial zone although some cracks went through aggregate particles rather than around them. The orientation of the individual microcracks had little relationship with the direction of the predominant crack - they were in all directions.

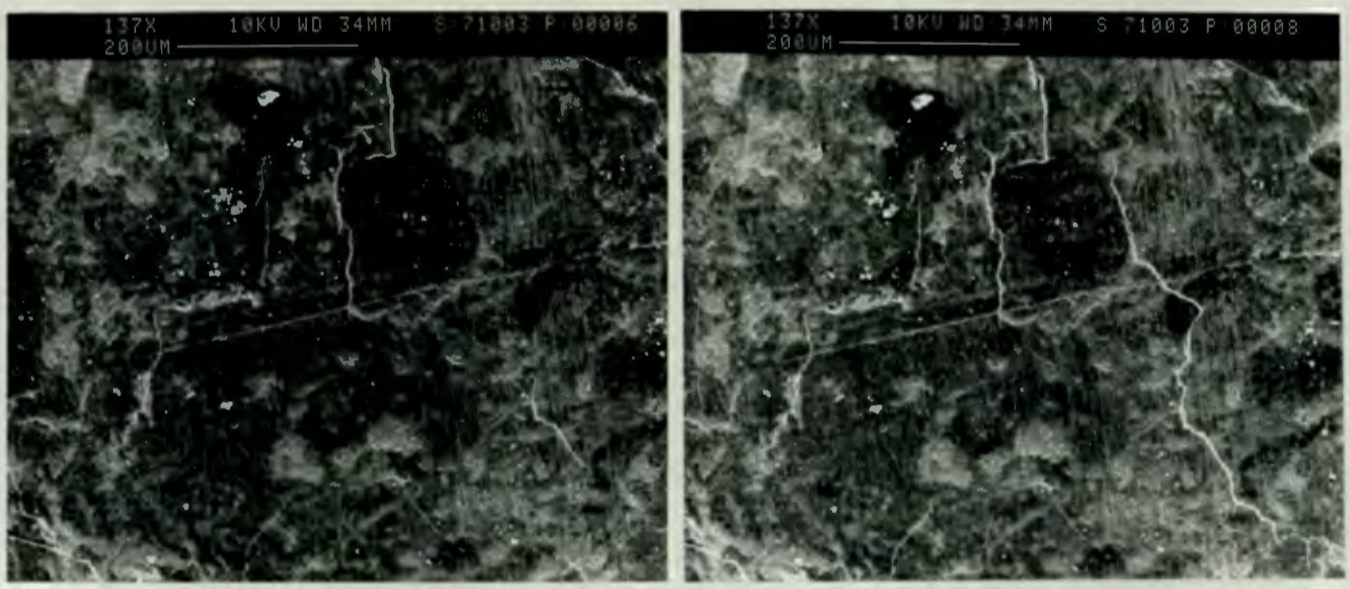

Figure 8.7: Two micrographs showing the development of a crack with increasing load. In the bottom right hand corner of (a) a short crack can be seen that is apparently not connected to that going around the sand particle. In the second image (b) the crack has grown back (main crack growth direction was from top to bottom) to join the other, but on the opposite side of the sand particle

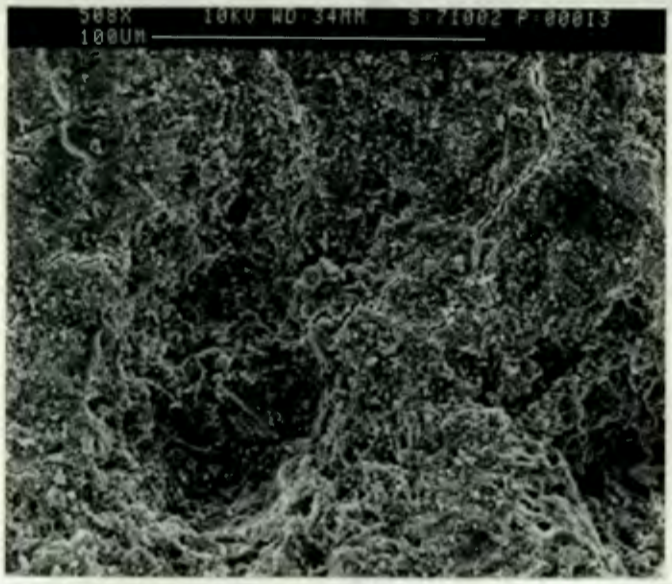

Figure 8.8: A bubble with small spherical particles inside which are probably fly ash. Note the microcracks running in all directions

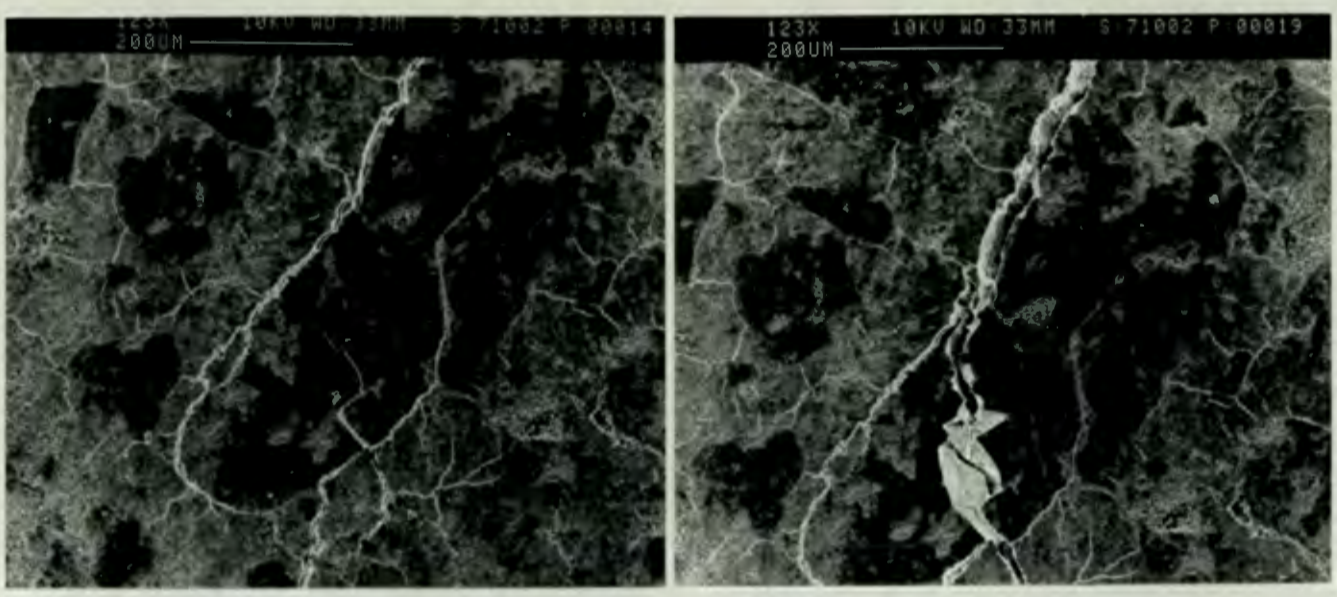

Figure 8.9: A pair of micrographs showing the progression of damage with increased load. In the first (a), the crack has gone around the interfacial zone of a large sand particle. In the second (b) the sand particle has split and the crack on the perimeter has closed slightly. Note the amount of debris that has fallen into the crack, providing potential material for wedging action on unloading

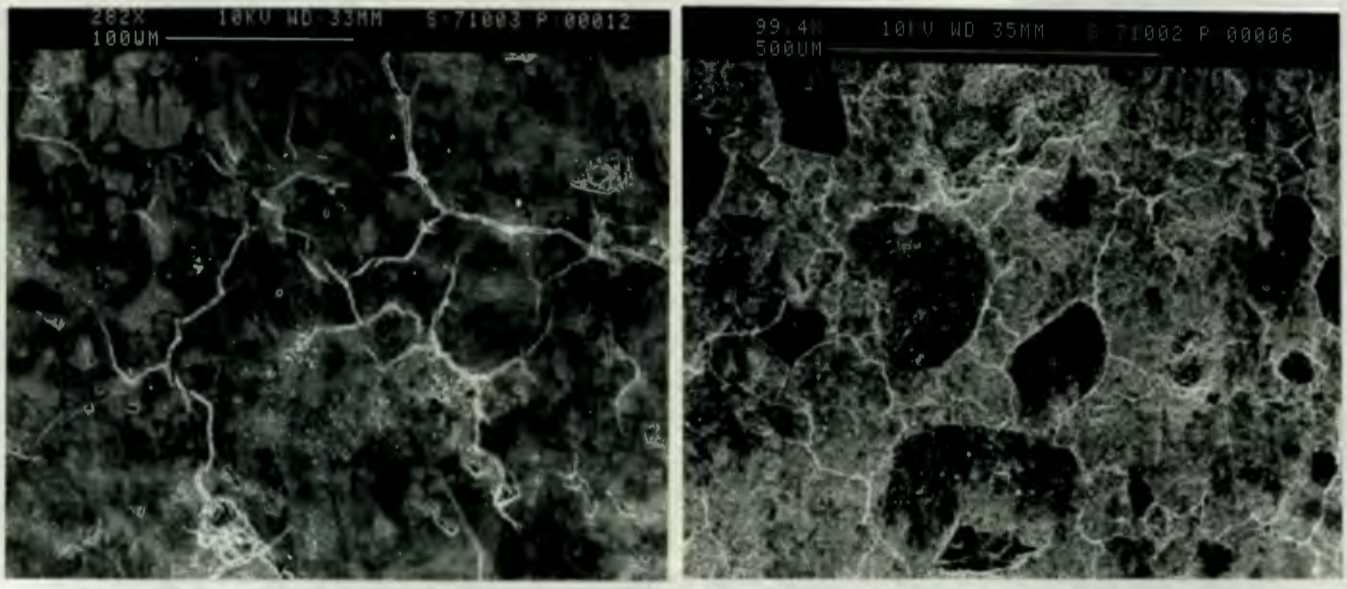

Figure 8.10: Two images from different samples showing the random direction of microcracking, the large number of discontinuous cracks, jumping and the predominance of cracks that have gone around the aggregate particles rather than through them. Such behaviour is not inconsistent with the concept of a process zone

The toughness (K_{Ic}) was determined as being 0,7 MPa$\sqrt{m}$ which was considerably lower than that of the full sized samples. There are two possible explanations for this. The aggregate size was large in relation to the thickness of the samples tested in the microscope. This would have the effect of lowering toughness as the interfacial zone around the larger aggregate pieces could be the full thickness of the sample, thus providing a short cut for the crack. The second cause could be the damage incurred in the sample in the preparation process.

8.4 Summary and discussion

The experimental observations were consistent with those reported in the literature, all of which help to explain the fracture behaviour of cementitious materials in that:

- at early ages the paste contains a large number of voids that decrease in number and size with continued hydration,

- large fly ash particles do not bond well with the paste, even after some reaction, but create round flaws that can effect toughness depending on their size in comparison with other flaws in the paste,

- microcracks in the paste are often discontinuous, multiple, within the interfacial zone with aggregate and seemingly random in direction,

- large cracks can contain debris which will cause further damage when the sample is unloaded.

The implications of these are discussed, in combination with the other experimental results, in the next chapter.

CHAPTER NINE - DISCUSSION

9.1 Introduction

This chapter discusses the implications and trends arising from the results presented in the previous three chapters. The discussion considers the present set of results in conjunction with those reported by other authors and leads to some conclusions about the fatigue behaviour and fracture mechanisms of cement mortar.

The chapter begins with an evaluation of the influences of fly ash content and specimen age on toughness and fatigue resistance, together with an attempt at a mechanistic explanation. This is followed by discussion on the effects of sample preparation and testing environment, followed by the loading effects. The chapter ends with a general discussion on the mechanisms of fatigue failure and the properties that affect toughness of cementitious materials.

9.2 Interpretation of results

As noted previously, there is a large amount of scatter inherent in the double torsion test method, particularly when used to evaluate non-homogenous materials such as cement mortars (see Section 4.4). Suresh has also noted[9.1] that the amount of scatter in brittle materials subject to cyclic stresses is considerable. These two effects together have led to a wide scatter that has made interpretation of the results difficult. It should also be noted that this technique uses relatively "large" specimens in a macrostructural system, thus making interpretation of microstructural effects an exercise to be approached with care.

The policy that has been adopted has been to compare on the various plots the positions of the various "clouds of data" with each other. In order to facilitate understanding, boundaries have been drawn around the clouds. In some cases the differences between these clouds have been of sufficient magnitude that it has been possible to infer that one set is distinct from another (bearing in mind

the extent of the scatter). In other cases the differences have been small enough to leave room for doubt about changes in behaviour due to the changing parameters.

A cloud of data on a V-K plot that is above and to the left of another may be considered to exhibit less resistance to fatigue damage in that for a given applied stress intensity, a higher crack velocity has been indicated.

Best fit lines based on least squares calculations for scatter in the Y direction have been shown on selected plots (eg Figure 7.15). However the correlation coefficients of these lines are poor, hence trend interpretation is generally better served using the "cloud of data" approach.

In following this approach, a different parameter is effectively being evaluated from that used by others. If the best fit line is described by the equation:

$$V = \mathbf{A}K^{\mathbf{n}}$$

then **A** and **n** are the material parameters to be compared. Traditionally it has been the slope of the line **n** (on a log-log scale) that has been the subject of discussion. If the position of clouds is the point of departure, then it is the parameter A that is being compared.

The determination of **n** for the present data can be carried out in different ways. If a least squares approach is considered, the line shown in Figure 9.1, for example, is obtained with a corresponding **n** value of 9. For the same data, a line drawn by eye through the cloud of data has an **n** value of 20.

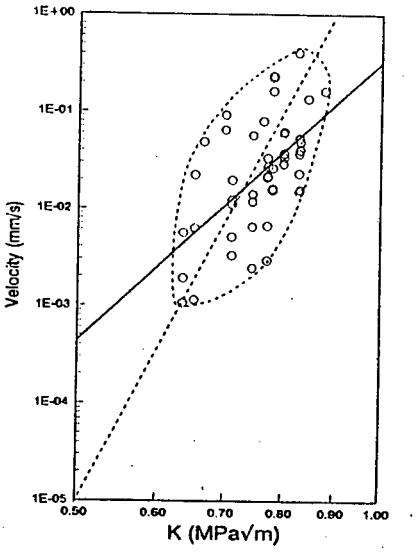

Figure 9.1: A V-K plot showing a typical set of results along with the least squares best fit line (solid) and the "eyeball" best fit line (dashed)

The justification for this latter approach is that there is scatter in both the X and Y directions. It is reasonable then that a better estimate of the true position of the mean line would be obtained by considering that which passes through the "centre of gravity" of the data points with a direction such that the "second moment of area" of the cloud is minimised. This approach has been used before in double torsion work.[9.2]

For the present work the **n** values obtained using the least squares approach were between 5 and 15 with an average of approximately 10. If the "eyeball" approach were used the **n** values would range from 15 - 25 with a mean of 20. These latter values are similar to those reported by Tait (26)[9.3] and Bazant (24)[9.4] for similar materials. Figure 9.2 showing typical sets of results from the different studies illustrates the above. It is also quite possible that the **n** value

varies with material composition and toughness and this aspect should be investigated in future work.

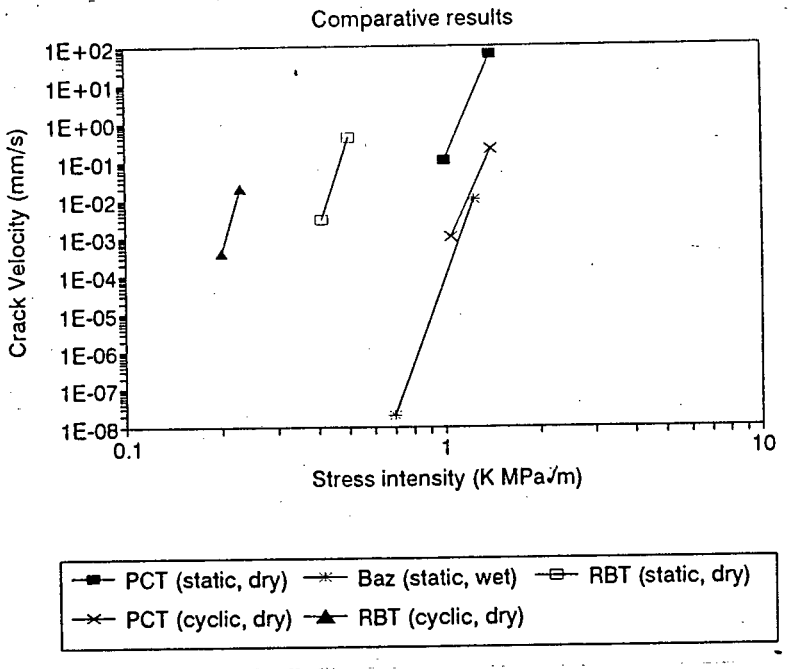

Figure 9.2: A V-K plot showing typical sets of results as reported by Tait and Bazant with those from the present study superimposed

9.3 Materials and environment

In this section the implications of the results presented in Chapter 7 are discussed with particular reference to the influence on fatigue crack growth of materials related effects within and external to, the samples.

9.3.1 Fly ash content and sample age

In this section the effects of fly ash content and sample age have been summarised from the results in terms of strength, fatigue resistance and toughness. The mechanisms for the observed effects are then discussed.

Strength

The compressive cube strengths of the three mixes were similar at seven days (Figure 7.1), whilst the greater the fly ash content the greater the strength at

higher ages. This is in accordance with reported trends as discussed in Section 2.3.4.

Fatigue

For the samples tested at an age of seven days, those containing fly ash exhibited a marginally slower crack growth rate than those with no fly ash (Figure 7.5). At 28 days there did not appear to be any significant difference between the sets, whilst at 90 and 180 days the fly ash seemed to have a slight detrimental effect (Figures 7.6 to 7.8). This is in agreement with work reported by Tait.[9.5]

For the 0 and 15% fly ash contents, there was a distinct improvement between 7 and 28 days and little or no change between the results for 28, 90 and 180 days. That is, the 7 day data cloud is distinctly to the left and above the rest of the data in Figures 7.2 to 7.4, which represents a reduction of crack velocity for a given applied stress intensity. There was little effect of time apparent in the fatigue resistance of the 25% mix.

Toughness

The trends observed in the V-K plots for fatigue resistance described above were largely the same as those in the recorded values of toughness (K_{Ic}) as shown in Figure 7.17.

There was a general increase in toughness with increasing fly ash content at 7 and 28 days but little effect of fly ash content at 90 and 180 days. With increasing age the toughness of all of the mixes increased with increasing hydration up to 90 days with little change between 90 and 180 days.

Discussion

It has been noted that there was a closing up of differences in fatigue results when the data was normalised as K_{rel} plots. This, and the similar trends observed in fatigue resistance and toughness, indicate that the fatigue

characteristics of the family of materials tested in this thesis are broadly related to its toughness when considering variations due to age and fly ash content.

It can also be seen from Figure 9.3 that at young ages cube strengths are independent of, but toughness varies with, changing fly ash content. However, at greater ages toughness is largely independent of, but strength varies with, fly ash content. This supports the contention that strength and toughness are not necessarily related for a given material.

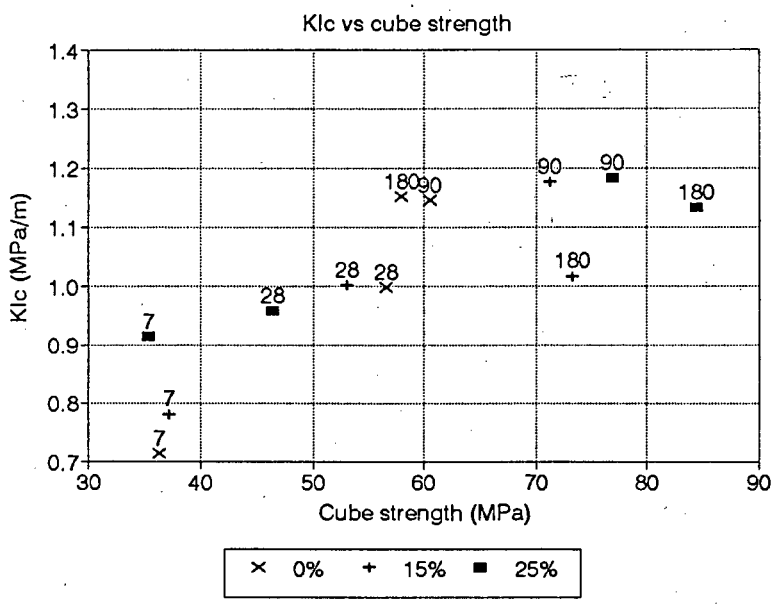

Figure 9.3: A plot showing some K_{Ic} results against their respective cube strengths.

As noted above, increasing fly ash content is beneficial to fatigue and toughness at early ages but slightly detrimental to fatigue resistance at greater ages (particularly if normalised against compressive strength). The cause of this behaviour is probably associated with the size and shape of the fly ash particles in relation to the size and shape of other flaws in the matrix as discussed below.

It has been established that the fly ash particles (particularly the larger ones) do not hydrate appreciably at an early age (Chapter 8), thus resulting in poor bond between the larger fly ash particles and the rest of the gel. At early ages,

the size of the particles (and their associated flaws) is of the same order of magnitude as the other flaws in the paste, therefore they do not further reduce toughness to any marked degree. However, the shape of the fly ash flaw is such that a crack is impeded because the radius of the crack tip around the fly ash particle is large. Cracks have been observed to go around such flaws before being forced to split or stop, thus effectively toughening the material as shown in Chapter 8.

The reduction in fatigue resistance with increasing fly ash content at greater ages is probably because many of the flaws in the paste reduce in number and magnitude with continued hydration, whilst those caused by the presence of large fly ash particles remain similar in size. These flaws therefore become **relatively** more significant and effectively reduce fatigue resistance when compared with the matrix without fly ash.

This concept of the relative importance (flaw magnitude and grain orientation) of the microstructure at the crack tip in influencing macro behaviour has similarly been expressed for metals by Miller [9.6].

There is a reported influence on fracture behaviour of cementitious materials due to the interfacial zone between paste and aggregate which may be modified by the presence of fly ash.[9.7] However, any beneficial influence of the very small fly ash particles reducing the effects of the interfacial zone appears to have been masked, in this case, by the deleterious influence of the larger, less reactive, fly ash particles.

9.3.2 Sample preparation and testing environment

In this section the effects of sample preparation and drying are discussed, along with the changes in fatigue behaviour observed when the samples were exposed to different environmental conditions.

Sample preparation

As discussed in Section 3.2.4, fatigue crack growth rates normally slow down in samples that have been dried compared with those kept wet. Similar behaviour is shown in Figures 7.13 and 7.14 in which the fatigue crack growth rate was lower in oven dried samples than those dried in air, which in turn was slower than that in un-dried (wet) samples.

In terms of toughness, it can be seen from Figure 7.18 that samples that were not dried were less tough than those that were dried, while air dried samples were less tough than those that were oven dried. This toughness behaviour is consistent with the fatigue crack growth behaviour described above.

These trends may be partially accounted for by the relative drying effects of the different methods (in that oven drying removes more water than air drying), coupled with the supposition that the mechanism may be dependent on the amount of water present.

There is also the complicating issue of the damage incurred in the matrix by the drying action which would effectively reduce toughness. The author has shown in another study[9.8] that cubes dried at 50°C, and tested in compression after resoaking, were less strong than those not dried. However those dried and tested only surface wet were considerably stronger than the permanently wet samples. The drying appeared to cause irreversible damage, whilst the presence of water reintroduced into the sample reduced strength.

Ballim and Parrot have also shown that the method of drying has a distinct effect on concrete samples used for durability index tests.[9.9, 9.10, 9.11] The cause of this effect is thought to be due to the formation of extensive microcracking at gel pore level when water is extracted from the gel, particularly water that may have been securely adsorbed onto the gel pore surfaces or loosely chemically bound into the CSH gel.[9.12, 9.13]

In summary: despite the damage incurred by drying, the absence of water from a matrix causes dry specimens to be tougher and more fatigue resistant than wetter samples. This indicates that the mechanism is strongly dependent on the presence of water, and may be associated with environmentally assisted cracking[9.14] and/or activation energy requirements.[9.15] This is discussed further in Section 9.5.

It is not only water from within the sample, but also that in the surrounding environment which will influence behaviour. This topic has been addressed in the following sections which examine the effects of relative humidity, as well as the type of fluids in submerged samples.

Relative humidity

Figures 7.10 to 7.12 show the effects on fatigue resistance of relative humidity (RH) on samples that were subjected to different preparation methods. Together, the figures do not show any clear **trend** due to changing humidity and the results for the oven dried samples (Figure 7.10) show a trend that changes direction with increasing RH.

In terms of toughness (Figure 7.18), the oven dried samples were sensitive to RH in that those tested at 0% appeared to be tougher than those at higher humidities. Wet samples did not show any significant effect of RH on toughness at the high RH values tested.

The sets of samples were prepared over a period of several months, in which time the ambient relative humidity changed from approximately 60 - 70% in the wet season to 30 - 40% in the dry season. This would have had some masking influence on the samples, particularly those that had been air dried.

Beaudoin has published a figure showing the influence of RH in a plot of stress intensity versus porosity (Figure 9.4). This has indicated that varying RH does not result in simple relationships or trends.[9.13, 9.16] Beaudoin has also noted[9.17]

that the RH at the crack tip of a "large" mortar specimen is likely to be different from that at a point remote from the crack tip. This means that despite controlling the RH in a glove box, the environment influencing crack growth rates is probably still unknown.

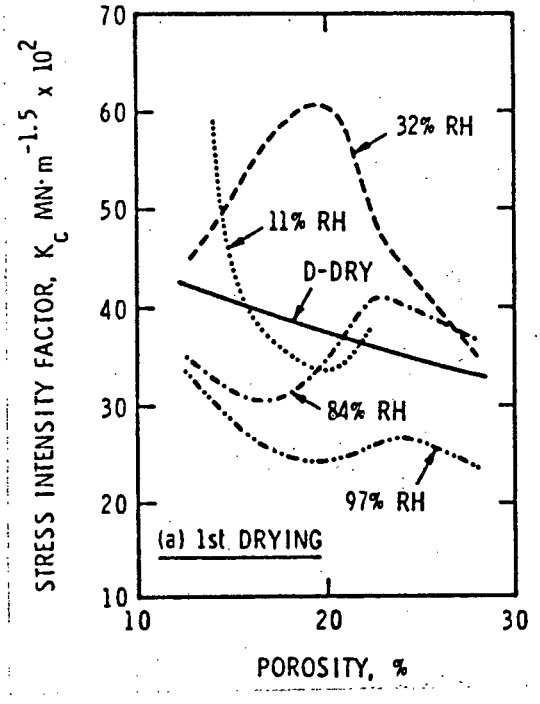

Figure 9.4: A plot of stress intensity vs porosity for families of RH[9.16]

However, it is reasonable to state that the amount of moisture external to the material at the crack tip, as well as the degree of wetness of the material (ie water adsorbed on the surface of the gel as well as contained in the capillaries) and the pore structure of the material at the crack tip are all critical in governing crack growth behaviour. These properties will vary with the different material phases at a microstructural level as well as with time, thus making measurement of the behaviour difficult to assess using specimens that are orders of magnitude larger that the zone of interest. This concept is discussed further in Section 9.5.

Fluids and temperature

From Figure 7.15, it can be seen that for the samples that were not dried before being tested in water, increasing water temperature resulted in increased fatigue crack velocity. This would be expected of an environmentally assisted

cracking (EAC) mechanism in which increasing temperature would promote chemical attack of stressed elements by providing some of the activation energy required. The activation energy for EAC cracking of the mortar was calculated as approximately 31 ± 5 kJ/mol using the equation given below and the results from Figure 7.15. This figure is of the same order of magnitude as that reported by Tait.[9.3]

$$V = A_o \exp(-\frac{\Delta H}{RT})\ K_I^{\ n} \quad \ldots\ldots\ldots\ldots\ldots\ldots\ldots\ldots\ldots\ldots\ldots\ldots \quad (9.1)$$

where V = crack velocity
A_o = a material constant
ΔH = Activation energy
R = Gas constant
T = temperature (°K)
K_I = stress intensity
n = slope of the V-K plot

Turning to those samples that were tested in alcohol, it should be noted that these had been dried whilst those tested in water had not. Therefore, to facilitate comparison between the alcohol and water tests, the results of a set of wet samples tested at high RH have been included in the water plot, and air dried samples tested at high RH included in the alcohol plot (Figure 7.16) to act as a basis of comparison.

In the case of the water plot (Figure 7.15), the immersed samples at 20°C exhibited fatigue crack velocities less than one order of magnitude higher than those in high RH air. The air dried samples tested in alcohol (Figure 7.16) had velocities somewhat more than one order of magnitude higher than the air dried high RH samples. It is reported that alcohol has little if any effect on the bulk properties of cementitious materials.[9.18, 9.19] However the above results indicate that the alcohol probably promoted cracking slightly more readily than water, even though the effect is small.

In terms of toughness (Figure 7.18), the wet samples were sensitive to temperature, with toughness decreasing with increasing temperature. Samples tested in alcohol were less tough than in those tested in high RH for both oven and air dried cases. Undried samples tested in water were also less tough than similar samples tested at high RH, by a similar amount. This indicates that the small effect of the alcohol may possibly be related to the cyclic loading rather than a chemical effect.

The influence of alcohol on the fatigue results may be connected to the relative moisture content of the dried samples. Air dried samples probably still contained some water, and so alcohol was prevented from entering the smaller capillaries. However the oven dried (and so dryer) samples would have allowed the alcohol, with its lower surface tension, to get into pores inaccessible to water. This means that the damage accumulation in fatigue due to wedging action[9.3] may have been greater in the oven dried, alcohol immersed samples than in others.

Comparative tests need to be carried out with the samples subjected to the same preparation methods and then immersed in alcohol, water and other fluids with strong hydroxyl ion concentrations or high dielectric constants.

9.3.3 Summary

As noted in most of the above discussion, there is an apparent relationship between fatigue resistance and toughness for the materials tested.

The effects of fly ash and age point to the increasing toughness of mortar with increasing age and the toughening effect of fly ash particles at young ages when they are the same size as the rest of the flaws in the matrix, probably due to their shape. In addition, they appear to result in a detrimental effect when they are relatively large with respect to the other matrix flaws at greater ages.

The effects of preparation, RH, temperature and fluid type point to fluid dependant mechanisms such as EAC and wedging, amongst others, in the fatigue of mortars. These mechanisms are studied more closely in the next section by looking at the results of loading parameter tests and discussing them in relation to V-K (EAC) or Paris (plasticity) models.

9.4 Loading parameters

9.4.1 Introduction

As discussed in Chapter 3, two models are presently used to describe fatigue behaviour of materials using fracture mechanics parameters. One is the empirically derived Paris equation which is used to describe the behaviour of metals subject to plasticity controlled mechanisms.[9.20, 9.21] The other model is the V-K plot for brittle materials including ceramics and to a lesser extent cementitious materials which are subject to environmentally assisted cracking (EAC).[9.3, 9.22]

There is some question as to which of these relationships is more applicable to cementitious materials. The following sections address this topic with particular reference to the experimental results reported in Chapters 6 and 7.

The next two sections look at the measured effects of cyclic frequency and amplitude and compare the observed trends with those that would be expected from the two models as discussed in Chapter 3. Figures of the trends to be expected under each model are presented in order to facilitate comparison with the experimental results.

9.4.2 Cyclic frequency

Part of the discussion about whether mortars and other cementitious materials behave in a manner consistent with the Paris or the V-K approaches hinges on the effect of cyclic frequency. This section compares the type of behaviour to be expected of materials perfectly complying with these two mechanisms, with the observed behaviour.

Paris model

For the Paris relationship, the rate of crack growth (per unit cycle) is described as being independent of cyclic frequency for stage B (Figure 3.16). If a mechanism was purely controlled by a plasticity mechanism, a plot of the relevant portion of da/dn vs ΔK for families of different frequencies would appear as shown in Figure 9.5 with little separation apparent between the data sets.

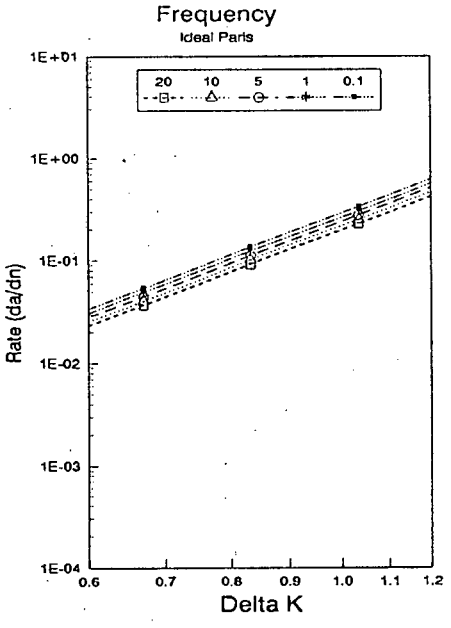

Figure 9.5: da/dn vs ΔK for ideal plasticity (Paris) behaviour. The lines at different frequencies effectively occur on the same line, with minimal separation

If the **same** data were to be presented on a V-K plot (where V = da/dt), then it would be expected that a sensitivity to frequency would appear as shown in Figure 9.6, ie a marked separation would appear between the data sets. Where growth per cycle is constant and cycles per second (frequency) is increased, then growth per second would be expected to increase.

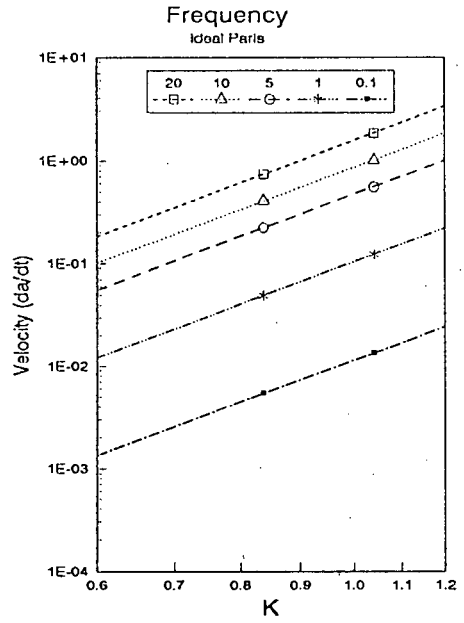

Figure 9.6: V vs K for ideal plasticity (Paris) behaviour.

V-K relationship

In the case of the V-K model the rate of crack growth (per unit time) is said to be independent of cyclic frequency (see Section 3.3.3). If it is assumed that there is sufficient time for transportation of reagents and corrosion products to and from the crack tip, plots of V vs K and da/dn vs ΔK for families of different frequencies would appear as shown in Figure 9.7, with the data appearing to be bunched in the V-K plot and separated in the da/dn-ΔK plot.

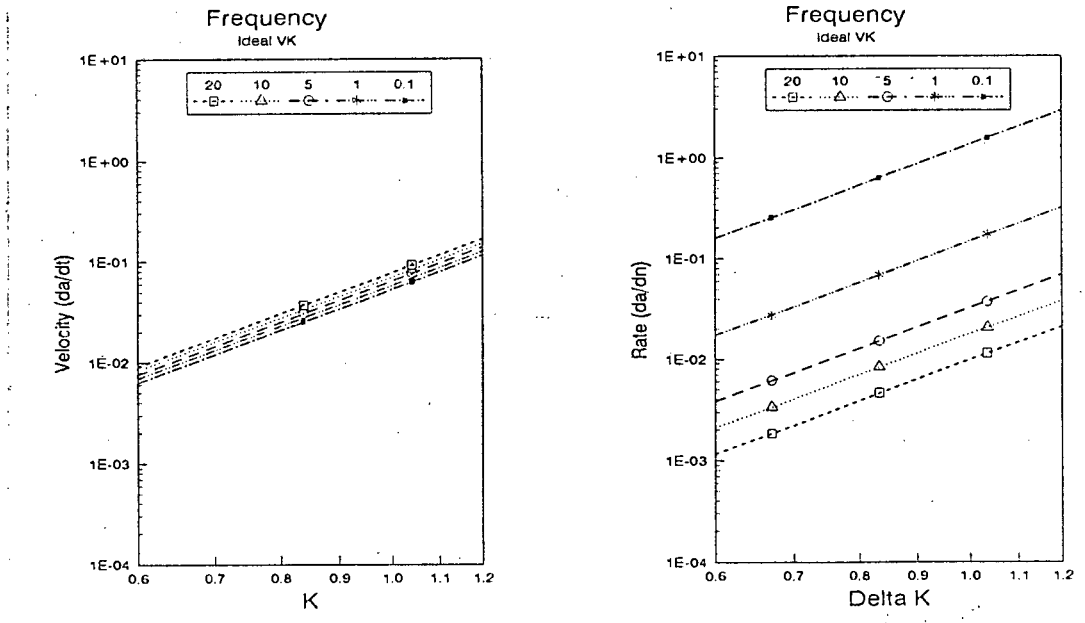

Figure 9.7: V vs K and da/dn vs ΔK plots of the same data for ideal EAC (V-K) behaviour

Results

The plots given in Chapter six (Figures 6.4 and 6.5) showing the results of the tests carried out in this study are presented again in summarised form in Figure 9.8 (a and b), represented here as lines for clarity.

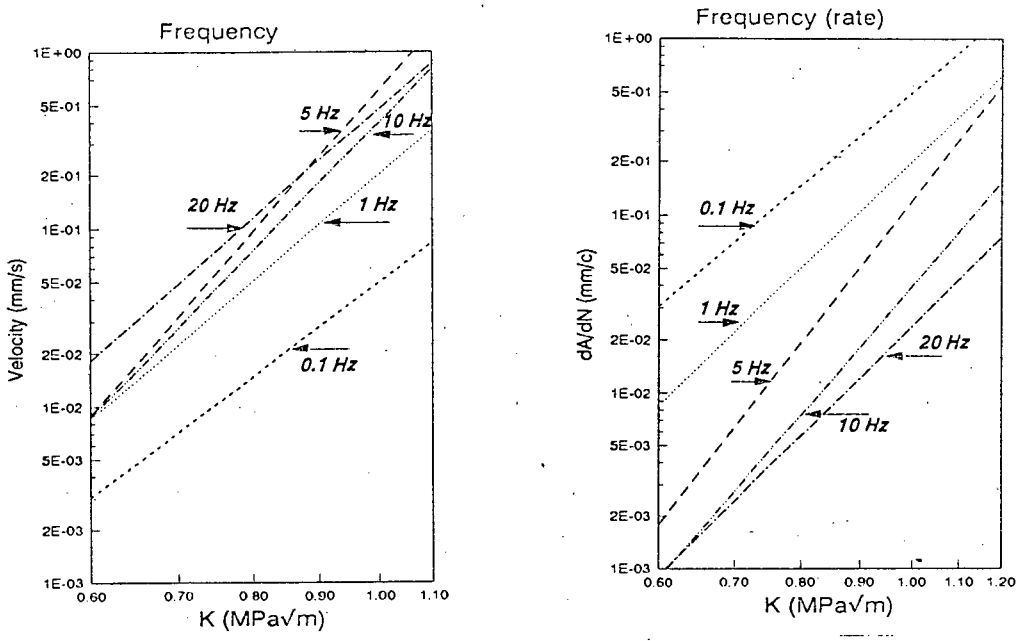

Figure 9.8: Experimental results presented as V-K and da/dn-K plots

In comparing Figures 9.5 to 9.7 with 9.8 It can be seen that the mortar tested in this study did not behave in conformance with either the pure Paris, or pure V-K models.

In the V-K plot (Figure 9.8a), frequencies between 1 and 20 Hz are effectively bunched into a single zone as expected in a V-K model (Figure 9.7a). While there are small separations between them, there is no general trend, and this is not likely to be significant bearing in mind the range of scatter. The 0,1 Hz line, on the other hand, is distinctly separate with a slower crack velocity for a given applied stress intensity; as would be expected in a Paris model (Figure 9.5).

If the Paris model were to be completely applicable, then there should be more separation of the lines for frequencies 1, 5, 10 and 20 Hz than was the case.

It still appears that the dominant mechanism is V-K controlled because of the bunching of the frequencies, with the exception of 0.1 Hz.

It is also possible that there may be some form of transport limitation in the V-K type EAC mechanism to explain the separation of the 0,1 Hz line. Normally, discussions about transport limitations refer to insufficient aggressive species being able to reach the stressed crack tip (and this may be related to inadequate time at high frequencies). The effect is that increased stress (and stress intensity) does not lead to increased crack growth rate at this plateau condition. However, this does not appear to have occurred in the range of frequencies tested in this study. At very low frequencies it may also be possible that reagents within the fluid pumped into the crack tip by the fatigue action are fully consumed or neutralised some time before the cycle is completed. This would mean that there is a period of time before they are replaced in the next cycle in which little or no EAC can occur. This would effectively slow crack growth dominated by EAC mechanisms at low frequencies, and could possibly explain the position of the 0,1 Hz data set in Figure 9.8a.

On the other hand, if hydrowedging were to be considered as a contributing mechanism, then the stresses at the crack tip due to this mechanism would also be dependant on frequency.[9.3] At low frequency, fluid flow under a slowly closing crack would be unimpeded and crack tip stresses low, but at higher frequencies stresses due to hydrowedging would be greater. It may well be that at 0.1 Hz in the present tests, any hydrowedging contribution was very much less than that at high frequencies.

It was not possible to carry out tests at frequencies lower than 0,1 Hz to see if the trend continued due to the limitations of the signal generator available, but it would be worth pursuing this concept in future work.

In summary, it appears that the fatigue behaviour is dominated by the V-K model, but with a possible element of Paris type behaviour occurring. The

comparison between the two models will be discussed further in the next section which looks at the amplitude results.

9.4.3 Load amplitude

The other aspect to the discussion regarding V-K or Paris is the effect of load amplitude on crack velocity; that is to look at the X axis parameters, as opposed to the Y-axis parameters discussed so far.

It can be observed from the normalised K_{rel} plots of Chapter 6 that the K_{rel} values were all above 60%. This could be interpreted as an apparent fatigue limit. That is, below a given applied peak stress intensity of $K_{max} \approx 60\%\ K_{Ic}$, there was no **observable** crack growth. It is possible that this is due to the relatively limited size and form of the stress field in the double torsion test, and that tests did not go beyond a few thousand cycles. The small stress field, combined with crack shielding of the multiple crack tips in the process zone would result in the stress intensity at all of the crack tips being less than critical and crack growth would effectively stop. This is in contrast to the stress distribution in other test configurations which is generally over a greater area, and so across more flaws that have the potential to be critical, so leading to the reported absence of fatigue limit in cementitious materials.

Paris relationship

For materials that behave according to the Paris model in fatigue loading, the cyclic stress intensity **amplitude** is reported to be the dominant factor rather than the magnitude of K_{max} (see Chapter 3). To illustrate this effect, the test programme of the relative amplitude effect as described in Section 6.4 has been described in terms of a bar chart showing K_{max} and K_{min} in Figure 9.9. If the fatigue crack results were consistent with pure Paris behaviour, then the theoretical da/dn vs ΔK plot for families of constant K_{max} would be as shown in Figure 9.10a. This theoretical position can also be processed as a V-K plot (but still showing pure Paris mechanistic behaviour) and presented as families of constant amplitude, normalised with respect to K_{max} in Figure 9.10b.

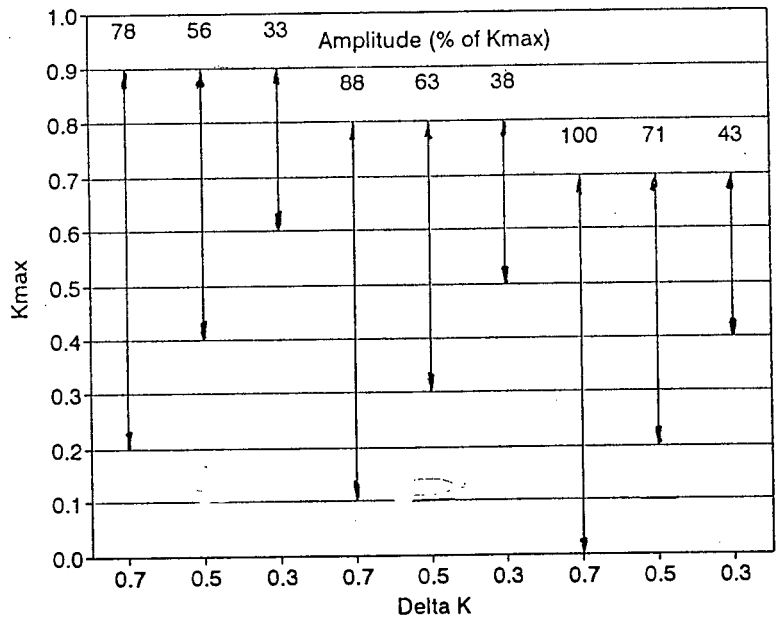

Figure 9.9: Bar chart describing the cyclic load ranges in terms of K_{max}, K_{min}, amplitude and ΔK

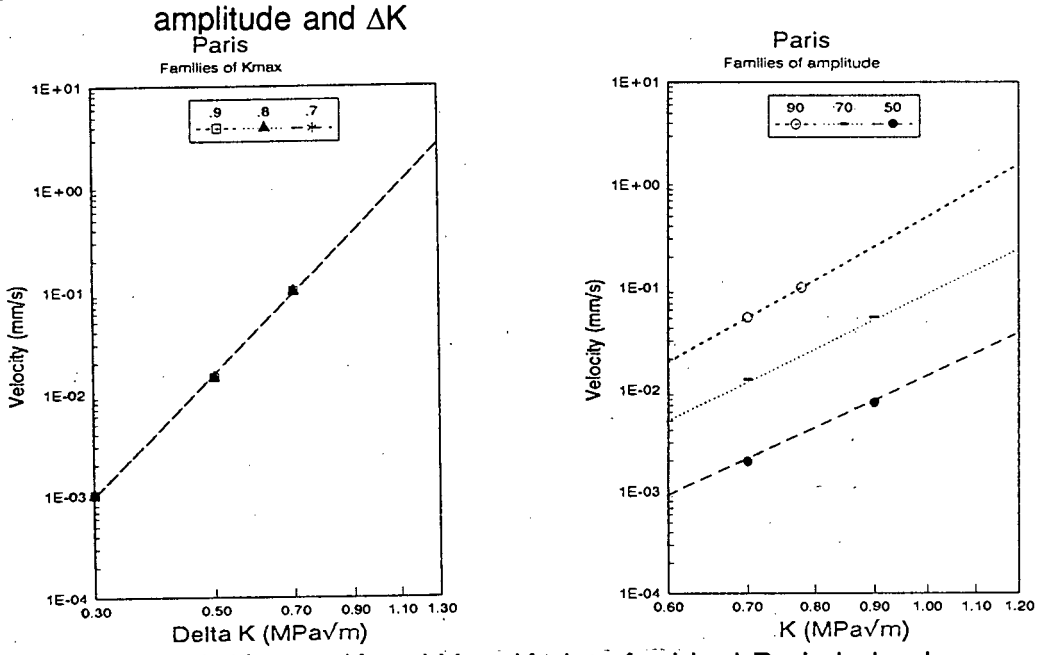

Figure 9.10: da/dn vs ΔK and V vs K plots for ideal Paris behaviour

V-K relationship

Conversely, for materials that are consistent with the V-K model, it is K_{max} that is critical as shown in Figure 9.11a and b.

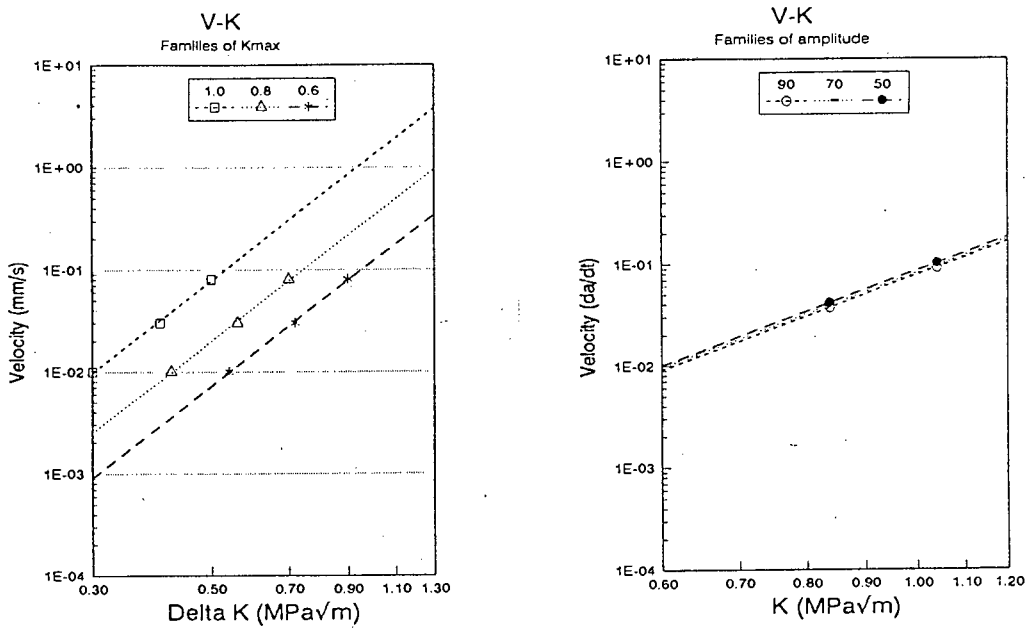

Figure 9.11: da/dn vs ΔK and V vs K plots for ideal V-K behaviour for different load amplitudes

Results

again the results previously presented in Figures 6.6 and 6.7 are repeated in Figures 9.12a and b in the form of least squares lines. All of these results are from tests carried out at 1 Hz in order to avoid variations as a result of frequency effects.

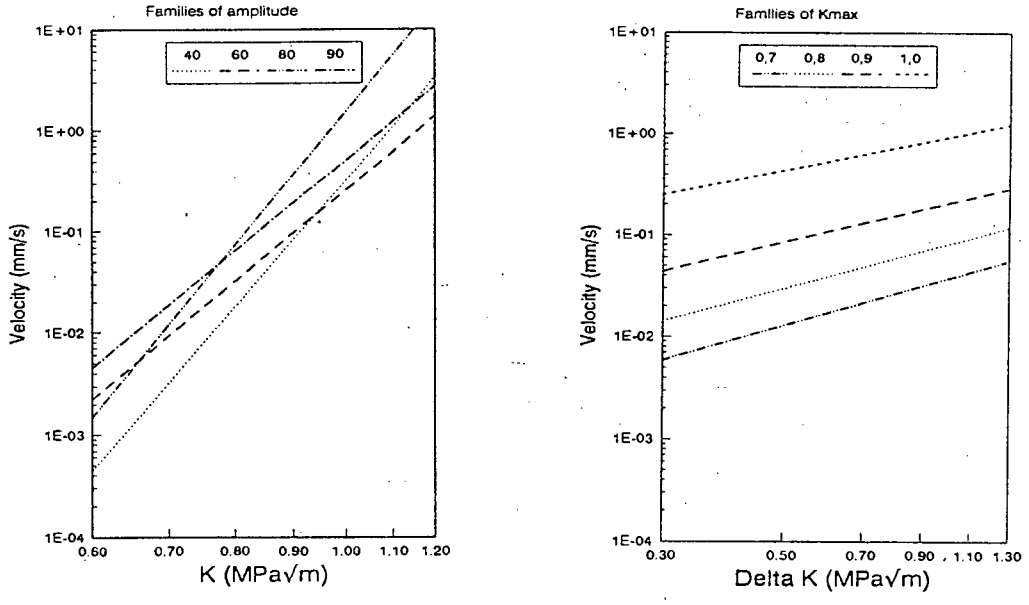

Figure 9.12: Experimental results presented as V vs K and da/dn vs ΔK plots

From Figure 9.12 it appears that the mechanism is dominated by the V-K model, but there is an element of "plasticity" control, as discussed together with frequency effects in the next section. There is a small but distinct spread in the V-K plot, whilst the spread is somewhat larger in the da/dn-ΔK plot.

9.4.4 Summary

This section has considered in some detail the relative contributions of the Paris plasticity dominated mechanism and the EAC (VK) mechanism. It would appear from the interpretation of both the frequency and amplitude results that the fatigue cracking in the mortars tested is consistent with a mechanism dominated by the VK model. There appears, however, to be a contribution, albeit less significant, from the Paris model as well.

This is also consistent with the observation in Section 9.3 that the fatigue behaviour is toughness dominated, ie when the fatigue data is normalised with respect to material toughness, as shown in the K_{rel} plots, many of the trends seem to be nullified. Dauskardt et al (as described by Suresh[9.1]) also report an increased crack growth rate with decreased toughness from Mg-PSZ ceramics. The implication of this is that the crack mechanism in the material is dominated by EAC behaviour rather than the Paris model. In metals, in contrast, high fatigue resistance is often associated with hard, brittle (low toughness) characteristics, and more ductile, tougher alloys show poorer fatigue resistance.

It is also notable that, as shown in Figure 6.8, the measured data is consistent with the Modified Goodman Diagram approach. This approach considers both peak load and load amplitude as variables in its formulation, once again pointing to a mixture of mechanisms.

The next section presents a mechanistic model to explain the observed behaviour that has been discussed above.

9.5 Crack growth mechanisms

The development of an understanding of the mechanisms of fatigue in brittle materials such as cement mortars is presently limited. Indeed, Suresh has recently reported "the cyclic fracture mechanisms in ceramics are by no means completely understood".[9.1] However efforts are presently being focused on solving this problem.

In order to explain the mix of V-K and Paris type behaviours that are apparent from the above discussion, this section presents a model that approaches the question at two distinct levels. The crack growth mechanisms at an extreme localised microscopic level will not necessarily be the same as the apparent macro mechanisms suggested by experimental work due to the heterogenous nature of mortar and due to the number of different mechanisms occurring. For this reason the discussion is presented at different levels of magnitude, the first at the (microscopic) localised level where crack growth is occurring, and the other at the mesoscopic (or process zone) level where it is being observed.

9.5.1 Localised crack growth mechanisms

There are six different failure mechanisms that are defined and discussed in this section, none of which are new, but the manner in which they presumed to interact is. The mechanisms under consideration in this section are at a micro-localised level (see Section 2.2.2), ie individual fibres, plates or crystals in the gel, fly ash particles or sand grains, hereafter referred to as elements (in the sense of discrete elements, not chemical elements). The mechanisms discussed are:

- plasticity,
- environmentally assisted cracking (EAC),
- brittle shear failure,
- creep,
- slippage,
- wedging.

Plasticity

Plasticity is the failure mechanism, commonly occurring in metals, where high stresses at individual grains cause them to be stressed beyond their elastic limit and to deform plastically. This mechanism can be characterised [9.23] by dislocation dynamics, ie dislocation development and movement in polycrystalline materials. In cyclic fatigue this mechanism results in incremental growth of a crack with each cycle by local shear failure occurring in the plastically deformed zones. Fatigue fracture surfaces of ductile polycrystalline materials (eg aluminium alloys) are characterised by ductile fatigue striations visible in electron microscopy. This mechanism is modelled by the so called Paris equation as discussed above.

Cementitious materials, particularly at localised individual element level are generally considered to be non polycrystalline and amorphous, yet brittle,[9.3] with minimal micro-plastic deformation occurring, thus effectively precluding this mechanism from being likely.

Environmentally assisted cracking (EAC)

EAC is the mechanism in which individual stressed elements are attacked and broken by external aggressive agents from the local environment. Stress corrosion cracking (SCC) in glass is a special case of this in which hydroxyl ions in water[9.24] attack stressed silica bonds resulting in crack propagation.

For this mechanism to occur, all three of the following are required: the material must be susceptible to EAC, there must be a sufficiently high local stress and a suitable aggressive species must be present.

The mechanism is modelled by the so called V-K relationship in which crack growth velocity is a function of stress intensity and time, and independent of cyclic frequency.

Brittle shear failure

Brittle shear failure is the fast fracture of elements, normally in shear, due to overload. If this was the dominant mode at macro level, the material could be modelled by linear elastic fracture mechanics (LEFM). It is likely that this mechanism is significant for cementitious materials at element or micro-localised level, but is masked at process zone level (thus making LEFM invalid, see Section 3.3.2) as discussed in the Section 9.5.2.

Creep

Creep is a term that is often loosely used in connection with cementitious materials. In this context, the term will be taken to refer to "the effect of water movement at gel pore level as a result of applied load, thus causing deformation of the material" (see Section 3.2.5). In this case creep can only occur in samples in which water is present and will not occur in samples that have been completely dried.

It is virtually impossible (with present technology) to separate this mechanism from EAC in any experimental test programme, because both mechanisms, by definition, involve the action of water on gel. For this reason, this mechanism will not be separated from EAC in further discussion. It must be borne in mind that such a mechanism may well be playing a significant role. Assessment of the degree of such significance would have to be the topic of further work.

The more general use of the word "creep" as applied to the macro deflection of concrete under sustained loading is potentially misleading as the mechanism of such macro deflection is probably a combination of several of the above.

Slippage

By slippage, is meant the separation or debonding of CSH fibres that have grown from different cement grains and meshed together, not unlike fibre pullout in composites, except that in this case the fibres also form the matrix. No direct evidence is available for this occurring, or not occurring, but it has

been suggested as a mechanism of macro-creep.[9.25] This should be kept in mind as a potential complicating factor, and as an interesting point for further work.

It is more likely to occur in poorly hydrated matrices in which the gel is predominantly Type I or II as opposed to the dense matrix of Type III or IV (see Table 2.2).

Wedging

Wedging is a mechanism that can only occur in cyclic fatigue, as a result of fluid molecules or grains of solid material acting as wedges during the unloading cycle. These would have the effect of increasing stresses at the crack tip and thus promoting all of the other element level mechanisms. Tait has suggested that hydrowedging is a possibility,[9.3] and micrographs such as those in Figure 8.10 have also shown that broken materials acting as wedges is a reality.

The effects of immersion in alcohol (Section 9.3.2) also indicate that this mechanism may be significant. This is indicated by the tests carried out in alcohol where fatigue cracks appeared to be growing faster than those tested in water, despite the reported lack of chemical aggressiveness of the alcohol. It is suggested that the alcohol with its lower viscosity was able to penetrate further into cracks, and so promote the wedging mechanism.

The mechanism could occur at all levels from the element level up to a certain macro structural level, and would also be one of the contributing factors to the observed accumulation of damage during the unloading phase of a loading cycle.[9.3]

This mechanism also needs to be borne in mind as a complicating factor in the following discussion.

General

It should be noted that many or all of the above micro-mechanisms could occur in most situations; and it is the relative dominance of each that will govern the macro (and measurable) behaviour of the sample in question.[9.1, 9.6] There is also likely to be some overlap in the mechanisms; for instance it has already been stated that it is unlikely that EAC and creep will act independently. The combinations of these mechanisms at a larger dimensional level are discussed in the next section.

9.5.2 Process zone level crack growth mechanisms

The process zone has been described as a zone of microcracking in front of a crack tip in which the mechanical properties of the material have been changed due to damage (see Section 3.2.5). The physical size of such a zone is debated and is thought to be related to sample size, but is in the order of mm rather than μm in these specimens and thus becomes a useful reference of magnitude for discussion of mechanisms which are discernible in experimental tests.

Mechanisms which are discernible at process zone level would occur as a result of the combination of the above element level mechanisms. It is proposed that environmentally assisted cracking (EAC) would be the dominant mechanism at this level. However it would not be the only mechanism acting, with others (referred to by Suresh as cyclic fracture mechanisms[9.1]) also contributing to damage accumulation. It is therefore proposed that another mechanism, called for convenience pseudo plasticity (PP), acts as the sum of the other micro level cracking mechanisms in cyclic loading, albeit to a lesser extent than the EAC.

Environmentally assisted cracking (EAC)

As discussed in Section 3.2.4, Evans and Fuller[9.22] have reported a theoretical correlation between static and cyclic fatigue crack growth behaviour that is applicable, but only if the mechanism of crack advance is the same in both

static and cyclic cases. They provide a method where a fatigue data line (in a V-K plot) can be derived from the static data if it is assumed that the mechanism is EAC. If the Evans & Fuller prediction is not accurate, the implication is that the mechanisms for the two cases are different.

Crack growth rate would be expected to be related to the length of time for which fibre elements are stressed, and the value of the maximum stress intensity (rather than cyclic amplitude). The relationship has been derived as an integration of the amount of time during which the material is at a particular stress or stress intensity.

Both the results of this work (Figure 9.13) and others[9.3] have indicated that cement mortars do exhibit broad compliance with this relationship indicating that EAC is a dominant mechanism of crack propagation in cementitious materials. This relatively close correlation with the Evans and Fuller prediction is regarded as of particular significance and strong support for the argument that the EAC mechanism is dominant.

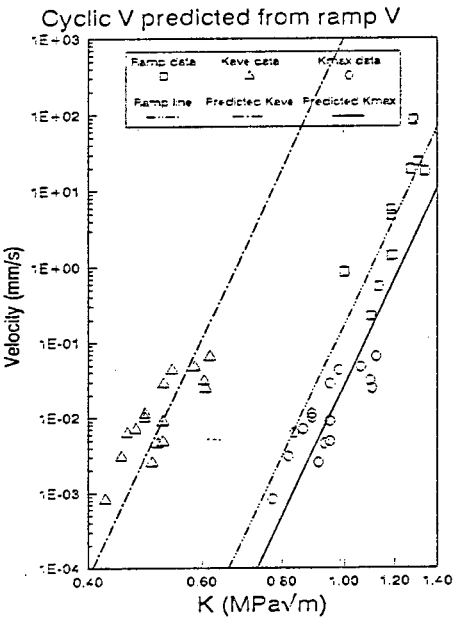

Figure 9.13: Comparison of observed static and cyclic fatigue tests and predicted cyclic behaviour

Pseudo-plasticity (PP)

Pseudo-plasticity is suggested as a model in which considerable microcracking at a localised level (the process zone) may cause a brittle material to behave in a manner that resembles plastic behaviour. That is, there is some deformation without catastrophic failure, but with decreasing load carrying capacity, as described by the non-linear portion of the stress strain curve. It has been suggested[9.4] that the larger the process zone, so the material will appear to be less brittle and more plastic, thus moving away from **linear elastic** fracture mechanics validity towards a more elastic plastic fracture mechanics approach.

It is proposed that fatigue or fracture behaviour where this mode is predominant will be better described by the Paris model than the V-K model in that the cracking is occurring within the pseudo-plastic process zone, albeit due to a number of different micro-mechanisms within the process zone. A (tenuous) parallel may be drawn between the dislocations of true plasticity, and the microcracks of pseudo plasticity. Note that the Paris model, as a fit to fatigue crack growth data, is empirical, rather than rigorously mechanistically based, and therefore could well be valid for another mechanism which results in similar behaviour on a similar scale.

The cause of the microcracking may be any of the element level mechanisms described above, but it is proposed that brittle fracture is the most likely, particularly at the tips of the multitude of flaws in a normal concrete or mortar. Brittle cracking would be independent of time or rate effects (at the levels pertaining to this study), and the damage incurred would be irreversible and permanent. Creep (due to water movement) would also contribute to this mechanism by redistributing the stresses in a rate dependent way, and with a degree of reversibility. Slippage could also contribute as fibres are pulled apart with some presumed slight rate dependence.

Pseudo-plasticity is an effect not a cause, and as a model helps to explain the observed partial Paris type behaviour. The multitude of small discontinuous cracks and flaws will reduce the notch sensitivity of a mortar (making LEFM less valid) as well as acting as an energy absorber and permitting relatively large deformations whilst retaining some load carrying capacity across the crack bridges. Crack shielding and redistribution of stresses could also occur within the process zone, thus contributing to the apparent "plasticity" (or non-linear) behaviour.

9.5.3 Discussion

This section compares the behaviour that would be expected in terms of some of the variables used in this study (ie preparation, relative humidity, cyclic load amplitude, cyclic frequency, and material toughness) on the basis of the mechanisms at the process zone level described above.

A paper by Bazant & Gettu[9.4], has discussed several of these aspects based on experimental static testing, including reference to the apparent differences in brittleness of cementitious materials due to changing loading rates. The difference in brittleness is described as being related to the process zone size: the smaller the process zone, the more brittle the material and the closer to LEFM behaviour.

Reference is made in the Bazant & Gettu paper to creep, but the term has not been defined and has been interpreted here as referring to macro deformation. This deformation could be due to any of the element level mechanisms described above. It is proposed that the macro-properties of cementitious materials known as creep, fatigue and static fatigue are all due to varying combinations of the same micro-mechanisms. These mechanisms will result in the formation and accumulation of damage, which is exhibited as the different macro-properties due to the loading conditions prevailing.

Sample preparation and relative humidity

Differences in sample moisture content due to different drying methods and environmental conditions would be expected to result in the following changes in fatigue behaviour on the basis of the mechanisms proposed above.

The act of drying would tend to cause damage and so promote pseudo plasticity, and may result in a larger process zone. Creep and EAC would be precluded as micro-mechanisms unless sufficient external water were permitted to re-enter the matrix. Carbonation and consequent densification of the surface after drying would make it harder for external water to get back into the crack tip. Fatigue tests carried out in low relative humidity environments would be expected to reduce the effect of environmentally assisted cracking due to the absence of water to take part in the reaction. All of these would result in slower crack growth.

As discussed in Section 9.3.2, the observed trends were that, in general, decreased moisture resulted in decreased crack velocity/increased toughness which is consistent with that described above.

Temperature

Bazant has indicated that a higher temperature leads to a smaller process zone[9.4] due to a lower activation energy requirement.[9.26] This is consistent with the EAC mechanism in which case the activation energy referred to is the energy required to break bonds chemically. This mechanism would also lead to faster crack growth with increasing temperature. An increase in temperature would also promote micro-localised brittle failure and pseudo-plasticity behaviour. This point could be clarified by tests carried out on dry samples over a range of temperatures.

The observed behaviour shows increased temperature of samples tested in water leading to higher velocities, again as consistent with the models.

Cyclic load amplitude

Evans and Fuller's model for pure environmentally assisted cracking (Appendix B) predicts a very slight increase in crack velocity at a given applied stress intensity peak with decreasing cyclic load amplitude. Pseudo plasticity, if modelled by the Paris relationship, would be expected to lead to a large reduction in velocity with reducing amplitude.

The observed behaviour agrees with the EAC model in that there was a shift from static loading to cyclic loading in the right direction and of approximately the right magnitude (Figure 9.12). However, with decreasing amplitude, the velocity was slightly reduced, opposite to that expected from the EAC model but in agreement with the direction (but not necessarily the magnitude) predicted by the Paris model. This backs up the argument that both mechanisms were occurring, the difference between static and cyclic being well modelled by EAC, but with a small influence of pseudo plasticity in addition.

Frequency

Frequency effects are complex due to transportation limitations (at both extremes of high and low frequencies) and the effects of the different mechanisms.

Bazant[9.4] has stated that slower monotonic load application leads to a smaller process zone and less crack shielding and so a higher crack velocity. In the present study this may be compared with lower frequency tests. In this study, ramp tests at higher rates resulted in higher measured K_{Ic} values and higher velocities which is in agreement with Bazant (see Figure 6.10). In fatigue tests, there was a noticeable difference between 0,1 and 1 Hz, probably due to transport effects, but little further change with increasing frequency, as would be expected from the EAC model.

Material toughness

Bazant has reported that younger (and presumably less tough) cementitious materials have a smaller process zone.[9.4] It is possible that a higher K_{Ic} may lead to a larger process zone because the same amount of energy is absorbed in creating the same number of new surfaces (micro-cracks) that are further apart and over a larger area. This would be due to both pseudo plasticity and environmentally assisted cracking mechanisms.

Whilst all the mortars tested in this present work were of similar toughness, the results can be compared with Tait who used a mortar with lower K_{Ic}. What is notable is that despite the large difference in K_{Ic}, the velocities are of the same order, indicating a limiting maximum velocity, as would be expected of an EAC mechanism.

9.5.4 Summary

A model describing the mechanisms of crack growth of cementitious materials on the basis of different dimensional levels has been considered. The observed experimental behaviour of this and other studies have been shown to be consistent with the models.

It is proposed that several mechanisms occur at individual element level, which combine at process zone level into two basic mechanisms, environmentally assisted cracking and pseudo plasticity. The relative dominance and effects of these mechanisms is largely dependent on the reagents available (environment), as well as loading configuration, strength, materials in the concrete or mortar, stress field, time, temperature, amplitude, and loading rates.

The key points discussed in this Chapter are summarised in the following conclusion chapter, along with some thoughts on the implications of these findings on the design of structural concrete, and recommendations for future work.

CHAPTER TEN - CONCLUSION

10.1 Introduction

The chapter summarises the conclusions reached in the foregoing discussion. The first two sections address the effects of fly ash at various ages, and the effects of environment and loading variables in the fatigue performance and fracture toughness of cementitious mortars. This is followed by a description of the mechanisms thought to be responsible for these and other trends.

The final two sections in the chapter contain some recommendations for future work to address some of the outstanding and new questions raised by this study, and a comment on the implications of these findings on engineering design as stated as one of the thesis objectives.

10.2 Fly ash

Fly ash, when used as a partial cement replacement in mortar, has been recorded as improving fracture toughness at early ages, but reducing toughness at greater ages. This appears to be due to the poor bond between larger fly ash particles and hydrated cement gel. At early ages the particles tend to blunt microcracks and so marginally improve toughness. At greater ages the size of the poorly bonded particles, with respect to the other flaws in the matrix, become critical, and so toughness is reduced when compared with similar OPC mortars. This reduction in toughness is despite any improvements in properties in the interfacial zone due to the presence of fly ash.

There appears to be a close correlation between the fatigue resistance characteristics of mortars and their toughness. This is useful because it could be implied that when designing for fatigue, a change of mix proportions or binder type would require the determination of toughness characteristics only. The fatigue characteristics would only need to be measured once, rather than for every mix.

The next section summarises the findings regarding the influences of environment and loading on fatigue behaviour of the mortars tested.

10.3 Environment and load variables

Observations of the changes in measured crack growth rates in mortars due to variations in the environment, point to crack growth mechanisms that are dominated by fluid dependency such as EAC and, possibly, hydro wedging.

Interpretation of the frequency and amplitude results has also indicated that the crack growth mechanisms are dominated by EAC, but with a certain small amount of a plasticity type of mechanism.

The correlation between fatigue resistance and toughness for mortars was also apparent in this set of tests. This correlation is also consistent with a V-K dominant model.

Some of the mechanisms behind the fatigue and fracture of cementitious materials are described in more detail in the next section.

10.4 Mechanisms

The mechanisms of crack growth in mortars need to be considered at different levels. At the localised microstructural level, there is evidence of a number of different mechanisms acting. These include brittle (LEFM) fracture, environmentally assisted cracking (EAC), creep, slippage and wedging. All of these will occur at any given location, but it is the prevailing loading and environmental conditions that will determine their relative importance.

At the process zone level, it has been suggested that the above mechanisms will superimpose to result in two principal mechanisms governing the observed behaviour. Environmentally assisted cracking appears to be the dominant mechanism when there is sufficient moisture available. The presence of water results in the acceleration of crack growth rates, probably due to the lowering

of the activation energy requirement to cause failure of individual chemical bonds. This mechanism appears to be well modelled by the V-K relationship. Pseudo plasticity is, in effect, a result of all of the microstructural mechanisms taking place causing a sample to behave with some plasticity (Paris) characteristics.

The variables that influence the relative effect of the mechanisms include:

- the presence of water; the more water there is the faster the fatigue crack growth,

- the presence of other fluids; ethyl alcohol has the effect of accelerating crack growth rates,

- temperature; crack growth rates were accelerated with increasing temperature,

- sample preparation; those samples that had been dried showed increased fatigue resistance and toughness compared to those that had not been dried, despite the damage incurred in the drying process,

- strain rate or cyclic frequency; increasing crack velocities were observed with an increased loading rate between 0,1 and 1 Hz, above which there was little effect,

- cyclic amplitude; greater cyclic amplitude lead to marginally faster crack growth,

- peak load; increased peak stress or stress intensity lead to accelerated crack velocity,

- the shape or pattern of the stress field due to the configuration of the member and the applied loads,
- the toughness of the material.

The V-K model was found to be the dominant model and there was good correlation between the measured relationship between static and cyclic fatigue and the theoretical position derived using an Evans and Fuller analysis. However, there was consistently discernible plasticity behaviour as well.

The mechanisms as proposed provide a means of describing and understanding fatigue behaviour of mortars. They are not mutually exclusive, but indeed have a large element of overlap and commonality and in some cases may not be easily separable. Considerable work is still required in order to be able to quantify the effects of the individual mechanisms for all materials, loads and environments.

10.5 Future Work

The following suggestions are made for future work to address some of the new questions raised, and old questions not resolved in this work.

It would be of use for a wider range of double torsion fatigue tests to be carried out in a variety of environments using samples which have been prepared in different ways. One of the suggested environments includes the immersion in fluids, particularly those with varying dielectric constants, hydroxyl ion concentrations and viscosities. This information would assist in defining which fluid properties are critical in governing environmentally assisted cracking.

Further use of the in situ double torsion testing facility inside a scanning electron microscope, particularly a wet cell microscope in which moisture content can be controlled, would help in observing the different mechanisms under different environmental conditions.

An investigation into the effects of silica fume on the fly ash - CSH gel interfacial bond in such a facility would be very interesting to carry out.

Full sized tests on dried samples in a low humidity environment over a range of temperatures would help to quantify the extent of the brittle fracture mechanism occurring at a microstructural level.

A test programme designed to investigate the amount of creep, slippage and wedging occurring would also be of great use in separating out the individual mechanisms at microstructural level. Design of such a programme would have to try to exclude (or at least quantify) EAC effects.

10.6 Implications

As detailed above, the variables influencing fatigue behaviour of cementitious materials are numerous. So numerous that to try and model or include corrections for all of them from a fundamental mechanistic point of view in structural design would be risky with present knowledge, particularly as their relative effects are as yet not fully quantified.

Therefore, until they are well quantified, structural design will have to continue to rely on previously acceptable empirically based systems. A re-assuring factor has been that this study has demonstrated the validity of the Goodman Diagram approach from the point of view of taking cognizance of amplitude and peak stress effects. It should also be accepted that empirical methods are not all bad; for example, the slump test. It is often said that if someone was seeking to invent a test to determine consistence of concrete, the last test that would be accepted would be the slump test. However, in the words of Popovics[10.1] misquoting Churchill "The slump test is the worst possible test method for fresh concrete except for any other invented".

A point that is not covered by the Goodman model is the time for crack initiation. It is probable that for cementitious materials with their inherently flawed microstructure, the initiation time for microcracking to develop is relatively small, although the time for macrocracks to become significant may be appreciable. From the design point of view, to ignore initiation time would be conservative.

It is felt that this study has met the overall aim in establishing that the present design methods are based on sound technology. At the same time, some new models or new ways of looking at fracture processes have been proposed that appear to assist in understanding, and possibly modelling in the future, fatigue and fracture behaviour of cementitious materials, including those containing fly ash.

REFERENCES

CHAPTER 1

1.1 Davis, R.E. et al, Properties of cements and concretes containing fly ash, **Proceedings ACI,** vol.33, May-June 1937, pp.577-612.

1.2 Owens, P.L. Fly ash and its use in concrete, **Concrete,** July 1979, pp.21- 26.

1.3 Ho, D.W.S. and Lewis, R.K. Effectiveness of fly ash for strength and durability of concrete, **Cement & Concrete Research,** vol.15, no.5, 1985, pp.793-800.

1.4 Diamond, S. Particle morphologies in fly ash, **Cement & Concrete Research,** vol.16, 1986, pp.569-579.

1.5 Tse, E.W., Lee, D.Y. and Klaiber, F.W. Fatigue behaviours of concrete containing fly ash, **Fly Ash, silica fume and slag, proceedings of the second international conference, Madrid, Spain**, 1986, pp.273-290. (ACI SP-91).

1.6 Swamy, R.N. Fly ash concrete - potential without misuse, **Materials & Structures,** vol.23, 1990, pp.397-411.

1.7 Thomas, M.D.A. and Matthews, J.D. Durability studies of PFA concrete structures, **BRE Information Paper,** 11/91, June 1991.

1.8 Sarkar, S.L., Baalbaki, M. and Aitcin, P.C. Microstuctural development in a high strength concrete containing a ternary cementitious system, **Cement, Concrete and Aggregates,** vol.13, no.2, Winter 1991, pp.81-87.

1.9 Dhir, R.K. A fundamental look at PFA, **Concrete,** July 1992, pp.45-48.

1.10 Larbi, J.A. and Bijen, J.M. Effect of mineral admixtures on the cement paste aggregate interface, **Fly ash, silica fume, slag, and natural pozzolans in concrete, proceedings of the fourth international conference, Istanbul, Turkey,** 1992, pp.655-669. (ACI SP-132).

1.11 **Symposium on the utilisation of pulverised fuel ash, CSIR, Pretoria**, 1979.

1.12 **Fly Ash, silica fume and slag, proceedings of the second international conference, Madrid, Spain**, 1986, (ACI SP-91).

1.13 **ASH - A Valuable Resource, Proceedings,** Pretoria, CSIR, 2-6 Feb 1987.

1.14 **Fly ash, silica fume, slag, and natural pozzolans in concrete, proceedings of the fourth international conference, Istanbul, Turkey,** 1992, (ACI SP-132).

1.15 **Fifth CANMET/ACI International Conference on Fly Ash, Silica Fume, Slag and Natural Pozzolans in Concrete,** Milwaukee, June 1995, (in publication).

1.16 Dhir, R.K. and Green, J.W. ed, **Protection of concrete, proceedings of the international conference held in Scotland,** London: Spon, 1990.

1.17 Holmen, J.O. Fatigue design evaluation of offshore concrete structures, **Materiaux et Constructions,** vol.17, no.97, pp.39-42.

1.18 Hoff, G.C. Considerations for the use of concrete for offshore structures, **SP Evaluation and rehabilitation of concrete structures and innovations in design, proceedings of an ACI international conference,** Hong Kong, 1991, vol.2, pp.749-788. (ACI special publication 128).

1.19 Kiyomiya, O. et al. Fatigue properties of prestressed beam column joints, with emphasis on offshore structures subject to wave loading, **ACI journal,** Nov. 1988, pp.138-162.

1.20 American Concrete Institute, Committee 215, Considerations for design of concrete structures subjected to fatigue loading, (ACI 215R-74, revised 1992), **ACI manual of concrete practice**, Detroit: ACI, 1993, part 1, pp.215R-2 to 215R-5.

1.21 Portland Cement Association, **Design of reinforced concrete for fatigue,** Research & Development Bulletin RD 059.01D, Skokie: PCA, 1978.

1.22 Siemes, A.J.M. Fatigue evaluation of concrete structures - preliminary studies, procedure and examples, **Heron,** vol.33, no.3, 1988.

CHAPTER 2

2.1 **Highlights in the history of concrete,** Wexham Springs, Slough: British Cement Association, 1986.

2.2 Betterton, E.A. The romans did it in the forum, **Chemsa,** Jan 1984, pp.267-268.

2.3 Stevenson, J. and Spooner, D. Concrete and the environment, **Concrete Quarterly,** Autumn 1992, pp.8-11.

2.4 Addis, B.J. ed. **Fulton's concrete technology**, 6th ed, Midrand: Portland Cement Institute, 1986, p.6.

2.5 Abrams, D.A. Design of concrete mixtures, **A selection of historic american papers on concrete 1876-1926,** Detroit: ACI, 1976, pp.309-330. (ACI SP-52)

2.6 Neville, A. Concrete research on a micro- and a macro-scale, **Cement & Concrete Research,** vol.22, 1992, pp.1067-1076.

2.7 Dhir, R.K. and Green, J.W. ed, **Protection of concrete, proceedings of the international conference held in Scotland,** London: Spon, 1990.

2.8 Hine, W.G. The corrosion of steel - Random thoughts and wishful thinking, **Concrete International,** October 1993, pp.54-57.

2.9 Basson, J.J. **Deterioration of concrete in aggressive waters - measuring aggressiveness and taking counter measures,** Midrand: Portland Cement Institute, 1989.

2.10 Blight, G.E. et al, Effect of AAR on the performance of a reinforced structure over a six year period, **Magazine of Concrete Research,** vol.41, no.147, June 1989, pp.69-77.

2.11 **ASH - A valuable resource, international symposium, CSIR, Pretoria,** 2-6 Feb.1987.

2.12 Guozho, L.Investigation of fly ash concretes with application of SEC technology, **Concrete Precasting Plant & Technology,** vol.11, 1992, pp.54-62.

2.13 Grieve, G.R.H. The properties of fresh concrete made with portland cements, milled granulated blastfurnace slag, fly ash or silica fume, **Symposium: Practical guidelines on the selection and use of portland cement, mgbs, fly ash and silica fume in concrete,** Midrand: Portland Cement Institute, 1987

2.14 Ballim, Y. Curing and the durability of OPC, fly ash and blastfurnace slag concretes, **Materials and Structures,** vol.26, 1993, pp.240-244.

2.15 Jennings, H.M. Aqueous solubility relationships for two types of calcium silicate hydrate, **Journal of the American Ceramic Society,** vol.69, no.8, 1986, pp.614-618.

2.16 Czernin, W. **Cement, chemistry and physics for civil engineers,** 2nd English ed, Wiesbaden: Bauverlag, 1980.

2.17 Mantel, D.G. The chemistry of portland cement, **Cement Technology Course,** Johannesburg: Pretoria Portland Cement Company (Pty) Ltd, 1992.

2.18 Pratt, P.L. and Jennings, H.M. The microchemistry and microstructure of portland cement, **Annual Review of Materials Science,** vol.11, 1981, pp.123-149.

2.19 Taylor, H.F.W. Mineralogy, microstructure and mechanical properties of cements, **Proceedings of the British Ceramic Society,** edited by D. Taylor and P.S. Rogers, vol.28, 1979, pp.147-163.

2.20 Lea, F.M. **The chemistry of cement and concrete**, 2nd.ed, London: Edward Arnold, 1956.

2.21 Jennings, H.M. Design of high strength cement based materials: Part 2 Microstructure, **Materials Science and Technology,** vol.4, April 1988, pp.285-290.

2.22 Jennings, H.M. and Pratt, P.L. On the hydration of portland cement, **Proceedings of the British Ceramic Society,** edited by D. Taylor and P.S. Rogers, vol.28, 1979, pp.179-193.

2.23 Beaudoin, J.J. and Ramachandran, V.S. A new perspective on the hydration characteristics of cement pastes, **Cement & Concrete Research,** vol.22, no.4, 1992, pp.689-694.

2.24 Bogue, R.H. **The chemistry of portland cement,** 2nd ed, New York: Reinhold, 1955, p.248.

2.25 Diamond, S. Cement paste microstructure - an overview at several levels, **Hydraulic cement pastes: their structure and properties, proceedings of a conference at Sheffield**, 8-9 April, 1976, pp.2-31.

2.26 Taylor, H.F.W. **The chemistry of cements, vol. 1,** London: Academic Press, 1964, p.6.

2.27 Jawed, I., Skalny, J. and Young, J.F. Hydration of portland cement, **Structural performance of cements,** edited by P. Barnes, London: Applied Science, 1983, pp.240-241.

2.28 Dalgliesh, B.J. and Pratt, P.L. Fractographic studies of microstructural development in hydrated portland cement, **Journal of Materials Science**, vol.17, 1982, pp.2199-2207.

2.29 McCarter, W.J. and Afshar, A.B. Monitoring the early hydration mechanisms of hydraulic cement, **Journal of Materials Science,** vol.23, 1988, pp.488-496.

2.30 Addis, B.J. ed. **Fulton's concrete technology**, 6th ed, Midrand: Portland Cement Institute, 1986, p.132.

2.31 Lea, F.M. **The chemistry of cement and concrete**, 2nd.ed, London: Edward Arnold, 1956, p.84.

2.32 Addis, B.J. ed. **Fulton's concrete technology**, 6th ed, Midrand: Portland Cement Institute, 1986, p.459.

2.33 Sarkar, S.L. The importance of microstructure in evaluating concrete, **Advances in Concrete Technology,** ed. V.M. Malhotra, Ottawa: Minister of Supply and Services Canada, 1992, pp.123-158.

2.34 Barnes, B.D., Diamond, S. and Dolch, W.L. Hollow shell hydration of cement particles in bulk cement paste, **Cement & Concrete Research,** vol.8, no.3, 1978, pp.263-272.

2.35 Kjellsen, K.O., Detwiler, R.J. and Gjorv, O.E. Development of microstructures in plain cement pastes hydrated at different temperatures, **Cement & Concrete Research,** vol.21, no.1, 1991, pp.179-189.

2.36 Kjellsen, K.O., Detwiler, R.J. and Gjorv, O.E. Backscattered electron imaging of cement pastes, **Cement & Concrete Research,** vol.20, no.2, 1990, pp.308-311.

2.37 Mehta, P.K. **Concrete: structure, properties and materials,** Englewood Cliffs: Prentice Hall, 1986, p.23.

2.38 Wecharatana, M. and Shah, S.P. Double torsion tests for studying slow crack growth of portland cement mortar, **Cement & Concrete Research,** vol.10, 1980, pp.833-844.

2.39 Mehta, P.K. **Concrete: structure, properties and materials,** Englewood Cliffs: Prentice Hall, 1986, p.36.

2.40 Attiogbe, E.K. and Darwin, D. Strain due to submicrocracking in cement paste & mortar, **ACI Materials Journal,** Jan.1988, pp.3-11.

2.41 Robler, M. and Odler, I. Investigations on the relationship between porosity, structure and strength of hydrated portland cement pastes. I. Effect of porosity, **Cement and Concrete research,** vol.15, no.2, 1985, pp.320-330.

2.42 Odler, I. and Robler, M. Investigations on the relationship between porosity, structure and strength of hydrated portland cement pastes. II. Effect of pore structure and of degree of hydration, **Cement and Concrete Research,** vol.15, no.3, 1985, pp.401-410.

2.43 Howard, A.J. and Kendall, K. Flexural strength and porosity of cements, **Nature,** vol.289, Jan.1981, pp.388-389.

2.44 Jennings, H.M. Design of high strength cement based materials: Part 3 state of the art, **Materials Science and Technology,** vol.4, April 1988, pp.291-299.

2.45 Diamond, S. et al, SEM investigations of the contact zones between rock surfaces and cement paste, **Interfaces in cementitious composites, proceedings of the international conference held by RILEM, Toulouse**, 1992, pp.13-22.

2.46 Jennings, H.M. Design of high strength cement based materials: Part 1 Fracture Mechanics, **Materials Science and Technology,** vol.4, April 1988, pp.277-284.

2.47 Dhir, R.K. et al, Application of fracture mapping to the study of coarse aggregate influence on microcracking in concrete, **Res Mechanica,** vol.5, 1982, pp.183-201.

2.48 Attiogbe, E.K. and Darwin, D. Submicrocracking in cement paste and mortar, **ACI Materials Journal,** vol.84, Nov.1987, pp.491-500.

2.49 Chen, A.C.T. and Chen, W. Constitutive relations for concrete, **Journal of Engineering Mechanics,** Aug.1975, pp.466-481.

2.50 Mehta, P.K. **Concrete: structure, properties and materials,** Englewood Cliffs: Prentice Hall, 1986, pp.60-61.

2.51 Stroeven, P. Some mechanical effects of interface debonding in plain concrete, **Interfaces in cementitious composites, proceedings of the international conference held by RILEM, Toulose**, 1992, pp.187-196.

2.52 Bascoul, A. and Maso, J.C. Microcracking and cracking limit state as functions of strain gradients for concrete, **Cement & Concrete Research,** vol.17, no.4, 1987, pp.661-672.

2.53 Bascoul, A., Olivier, J.P. and Poushanchi, M. Stable microcracking of concrete subjected to tensile strain gradient, **Cement & Concrete Research,** vol.19, no.1, 1989, pp.81-88.

2.54 Chudnovsky, A. and Wu, S. Effect of crack - microcracks interaction on energy release rates, **International Journal of Fracture,** vol.44, 1990, pp.43-56.

2.55 Rose, L.R.F. Microcrack interaction with a main crack, **International Journal of Fracture,** vol.31, 1986, pp.233-242.

2.56 Mehta, P.K. **Concrete: structure, properties and materials,** Englewood Cliffs: Prentice Hall, 1986, p.72.

2.57 Eden, N.B. and Bailey, J.E. On the factors effecting strength of portland cement, **Journal of Materials Science,** vol.19, 1984, pp.150-158.

2.58 Ansari, F. Stress strain response of microcracked concrete in direct tension, **ACI Materials Journal,** vol.84, Nov.1987, pp.481-490.

2.59 Macdonald, H.K.J. **The properties of concrete in uniaxial tension,** PhD Thesis, University of the Witwatersrand, 1980.

2.60 Tait, R.B. In situ scanning electron microscopy of doubler torsion fracture of concrete, **Proceedings of Electron Microscopy Society of Southern Africa,** December 1980, p.29.

2.61 Bentur, A. and Mindess, S. The effect of concrete strength on crack patterns, **Cement & Concrete Research,** vol.16, no.1, 1986, pp.59-66.

2.62 Diamond, S. and Mindess, S. SEM investigations of fracture surfaces using stereo pairs: 1. Fracture surfaces of rock and cement paste, **Cement & Concrete Research,** vol.22, no.1, 1992, pp.67-78.

2.63 Mindess, S. and Diamond, S. SEM investigations of fracture surfaces using stereo pairs. Part 11: Fracture surfaces of rock-cement paste composite specimens, **Cement & Concrete Research,** vol.22, no.4, 1992, pp.678-688.

2.64 Rossi, P. A physical phenomenon which can explain the mechanical behaviour of concrete under high strain rates, **Materials and Structures,** vol.24, 1991, pp.422-424.

2.65 Harsh, S., Shen, Z. and Darwin, D. Strain rate sensitive behaviour of cement paste and mortar in compression, **ACI Materials Journal,** vol.87, Sept.1990, pp.508-516.

2.66 Beaudoin, J.J. Effect of water and other dialectrics on subcritical crack growth in portland cement paste, **Cement & Concrete Research,** vol.15, no.6, 1985, pp.988-994.

2.67 Paul, D. Weathering of hardened concrete - causes and suggested remedies, **Indian Concrete Journal,** April 1983, pp.97-99.

2.68 Davies, G. and Oberholster, R.E. Alkali silica reaction products and their development, **Cement & Concrete Research,** vol.18, no.4, 1988, pp.621-635.

2.69 Grosskurth, K.P., Malorny, W. and Ruthmann, W. Influence of the interfacial zone between cement paste and aggregate on the corrosive attack on concrete, **Interfaces in cementitious composites, proceedings of the international conference held by RILEM, Toulose**, 1992, pp.297-306.

2.70 Samaha, H.R. and Hover, K.C. Influence of microcracking on the mass transport properties of concrete, **ACI Materials Journal,** vol.89, July 1992, pp.416-424.

2.71 Moolman, F.S., Nienaber-Roberts, C.J. and van Rensburg, T.J.J. **Interim results of an investigation into the relationship between fly ash and pulverised fuel**, Pretoria: CSIR, n.d.

2.72 Matla: massive power for the eighties, **Eskom Brochure,** 1983.

2.73 Lesch, W. and Cornell, D.H. The mineralogy and morphology of fly ash from South African power stations, **ASH - A valuable resource, proceedings, CSIR, Pretoria**, 2-6 Feb.987, vol.1.

2.74 Woolley, G. The historical use of pfa in concrete by the electricity supply industry, **Concrete,** July/Aug.1992, pp.49-53.

2.75 Davis, R.E. et al, Properties of cements and concretes containing fly ash, **Proceedings ACI,** vol.33, May-June 1937, pp.577-612.

2.76 Cabrera, J.G. and Woolley, G.R. A study of twenty-five year old pulverised fuel ash concrete used in concrete structures, **Proceedings of the ICE,** vol.2, no.79, Mar.1985, pp.149-165.

2.77 Faber, J.H. and Babcock, A.W. 50 Years of ash marketing & utilisation in the USA, **ASH - A valuable resource, proceedings, CSIR, Pretoria**, 2-6 Feb.1987, vol.1.

2.78 Owens, P.L. Fly ash & its use in concrete, **Concrete,** July 1979, pp.21- 26.

2.79 Smith, M.A. and Harris, M.R. Ash utilisation in the United Kingdom, **ASH - A valuable resource, proceedings, CSIR, Pretoria**, 2-6 Feb.1987, vol.2.

2.80 Erel, Y., Matthews, A. and Nathan, Y. Potential use of coal ash in the Israel cement industry, **Cement & Concrete Research,** vol.18, 1988, pp.503-512.

2.81 Alberts, L. South African minerals and waste products, **ASH - A valuable resource, proceedings, CSIR, Pretoria**, 2-6 Feb.1987, vol.1.

2.82 Dalton, G.L.Ash production - problems and probabilities, **ASH - A valuable resource, proceedings, CSIR, Pretoria**, 2-6 Feb.1987, vol.2.

2.83 Kruger, J.E. Research at the NBRI on the utilisation of fly ash : an overview, **ASH - A valuable resource, proceedings, CSIR, Pretoria**, 2-6 Feb.1987, vol.2.

2.84 **Symposium on the utilisation of pulverised fuel ash, CSIR, Pretoria**, 1979.

2.85 CSIR, National Building Research Institute, **6th Interim report on studies of South African pulverised fuel ash (PFA) for use in mortar and concrete (1984/85 financial year),** Pretoria: CSIR, 1985.

2.86 Roy, D.M. Luke, K. and Diamond, S. Characterisation of fly ash and its reactions in concrete, **Materials Research Society symposium proceedings,** vol.43, 1985, pp.3-20.

2.87 Valenti, G.L., Cioffi, R. and Sersale, R. Chemical and physical properties of fly ashes and influence on the mechanical performance of the resultant cement mortars, **Il Cemento,** vol.4, 1986, pp.565-572.

2.88 Swamy, R.N. Fly ash concrete - potential without misuse, **Materials & Structures,** vol.23, 1990, pp.397-411.

2.89 Grieve, G.R.H. Viscosity measurements on cement and cement/fly ash blend pastes, **ASH - A valuable resource, proceedings,** CSIR, Pretoria, 2-6 Feb.1987, vol.2.

2.90 Baalbaki, M. et al, Properties and microstructure of high-performance concretes containing silica fume, slag, & fly ash, **Fly ash, silica fume, slag, and natural pozzolans in concrete, proceedings of the fourth international conference, Istanbul, Turkey,** 1992, pp.921-933. (ACI SP-132).

2.91 Ravina, D. and Mehta, P.K. Compressive strength of low cement/high fly ash concrete, **Cement & Concrete Research,** vol.18, 1988, pp.571-583.

2.92 Richartz, W., The influence of fly ashes on the properties of fly ash cement, **ASH - A Valuable Resource, Proceedings,** vol. 2, Pretoria, CSIR, 2-6 Feb 1987.

2.93 Dhir, R.K. Pulverised-fuel ash in the United Kingdom : research, development and use in concrete, **ASH - A valuable resource, proceedings,** CSIR, Pretoria, 2-6 Feb.1987, vol.2.

2.94 Scholz, H., Fly ash in concrete technology, **ASH - A valuable resource, proceedings,** CSIR, Pretoria, 2-6 Feb.1987, vol.1.

2.95 Schubert, P. Properties of cement and concrete with fly ash, **ASH - A valuable resource, proceedings,** CSIR, Pretoria, 2-6 Feb.1987, vol.1.

2.96 Tse, E.W., Lee, D.Y. and Klaiber, F.W. Fatigue behaviours of concrete containing fly ash, **Fly Ash, silica fume and slag, proceedings of the second international conference, Madrid, Spain**, 1986, pp.273-290. (ACI SP-91).

2.97 ASTM C618-83, **Fly ash and raw or calcined natural pozzolans for use as a mineral admixture in portland cement concrete**, Philadelphia, American Society for Testing Materials, 1983.

2.98 SABS 1491: Part II - 1989, **Standard specification for portland cement extenders: Fly ash,** Pretoria: South African Bureau of Standards, 1989.

2.99 BS 3892: Part 1:1982, **Pulverized-fuel ash. Part 1: Specification for pulverized-fuel-ash for use in as a cementitious component in structural concrete,** London: British Standards Institution, 1982.

2.100 DIN 1045: 1988, **Structural use of concrete: design and construction,** 1988.

2.101 Osbaeck, B. Influence of residual carbon in fly ash when assessing the water requirement and pozzolanic activity of fly ash in mortar tests, **Use of fly ash, silica fume, slag and natural pozzolans in concrete, second international conference, supplementary papers, Madrid, Spain**, 1986, paper 26.

2.102 Dhir, R.K. et al, Physical characterization of UK pulverized fuel ashes for use in concrete, **Magazine of Concrete Research**, vol.37, no.131, June 1985, pp.75-87.

2.103 Kautz, K.M. The range of fly ash quality in the Federal Republic of Germany, **ASH - A valuable resource, proceedings,** CSIR, Pretoria, 2-6 Feb.1987, vol.2.

2.104 Diamond, S. **Selection & use of fly ash for highway concrete**, Lafayette: Purdue University, 1985. (Joint Highway Research Report FHWA/IN/JHRP-85/8).

2.105 Hubbard, F.H. et al, Clay and pyrite transformations during ignition of pulverised coal, **Mineralogical Magazine,** vol.48, June 1984, pp.251-256.

2.106 Diamond, S. and Kilgour, C.L. A procedure for the interpretation of fly ash particle size data, **Materials Research Society symposium proceedings,** vol.65, 1986, pp.105-114.

2.107 Brink, R.H. and Halstead, W.J. Studies relating to the testing of fly ash for use in concrete, **Proceedings ASTM,** vol.56, 1956, pp.1161-1214.

2.108 Ravina, D. Fly ash performance in plastic concrete, **ASH - A valuable resource, proceedings,** CSIR, Pretoria, 2-6 Feb 1987, vol.2.

2.109 Dhir, R.K. A fundamental look at PFA, **Concrete,** July 1992, pp.45-48.

2.110 Diamond, S. Particle morphologies in fly ash, **Cement & Concrete Research,** vol.16, 1986, pp.569-579.

2.111 Montgomery, D. and Diamond, S. The influence of fly ash cenospheres on the details of cracking in fly ash bearing cement pastes, **Cement & Concrete Research,** vol.14, no.6, 1984, pp.767-775.

2.112 Dhir, R.K. et al, Contribution of PFA to concrete workability and strength development, **Cement & Concrete Research,** vol.18, no.2, 1988, pp.277-289.

2.113 Sharma, R.C. and Jain, N.K. An Indian fly ash with high percentage of cenospheres, **Cement & Concrete Research,** vol.23, no.1, 1993, pp.239-240.

2.114 ASTM C311 -93, **Standard test methods for sampling and testing fly ash or natural pozzolans,** Philadelphia, American Society for Testing Materials, 199.

2.115 Ho, D.W.S. and Lewis, R.K. Effectiveness of fly ash for strength and durability of concrete, **Cement & Concrete Research,** vol.15, no.5, 1985, pp.793-800.

2.116 Kuo, S.T., Hsu, C.C. and Quo, L.W. Stabilised fly ash as a light weight concrete construction material, **ASH - A valuable resource, proceedings,** CSIR, Pretoria, 2-6 Feb.1987, vol.2.

2.117 Dhir, R.K., Jones, M.R. and Munday, J.G.L. Physical characterization of UK pulverised fuel ashes for use in concrete, **Magazine of Concrete Research,** vol.37, no.131, June 1985, pp.75-87.

2.118 Mehta, P.K. Influence of fly ash characteristics on the strength of portland fly ash mixtures, **Cement & Concrete Research,** vol.15, no.4, 1985, pp.669-674.

2.119 Sharma, R.C., Jain, N.K. and Gosh, S.N. Semi-theoretical method for the assessment of reactivity of fly ashes, **Cement & Concrete Research,** vol.23, no.1, 1993, pp.41-45.

2.120 Osborne, G.L. and Nixon, P.J. A comparative study of PFA cement made by blending and intergrinding 5 and 20% ash, **Silicates Industriels,** vol.1, 1982, pp.23-28.

2.121 Marusin, S.L. Experimental examination of fly ash concrete, **Cement, Concrete & Aggregates,** vol.6, no.2, Winter 1984, pp.125-136.

2.122 Kruger, R.E. Ash Resources, **The chemistry of fly ash and the pozzolanic reaction,** Personal communication, 1992, 10pp.

2.123 Haque, M.N., Ward, M.A. and Langan, B.W. Effect of sulphate content on the hydration & strength of cement/fly ash systems with & without water reducing admixture, **Magazine of Concrete Research,** vol.39, no.139, June 1987, pp.102-108.

2.124 Marsh, B.K., Day, R.L. and Bonner, D.G. Strength gain and CaOH depletion in hardened cement pastes containing fly ash, **Magazine of Concrete Research,** vol.38, no.134, Mar.1986, pp.23-29.

2.125 Gopolan, M.K. and Haque, M.N. Mix design for optimal strength development of fly ash concrete, **Cement & Concrete Research,** vol.19, 1989, pp.634-641.

2.126 Fraay, A.L.A., Bijen, J.M. and de Haan, Y.M. The reaction of fly ash in concrete. A critical examination, **Cement & Concrete Research,** vol.19, 1989, pp.235-246.

2.127 Dalziel, J.A. and Gutteridge, W.A. **The influence of pulverized-fuel ash upon the hydration characteristics and certain physical properties of a portland cement paste**, Wexham Springs, Slough: Cement and Concrete Association, 1986. (C&CA TR 42.560).

2.128 Dhir, R.K., Ho, N.Y. and Munday, J.G.L. Pulverised fuel ash in structural precast concrete, **Concrete,** June 1985, pp.32-35.

2.129 Berry, E.E. and Malhotra, V.M. Fly ash for use in concrete - a critical review, **ACI Journal,** Mar.1980, pp.59-73.

2.130 Ravina, D. Efficient utilisation of coarse and fine fly ash in precast concrete by incorporating thermal curing, **ACI Journal,** May-June 1981, pp.194-200.

2.131 Al-ani, M.N.A. and Hughes, B.P. PFA concrete mix design for the 1990's, **Cement & Concrete Composites,** vol.13, 1991, pp.187-195.

2.132 Addis, B.J. ed. **Fulton's concrete technology**, 6th ed, Midrand: Portland Cement Institute, 1986, p.67.

2.133 Helmuth, R.A. Water reducing properties of fly ash in cement pastes, mortars and concretes: causes and test methods, **Fly ash, silica fume, slag, and natural pozzolans in concrete, proceedings of the second international conference, Madrid, Spain,** vol.1, 1986, pp.723-741. (SP-91).

2.134 Thomas, M.D.A. and Matthews, J.D. Durability studies of PFA concrete structures, **BRE Information Paper,** 11/91, June 1991.

2.135 Dhir, R.K., Munday, J.G.L. and Ong, L.T. Investigations of the engineering properties of OPC/PFA concrete: Strength development and maturity, **Proceedings of the ICE,** Part 2, vol.77, June 1984, pp.239-254.

2.136 Thomas, M.D.A. An investigation of conventional ordinary portland cement and pulverised fuel ash concrete in 10 year old concrete bridges, **Proceedings of the ICE,** Part 1, Dec.1989, pp.1111-1128.

2.137 Hedegaard, S.E. and Hansen, T.C. Modified water/cement ratio law for compressive strength of fly ash concretes, **Materials & Structures,** vol.25, 1992, pp.273-283.

2.138 Saito, M. and Kawamura, M. Effect of fly ash and slag on the interfacial zone between cement and aggregate, **Fly ash, silica fume, slag, and natural pozzolans in concrete, proceedings of the third international conference, Trondheim, Norway,** 1989, pp.669-688. (ACI SP-114).

2.139 Swamy, R.N., Ali, S.A.R. and Theodorakopoulos, D.D. Early strength fly ash concrete for structural applications, **ACI Journal,** no.80-40, Sept./Oct.1983, pp.414-423.

2.140 Dhir, R.K. et al, PFA in structural precast concrete: measurement of permeability. **Concrete,** Dec.1986, pp.4-8.

2.141 Taylor, P.C. et al, Comparative testing of portland cement, fly ash, ground granulated blastfurnace slag and silica fume concretes for potential durability, **Fifth CANMET/ACI International Conference on Fly Ash, Silica Fume, Slag and Natural Pozzolans in Concrete,** Milwaukee, June 1995, (in publication).

2.142 Amtsbuchler, R. Effect of different curing regimes on fly ash concrete, **ASH - A valuable resource, proceedings,** CSIR, Pretoria, 2-6 Feb.1987, vol.2.

2.143 van Dijk, J. The influence of fly Ash on the properties of hardened concrete cured under various conditions. **ASH - A valuable resource, proceedings,** CSIR, Pretoria, 2-6 Feb.1987, vol.2.

2.144 Dhir, R.K., Munday, J.G.L. and Ong, L.T. Strength variability of OPC/PFA concrete. **Concrete,** June 1981, pp.33-37.

2.145 Meyer, A. Use of fly ash in cement, **ASH - A valuable resource, proceedings,** CSIR, Pretoria, 2-6 Feb.1987, vol.2.

2.146 Dhir, R.K., Munday, J.G.L. and Ong, L.T. Investigations of the engineering properties of OPC/pulverised fuel ash concrete deformation, **The Structural Engineer,** vol.64, no.2, June 1986, pp.36-42.

2.147 Ellis, W.E. For durable concrete, fly ash does not replace cement, **Concrete International,** July 1992, pp.47-51.

2.148 Haque, M.N. and Kayyali, O.A. Strength & porosity of hardened cement fly ash pastes in a hot environment, **ACI Materials Journal,** vol.86, Mar.1989, pp.128-134.

2.149 Kayyali, O.A. and Haque, M.N. Effect of carbonation on the chloride concentration in pore solution of mortars with and without fly ash, **Cement & Concrete Research,** vol.18, 1988, pp.636-648.

2.150 Thomas, M.D.A. and Matthews, J.D. Carbonation of fly ash concrete, **Magazine of Concrete Research,** vol.44, no.160, Sept.1992, pp.217-228.

2.151 Butler, W. and Baweja, D. Long-term durability of fly ash concretes in civil engineering structures, **Concrete durability, Katharine and Bryant Mather international conference,** Detroit: American Concrete Institute, 1987, pp.519-540. (ACI SP-100).

2.152 Dunster, A.M. A comparison between the carbonation of OPC and PFA concrete in a mass concrete structure, **Advances in Cement Research,** vol.4, no.14, Apr.1992, pp.69-74.

2.153 Addis, B.J. The effect on properties of hardened concrete of substituting milled granulated blastfurnace slag, fly ash, or silica fume for part of the portland cement, **Practical guidelines on the selection and use of portland cement, MGBS, fly ash and silica fume in concrete, symposium, Midrand, Portland Cement Institute**, 1987.

2.154 Ravina, D. Early longitudinal dimensional changes of fresh fly ash mortar exposed to drying conditions, **Cement & Concrete Research,** vol.16, no.6, 1986, pp.902-910.

2.155 Oberholster, R.E. Inhibiting alkali-silica reaction: The role of portland cement, milled granulated blastfurnace slag, fly ash and silica fume, **Symposium: Practical guidelines on the selection and use of portland cement, MGBS, fly ash and silica fume in concrete, symposium, Midrand, Portland Cement Institute**, 1987.

2.156 Nixon, P.J. et al, The effect of PFA with a high total alkali content on pore solution composition and ASR, **Magazine of Concrete Research,** vol.38, no.134, Mar.1986, pp.30-35.

2.157 Davies, G. and Oberholster, R.E. Use of NBRI accelerated test to evaluate the effectiveness of mineral admixtures in preventing the alkali-silica reaction, **Cement & Concrete Research,** vol.17, no.1, 1987, pp.97-107.

2.158 Sarkar, S.L., Baalbaki, M. and Aitcin, P.C. Microstuctural development in a high strength concrete containing a ternary cementitious system, **Cement, Concrete and Aggregates,** vol.13, no.2, Winter 1991, pp.81-87.

2.159 Brooks, J.J. and Sikharulidze, Z.D. Strength and fracture energy of concrete with and without fly ash cured in water at different constant temperatures, **Fly ash, silica fume, slag, and natural pozzolans in concrete, proceedings of the fourth international conference, Istanbul, Turkey**, 1992, pp.300-317. (ACI SP-132).

2.160 Larbi, J.A. and Bijen, J.M. Effect of mineral admixtures on the cement paste aggregate interface, **Fly ash, silica fume, slag, and natural pozzolans in concrete, proceedings of the fourth international conference, Istanbul, Turkey,** 1992, pp.655-669. (ACI SP-132).

CHAPTER 3

3.1 Tse, E.W., Lee, D.Y. and Klaiber, F.W. Fatigue behaviour of concrete containing fly ash, **Fly ash, silica fume, slag, and natural pozzolans in concrete, proceedings of the second international conference,** Madrid, 1986, SP 91-12. (ACI special publication 91).

3.2 Bennett, E.W. Fatigue in concrete, **Concrete,** vol.8, no.5, May 1974, pp.43-45.

3.3 Holmen, J.O. Fatigue design evaluation of offshore concrete structures, **Materiaux et Constructions,** vol.17, no.97, pp.39-42.

3.4 Hoff, G.C. Considerations for the use of concrete for offshore structures, **SP Evaluation and rehabilitation of concrete structures and innovations in design, proceedings of an ACI international conference,** Hong Kong, 1991, vol.2, pp.749-788. (ACI special publication 128).

3.5 BS5400: Part 10: 1980, **Code of practice for fatigue,** London: British Standards Institution, 1980.

3.6 Bennett, E.W. and St Muir, S.E. Some fatigue tests of high strength concrete in axial compression, **Magazine of concrete research,** vol.19, 1967, pp.113-117.

3.7 American Concrete Institute, Committee 215, Considerations for design of concrete structures subjected to fatigue loading, (ACI 215R-74, revised 1992), **ACI manual of concrete practice**, Detroit: ACI, 1993, part 1, pp.215R-2 to 215R-5.

3.8 Siemes, A.J.M. Fatigue evaluation of concrete structures - preliminary studies, procedure and examples, **Heron,** vol.33, no.3, 1988.

3.9 Destrebecq, J.F. and Szerszen, M. A model of prediction for plain concrete subjected to high level compressive cyclic loading, **International conference on concrete & structures,** Hong Kong, March 1993, pp.45-49.

3.10 Tait, R.B. **Fatigue and fracture of cement mortars,** PhD Thesis, Cape Town: University of Cape Town, 1985.

3.11 Hsu, T.T.C. Fatigue of plain concrete, **ACI journal,** July-Aug. 1981, pp.292-305.

3.12 Matsufuji, Y. and Ohkubo, T. On the estimating method of fatigue strength of the brittle materials under repeated impulsive bending load, **SEM/RILEM international conference on fracture of concrete and rock,** Houston Texas, June 1987.

3.13 Garrett, G.G. Failure by Fatigue, **Engineering Applications of Fracture Analysis,** ed. G.G. Garrett and D.L. Marriott, Pergaman Press, 1980.

3.14 Raju, N.K. Comparative study of the fatigue behaviour of concrete mortar and paste in uniaxial compression, **ACI journal,** June 1970, pp.461-463.

3.15 Tepfers, R. Tensile fatigue strength of plain concrete, **ACI journal,** Aug. 1979, pp.919-933.

3.16 Petkovic, G. et al. Fatigue of high-strength concrete, **High-strength concrete, second international symposium,** Detroit: American Concrete Institute,1990, pp.505-525. (ACI special publication 121).

3.17 Oh, B.H. Fatigue life distributions of concrete for various stress levels, **ACI materials journal,** vol.88, no.2, Mar. 1991, pp.122-128.

3.18 Evans, A.G. Fatigue in ceramics. **International journal of fracture,** vol.16, 1980, pp 484-498.

3.19 Holmen, J.O. Fatigue of concrete by constant and variable amplitude loading, **Fatigue of concrete structures**, edited by S.P. Shah, Detroit: American Concrete Institute, 1982, pp.71-110. (ACI special publication 75).

3.20 Krokosky, E.M. Static fatigue in hydrated portland cement, **Materials and construction,** vol.6, no.36, 1973, pp.447-452.

3.21 Tepfers, R. and Kutti, T. Fatigue strength of plain ordinary and lightweight concrete, **ACI journal,** May 1979, pp.635-653.

3.22 Horii, H., Shin, H.C. and Pallewatta, T.M. Mechanism of fatigue crack growth in concrete, **Cement & concrete composites,** vol.14, 1992, pp.83-89.

3.23 Paris, P.C., Gomez, M.P. and Anderson, W.P. A rational analytic theory of fatigue, **The Trend in Engineering,** vol.13, 1961, pp.9-14.

3.24 Paris, P.C. and Erdogan, F A critical analysis of crack propagation laws, **Journal of Basic Engineering,** vol.85, 1963, pp.528-534.

3.25 Baluch, M.H., Qureshy, A.B. and Azad, A.K. Fatigue crack propagation in plain concrete, **SEM/RILEM international conference on fracture of concrete and rock,** June 1987, pp.112-119.

3.26 Van Ornum, J.L. The fatigue of concrete, **Transactions of the American Society of Civil Engineers,** vol.58, June 1957, pp.294-320.

3.27 Mallet, G. **Fatigue of reinforced concrete,** London: HMSO, 1991. (TRRL state of the art review /2).

3.28 Darter, M.I. Concrete slab vs beam fatigue models, **2nd International workshop on the theoretical design of concrete pavements,** Siguenza Spain, 4-5 October 1990, pp.472-481.

3.29 Klaiber, F.W. and Lee, D.Y. The effects of air content, water cement ratio and aggregate type on the flexural fatigue strength of plain concrete, **Fatigue of concrete structures**, edited by S.P. Shah, Detroit: American Concrete Institute, 1982, pp.111-131. (ACI special publication 75).

3.30 Wilkes, W.J. Fatigue, concrete vs steel, **ACI Journal,** July August 1989, pp.76-79.

3.31 Howells, H. and Raithby, K.D. **Static and repeated loading tests on lightweight prestressed concrete bridge beams**, Crowthorne, Berks: Transport and Road Research Laboratory, 1977. (TRRL laboratory report 804).

3.32 Waagaard, K. Fatigue strength evaluation of off-shore concrete structures, **Fatigue of concrete structures**, edited by S.P. Shah, Detroit: American Concrete Institute, 1982, pp.373-397. (ACI special publication 75).

3.33 Libby, J.R. Critique of a post-tensioned roof slab failure, **Concrete Beton,** First quarter 1987, pp.10-15.

3.34 Tait, R.B. and Willmott, S.S. **Impact fracture of dolosse**, Johannesburg: University of the Witwatersrand, Department of metallurgy fracture, 1982.

3.35 Oh, B.H. and Kim, J.S. Fatigue damage analysis of concrete structures under variable amplitude cyclic loadings, **The third east Asia Pacific conference on structural engineering construction,** Shanghai, 23-26 April 1991, pp.306-310.

3.36 Hsu, T.T.C. Fatigue of plain concrete, **ACI Journal,** vol.78, no.4, July-August 1981, pp.292-305.

3.37 Award, M.E. and Hilsdorf, H.K. Fatigue, strength and deformation characteristics of plain concrete subjected to high repeated & sustained loads, **Abeles symposium on fatigue of concrete**, Detroit: American Concrete Institute, 1974, pp.1-13. (ACI special publication 41).

3.38 Pons, G., Ramoda, S.A. and Maso, J.C. Influence of the loading history on fracture mechanics parameters of microconcrete: effects of low frequency cyclic loading, **ACI materials journal,** Sept.1988, pp.341-346.

3.39 Oh, B.H. Cumulative damage theory of concrete under variable amplitude fatigue loadings, **ACI materials journal,** vol.88, no.1, Jan. 1991, pp.41-48.

3.40 Lloyd, J.P., Lott, J.L. and Kessler, C.E. **Fatigue of concrete**, Urbana, Illinois: University of Illinois, Department of Theoretical and Applied Mechanics, 1967. (T. & A.M. report 675).

3.41 Kiyomiya, O. et al. Fatigue properties of prestressed beam column joints, with emphasis on offshore structures subject to wave loading, **ACI journal,** Nov. 1988, pp.138-162.

3.42 Ozaki, S. and Sugata, N. Fatigue of concrete composed of BFS or SF under submerged conditions, **Fly ash, silica fume, slag, and natural pozzolans in concrete, proceedings of the fourth international CANMET/ACI conference,** Turkey, Detroit: American Concrete Institute, 1992, pp.1509-1524. (ACI special publication 132).

3.43 Husak, A.D. and Krokosky, E.M. Static fatigue of hydrated cement concrete, **ACI journal,** April 1971, pp.263-271.

3.44 Nelson, E.L., Carrasquillo, R.L. and Fowler, D.W. Behaviour and failure of high strength concrete subjected to biaxial cyclic compression loading, **ACI materials journal,** vol.85, July 1988, pp.248-253.

3.45 Nishibayashi, S., Inoue, S. and Yamura, K. Fatigue characteristics of reinforced concrete in water, **Concrete in marine environment, proceedings of the second CANMET/ACI international conference,** Canada, 1988, pp.543-561.

3.46 Schneider, U., Nagele, E. and Dujardin, N. The durability of cementitious materials subjected to chemo-mechanical stresses, **Durability of construction materials, proceedings of the first international RILEM congress,** London: Chapman & Hall, 1987, vol.3, pp.982-989.

3.47 Petkovic, G. et al. Fatigue of high-strength concrete, **High-strength concrete, second international symposium,** Detroit: American Concrete Institute,1990, pp.505-525. (ACI special publication 121).

3.48 Bazant, Z.P. and Xu, K. Size effect in fatigue fracture of concrete, **ACI materials journal,** vol.88, no.4, July-Aug. 1991, pp.390-399.

3.49 Neal, J.A. and Kessler, C.E. **Some aspects of fatigue of concrete**, Urbana, Illinois: University of Illinois, Department of Theoretical and Applied Mechanics, 1965. (T.& A.M. report 657).

3.50 Shah, S.P. and Chandra, S. Fracture of concrete subjected to cyclic and sustained loading, **ACI journal,** Oct. 1970, pp.816-825.

3.51 Maher, A. and Darwin, D. Mortar constituent of concrete in compression, **ACI materials journal,** vol.79, Mar. 1982, pp.100-109.

3.52 Yankelevsky, D.Z. and Reinhardt, H.W. Response of plain concrete to cyclic tension, **ACI materials journal,** vol.84, Sept. 1987, pp.365-373.

3.53 Tait, R.B. and Garrett, G.G. A fracture mechanics evaluation of static and fatigue crack growth in cement mortar, **Proceedings of International Conference on Fracture Mechanics in Concrete: Fundamentals and Applications,** Lausanne: October 1-3 1985, pp.13-22.

3.54 Ruimin, W., Guofan, Z. and Yupu, S. Fatigue of plain concrete under compression, **The third east Asia Pacific conference on structural engineering construction,** Shanghai, 23-26 April 1991, pp.311-316.

3.55 Binsheng, Z., Zhaohong, Z. and Keru, W. Fatigue rupture of plain concrete, **SEM/RILEM international conference on fracture of concrete and rock,** Houston, Texas, June 1987, pp.90-95.

3.56 Perdikaris, P.C. and Calomino, A.M. Kinetics of crack growth in plain concrete, **SEM/RILEM international conference on fracture of concrete and rock,** Houston, Texas, June 1987, pp.96-100.

3.57 Otter, D.E. and Naaman, A.E. Model for response of concrete to random compressive loads, **Journal of structural engineering,** vol.115, no.11, Nov. 1989, pp.2794-2809.

3.58 Garrett, G.G., Jennings, H.M. and Tait, R.B. The fatigue hardening behaviour of cement based materials, **Journal of materials science,** vol.14, 1979, pp.296-306.

3.59 Evans, A.G. and Fuller, E.R. Crack propogation in ceramic materials under cyclic loading conditions, **Metallurgical Transactions,** January 1974, vol. 5, pp.27-33.

3.60 Siemes, A.J.M. Miners rule with respect to plain concrete variable amplitude tests, **Fatigue of concrete structures**, edited by S.P. Shah, Detroit: American Concrete Institute, 1982, pp.343-372. (ACI special publication 75).

3.61 Bennett, E.W. and Jinawath, P. Compressive strength of concrete under repeated loading of varying intensity, **Conference on service life of supporting structures in concrete and panel buildings,** Brno, Oct 1975.

3.62 Tepfers, R., Friden, C. and Georgsson, L. A study of the applicability to the fatigue of concrete of the palmgren-miner partial damage hypothesis, **Magazine of concrete research,** vol.29, no.100, Sept. 1977, pp.123-130.

3.63 van Leeuwen, J. and Siemes, A.J.M. Miners rule with respect to plain concrete, **Heron,** vol.24, no.1, 1979.

3.64 Akutagawa, S. et al. Effects of loading history on fracture properties of concrete, **ACI materials Journal,** vol.88, no.2, Mar. 1991, pp.170-180.

3.65 Alliche, A. and Francois, D. Fatigue behaviour of hardened cement paste, **Cement & concrete research,** vol.16, no.2, 1986, pp.199-206.

3.66 Cornelissen, H.A.W. Fatigue failure of concrete in tension, **Heron,** vol.29, no.4, 1984.

3.67 Cornelissen, H.A.W. **Constant-amplitude tests on plain concrete in uniaxial tension and tension-compression**, Delft: Delft University of Technology, Department of Civil Engineering, 1984. (Report 5-84-1).

3.68 Ramakrishnan, V., Bremner, T.W. and Malhotra, V.M. Fatigue strength and endurance limit of lightweight concrete, **Structural lightweight aggregate concrete performance**, edited by T.A. Hole, Detroit: American Concrete Institute, 1992, pp.397-421. (ACI special publication 136).

3.69 Alexander, M.G. **Fracture of plain concrete - a comparative study of notched beams of varying depth**, PhD thesis, Johannesburg: University of the Witwatersrand, 1986.

3.70 Stroeven, P. Mechanics of microcracking in concrete subjected to fatigue loading, **Proceedings of the 3rd Conference of ICM on mechanical behaviour of materials,** vol.3, Aug. 1979, pp.141-150.

3.71 Bascoul, A. and Maso, J.C. Microcracking and cracking limit state as functions of strain gradients for concrete, **Cement & concrete research,** vol.17, 1987, pp.661-672.

3.72 Wecharatana, M. and Shah, S.P. Double torsion tests for studying slow crack growth of portland cement mortar, **Cement & Concrete Research,** vol.10, 1980, pp.833-844.

3.73 Pletka, B.J., Fuller Jr, E.R. and Koepke, B.G. An evaluation of double-torsion testing - analysis, **Fracture mechanics applied to brittle materials,** edited by S.W. Freiman, Philadelphia: American Society for Testing and Materials, 1979, pp.7-18. (ASTM STP 678).

3.74 Fry, P.R. **Review of the double torsion test method**, MSc Thesis, Johannesburg: University of the Witwatersrand, 1982, chapter 3, pp.68-114.

3.75 Evans, A.G. Fracture mechanics determinations, **Fracture mechanics of ceramics,** ed. R.C. Bradt et al, New York: Plenium Press, 1974.

3.76 Yon, J-H., Hawkins, N.M. and Kobayashi, A.S. Strain rate sensitivity of concrete mechanical properties, **ACI materials journal,** vol.89, March 1992, pp.146-153.

3.77 Harsh, S. Shen, Z. and Darwin, D. Strain rate sensitive behaviour of cement paste and mortar in compression, **ACI materials journal,** vol.87, Sept. 1990, pp.508-516.

3.78 Fu, H.C., Erki, M.A. and Seckin, M. Review of effects of loading rate on concrete in compression, **Journal of structural engineering,** vol.117, no.12, Dec. 1991, pp.3645-3659.

3.79 Bischoff, P.H. and Perry, S.H. Compressive behaviour of concrete at high strain rates, **Materials & structures,** vol.24, 1991, pp.425-450.

3.80 Rossi, P. et al. The dynamic behaviour of concrete: influence of free water, **Materials & structures,** vol.25, 1992, pp.509-514.

3.81 Rossi, P. A physical phenomenon which can explain the mechanical behaviour of concrete under high strain rates, **Materials & structures,** vol.24, 1991, pp.422-424.

3.82 Sparks, P.R. and Menzies, J.B. The effect of rate of loading upon the static and fatigue strengths of plain concrete in compression, **Magazine of concrete research,** vol.25, no.83, June 1973, pp.73-80.

3.83 Hirst, G.A. and Neville, A.M. A discussion on "Creep of concrete under cyclically varying dynamic loads", **Cement & concrete research,** vol.6, 1976, pp.715-718.

3.84 Cornelissen, H.A.W. and Timmers, G. **Fatigue of plain concrete in uniaxial tension and in alternating tension-compression: experiment and results,** Delft: Delft University of Technology, Department of Civil Engineering, 1981. (Report 5-81-7).

3.85 Murdock, J.W. and Kessler, C.E. Effect of range of stress on fatigue strength of plain concrete beams, **Proceedings of the American Concrete Institute,** vol.55, Aug. 1958, pp.221-231.

3.86 Rusch, H. Researches toward a general flexural theory for structural concrete, **Journal of the American Concrete Institute,** vol.57, July 1960, pp.1-28.

3.87 Barrick, E. and Krokosky, E.M. The effects of temperature & relative humidity on static strength of hydrated portland cement, **Journal of testing & evaluation,** vol.4, no.1, Jan. 1976, pp.61-73.

3.88 Bazant, Z.P. and Pratt, P.C. Effect of temperature and humidity on fracture energy of concrete, **ACI materials journal,** vol.85, July 1988, pp.262-271.

3.89 Raithby, K.D. and Galloway, J.D. Effects of moisture condition, age and rate of loading on fatigue of plain concrete, **Abeles symposium on fatigue of concrete**, Detroit: American Concrete Institute, 1974, pp.15-33. (ACI special publication 41).

3.90 Schneider, U. and Nagele, E. Stress corrosion of cement mortars in ammonium sulphate solution, **Cement & concrete research,** vol.23, no.1, 1993, pp.13-19.

3.91 Beaudoin, J.J. Effect of water and other dielectrics on subcritical crack growth in portland cement paste, **Cement & concrete research,** vol.15, no.6, 1985, pp.988-994.

3.92 Tait, R.B. and Garrett, G.G. Effect of moisture and time on static and fatigue crack growth in cement mortar, **From materials science to construction materials engineering. Volume 3 - Durability of construction materials**, edited by J.C. Maso, London: Chapman and Hall, 1987, pp.1162-1169.

3.93 Abdel-Jawad, Y. and Haddad, R. The effect of early overloading of concrete on strength at later ages, **Cement & concrete research,** vol.22, no.5, 1992, pp.927-936.

3.94 Barrick, II, J.E., **PhD Thesis,** Ann Arbor, Carnegie-Mellon University, 1972.

3.95 Beaudoin, J.J. Effect of humidity and porosity on fracture of hardened concrete, **Cement & concrete research,** vol.12, no.6, 1982, pp.705- 716.

3.96 Schneider, U., Nagele, E. and Dumat, F. Stress corrosion initiated cracking of concrete, **Cement & concrete research,** vol.16, no.4, 1986, pp.535- 544.

3.97 Hanson, T.C. Cracking and fracture of concrete and cement paste, **Causes, mechanism, and control of cracking in concrete,** Detroit: American Concrete Institute, 1968, pp.43-65. (ACI special publication 20).

3.98 Bentur, A. and Mindess, S. The effect of concrete strength on crack patterns, **Cement & concrete research,** vol.16, no.1, 1986, pp.59-66.

3.99 Schlangen, E. and van Mier, J.G.M. Experimental and numerical analysis of micromechanisms of fracture of cement based composites, **Cement & concrete composites,** vol.14, 1992, pp.105- 118.

3.100 Suter, G.T. and Mickleborough, N.C. Creep of concrete under cyclically varying dynamic loads, **Cement & concrete research,** vol.5, no.6, 1975, pp.565-576.

3.101 Cornelissen, H.A.W. and Reinhardt, H.W. Service life prediction based on secondary strain rate for plain concrete in tension, **Durability of construction materials, proceedings of the first international RILEM congress,** London: Chapman & Hall, 1987, vol.3, pp.1286-1293.

3.102 Bazant, Z.P. and Gettu, R. Rate effects and load relaxation in static fracture of concrete, **ACI materials journal,** Sept. 1992, pp.456-468.

3.103 Alexander, M.G. **Fulton's concrete technology**, Addis, B.J. ed., 7th revised edition, Midrand: Portland Cement Institute, 1994, pp.128.

3.104 Garrett, G.G., Tait, R.B. and James, N. **Introduction to fracture mechanics,** Johannesburg: University of the Witwatersrand, Division of Continuing Engineering Education, July 1986.

3.105 Gordon, J.E. **The new science of strong materials,** 2nd ed. Hammondsworth: Pelican Books, 1976.

3.106 Griffith A.A. The phenomena of rupture and flow in solids, **Philosophical Transactions, Royal Society of London,** vol.A221, 1921.

3.107 Reinhardt, H.W., Basic types of fracture, **Fracture mechanics of concrete structures,** edited by L. Elfgren, London: Chapman & Hall, 1989.

3.108 Watson, T. et al. An evaluation of the short rod technique to measure the fracture toughness of polymers, **Journal of materials science,** vol.22, 1987, pp.1249-1258.

3.109 Krell, A. and Pompe, W. The influence of subcritical crack growth on the strength of ceramics, **Materials science and engineering,** vol.89, 1987, pp.161-168.

3.110 Ritchie, R.O. and Lankford, J. Small fatigue cracks: a statement of the problem and potential solutions, **Materials science and engineering,** vol.84, 1986, pp.11-16.

3.111 BS 5447:1977, **Methods of test for plane strain fracture toughness (K_{IC}) for metallic materials,** London: British Standards Institution, 1977.

3.112 Zahoor, A. J-integral analysis of three-point bend specimen, **Transactions of the ASME,** vol.111, April 1989, pp.132-144.

3.113 Jennings, H.M. The design of high strength cement based materials: part 1, **Materials science & technology,** vol.4, Apr. 1988, pp.277-284.

3.114 Alvarado, M.A., Shah, S.P. and John, R. Mode 1 fracture in concrete using centre-cracked plate specimens, **Journal of engineering mechanics,** vol.115, no.2, Feb.1989, pp.366-383.

3.115 Ratanalert, S. and Wecharatana, M. Evaluation of existing fracture models in concrete, **Fracture mechanics: application to concrete,** Detroit: American Concrete Institute, 1989, pp.113-146. (ACI special publication 118).

3.116 Shah, S.P. and Tasdemir, M.A. Role of fracture mechanics in concrete technology, **Advances in concrete technology, Canmet international conference,** Athens, May 1992.

3.117 Cotterell, B., Paramasivam, P. and Lam, K.Y. Modelling the fracture of cementitious materials, **Materials and structures,** no.25, 1992, pp.14-20.

3.118 Gylltoft, K. Cyclic loading, **Fracture mechanics of concrete structures,** edited by L. Elfgren, London: Chapman & Hall, 1989, pp.172-177.

3.119 Carpinteri, A. Preface, **Applications of fracture mechanics to reinforced concrete,** London: Elsevier, 1992, pp.v-viii.

3.120 Van Mier, J.G.M. Scaling in tensile and compressive fracture of concrete, **Applications of fracture mechanics to reinforced concrete,** London: Elsevier, 1992, pp.95-136.

3.121 Mindess, S. An application of fracture mechanics to cement & concrete: A historical review, **Fracture mechanics of concrete**, edited by F.H. Whittmann, London: Elsevier, 1983, pp.1-25.

3.122 Hillerborg, A. Fracture mechanics and the concrete codes, **Fracture mechanics: application to concrete,** Detroit: American Concrete Institute, 1989, pp.157-169. (ACI special publication 118).

3.123 Hillerborg, A., Modeer, M. and Petersson, P.E. Analysis of crack formation and crack growth in concrete by means of fracture mechanics and finite elements, **Cement & concrete research,** vol.6, no.6, 1976, pp.773-782.

3.124 Bazant, Z.P. and Oh, .H. Crack band theory for fracture of concrete, **Applied Mechanics Review,** 1986, vol.39, no.5, pp.675-705.

3.125 Jenq, Y-S. and Shah, S.P. On the fundamental issues of mixed mode crack propagation in concrete, **Fracture of concrete & rock, recent developments,** edited by S.P. Shah, London: Elsevier, 1989, pp.27-38.

3.126 Wecharatana, M. and Shah, S.P. Slow crack growth in cement composites, **ASCE structures,** vol.108, no.st6, June 1982, pp.1400-1413.

3.127 Alexander, M.G. and Blight, G.E., A comparative study of fracture parameters in notched concrete beams, **Magazine of concrete research,** vol.40, no.142, March 1988, pp.50-58.

3.128 Planas, J., Elices, M. and Toribio, J. Approximation of cohesive crack models br R-CTOD curves, **Fracture of concrete & rock, recent developments,** edited by S.P. Shah, London: Elsevier, 1989, pp.213-222.

3.129 Alexander, M.G., Tait, R.B. and Gill, L.M. Characterisation of microcracking and crack growth in notched concrete and mortar using the J-integral approach, **Fracture of concrete & rock, recent developments,** edited by S.P. Shah, London: Elsevier, 1989, pp.317-326.

3.130 Mazars, J. and Pijaudier-Cabot, J. Continuum damage theory - application to concrete, **ASCE journal of engineering mechanics,** vol.115, no.2, Feb. 1989, pp.345-365.

3.131 Mazars, J. A description of micro- and macroscale damage of concrete structures, **Engineering fracture mechanics,** vol.25, no.5/6, 1986, pp.729-737.

3.132 Van Mier, J.G.M. Mode I fracture of concrete: Discontinuous crack growth and crack interface grain bridging, **Cement & concrete research,** vol.21, 1991, pp.1-15.

3.133 Hu, X.Z. and Wittmann, F.H. Fracture energy and fracture process zone, **Materials and structures,** vol.25, 1992, pp.319-326.

3.134 Alexander, M.G. The use of ultrasonic pulse velocity for fracture testing of cemented materials, **Cement, concrete & aggregates,** vol.10, no.1, Summer 1988, pp.9-14.

3.135 Alexander, M.G. and Blight, G.E. Behaviour of fracture zones in notched concrete beams, **International journal of fracture**, vol.44, 1990, pp.71-77.

3.136 Hu, X.Z. and Whittman, F.H. An analytical method to determine the bridging stress transferred within the fracture process zone: II, Application to mortar, **Cement & concrete research,** vol.22, 1992, pp.559-570.

3.137 Yu C.T., Kobayashi A.S. and Hawkins N.M. Energy dissipation mechanisms associated with rapid fracture of concrete, **Experimental mechanics,** Sept. 1993, pp.205-211.

3.138 Shah, S.P. Wither fracture mechanics for concrete, **Fracture of concrete & rock, recent developments,** edited by S.P. Shah, London: Elsevier, 1989, pp.1-4.

3.139 Howard, A.J. and Kendall, K. Flexural strength and porosity of cements, **Nature**, vol.289, Jan. 1981, pp.388-389.

3.140 Jennings, H.M. The design of high strength cement based materials: part 3, **Materials science & technology,** vol.4, Apr. 1988, pp.291-299.

3.141 Birchall, J.D. Cement in the context of new materials for an energy-expensive future, **Philosophical Transactions, Royal Society of London,** vol.A310, 1983, pp.31-42.

3.142 Pye, G.B. and Beaudoin, J.J. An energy approach to bond strength determinations in cement systems, **Cement & concrete research,** vol.22, 1992, pp.551-558.

3.143 Eden, N.B. and Bailey, J.E. On the factors effecting strength of portland cement, **Journal of materials science,** vol.19, 1984, pp.150-158.

3.144 Evans, A.G., Clifton, J.R. and Anderson, E. The fracture mechanics of mortars, **Cement & concrete research,** vol.6, no.4, 1976, pp.535-548.

3.145 Schlangen, E. Experimental and numerical analysis of fracture processes in Concrete, **Heron,** vol.38, no.2, 1993, pp.1-56.

3.146 Barr, B. and Tokatly, Z.Y. Size effects in two compact test specimen geometries, **Applications of fracture mechanics to reinforced concrete,** London: Elsevier, 1992, pp.63-94.

3.147 Nallathambi, P. and Karihaloo, B.L. Determination of specimen-size independent fracture toughness of plain concrete, **Magazine of concrete research,** vol.38, no.135, June 1986, pp.67-76.

3.148 Carpinteri, A. Decrease of apparent tensile & bending strength with specimen size: 2 different explanations based on fracture mechanics, **International journal of solids & structures,** vol.25, no.4, 1989, pp.407-429.

3.149 Bazant, Z.P. Should design codes consider fracture mechanics size effect, **Concrete design based on fracture mechanics,** edited by W.Gertsle, Detroit: American Concrete Institute, 1992, pp.11-13. (ACI special publication 134).

3.150 Planas, J., Elices, M. and Guinea, G.V. Measurement of the fracture energy using three point bend tests: Part 2 Influence of bulk energy dissipation, **Materials & structures,** vol.25, 1992, pp.305-312.

3.151 Zielinski, A.J. Model for tensile fracture of concrete at high rates of loading, **Cement & concrete research,** vol.14, no.2, 1984, pp.215-224.

3.152 Wolinski, S. et al. Influence of aggregate size on fracture mechanics parameters of concrete, **International journal of cement composites and lightweight concrete,** vol.9, no.2, May 1987, pp.95-103.

3.153 Tait, R.B. and Garrett, G.G. A fracture mechanics evaluation of static and fatigue crack growth in cement mortar, **Fracture toughness & fracture energy of concrete,** edited by F.H. Whittmann, London: Elsevier, 1986, pp.21-30.

3.154 Bazant, Z.P. and Xu, K. Size effect in fatigue fracture of concrete, **ACI materials journal,** vol.88, no.4, July 1991, pp.390-399.

3.155 Swartz, S.E., Huang, C.M.J. and Hu, K.K. Crack growth and fracture in plain concrete-static versus fatigue loading, **Fatigue of concrete structures**, edited by S.P. Shah, Detroit: American Concrete Institute, 1982, pp.47-68. (ACI special publication 75).

3.156 Bazant Z.P. and Schell W.F. Fatigue fracture of high strength concrete and size effect, **ACI materials journal,** vol.90, no.5, Sept. 1993, pp.472-478.

3.157 Horii, H., Shin, H.C. and Pallewatta, T.M. Mechanism of fatigue crack growth in concrete, **Cement & concrete composites,** vol.14, 1992, pp.83-89.

3.158 Mazumdar, P.K. and Jeelani, S. Plastic deformation - its role in fatigue crack propagation, **Journal of materials science,** no.21, 1986, pp.3611-3614.

3.159 Demaid, A.P.A. **Fracture mechanics applied to fatigue crack growth**, Milton Keynes: Open University, n.d.

3.160 Ritchie, R.O. Slow crack growth: Macroscopic and microscopic Aspects, **Fracture and Fracture Mechanics, Case Studies,** Eds R.B. Tait & G.G. Garrett, Johannesburg: Pergamon Press, 1984, pp.93-124.

3.161 Suresh, S. and Brokenborough, J.R. Theory and experiments of fracture in cyclic compression: Single phase ceramics, transformation ceramics and ceramic components, **Acta metallurgica,** vol.36, no.6, 1988, pp.1455-1470.

3.162 Prasad, N.E. and Bhaduri, S.B. Subcritical growth of long cracks in heterogenous materials, **Journal of materials science,** vol.23, 1988, pp.2167-2173.

3.163 Kim, K. and Mubeen, A. Relationship between differential stress intensity factor and crack growth rate in cyclic tension in westerly granite, **Fracture mechanics methods for ceramics, rock and concrete,** Philadelphia: American Society for Testing and Materials, 1981, pp.157-168. (ASTM STP 745).

CHAPTER 4

4.1 Evans, A.G. Fracture mechanics determinations, **Fracture mechanics of ceramics,** edited by R.C. Bradt et al, New York: Plenum Press, 1974. vol.1, pp.17-48.

4.2 Guinea, G.V., Planas, J. and Elices, M. Measurement of fracture energy using three point bend test: part 1 - influence of experimental procedures, **Materials & Structures,** vol.25, 1992, pp.212-218.

4.3 Tait, R.B., Fry, P.R. and Garrett, G.G. Review & evaluation of the double torsion technique for fracture toughness and fatigue testing of brittle materials, **Experimental Mechanics,** Mar.1987, pp.14-22.

4.4 Wecharatana, M. and Shah, S.P. Slow crack growth in cement composites, **ASCE Structures,** vol.108, no.st6, June 1982, pp.1400-1413.

4.5 Tait, R.B. **Fatigue and fracture of cement mortars**, PhD Thesis, Cape Town: University of Cape Town, 1985.

4.6 Fuller Jr, E.R. An evaluation of double-torsion testing - analysis, **Fracture mechanics applied to brittle materials,** edited by S.W. Freiman, Philadelphia: American Society for Testing and Materials, 1979, pp.3-18. (ASTM STP 678).

4.6a Outwater, J.O. et al, Double-torsion technique as a universal fracture toughness test method, **Fracture Toughness and Slow Stable Cracking**, Philadelphia: American Society for Testing and Materials, 1974, pp.127-138. (ASTM STP 559).

4.6b Kies, J.A. and Clark, B.J. **Fracture 1969**, edited by P.L. Pratt, London: Chapman and Hall, 1969, pp.483-491.

4.7 Leevers, P.S. and Williams, J.G. Double torsion testing of high velocity crack resistance, **Journal of Materials Science,** no.22, 1987, pp.1097-1107.

4.8 Pickles C.S.J. and Field J.E. Dependence of the strength of zinc sulphide on temperature and environment, **Journal of Materials Science,** vol.29, no.4, Feb.1994, pp.1115-1120.

4.9 Sano, O. A revision of the double torsion technique for brittle materials, **Journal of Materials Science,** vol.23, 1988, pp.2505-2511.

4.10 Kim, K. and Mubeen, A. Relationship between differential stress intensity factor and crack growth rate in cyclic tension in westerly granite, **Fracture mechanics methods for ceramics, rock and concrete, symposium,** 1981, pp.157-168. (ASTM STP 745).

4.11 Evans, A.G., Clifton, J.R. and Anderson, E. The fracture mechanics of mortars, **Cement & Concrete Research,** vol.6, no.4, 1976, pp.535-548.

4.12 Tait, R.B. and Garrett, G.G. A fracture mechanics evaluation of static and fatigue crack growth in cement mortar, **Fracture toughness & fracture energy of concrete,** edited by F.H. Whittmann, London: Elsevier, 1986, pp.21-30.

4.13 Detwiler, R.J. Subcritical crack growth in the cement paste - steel transition zone, **Cement & Concrete Research,** vol.20, 1990, pp.277-284.

4.14 Wecharatana, M. and Shah, S.P. Double torsion tests for studying slow crack growth of portland cement mortar, **Cement & Concrete Research,** vol.10, 1980, pp.833-844.

4.15 Yam, A.S. and Mindess, S. The effects of fibre reinforcement on crack propagation in concrete, **International Journal of Cement Composites and Lightweight Concrete**, vol.4, no.2, May 1992, pp.83-93.

4.16 Fry, P.R. **Review of the double torsion test method**, MSc Thesis, Johannesburg: University of the Witwatersrand, 1982, chapter 3, pp.68-114.

4.17 Michalske, T.A., Singh, M. and Frechette, V.D. Experimental observation of crack velocity and crack front shape effects in double torsion fracture mechanics tests, **Fracture mechanics for ceramics, rocks and concrete, symposium,** 1981, pp.3-12. (ASTM STP 745).

4.18 Tait, R.B and Garrett, G. Effect of moisture and time on static and fatigue crack growth in cement mortar, **Fracture toughness & fracture energy of concrete,** edited by F.H. Wittmann, London: Elsevier, 1986, pp.21-30.

4.19 Beaudoin, J.J. Effect of water and other dielectrics on subcritical crack growth in portland cement paste, **Cement & Concrete Research,** vol.15, no.6, 1985, pp.988-994.

4.20 Pabst, R.F. and Weick, J. Double torsion measurements with & without a guiding notch, **Journal of Materials Science,** vol.16, 1981, pp.836-838.

4.21 Hillerborg, A. Theoretical analysis of the double torsion test, **Cement and Concrete Research,** vol.13, 1983, pp.69-80.

4.22 Demaid, A.P.A. **Fracture mechanics applied to fatigue crack growth.**

4.23 Montgomery, D. and Diamond, S. The influence of fly ash cenospheres on the details of cracking in fly ash bearing cement pastes, **Cement & Concrete Research,** vol.14, 1984, pp.767-775.

4.24 Hassanzadeh, M. and Hillerborg, A. Theoretical analyses of test methods, **Fracture of concrete and rock, SEM/RILEM international conference,** Houston, Texas, 1987, pp.388-395.

4.25 Pletka, B.J., Fuller Jr, E.R. and Koepke, B.G. An evaluation of double-torsion testing - experimental, **Fracture mechanics applied to brittle materials,** edited by S.W. Freiman, Philadelphia: American Society for Testing and Materials, 1979, pp.19-37. (ASTM STP 678).

4.26 Epstein, D. **Stress analysis of of the double torsion specimen,** BSc Thesis, University of Cape Town, 1991.

CHAPTER 5

5.1 Hassanzadeh, M. and Hillerborg, A. Theoretical analyses of test methods, **SEM/Rilem international conference on fracture of concrete and rock,** Houston, Texas, June 1987, pp.388-395.

5.2 Hillerborg, A. Theoretical analysis of the double torsion test, **Cement and Concrete Research,** vol.13, no.1, 1983, pp.69-80.

5.3 ASTM C 109-92, **Standard test method for compressive strength of hydraulic cement mortars**, Philadelphia: American Society for Testing and Materials, 1992, pp.64-68.

5.4 Fry, P. **Review of the double torsion test method**, MSc Thesis, Johannesburg: University of the Witwatersrand, 1987, Chapter 3, pp.68-114.

5.5 Bazant, Z.P. and Xu, K. Size effect in fatigue fracture of concrete, **ACI Materials Journal,** vol.88, no.4, July 1991, pp.390-399.

5.6 BS 5447:1977, **Methods of test for plane strain fracture toughness (K_{Ic}) of metallic materials**, London: British Standards Institution, 1977.

5.7 Tait, R.B. **Fatigue and fracture of cement mortars**, PhD Thesis, Cape Town: University of Cape Town, 1985.

5.8 Tait, R.B., Fry, P.R. and Garrett, G.G. Review & evaluation of the double torsion technique for fracture toughness and fatigue testing of brittle materials, **Experimental Mechanics,** Mar.1987, pp.14-22.

5.9 Fuller Jr, E.R. An evaluation of double-torsion testing - analysis, **Fracture mechanics applied to brittle materials,** edited by S.W. Freiman, Philadelphia: American Society for Testing and Materials, 1979, pp.3-18. (ASTM STP 678).

5.10 Pletka, B.J., Fuller Jr, E.R. and Koepke, B.G. An evaluation of double-torsion testing - experimental, **Fracture mechanics applied to brittle materials,** edited by S.W. Freiman, Philadelphia: American Society for Testing and Materials, 1979, pp.19-37. (ASTM STP 678).

5.11 Hsu, T.T.C. Fatigue of plain concrete, **ACI Journal,** vol.78, no.4, July-August 1981, pp.292-305.

CHAPTER 6

6.1 Hsu, T.T.C. Fatigue of plain concrete, **ACI Journal,** vol.78, no.4, July-August 1981, pp.292-305.

6.2 Tait, R.B. **Fatigue and fracture of cement mortars**, PhD Thesis, Cape Town: University of Cape Town, 1985.

6.3 **Introduction to fracture mechanics,** Short course presented by the Fracture Research Group in the Department of Metallurgy and Materials Engineering, University of the Witwatersrand, July 1986.

CHAPTER 8

8.1 Sarkar, S.L. The importance of microstructure in evaluating concrete, **Advances in Concrete Technology,** Canmet, pp.123-158.

8.2 Diamond, S. and Mindess, S. SEM investigations of fracture surfaces using stereo pairs: 1. Fracture surfaces of rock and cement paste, **Cement & Concrete Research,** vol.22, no.1, 1992, pp.67-78.

8.3 Diamond, S., Ravina, D. and Lovell, J, The occurence of duplex films on flyash surfaces, **Cement & Concrete Research,** no.10, 1980, pp.297-300.

8.4 Diamond, S. et al, SEM investigations of the contact zones between rock surfaces and cement paste, **Interfaces in cementitious composites, proceedings of the international conference held by RILEM, Toulouse**, 1992, pp.13-22.

8.5 Diamond, S. The microstructure of cement paste in concrete, **8th International Congress on the Chemistry of Cement,** vol.1, Rio de Jeneiro, 1986, pp.123-147.

8.6 Taylor, P.C. and Tait, R.B. The effect of hydration age on morphology of fly ash cement, **Electron Microscopy Society of Southern Africa,** vol.20, 1990, pp.31-32.

8.7 Jennings, H.M. Design of high strength cement based materials: Part 2 Microstructure, **Materials Science and Technology,** vol.4, April 1988, pp.285-290.

8.8 Tait, R.B. **Fatigue and fracture of cement mortars**, PhD Thesis, Cape Town: University of Cape Town, 1985.

8.9 Wesche, K. (Ed) Fly Ash in Concrete, **Properties and Performance, Report of Technical Committee 67-FAB,** Rilem, E&FN Spon, pp.50-55.

8.10 Sarkar, S.L., Baalbaki, M. and Aitcin, P.C. Microstuctural development in a high strength concrete containing a ternary cementitious system, **Cement, Concrete and Aggregates,** vol.13, no.2, Winter 1991, pp.81-87.

8.11 Montgomery, D. and Diamond, S. The influence of fly ash cenospheres on the details of cracking in flyash-bearing cement pastes, **Cement & Concrete Research,** vol.14, no.5, 1984, pp.767-775.

8.12 Marusin, S.L. Experimental examination of fly ash concrete, **Cement, Concrete & Aggregates,** vol.6, no.2, Winter 1984, pp.125-136.

8.13 Tait, R.B. and Bohm, H. In situ scanning electron microscope observations of double torsion fracture of concrete, **Electron Microscopy Society of Southern Africa - Proceedings,** vol.10, 1980, pp.17-18.

8.14 Bentur, A. and Mindess, S. The effect of concrete strength on crack patterns, **Cement & Concrete Research,** vol.16, no.1, 1986, pp.59-66.

8.15 Tait, R.B. and Diamond, S. Backscatter and wet cell techniques for observing in situ fracture of double torsion cement samples, **Electron Microscopy Society of Southern Africa - Proceedings,** vol.16, 1986, pp.21-22.

CHAPTER 9

9.1 Suresh, S. Fatigue of brittle solids, Chapter 13, **Fatigue of materials,** Cambridge: Cambridge University Press, 1991, p.435.

9.2 Fry, P. **MSc Thesis,** Johannesburg: University of the Witwatersrand, 1987.

9.3 Tait, R.B. **Fatigue and fracture of cement mortars,** PhD Thesis, Cape Town: University of Cape Town, 1985.

9.4 Bazant, Z.P. and Gettu, R. Rate effects and load relaxation in static fracture of concrete, **ACI Materials Journal,** September-October 1992, vol.85, no.5, pp.456-468.

9.5 Tait, R.B. Comparative slow crack growth behaviour in hardened cement paste containing PFA, **ASH - A valuable resource, proceedings, CSIR, Pretoria,** 2-6 Feb.1987, vol.2.

9.6 Miller, K.J. Materials science perspective of metal fatigue resistance, **Materials Science and Technology,** June 1993, vol.9, pp.453-514.

9.7 Saito, M. and Kawamura, M. Effect of fly ash and slag on the interfacial zone between cement and aggregate, **Fly ash, silica fume, slag, and natural pozzolans in concrete, proceedings of the third international conference, Trondheim, Norway,** 1989, pp.669-688. (ACI SP-114).

9.8 Taylor, P.C., Influence of the duration of re-wetting of concrete samples on strength results, **Concrete Beton,** 1994.

9.9 Ballim, Y. **Curing and the durability of concrete,** PhD Thesis, Johannesburg: University of the Witwatersrand, 1994.

9.10 Ballim, Y., Taylor P.C., Lampacher, B.J, Assessment and control of concrete durability, **Concrete Meets the Challenge, National Convention of the CSSA,** Sept 1994.

9.11 Parrot, L.J. Moisture conditioning and transport properties of concrete test specimens, **Materials and Structures,** vol.27, 1994, pp.460-468.

9.12 Addis, B.J. ed. **Fulton's concrete technology**, 6th ed, Midrand: Portland Cement Institute, 1986. p.30.

9.13 Beaudoin, J.J. Effect of humidity and porosity on fracture of hardened portland cement, **Cement & Concrete Research,** vol.12, 1982, pp.705-716.

9.14 Schneider, U., Nagele, E. and Dumat, F. Stress corrosion initiated cracking of concrete, **Cement & Concrete Research,** vol.16, 1986, pp.535-544.

9.15 Cook, D.J. and Haque, M.N. Strength reduction and length changes in concrete and mortar on water and methanol sorption, **Cement & Concrete Research,** vol.4, 1974, pp.735-744.

9.16 Beaudoin, J.J. Feldman, R.F. and Tumidajski, P.J. Pore structure of hardened portland Cement pastes and its influence on properties, **Advanced Cement Based Materials**, vol. 1, 1994, pp.224-236.

9.17 Beaudoin, J.J. Personal communication, 1995.

9.18 Kleinlogel, A. **Influences on Concrete,** New York: Frederick Ungar Publishing, 1941.

9.19 Basson, J.J. Consultant chemist to Portland Cement Institute, Personal communication, 1994.

9.20 Paris, P.C. and Erdogan, F A critical analysis of crack propagation laws, **Journal of Basic Engineering,** vol.85, 1963, pp.528-534.

9.21 Suresh, S. **Fatigue of Materials,** Cambridge Solid State Science Series, Cambridge: Cambridge University Press, 1991.

9.22 Evans, A.G. and Fuller, E.R. Crack propagation in ceramic materials under cyclic loading conditions, **Metallurgical Transactions,** January 1974, vol. 5, pp.27-33.

9.23 Gordon, J.E. Cracks and dislocations, Chapter Four, **The New Science of Strong Materials 2nd Edition,** Pelican Books: Harmondsworth, 1976.

9.24 Tait, R.B. and Garrett, G.G. Effect of moisture and time on static and fatigue crack growth in cement mortar, **From materials science to construction materials engineering. Volume 3 - Durability of construction materials,** edited by J.C. Maso, London: Chapman and Hall, 1987, pp.1162-1169.

9.25 Addis, B.J. ed. **Fulton's concrete technology**, 7th ed, Midrand: Portland Cement Institute, 1994. p.128.

9.26 Bazant, Z.P. and Pratt, P.C. Effect of temperature and humidity on fracture energy of concrete, **ACI materials journal,** vol.85, July 1988, pp.262-271.

CHAPTER 10

10.1 Popovics, S. The slump test is useless - or is it?, **Concrete International,** September 1994, vol.16, no.9, pp.30-33.

APPENDIX A - DATA FOR V-K PLOTS

DATA POINTS FOR FIGURE 6.1

Scatter

V (mm/s)	K (MPa√m)	Krel (%)	Age (days)
2.24e-02	0.653	62.6	28
6.24e-03	0.653	62.6	28
6.65e-03	0.771	73.9	28
4.88e-02	0.831	79.6	28
2.12e-02	0.771	73.9	28
2.91e-03	0.771	73.9	28
1.57e-02	0.831	79.6	28
1.24e-02	0.711	70.8	28
1.14e-03	0.653	65.0	28
3.26e-03	0.711	70.8	28
3.35e-02	0.771	76.8	28
2.17e-02	0.771	76.8	28
3.40e-02	0.801	79.8	28
6.24e-02	0.801	79.8	28
3.72e-02	0.801	79.8	28
5.09e-03	0.711	70.8	28
4.03e-02	0.831	82.7	28
5.66e-02	0.745	75.4	28
1.42e-02	0.745	75.4	28
1.19e-02	0.745	75.4	28
6.51e-03	0.745	75.4	28
2.44e-03	0.745	75.4	28
2.74e-02	0.772	87.2	28
1.64e-01	0.780	83.3	28
2.24e-01	0.780	83.3	28
2.34e-01	0.780	83.3	28
4.87e-02	0.666	74.4	28
9.24e-02	0.699	70.6	28
6.48e-02	0.699	70.6	28
5.57e-03	0.636	64.3	28
1.06e-03	0.636	64.3	28
1.91e-03	0.636	64.3	28
7.98e-02	0.763	77.1	28
4.09e-01	0.826	83.5	28
1.61e-02	0.780	76.4	28
2.64e-02	0.780	76.4	28
1.36e-01	0.845	82.7	28
1.64e-01	0.878	85.9	28
1.57e-02	0.780	76.4	28

1.99e-02	0.711	70.5	28
V (mm/s)	**K (MPa√m)**	**Krel (%)**	**Age (days)**
1.11e-02	0.711	70.5	28
6.00e-02	0.800	79.4	28
2.92e-02	0.800	79.4	28
5.34e-02	0.829	82.3	28
3.71e-02	0.829	82.3	28
2.32e-02	0.829	82.3	28
1.50e-02	0.829	82.3	28

DATA POINTS FOR FIGURE 6.2

Orientation

V (mm/s)	K (MPa√m)	Krel (%)	Orientation
4.20e-02	0.698	73.4	Normal
1.41e-02	0.698	73.4	Normal
1.75e-02	0.577	60.7	Normal
1.75e-02	0.577	60.7	Normal
5.73e-02	0.759	79.8	Normal
1.78e-01	0.819	86.1	Normal
1.52e-01	0.819	86.1	Normal
7.43e-02	0.759	79.8	Normal
8.64e-02	0.759	79.8	Normal
1.37e-02	0.551	60.7	Normal
1.56e-02	0.771	81.8	Normal
7.65e-02	0.771	81.8	Normal
3.71e-02	0.712	75.6	Normal
5.05e-02	0.712	75.6	Normal
9.24e-02	0.771	81.8	Normal
4.60e-02	0.551	60.7	Normal
2.67e-02	0.551	60.7	Normal
4.44e-02	0.604	78.2	Normal
4.67e-02	0.604	78.2	Normal
1.40e-02	0.699	75.2	Normal
2.98e-02	0.597	77.7	Normal
2.73e-02	0.638	68.7	Normal
8.09e-03	0.638	68.7	Normal
1.64e-02	0.597	77.7	Normal
6.36e-03	0.654	85.2	Normal
1.21e-01	0.710	92.4	Normal
1.85e-02	0.597	77.7	Normal
4.93e-02	0.654	85.2	Normal
7.14e-03	0.578	62.2	Normal
2.59e-02	0.581	76.0	Normal
1.11e-01	0.639	83.6	Normal
2.36e-01	0.819	86.1	Normal
8.44e-02	0.581	76.0	Normal
7.22e-02	0.639	83.6	Normal
7.96e-02	0.639	83.6	Normal
8.18e-02	0.578	62.2	Normal
7.41e-02	0.639	83.6	Normal
6.84e-02	0.639	83.6	Normal
5.54e-02	0.595	66.1	Normal
2.88e-02	0.595	66.1	Normal
1.80e-01	0.872	87.6	Normal

2.00e-02	0.539	59.9	Normal

V (mm/s)	K (MPa√m)	Krel (%)	Orientation
2.94e-02	0.595	66.1	Normal
1.39e-02	0.539	61.3	Normal
3.66e-02	0.596	67.7	Normal
3.16e-02	0.595	66.1	Normal
1.68e-02	0.539	61.3	Normal
1.58e-01	0.872	87.6	Normal
6.33e-02	0.756	76.0	Normal
1.93e-02	0.756	76.0	Normal
3.11e-02	0.698	70.2	Normal
1.51e-02	0.698	70.2	Normal
7.31e-02	0.814	81.8	Normal
1.60e-01	0.872	87.6	Normal
1.11e-01	0.872	87.6	Normal
5.03e-02	0.814	81.8	Normal
5.85e-02	0.814	81.8	Normal
1.45e-02	0.668	73.4	Normal
5.52e-02	0.593	63.0	Normal
8.16e-02	0.726	79.8	Normal
2.64e-02	0.668	73.4	Normal
2.69e-02	0.593	63.0	Normal
3.22e-02	0.712	75.6	Normal
5.10e-02	0.653	69.3	Normal
3.61e-02	0.653	69.3	Normal
9.00e-02	0.653	69.3	Normal
5.25e-02	0.726	79.8	Normal
9.43e-02	0.709	80.6	Normal
1.78e-02	0.709	80.6	Normal
2.23e-02	0.596	67.7	Normal
5.38e-02	0.653	74.2	Normal
6.22e-02	0.709	80.6	Normal
1.00e-02	0.610	67.0	Normal
8.66e-02	0.726	79.8	Normal
2.44e-02	0.552	60.7	Normal
3.76e-02	0.610	67.0	Normal
2.93e-02	0.464	69.9	Sideways
4.23e-02	0.464	69.9	Sideways
4.69e-02	0.464	69.9	Sideways
3.82e-02	0.464	69.9	Sideways
1.94e-02	0.501	63.5	Sideways
1.54e-02	0.596	67.3	Sideways
1.32e-02	0.656	74.0	Sideways
1.52e-02	0.536	60.5	Sideways

1.15e-02	0.536	60.5	Sideways
1.11e-01	0.575	73.2	Sideways
3.30e-01	0.575	73.2	Sideways

V (mm/s)	K (MPa√m)	Krel (%)	Orientation
1.24e-01	0.596	75.8	Sideways
3.23e-02	0.575	73.2	Sideways
8.76e-02	0.594	82.8	Sideways
8.30e-02	0.607	75.6	Sideways
2.98e-01	0.639	81.3	Sideways
1.00e-01	0.653	84.5	Sideways
1.28e-01	0.775	87.5	Sideways
2.58e-02	0.715	80.7	Sideways
2.79e-02	0.715	80.7	Sideways
2.85e-02	0.544	70.4	Sideways
3.25e-01	0.653	84.5	Sideways
8.78e-02	0.599	77.5	Sideways
1.30e-02	0.544	70.4	Sideways
4.07e-02	0.667	73.4	Up side down
1.01e-01	0.725	79.8	Up side down
6.46e-02	0.725	79.8	Up side down
1.26e-02	0.540	56.3	Up side down
6.23e-03	0.483	50.4	Up side down
1.16e-02	0.516	62.0	Up side down
1.17e-02	0.653	68.1	Up side down
6.73e-02	0.653	68.1	Up side down
2.25e-03	0.596	62.1	Up side down
4.32e-02	0.516	62.0	Up side down
2.42e-02	0.527	63.8	Up side down
5.45e-02	0.472	57.1	Up side down
1.34e-02	0.472	57.1	Up side down
1.95e-02	0.583	70.6	Up side down
4.06e-02	0.583	70.6	Up side down
7.68e-02	0.527	63.8	Up side down
3.09e-02	0.710	74.0	Up side down
4.16e-02	0.609	73.2	Up side down
4.52e-02	0.609	73.2	Up side down
4.90e-02	0.609	73.2	Up side down
3.15e-02	0.667	73.4	Up side down
2.01e-02	0.609	67.0	Up side down
7.18e-02	0.609	67.0	Up side down
3.85e-01	0.699	83.1	Up side down
3.06e-02	0.577	68.6	Up side down
2.07e-01	0.609	79.5	Up side down
1.06e-01	0.767	80.0	Up side down
2.67e-02	0.638	75.9	Up side down

6.32e-02	0.638	75.9	Up side down
1.41e-02	0.577	68.6	Up side down

DATA POINTS FOR FIGURE 6.4

Frequency

V (mm/s)	K (MPa√m)	Krel (%)	f (Hz)
1.56e-02	0.774	84.7	0.1
1.45e-02	0.816	83.9	0.1
4.05e-03	0.763	72.7	0.1
2.44e-02	0.913	84.9	0.1
2.17e-02	0.845	78.3	0.1
5.98e-03	0.763	72.7	0.1
2.28e-01	1.035	93.8	0.1
6.44e-03	0.763	72.7	0.1
1.88e-02	0.974	84.1	0.1
1.58e-02	0.894	82.4	0.1
1.43e-02	0.805	72.7	0.1
1.19e-02	0.670	70.2	0.1
4.75e-02	0.922		0.1
5.38e-02	0.892	85.7	0.1
9.19e-03	0.842	77.5	0.1
1.55e-02	0.774		0.1
1.52e-02	0.833	76.6	0.1
2.73e-02	0.716	74.4	0.1
1.16e-01	0.956	85.8	0.5
3.64e-02	0.774	84.7	1
5.01e-02	0.894	82.4	1
1.77e-02	0.763	72.7	1
3.60e-02	0.746	74.4	1
1.91e-02	0.974	84.1	1
1.12e-01	0.922		1
6.06e-02	0.830	80.2	1
2.90e-02	0.763	72.7	1
1.19e-01	0.830	86.0	1
3.70e-02	0.670	70.2	1
1.21e-01	0.832	85.0	1
3.20e-01	0.915	87.2	1
6.11e-02	0.894	82.4	1
6.26e-02	0.805	72.7	1
5.54e-02	0.893	75.8	1
4.10e-01	0.915	87.2	1
3.08e-02	0.833	76.6	1
6.21e-02	0.816	83.9	1
3.52e-02	0.974	84.1	1
1.90e-02	0.774	65.0	1
1.36e-01	0.893	75.8	1
4.17e-01	0.945	93.9	1

7.96e-01	1.035	93.8	1

V (mm/s)	K (MPa√m)	Krel (%)	f (Hz)
8.47e-01	0.951	93.6	1
4.75e-02	0.892	85.7	1
8.17e-02	0.956	85.8	1
1.74e-02	0.716	74.4	1
3.04e-02	0.956	85.8	1
8.02e-02	0.845	78.3	1
6.69e-02	0.774		1
6.52e-02	0.845	78.3	1
1.50e-01	0.913	84.9	1
4.75e-01	0.915	87.2	1
3.91e-01	0.935	86.1	1
5.55e-02	0.842	77.5	1
3.93e-02	0.842	77.5	5
3.07e-01	0.816	83.9	5
1.12e+00	0.945	93.9	5
2.28e-01	0.834	79.5	5
1.37e-01	0.922		5
2.24e-01	0.892	85.7	5
3.67e-02	0.729	69.6	5
2.56e-01	0.805	72.7	5
5.53e-02	0.833	76.6	5
7.70e-01	0.915	87.2	5
2.30e-02	0.729	69.6	5
2.29e-01	0.805	72.7	5
6.61e-02	0.893	75.8	5
5.08e-02	0.893	75.8	5
3.13e-01	0.834	79.5	5
1.67e-01	0.816	83.9	5
4.56e-02	0.763	72.7	5
2.41e-01	0.845	78.3	5
2.53e-01	0.894	82.4	5
1.50e-01	0.842	77.5	10
3.77e-02	0.833	76.6	10
1.06e-01	0.833	76.6	10
6.71e-01	0.774	84.7	10
1.41e-02	0.774	65.0	10
1.97e-01	0.832	85.0	10
4.53e-02	0.729	69.6	10
1.22e-01	0.816	83.9	10
1.66e-02	0.729	69.6	10
7.75e-02	0.893	75.8	10
6.78e-02	0.893	75.8	10
6.84e-02	0.833	76.6	10

1.16e-01	0.833	76.6	10
2.63e-01	0.834	79.5	10
8.82e-02	0.956	85.8	10

V (mm/s)	K (MPa√m)	Krel (%)	f (Hz)
2.54e-01	0.922		10
2.02e-02	0.729	69.6	10
5.96e-02	0.845	78.3	10
1.91e-01	0.974	84.1	10
1.49e-01	0.894	82.4	10
9.05e-02	0.763	72.7	10
6.02e-02	0.805	72.7	10
1.99e-01	0.892	85.7	10
5.03e-02	0.746	74.4	10
1.38e-01	0.805	72.7	10
2.27e-01	0.834	79.5	10
2.91e+00	1.035	93.8	10
4.82e-02	0.845	78.3	10
7.18e-02	0.763	72.7	20
2.90e-01	0.892	85.7	20
4.28e-01	0.892	85.7	20
3.80e-01	0.956	85.8	20
1.73e-01	0.892	85.7	20
9.87e-02	0.763	72.7	20
3.48e-01	0.974	84.1	20
8.45e-02	0.763	72.7	20
8.99e-02	0.842	77.5	20
2.03e-01	0.893	75.8	20

DATA POINTS FOR FIGURE 6.5

(Frequency (Rate)

dA/dN (mm/c)	K (MPa√m)	Krel (%)	f (Hz)
0.156	0.774	84.7	0.1
0.145	0.816	83.9	0.1
0.041	0.763	72.7	0.1
0.244	0.913	84.9	0.1
0.217	0.845	78.3	0.1
0.060	0.763	72.7	0.1
2.280	1.035	93.8	0.1
0.064	0.763	72.7	0.1
0.188	0.974	84.1	0.1
0.054	0.956	85.8	0.1
0.158	0.894	82.4	0.1
0.143	0.805	72.7	0.1
0.119	0.670	70.2	0.1
0.475	0.922		0.1
0.538	0.892	85.7	0.1
0.092	0.842	77.5	0.1
0.155	0.774		0.1
0.152	0.833	76.6	0.1
0.273	0.716	74.4	0.1
0.232	0.956	85.8	0.5
0.036	0.774	84.7	1
0.050	0.894	82.4	1
0.018	0.763	72.7	1
0.036	0.746	74.4	1
0.004	0.774	65.0	1
0.019	0.974	84.1	1
0.112	0.922		1
0.061	0.830	80.2	1
0.029	0.763	72.7	1
0.119	0.830	86.0	1
0.037	0.670	70.2	1
0.121	0.832	85.0	1
0.320	0.915	87.2	1
0.061	0.894	82.4	1
0.063	0.805	72.7	1
0.055	0.893	75.8	1
0.410	0.915	87.2	1
0.031	0.833	76.6	1
0.062	0.816	83.9	1
0.035	0.974	84.1	1
0.019	0.774	65.0	1

0.136	0.893	75.8	1

dA/dN (mm/c)	K (MPa√m)	Krel (%)	f (Hz)
0.417	0.945	93.9	1
0.796	1.035	93.8	1
0.847	0.951	93.6	1
0.048	0.892	85.7	1
0.082	0.956	85.8	1
0.017	0.716	74.4	1
0.030	0.956	85.8	1
0.080	0.845	78.3	1
0.067	0.774		1
0.065	0.845	78.3	1
0.150	0.913	84.9	1
0.475	0.915	87.2	1
0.391	0.935	86.1	1
0.056	0.842	77.5	1
0.008	0.842	77.5	5
0.061	0.816	83.9	5
0.224	0.945	93.9	5
0.001	0.774	65.0	5
0.046	0.834	79.5	5
0.027	0.922		5
0.011	0.655	66.7	5
0.045	0.892	85.7	5
0.007	0.729	69.6	5
0.051	0.805	72.7	5
0.011	0.833	76.6	5
0.154	0.915	87.2	5
0.005	0.729	69.6	5
0.046	0.805	72.7	5
0.013	0.893	75.8	5
0.010	0.893	75.8	5
0.063	0.834	79.5	5
0.006	0.595	60.6	5
0.006	0.974	84.1	5
0.033	0.816	83.9	5
0.055	0.655	66.7	5
0.009	0.763	72.7	5
0.048	0.845	78.3	5
0.051	0.894	82.4	5
0.015	0.842	77.5	10
0.004	0.833	76.6	10
0.011	0.833	76.6	10
0.067	0.774	84.7	10
0.001	0.774	65.0	10

0.020	0.832	85.0	10
0.005	0.729	69.6	10
0.012	0.816	83.9	10

dA/dN (mm/c)	K (MPa√m)	Krel (%)	f (Hz)
0.002	0.729	69.6	10
0.008	0.893	75.8	10
0.007	0.893	75.8	10
0.007	0.833	76.6	10
0.012	0.833	76.6	10
0.026	0.834	79.5	10
0.009	0.956	85.8	10
0.025	0.922		10
0.002	0.729	69.6	10
0.006	0.845	78.3	10
0.019	0.974	84.1	10
0.015	0.894	82.4	10
0.009	0.763	72.7	10
0.006	0.805	72.7	10
0.001	0.862		10
0.020	0.892	85.7	10
0.005	0.746	74.4	10
0.014	0.805	72.7	10
0.023	0.834	79.5	10
0.291	1.035	93.8	10
0.005	0.845	78.3	10
0.004	0.763	72.7	20
0.015	0.892	85.7	20
0.021	0.892	85.7	20
0.019	0.956	85.8	20
0.009	0.892	85.7	20
0.005	0.763	72.7	20
0.017	0.974	84.1	20
0.004	0.763	72.7	20
0.004	0.842	77.5	20
0.010	0.893	75.8	20

DATA POINTS FOR FIGURE 6.6

Amplitude

V (mm/s)	K (MPa√m)	Krel (%)	Amplitude (%)
8.93e-03	0.773	68.6	90
1.92e-02	0.756	71.6	90
2.05e-02	0.842	80.6	90
2.48e-02	0.756	71.6	90
3.93e-02	0.761	77.8	90
4.11e-02	0.756	73.9	90
4.67e-02	0.773	68.6	90
4.87e-02	0.792	80.2	90
6.18e-02	0.792	80.2	90
6.74e-02	0.873	79.3	90
7.43e-02	0.864	78.8	90
9.64e-02	0.814	81.9	90
1.32e-01	0.861	92.6	90
1.62e-01	0.756	84.1	90
1.85e-01	0.893	84.4	90
2.09e-01	0.893	83.1	90
2.58e-01	0.756	84.1	90
2.82e-01	0.841	85.8	90
9.35e-01	0.952	91.8	90
2.34e-02	0.773	68.6	80
3.02e-02	0.761	77.8	80
3.03e-02	0.756	71.6	80
3.10e-02	0.792	80.2	80
1.01e-01	0.873	79.3	80
1.34e-01	0.814	81.9	80
2.07e-01	0.893	84.4	80
3.64e-01	0.861	92.6	80
5.98e-03	0.773	68.6	60
1.05e-02	0.823	77.5	63
1.06e-02	0.712	65.6	63
1.33e-02	0.702	76.2	60
1.50e-02	0.744	80.1	65
1.56e-02	0.800	73.7	72
1.67e-02	0.779	77.3	69
1.73e-02	0.792	80.2	60
1.89e-02	0.800	73.7	63
1.95e-02	0.823	77.5	73
1.97e-02	0.756	71.6	60
2.09e-02	0.724	75.8	60
2.21e-02	0.853	72.5	60
3.11e-02	0.833	89.7	65

3.72e-02	0.873	79.3	60

V (mm/s)	K (MPa√m)	Krel (%)	Amplitude (%)
4.51e-02	0.833	89.7	74
7.61e-02	0.798	87.9	60
1.14e-01	0.893		60
1.28e-01	0.814	81.9	60
1.64e-01	0.893	84.4	60
4.03e-01	0.861	92.6	60
2.01e-03	0.712	65.6	48
2.82e-03	0.655	70.4	57
4.81e-03	0.744	80.1	57
6.18e-03	0.744	80.1	57
7.63e-03	0.744	80.1	57
8.32e-03	0.792	80.2	40
9.21e-03	0.756	71.6	40
1.13e-02	0.800	73.7	54
1.48e-02	0.779	77.3	59
3.46e-02	0.833	89.7	57
3.65e-02	0.833	89.7	57
6.34e-02	0.814	81.9	40
2.10e-02	0.893	83.1	20

DATA POINTS FOR FIGURE 6.7

Amplitude (Delta K)

V (mm/s)	Delta K (Mpa√m)	Delta Krel (%)	K (MPa√m)
2.82e-03	0.262	28.2	0.655
1.33e-02	0.421	45.7	0.702
2.01e-03	0.285	26.2	0.712
1.06e-02	0.427	39.4	0.712
2.09e-02	0.434	45.5	0.724
1.50e-02	0.446	48.1	0.744
7.63e-03	0.298	32.0	0.744
6.18e-03	0.298	32.0	0.744
4.81e-03	0.298	32.0	0.744
1.97e-02	0.454	43.0	0.756
3.03e-02	0.605	57.3	0.756
4.11e-02	0.680	66.5	0.756
2.58e-01	0.680	75.7	0.756
1.62e-01	0.680	75.7	0.756
9.21e-03	0.302	28.6	0.756
1.92e-02	0.680	64.4	0.756
2.48e-02	0.680	64.4	0.756
3.02e-02	0.609	62.2	0.761
3.93e-02	0.685	70.0	0.761
5.98e-03	0.464	41.2	0.773
8.93e-03	0.696	61.7	0.773
4.67e-02	0.696	61.7	0.773
2.34e-02	0.618	54.9	0.773
1.48e-02	0.312	30.9	0.779
1.67e-02	0.467	46.4	0.779
1.73e-02	0.475	48.1	0.792
6.18e-02	0.713	72.2	0.792
4.87e-02	0.713	72.2	0.792
8.32e-03	0.317	32.1	0.792
3.10e-02	0.634	64.2	0.792
7.61e-02	0.479	52.7	0.798
1.89e-02	0.480	44.2	0.800
1.56e-02	0.480	44.2	0.800
1.13e-02	0.320	29.5	0.800
6.34e-02	0.326	32.8	0.814
1.28e-01	0.488	49.1	0.814
1.34e-01	0.651	65.5	0.814
9.64e-02	0.733	73.7	0.814
1.95e-02	0.494	46.5	0.823
1.05e-02	0.494	46.5	0.823
4.51e-02	0.500	53.8	0.833

3.65e-02	0.333	35.9	0.833

V (mm/s)	Delta K (Mpa√m)	Delta Krel (%)	K (MPa√m)
3.46e-02	0.333	35.9	0.833
3.11e-02	0.500	53.8	0.833
2.82e-01	0.757	77.2	0.841
2.05e-02	0.758	72.5	0.842
2.21e-02	0.512	43.5	0.853
1.32e-01	0.775	83.3	0.861
3.64e-01	0.689	74.1	0.861
4.03e-01	0.517	55.6	0.861
7.43e-02	0.778	70.9	0.864
1.01e-01	0.698	63.4	0.873
3.72e-02	0.524	47.6	0.873
6.74e-02	0.786	71.4	0.873
2.10e-02	0.179	16.6	0.893
1.14e-01	0.536		0.893
2.07e-01	0.714	67.5	0.893
1.64e-01	0.536	50.6	0.893
1.85e-01	0.804	76.0	0.893
2.09e-01	0.804	74.8	0.893
9.35e-01	0.857	82.6	0.952

DATA POINTS FOR FIGURE 6.8

Loading history

V (mm/s)	K (MPa√m)	Krel (%)	Loading case
1.67e-01	1.050	86.3	Base
1.55e-01	0.855	81.1	Base
1.11e-01	0.920	78.7	Base
5.70e-02	0.814	83.4	Base
5.42e-02	0.910	78.5	Base
4.95e-02	1.010	81.5	Base
4.42e-02	0.940	79.2	Base
3.96e-02	0.930	79.0	Base
3.32e-02	0.840	75.6	Base
2.69e-02	0.930	73.9	Base
2.19e-02	0.863	73.7	Base
1.95e-02	0.930	78.1	Base
1.10e-02	1.000	80.1	Base
2.18e-03	0.870	71.6	Base
1.80e-01	0.960	83.0	Above
1.60e-01	0.855	81.1	Above
7.50e-02	1.070	85.0	Above
6.52e-02	0.980	83.4	Above
6.26e-02	0.980	82.5	Above
4.54e-02	0.900	80.8	Above
2.80e-02	0.980	80.7	Above
2.56e-02	0.940	79.2	Above
1.62e-02	1.010	81.5	Above
8.64e-02	0.990	81.5	Below
3.29e-02	0.759	72.1	Below
2.62e-02	0.870	74.3	Below
2.17e-02	0.960	81.5	Below
4.03e-03	0.830	70.1	Below
1.47e-03	0.631	64.6	Below
1.47e-03	0.672	57.2	Below

DATA POINTS FOR FIGURE 6.9

Ramp tests

V (mm/s)	K (MPa√m)	Ramp rate (mm/s)
8.57e-01	1.001	0.0005
2.22e-01	1.103	0.0005
5.45e-01	1.134	0.0005
1.38e+00	1.187	0.002
1.41e+00	1.196	0.002
7.00e+00	1.109	0.007
4.67e+00	1.186	0.007
5.60e+00	1.185	0.007
4.94e+00	1.009	0.007
5.60e+00	1.043	0.007
5.25e+00	1.016	0.007
7.00e+00	1.046	0.007
3.82e+00	1.025	0.007
3.28e+00	1.112	0.007
3.76e+00	1.112	0.007
4.55e+00	1.107	0.007
1.80e+01	1.336	0.03
2.40e+01	1.304	0.03
1.90e+01	1.272	0.03
8.47e+01	1.281	0.12

DATA POINTS FOR FIGURE 7.2

0% fly ash

V (mm/s)	K (MPa√m)	Krel (%)	Age (days)
2.82e-02	0.753	66.9	180
2.82e-03	0.753	66.9	180
1.25e-03	0.753	66.9	180
3.27e-02	0.811	72.0	180
5.42e-03	0.811	72.0	180
7.71e-03	0.811	72.0	180
1.60e-02	0.811	72.0	180
5.06e-02	0.869	77.2	180
7.36e-02	0.869	77.2	180
1.39e-02	0.927	82.3	180
2.63e-02	0.927	82.3	180
1.92e-02	0.927	82.3	180
1.81e-02	0.927	82.3	180
2.33e-02	0.985	87.5	180
5.43e-02	0.985	87.5	180
1.83e-02	0.985	87.5	180
3.52e-02	0.985	87.5	180
4.04e-02	0.705	61.8	180
1.18e-02	0.705	61.8	180
8.26e-03	0.759	66.6	180
8.93e-03	0.759	66.6	180
1.23e-02	0.759	66.6	180
2.23e-02	0.813	71.3	180
2.34e-02	0.813	71.3	180
2.73e-02	0.813	71.3	180
9.95e-03	0.813	71.3	180
2.26e-02	0.868	76.1	180
8.42e-02	0.972	85.3	180
1.05e-01	0.754	67.0	180
1.18e-02	0.754	67.0	180
3.91e-02	0.754	67.0	180
1.44e-01	0.889	82.7	180
5.72e-02	0.889	82.7	180
1.48e-02	0.737	62.1	180
5.40e-03	0.737	62.1	180
8.34e-02	0.754	59.6	180
9.83e-03	0.754	59.6	180
1.87e-02	0.812	64.1	180
7.36e-03	0.812	64.1	180
1.93e-02	0.812	64.1	180
6.47e-03	0.812	64.1	180

1.07e-02	0.812	64.1	180

V (mm/s)	K (MPa√m)	Krel (%)	Age (days)
1.62e-02	0.870	68.7	180
7.75e-02	0.920	72.7	180
5.53e-02	0.986	77.9	180
1.76e-01	1.044	82.5	180
3.05e-02	0.775	76.1	180
3.23e-02	0.775	76.1	180
2.86e-02	0.775	76.1	180
3.90e-02	0.837	82.1	180
9.46e-02	0.837	82.1	180
6.72e-02	0.837	82.1	180
3.51e-02	0.782	65.6	180
1.35e-02	0.782	65.6	180
2.20e-02	0.840	70.5	180
1.55e-02	0.840	70.5	180
1.88e-02	0.840	70.5	180
2.65e-03	0.840	70.5	180
2.35e-02	0.897	75.3	180
2.32e-02	0.897	75.3	180
2.33e-02	0.897	75.3	180
3.73e-02	0.765	67.9	180
2.89e-03	0.694	62.6	90
7.45e-03	0.694	62.6	90
9.97e-04	0.694	62.6	90
5.28e-03	0.749	67.5	90
6.37e-03	0.749	67.5	90
7.98e-03	0.805	72.6	90
3.14e-03	0.805	72.6	90
8.11e-02	0.794	62.4	90
5.97e-03	0.794	62.4	90
2.59e-02	0.851	66.8	90
8.19e-03	0.851	66.8	90
2.88e-02	0.907	71.2	90
1.61e-02	0.964	75.7	90
8.00e-03	0.964	75.7	90
3.06e-03	0.964	75.7	90
4.30e-03	0.992	77.9	90
3.45e-02	1.021	80.2	90
3.51e-01	0.831	70.0	90
2.05e-01	0.831	70.0	90
1.20e-01	0.831	70.0	90
2.08e-01	0.891	75.1	90
8.06e-02	0.891	75.1	90
1.40e-01	0.950	80.0	90

5.64e-02	0.950	80.0	90
1.30e-01	0.950	80.0	90
3.75e-01	1.009	85.0	90

V (mm/s)	K (MPa√m)	Krel (%)	Age (days)
1.50e-01	1.009	85.0	90
3.54e-02	0.742	62.4	90
5.46e-02	0.860	72.3	90
2.75e-02	0.860	72.3	90
1.13e-01	0.920	77.3	90
7.68e-02	0.920	77.3	90
6.53e-02	0.920	77.3	90
4.44e-02	0.920	77.3	90
2.19e-01	0.860	78.5	90
2.12e-02	0.816	76.7	90
2.03e-02	0.816	76.7	90
1.94e-02	0.816	76.7	90
2.18e-02	0.816	76.7	90
2.80e-02	0.796	71.0	90
8.29e-02	0.796	71.0	90
4.75e-02	0.796	71.0	90
1.61e-01	0.859	76.6	90
4.35e-02	0.859	76.6	90
2.37e-02	0.891	79.5	90
2.63e-02	0.891	79.5	90
1.35e-02	0.891	79.5	90
2.14e-02	0.891	79.5	90
3.65e-02	0.709	69.3	90
2.16e-02	0.709	69.3	90
3.75e-02	0.708	65.1	90
6.30e-03	0.708	65.1	90
1.74e-02	0.764	70.3	90
1.75e-02	0.821	75.5	90
1.58e-02	0.821	75.5	90
1.40e-02	0.821	75.5	90
1.58e-02	0.821	75.5	90
1.71e-02	0.878	80.8	90
2.90e-02	0.878	80.8	90
2.05e-02	0.823	73.9	90
2.18e-02	0.823	73.9	90
2.54e-02	0.823	73.9	90
6.48e-03	0.823	73.9	90
3.14e-02	0.880	79.1	90
6.11e-02	0.880	79.1	90
2.92e-02	0.880	79.1	90
4.11e-02	0.880	79.1	90

6.22e-02	0.936	84.1	90
3.77e-02	0.936	84.1	90
4.37e-02	0.936	84.1	90
2.24e-02	0.653	62.6	28
6.24e-03	0.653	62.6	28

V (mm/s)	K (MPa√m)	Krel (%)	Age (days)
6.65e-03	0.771	73.9	28
4.88e-02	0.831	79.6	28
2.12e-02	0.771	73.9	28
2.91e-03	0.771	73.9	28
1.57e-02	0.831	79.6	28
1.24e-02	0.711	70.8	28
1.14e-03	0.653	65.0	28
3.26e-03	0.711	70.8	28
3.35e-02	0.771	76.8	28
2.17e-02	0.771	76.8	28
3.40e-02	0.801	79.8	28
6.24e-02	0.801	79.8	28
3.72e-02	0.801	79.8	28
5.09e-03	0.711	70.8	28
4.03e-02	0.831	82.7	28
5.66e-02	0.745	75.4	28
1.42e-02	0.745	75.4	28
1.19e-02	0.745	75.4	28
6.51e-03	0.745	75.4	28
2.44e-03	0.745	75.4	28
2.74e-02	0.772	87.2	28
1.64e-01	0.780	83.3	28
2.24e-01	0.780	83.3	28
2.34e-01	0.780	83.3	28
4.87e-02	0.666	74.4	28
9.24e-02	0.699	70.6	28
6.48e-02	0.699	70.6	28
5.57e-03	0.636	64.3	28
1.06e-03	0.636	64.3	28
1.91e-03	0.636	64.3	28
7.98e-02	0.763	77.1	28
4.09e-01	0.826	83.5	28
1.61e-02	0.780	76.4	28
2.64e-02	0.780	76.4	28
1.36e-01	0.845	82.7	28
1.64e-01	0.878	85.9	28
1.57e-02	0.780	76.4	28
1.99e-02	0.711	70.5	28
1.11e-02	0.711	70.5	28

6.00e-02	0.800	79.4	28
2.92e-02	0.800	79.4	28
5.34e-02	0.829	82.3	28
3.71e-02	0.829	82.3	28
2.32e-02	0.829	82.3	28
1.50e-02	0.829	82.3	28
2.19e-02	0.394	66.6	7

V (mm/s)	K (MPa√m)	Krel (%)	Age (days)
1.28e-02	0.394	66.6	7
1.53e-02	0.394	66.6	7
7.74e-02	0.393	59.3	7
3.58e-02	0.426	53.1	7
1.73e-02	0.426	53.1	7
4.17e-02	0.482	60.2	7
2.17e-02	0.482	60.2	7
1.30e-02	0.539	67.2	7
5.19e-02	0.539	67.2	7
2.37e-02	0.596	74.4	7
8.74e-02	0.653	81.5	7
8.19e-02	0.522	79.2	7
3.42e-02	0.522	79.2	7
9.38e-03	0.522	79.2	7
3.27e-02	0.522	79.2	7
6.76e-02	0.497	84.7	7
1.79e-01	0.497	84.7	7
1.06e-01	0.497	84.7	7
4.72e-02	0.485	71.4	7
2.30e-02	0.485	71.4	7
2.11e-02	0.485	71.4	7
2.49e-02	0.485	71.4	7
2.29e-02	0.444	59.9	7
1.79e-02	0.499	67.4	7
1.73e-02	0.610	82.3	7
1.04e-01	0.653	83.5	7
3.67e-02	0.653	83.5	7
2.99e-02	0.653	83.5	7
3.49e-02	0.653	83.5	7
4.86e-02	0.653	83.5	7
1.58e-02	0.566		7
2.48e-02	0.566		7
1.63e-02	0.565		7
7.25e-02	0.595		7
8.84e-02	0.552		7
1.66e-02	0.523		7
3.37e-02	0.523		7

1.63e-03	0.495		7
1.36e-04	0.465		7
4.50e-03	0.495		7
3.79e-02	0.523		7
3.79e-02	0.523		7
2.89e-02	0.609		7
4.31e-02	0.639		7
5.12e-02	0.669		7
4.28e-02	0.700		7

V (mm/s)	K (MPa√m)	Krel (%)	Age (days)
2.23e-02	0.731		7
1.01e-01	0.754		7
7.11e-03	0.524		7
1.33e-02	0.551		7
2.77e-02	0.581		7
4.47e-02	0.610		7
5.23e-02	0.610		7
5.56e-02	0.610		7
8.46e-03	0.592		7
7.33e-03	0.592		7
4.92e-03	0.592		7
1.98e-02	0.654		7
1.54e-02	0.654		7
1.26e-02	0.654		7
8.38e-02	0.717		7
2.42e-01	0.699		7
3.60e-03	0.577		7
3.85e-02	0.638		7
1.25e-03	0.654		7
4.55e-03	0.713		7
3.45e-02	0.713		7
3.36e-02	0.713		7
6.37e-04	0.653		7
6.08e-03	0.711		7
5.91e-02	0.771		7
3.97e-02	0.712		7
2.74e-02	0.712		7
1.68e-02	0.712		7

DATA POINTS FOR FIGURE 7.3

15% fly ash

V (mm/s)	K (MPa√m)	Krel (%)	Age (days)
2.42e-03	0.681	60.6	180
1.66e-03	0.681	60.6	180
1.20e-02	0.741	65.9	180
7.25e-03	0.770	68.5	180
1.64e-02	0.829	73.8	180
1.46e-02	0.888	79.0	180
2.72e-02	0.653	72.3	180
8.76e-03	0.653	72.3	180
1.19e-02	0.712	78.9	180
2.32e-02	0.772	85.5	180
5.61e-02	0.772	85.5	180
1.93e-02	0.772	85.5	180
8.24e-02	0.801	88.8	180
2.94e-02	0.710	73.5	180
1.74e-02	0.741	76.6	180
7.02e-02	0.770	79.7	180
6.82e-02	0.770	79.7	180
6.88e-02	0.770	79.7	180
7.88e-02	0.799	82.7	180
2.36e-02	0.667	76.8	180
1.41e-02	0.638	73.4	180
4.41e-02	0.711	71.3	180
3.09e-02	0.711	71.3	180
3.13e-02	0.711	71.3	180
3.84e-02	0.711	71.3	180
2.57e-02	0.711	71.3	180
4.86e-02	0.681	64.0	180
1.20e-02	0.652	61.3	180
4.28e-02	0.681	64.0	180
2.18e-02	0.652	61.3	180
2.99e-02	0.681	64.0	180
5.78e-02	0.681	64.0	180
4.84e-02	0.710	66.8	180
2.83e-02	0.710	66.8	180
6.05e-02	0.712	76.9	180
3.88e-02	0.712	76.9	180
7.14e-02	0.712	76.9	180
1.41e-01	0.743	80.2	180
1.27e-01	0.743	80.2	180
2.17e-01	0.743	80.2	180
1.45e-02	0.730	66.6	180

4.08e-02	0.730	66.6	180

V (mm/s)	K (MPa√m)	Krel (%)	Age (days)
1.82e-02	0.761	69.5	180
1.61e-02	0.794	72.4	180
2.74e-02	0.794	72.4	180
2.65e-02	0.825	75.3	180
3.94e-02	0.857	78.1	180
4.37e-02	0.857	78.1	180
4.77e-02	0.857	78.1	180
6.08e-02	0.857	78.1	180
4.89e-02	0.857	78.1	180
6.12e-03	0.745	59.1	90
4.24e-02	0.745	59.1	90
2.83e-03	0.713	56.6	90
1.91e-02	0.713	56.6	90
4.89e-02	0.751	67.1	90
6.86e-02	0.751	67.1	90
5.02e-02	0.717	64.0	90
1.21e-02	0.683	61.0	90
1.62e-02	0.683	61.0	90
1.32e-02	0.683	61.0	90
1.10e-02	0.649	57.9	90
1.36e-01	0.751	67.1	90
2.20e-02	0.751	67.1	90
2.31e-01	0.819	73.2	90
8.45e-02	0.854	76.3	90
2.71e-02	0.808	66.8	90
1.67e-02	0.838	69.3	90
3.07e-02	0.869	71.9	90
2.43e-02	0.901	74.5	90
1.92e-02	0.932	77.1	90
7.14e-03	0.932	77.1	90
7.82e-02	0.932	77.1	90
6.35e-03	0.932	77.1	90
1.76e-02	0.932	77.1	90
9.73e-02	0.994	82.2	90
2.44e-02	0.686	71.1	28
7.22e-03	0.686	71.1	28
9.99e-03	0.686	71.1	28
1.10e-02	0.686	71.1	28
3.32e-02	0.748	77.5	28
3.72e-03	0.748	77.5	28
3.81e-03	0.748	77.5	28
1.39e-01	0.777	76.1	28
2.22e-01	0.777	76.1	28

2.18e-01	0.777	76.1	28
1.19e-02	0.715	70.1	28
1.18e-02	0.715	70.1	28

V (mm/s)	K (MPa√m)	Krel (%)	Age (days)
1.14e-02	0.715	70.1	28
6.70e-04	0.653	63.9	28
6.98e-04	0.653	63.9	28
9.68e-04	0.653	63.9	28
3.33e-02	0.654	69.5	28
4.13e-02	0.654	69.5	28
4.79e-02	0.684	72.7	28
1.00e-02	0.684	72.7	28
2.16e-01	0.713	75.9	28
3.00e-01	0.713	75.9	28
8.52e-02	0.727	78.1	28
3.56e-01	0.786	84.4	28
3.26e-01	0.786	84.4	28
7.79e-01	0.815	87.5	28
1.84e-02	0.652	60.5	28
5.47e-02	0.652	60.5	28
5.00e-03	0.621	57.7	28
1.57e-03	0.621	57.7	28
6.30e-03	0.621	57.7	28
1.50e-02	0.681	63.2	28
2.08e-03	0.681	63.2	28
8.19e-03	0.710	65.9	28
1.61e-02	0.741	68.7	28
1.45e-02	0.770	71.5	28
8.14e-03	0.799	74.2	28
4.42e-02	0.799	74.2	28
8.00e-03	0.681	63.2	28
3.54e-02	0.667	68.1	28
3.04e-02	0.636	64.9	28
3.15e-02	0.636	64.9	28
6.76e-03	0.604	61.6	28
1.38e-02	0.640	58.0	28
2.35e-02	0.640	58.0	28
1.56e-02	0.640	58.0	28
5.68e-02	0.653	72.3	28
1.44e-02	0.668	68.6	28
5.89e-02	0.730	74.9	28
3.50e-02	0.668	68.6	28
1.09e-02	0.668	68.6	28
3.40e-02	0.791	81.1	28
5.10e-02	0.821	84.2	28

3.39e-02	0.821	84.2	28
1.03e-01	0.821	84.2	28
5.88e-03	0.668	68.6	28
1.98e-02	0.546		7
1.83e-02	0.546		7

V (mm/s)	K (MPa√m)	Krel (%)	Age (days)
8.19e-03	0.546		7
5.82e-02	0.637		7
5.00e-02	0.637		7
2.46e-02	0.637		7
1.00e-02	0.546		7
2.40e-02	0.607		7
1.32e-02	0.575		7
3.28e-02	0.637		7
4.37e-02	0.637		7
2.50e-02	0.548		7
1.04e-01	0.591		7
1.48e-02	0.548		7
9.46e-03	0.548		7
1.98e-02	0.578		7
5.71e-02	0.609		7
3.77e-02	0.639		7
5.66e-02	0.639		7
1.70e-02	0.639		7
2.27e-02	0.669		7
2.55e-02	0.700		7
3.08e-02	0.524	63.5	7
4.79e-02	0.524	63.5	7
2.50e-02	0.583	70.6	7
2.14e-01	0.700	84.8	7
3.90e-03	0.548	69.6	7
8.79e-03	0.610	77.4	7
9.94e-03	0.610	77.4	7
3.07e-03	0.610	77.4	7
1.04e-02	0.610	77.4	7
6.56e-02	0.670	85.1	7
5.08e-02	0.670	85.1	7
5.33e-02	0.670	85.1	7
2.91e-01	0.731	92.8	7
5.77e-02	0.559	78.2	7
1.13e-01	0.621	87.0	7
1.95e-01	0.621	87.0	7
2.24e-01	0.621	87.0	7
5.53e-02	0.546	65.3	7
1.04e-02	0.653		7

1.14e-02	0.653		7
7.14e-03	0.653		7
1.01e-02	0.653		7
1.12e-02	0.653		7
1.38e-02	0.653		7
2.48e-03	0.621		7
6.98e-03	0.684		7

V (mm/s)	K (MPa m)	Krel (%)	Age (days)
4.88e-02	0.746		7
6.94e-03	0.729		7
7.69e-03	0.729		7
1.86e-02	0.729		7
3.12e-02	0.712		7
1.15e-02	0.712		7
2.78e-02	0.712		7

DATA POINTS FOR FIGURE 7.4

25% fly ash

V (mm/s)	K (MPa m)	Krel (%)	Age (days)
7.22e-02	0.834	71.7	180
2.99e-02	0.834	71.7	180
5.67e-02	0.834	71.7	180
4.80e-02	0.834	71.7	180
2.19e-01	0.852	67.5	180
8.37e-02	0.852	67.5	180
1.91e-02	0.852	67.5	180
1.14e-01	0.814	76.7	180
7.50e-02	0.814	76.7	180
2.26e-02	0.756	71.3	180
4.53e-02	0.756	71.3	180
7.14e-02	0.756	71.3	180
4.21e-02	0.756	71.3	180
7.28e-03	0.698	65.8	180
3.82e-02	0.698	65.8	180
1.89e-02	0.698	65.8	180
1.36e-01	0.829	71.3	180
7.41e-03	0.829	71.3	180
6.67e-03	0.829	71.3	180
1.16e-01	0.765	67.6	180
6.62e-02	0.765	67.6	180
5.43e-02	0.715	63.2	180
1.70e-02	0.715	63.2	180
4.31e-03	0.715	63.2	180
5.59e-02	0.774	68.4	180
1.64e-02	0.774	68.4	180
1.00e-02	0.834	73.7	180
3.67e-02	0.834	73.7	180
6.30e-02	0.830	75.1	180
3.16e-02	0.830	75.1	180
1.20e-01	0.894	80.9	180
1.53e-01	0.853	73.0	180
8.59e-02	0.815	70.6	180
1.63e-02	0.815	70.6	180
5.04e-02	0.873	75.6	180
7.20e-02	0.931	80.7	180
9.10e-02	0.990	85.8	180
1.24e-01	1.048	90.8	180
2.85e-01	1.056	91.5	180
2.05e-01	0.873	75.6	90
5.00e-02	0.873	75.6	90

1.36e-01	0.873	75.6	90

V (mm/s)	K (MPa m)	Krel (%)	Age (days)
5.25e-01	0.873	71.2	90
1.09e-01	0.873	71.2	90
4.47e-02	0.873	71.2	90
1.59e-01	0.834	62.8	90
2.04e-02	0.834	62.8	90
3.12e-02	0.893	67.2	90
3.40e-02	0.893	67.2	90
9.02e-02	0.953	71.8	90
1.00e-01	0.953	71.8	90
8.39e-02	0.953	71.8	90
1.00e-01	0.953	71.8	90
1.90e-01	1.012	76.2	90
3.12e-01	1.012	76.2	90
2.30e-01	1.012	76.2	90
4.63e-01	1.072	80.7	90
4.84e-02	0.814	77.0	90
9.85e-02	0.814	77.0	90
1.58e-01	0.814	77.0	90
2.50e-02	0.834	72.2	90
3.28e-02	0.893	77.3	90
3.54e-02	0.893	77.3	90
7.38e-01	0.953	82.5	90
1.29e-01	0.814	80.6	90
5.00e-02	0.814	80.6	90
4.72e-02	0.814	80.6	90
5.54e-02	0.814	80.6	90
2.89e-01	0.873	86.4	90
2.09e-01	0.873	86.4	90
1.21e-01	0.873	86.4	90
1.71e-01	0.914	84.2	90
3.43e-01	0.914	84.2	90
2.27e-01	0.914	84.2	90
1.36e-01	0.893	72.1	90
3.03e-02	0.953	76.9	90
5.13e-02	1.012	81.7	90
6.14e-02	1.012	81.7	90
3.93e-02	0.637	79.5	28
7.50e-02	0.637	79.5	28
4.12e-02	0.637	79.5	28
5.36e-02	0.637	79.5	28
4.82e-02	0.626	65.1	28
4.51e-02	0.626	65.1	28
7.86e-03	0.596	62.0	28

6.82e-03	0.596	62.0	28
5.48e-03	0.596	62.0	28
4.77e-03	0.596	62.0	28

V (mm/s)	K (MPa m)	Krel (%)	Age (days)
2.71e-02	0.685	71.3	28
4.22e-02	0.715	74.4	28
2.21e-02	0.715	74.4	28
2.18e-02	0.628	67.5	28
2.13e-02	0.628	67.5	28
3.00e-02	0.628	67.5	28
4.83e-02	0.628	67.5	28
2.39e-02	0.746	82.9	28
3.50e-02	0.746	82.9	28
2.59e-02	0.746	82.9	28
6.37e-03	0.757	70.8	28
1.49e-02	0.757	70.8	28
1.79e-02	0.816	76.3	28
3.98e-02	0.816	76.3	28
3.01e-02	0.816	76.3	28
4.99e-02	0.845	79.1	28
9.08e-02	0.845	79.1	28
1.00e-02	0.655	68.9	28
1.90e-02	0.655	68.9	28
1.89e-02	0.655	68.9	28
1.51e-02	0.655	68.9	28
1.04e-01	0.779	82.0	28
1.23e-02	0.779	82.0	28
3.00e-02	0.842	88.6	28
5.79e-03	0.686	72.2	28
6.84e-03	0.748	78.7	28
3.45e-02	0.748	78.7	28
6.63e-03	0.748	78.7	28
1.39e-02	0.748	78.7	28
1.84e-02	0.811	85.3	28
8.67e-02	0.811	85.3	28
1.48e-02	0.811	85.3	28
3.39e-02	0.811	85.3	28
6.31e-02	0.872	91.7	28
6.21e-02	0.872	91.7	28
7.36e-02	0.872	91.7	28
4.12e-01	0.935	98.3	28
2.69e-01	0.935	98.3	28
3.03e-01	0.935	98.3	28
3.11e-02	0.698	70.2	7
1.51e-02	0.698	70.2	7

3.92e-03	0.698	70.2	7
6.33e-02	0.756	76.0	7
1.93e-02	0.756	76.0	7
3.57e-03	0.756	76.0	7
7.31e-02	0.814	81.8	7

V (mm/s)	K (MPa m)	Krel (%)	Age (days)
5.03e-02	0.814	81.8	7
5.85e-02	0.814	81.8	7
1.60e-01	0.872	87.6	7
1.11e-01	0.872	87.6	7
1.58e-01	0.872	87.6	7
1.80e-01	0.872	87.6	7
2.00e-02	0.539	59.9	7
5.54e-02	0.595	66.1	7
2.88e-02	0.595	66.1	7
2.94e-02	0.595	66.1	7
3.16e-02	0.595	66.1	7
1.68e-02	0.539	61.3	7
1.39e-02	0.539	61.3	7
3.66e-02	0.596	67.7	7
2.23e-02	0.596	67.7	7
5.38e-02	0.653	74.2	7
9.43e-02	0.709	80.6	7
1.78e-02	0.709	80.6	7
6.22e-02	0.709	80.6	7
2.44e-02	0.552	60.7	7
3.76e-02	0.610	67.0	7
1.00e-02	0.610	67.0	7
1.45e-02	0.668	73.4	7
2.64e-02	0.668	73.4	7
8.16e-02	0.726	79.8	7
5.25e-02	0.726	79.8	7
8.66e-02	0.726	79.8	7
5.52e-02	0.593	63.0	7
2.69e-02	0.593	63.0	7
3.61e-02	0.653	69.3	7
9.00e-02	0.653	69.3	7
5.10e-02	0.653	69.3	7
3.22e-02	0.712	75.6	7
3.71e-02	0.712	75.6	7
5.05e-02	0.712	75.6	7
1.56e-02	0.771	81.8	7
7.65e-02	0.771	81.8	7
9.24e-02	0.771	81.8	7
4.44e-02	0.604	78.2	7

4.67e-02	0.604	78.2	7
4.60e-02	0.551	60.7	7
2.67e-02	0.551	60.7	7
1.37e-02	0.551	60.7	7
1.75e-02	0.577	60.7	7
1.75e-02	0.577	60.7	7
4.20e-02	0.698	73.4	7

V (mm/s)	K (MPa m)	Krel (%)	Age (days)
1.41e-02	0.698	73.4	7
5.73e-02	0.759	79.8	7
7.43e-02	0.759	79.8	7
8.64e-02	0.759	79.8	7
1.78e-01	0.819	86.1	7
1.52e-01	0.819	86.1	7
2.36e-01	0.819	86.1	7
8.44e-02	0.581	76.0	7
2.59e-02	0.581	76.0	7
1.11e-01	0.639	83.6	7
7.22e-02	0.639	83.6	7
7.41e-02	0.639	83.6	7
6.84e-02	0.639	83.6	7
7.96e-02	0.639	83.6	7
3.53e-03	0.607		7
7.79e-02	0.667		7
6.49e-02	0.638		7
1.29e-01	0.638		7
8.23e-02	0.638		7
1.65e-03	0.593		7
4.47e-02	0.682		7
4.92e-02	0.682		7
3.87e-02	0.682		7
1.34e-02	0.623		7
1.54e-02	0.623		7
2.14e-02	0.610		7
1.88e-01	0.697		7
3.33e-02	0.638		7
4.19e-02	0.638		7
3.46e-03	0.608		7
1.68e-03	0.608		7
2.11e-01	0.547		7
5.22e-01	0.699		7
2.49e-02	0.596		7
4.62e-03	0.596		7
5.58e-03	0.596		7
3.44e-02	0.653		7

6.27e-02	0.653		7
1.14e-01	0.653		7
7.24e-03	0.568		7
3.25e-02	0.596		7
6.79e-02	0.653		7
4.18e-02	0.653		7
5.22e-02	0.653		7
2.11e-02	0.710		7
8.70e-02	0.738		7

V (mm/s)	**K (MPa m)**	**Krel (%)**	**Age (days)**
4.62e-02	0.738		7
6.61e-02	0.738		7
6.77e-02	0.767		7
6.01e-02	0.767		7
2.03e-01	0.795		7
1.67e-02	0.568		7
4.28e-02	0.543		7
3.71e-03	0.543		7
3.30e-03	0.543		7
1.36e-02	0.652		7
1.95e-03	0.598		7
4.53e-02	0.639		7
9.80e-04	0.639		7
1.81e-02	0.726		7
3.44e-02	0.726		7
7.50e-01	0.709		7
9.37e-02	0.624		7
5.52e-02	0.624		7
2.25e-02	0.624		7
5.43e-02	0.624		7

DATA POINTS FOR FIGURE 7.5

Fly ash content (7 days)

V (mm/s)	K (MPa m)	Krel (%)	Fly ash content (%)
1.06e-01	0.497	84.7	0
6.76e-02	0.497	84.7	0
1.79e-01	0.497	84.7	0
3.49e-02	0.653	83.5	0
2.99e-02	0.653	83.5	0
1.04e-01	0.653	83.5	0
3.67e-02	0.653	83.5	0
4.86e-02	0.653	83.5	0
1.73e-02	0.610	82.3	0
8.74e-02	0.653	81.5	0
3.27e-02	0.522	79.2	0
9.38e-03	0.522	79.2	0
3.42e-02	0.522	79.2	0
8.19e-02	0.522	79.2	0
2.37e-02	0.596	74.4	0
2.49e-02	0.485	71.4	0
2.11e-02	0.485	71.4	0
4.72e-02	0.485	71.4	0
2.30e-02	0.485	71.4	0
1.79e-02	0.499	67.4	0
1.30e-02	0.539	67.2	0
5.19e-02	0.539	67.2	0
2.19e-02	0.394	66.6	0
1.53e-02	0.394	66.6	0
1.28e-02	0.394	66.6	0
2.17e-02	0.482	60.2	0
4.17e-02	0.482	60.2	0
2.29e-02	0.444	59.9	0
7.74e-02	0.393	59.3	0
1.73e-02	0.426	53.1	0
3.58e-02	0.426	53.1	0
4.47e-02	0.610		0
8.38e-02	0.717		0
6.37e-04	0.653		0
2.77e-02	0.581		0
1.26e-02	0.654		0
8.46e-03	0.592		0
5.23e-02	0.610		0
7.33e-03	0.592		0
5.56e-02	0.610		0
1.98e-02	0.654		0

3.97e-02	0.712		0

V (mm/s)	K (MPa m)	Krel (%)	Fly ash content (%)
1.54e-02	0.654		0
4.92e-03	0.592		0
6.08e-03	0.711		0
3.60e-03	0.577		0
3.45e-02	0.713		0
3.36e-02	0.713		0
5.91e-02	0.771		0
1.63e-03	0.495		0
2.23e-02	0.731		0
1.01e-01	0.754		0
4.55e-03	0.713		0
3.85e-02	0.638		0
2.42e-01	0.699		0
4.28e-02	0.700		0
1.68e-02	0.712		0
2.74e-02	0.712		0
1.58e-02	0.566		0
1.63e-02	0.565		0
2.48e-02	0.566		0
7.25e-02	0.595		0
2.89e-02	0.609		0
4.31e-02	0.639		0
5.12e-02	0.669		0
4.50e-03	0.495		0
3.79e-02	0.523		0
3.79e-02	0.523		0
7.11e-03	0.524		0
8.84e-02	0.552		0
1.36e-04	0.465		0
3.37e-02	0.523		0
1.33e-02	0.551		0
1.66e-02	0.523		0
1.25e-03	0.654		0
1.60e-01	0.872	87.6	25
1.58e-01	0.872	87.6	25
1.80e-01	0.872	87.6	25
1.11e-01	0.872	87.6	25
1.52e-01	0.819	86.1	25
2.36e-01	0.819	86.1	25
1.78e-01	0.819	86.1	25
1.11e-01	0.639	83.6	25
7.22e-02	0.639	83.6	25
6.84e-02	0.639	83.6	25

7.96e-02	0.639	83.6	25
7.41e-02	0.639	83.6	25
7.65e-02	0.771	81.8	25

V (mm/s)	K (MPa m)	Krel (%)	Fly ash content (%)
9.24e-02	0.771	81.8	25
1.56e-02	0.771	81.8	25
5.03e-02	0.814	81.8	25
5.85e-02	0.814	81.8	25
7.31e-02	0.814	81.8	25
9.43e-02	0.709	80.6	25
1.78e-02	0.709	80.6	25
6.22e-02	0.709	80.6	25
7.43e-02	0.759	79.8	25
5.73e-02	0.759	79.8	25
8.64e-02	0.759	79.8	25
8.66e-02	0.726	79.8	25
8.16e-02	0.726	79.8	25
5.25e-02	0.726	79.8	25
4.44e-02	0.604	78.2	25
4.67e-02	0.604	78.2	25
8.44e-02	0.581	76.0	25
2.59e-02	0.581	76.0	25
6.33e-02	0.756	76.0	25
1.93e-02	0.756	76.0	25
3.57e-03	0.756	76.0	25
3.71e-02	0.712	75.6	25
5.05e-02	0.712	75.6	25
3.22e-02	0.712	75.6	25
5.38e-02	0.653	74.2	25
2.64e-02	0.668	73.4	25
1.45e-02	0.668	73.4	25
4.20e-02	0.698	73.4	25
1.41e-02	0.698	73.4	25
3.11e-02	0.698	70.2	25
1.51e-02	0.698	70.2	25
3.92e-03	0.698	70.2	25
5.10e-02	0.653	69.3	25
3.61e-02	0.653	69.3	25
9.00e-02	0.653	69.3	25
3.66e-02	0.596	67.7	25
2.23e-02	0.596	67.7	25
3.76e-02	0.61	67.0	25
1.00e-02	0.61	67.0	25
3.16e-02	0.595	66.1	25
5.54e-02	0.595	66.1	25

2.88e-02	0.595	66.1	25
2.94e-02	0.595	66.1	25
2.69e-02	0.593	63.0	25
5.52e-02	0.593	63.0	25
1.39e-02	0.539	61.3	25

V (mm/s)	**K (MPa m)**	**Krel (%)**	**Fly ash content (%)**
1.68e-02	0.539	61.3	25
4.60e-02	0.551	60.7	25
2.67e-02	0.551	60.7	25
1.37e-02	0.551	60.7	25
1.75e-02	0.577	60.7	25
1.75e-02	0.577	60.7	25
2.44e-02	0.552	60.7	25
2.00e-02	0.539	59.9	25
6.01e-02	0.767		25
3.44e-02	0.653		25
9.80e-04	0.639		25
2.11e-02	0.710		25
4.53e-02	0.639		25
2.03e-01	0.795		25
1.81e-02	0.726		25
1.65e-03	0.593		25
4.47e-02	0.682		25
5.43e-02	0.624		25
9.37e-02	0.624		25
3.71e-03	0.543		25
5.58e-03	0.596		25
1.29e-01	0.638		25
6.79e-02	0.653		25
3.25e-02	0.596		25
3.30e-03	0.543		25
1.67e-02	0.568		25
6.27e-02	0.653		25
6.49e-02	0.638		25
1.95e-03	0.598		25
7.79e-02	0.667		25
1.36e-02	0.652		25
1.14e-01	0.653		25
6.61e-02	0.738		25
7.50e-01	0.709		25
8.70e-02	0.738		25
4.28e-02	0.543		25
2.14e-02	0.610		25
7.24e-03	0.568		25
5.22e-02	0.653		25

4.92e-02	0.682		25
1.88e-01	0.697		25
4.19e-02	0.638		25
3.33e-02	0.638		25
1.68e-03	0.608		25
3.53e-03	0.607		25
5.22e-01	0.699		25

V (mm/s)	**K (MPa m)**	**Krel (%)**	**Fly ash content (%)**
2.11e-01	0.547		25
1.54e-02	0.623		25
2.25e-02	0.624		25
3.44e-02	0.726		25
5.52e-02	0.624		25
3.87e-02	0.682		25
1.34e-02	0.623		25
3.46e-03	0.608		25
8.23e-02	0.638		25
4.62e-02	0.738		25
6.77e-02	0.767		25
2.49e-02	0.596		25
4.62e-03	0.596		25
4.18e-02	0.653		25

DATA POINTS FOR FIGURE 7.6

Fly ash content (28 day)

V (mm/s)	K (MPa m)	Krel (%)	Fly ash content (%)
5.09e-03	0.711	70.8	0
4.03e-02	0.831	82.7	0
3.72e-02	0.801	79.8	0
3.40e-02	0.801	79.8	0
6.24e-02	0.801	79.8	0
5.66e-02	0.745	75.4	0
2.44e-03	0.745	75.4	0
2.74e-02	0.772	87.2	0
6.51e-03	0.745	75.4	0
1.42e-02	0.745	75.4	0
1.19e-02	0.745	75.4	0
2.17e-02	0.771	76.8	0
4.88e-02	0.831	79.6	0
2.12e-02	0.771	73.9	0
6.65e-03	0.771	73.9	0
2.24e-02	0.653	62.6	0
6.24e-03	0.653	62.6	0
2.91e-03	0.771	73.9	0
3.26e-03	0.711	70.8	0
3.35e-02	0.771	76.8	0
1.14e-03	0.653	65.0	0
1.57e-02	0.831	79.6	0
1.24e-02	0.711	70.8	0
1.64e-01	0.780	83.3	0
1.99e-02	0.711	70.5	0
1.11e-02	0.711	70.5	0
1.57e-02	0.780	76.4	0
1.36e-01	0.845	82.7	0
1.64e-01	0.878	85.9	0
6.00e-02	0.800	79.4	0
2.32e-02	0.829	82.3	0
1.50e-02	0.829	82.3	0
3.71e-02	0.829	82.3	0
2.92e-02	0.800	79.4	0
5.34e-02	0.829	82.3	0
2.64e-02	0.780	76.4	0
9.24e-02	0.699	70.6	0
6.48e-02	0.699	70.6	0
4.87e-02	0.666	74.4	0
2.24e-01	0.780	83.3	0
2.34e-01	0.780	83.3	0

5.57e-03	0.636	64.3	0

V (mm/s)	K (MPa m)	Krel (%)	Fly ash content (%)
4.09e-01	0.826	83.5	0
1.61e-02	0.780	76.4	0
7.98e-02	0.763	77.1	0
1.06e-03	0.636	64.3	0
1.91e-03	0.636	64.3	0
1.23e-02	0.779	82.0	25
1.04e-01	0.779	82.0	25
1.51e-02	0.655	68.9	25
6.84e-03	0.748	78.7	25
5.79e-03	0.686	72.2	25
3.00e-02	0.842	88.6	25
1.89e-02	0.655	68.9	25
4.99e-02	0.845	79.1	25
3.01e-02	0.816	76.3	25
3.98e-02	0.816	76.3	25
1.90e-02	0.655	68.9	25
1.00e-02	0.655	68.9	25
9.08e-02	0.845	79.1	25
7.36e-02	0.872	91.7	25
6.21e-02	0.872	91.7	25
6.31e-02	0.872	91.7	25
3.03e-01	0.935	98.3	25
2.69e-01	0.935	98.3	25
4.12e-01	0.935	98.3	25
3.39e-02	0.811	85.3	25
1.39e-02	0.748	78.7	25
6.63e-03	0.748	78.7	25
3.45e-02	0.748	78.7	25
1.48e-02	0.811	85.3	25
8.67e-02	0.811	85.3	25
1.84e-02	0.811	85.3	25
4.77e-03	0.596	62.0	25
5.48e-03	0.596	62.0	25
6.82e-03	0.596	62.0	25
2.21e-02	0.715	74.4	25
4.22e-02	0.715	74.4	25
2.71e-02	0.685	71.3	25
7.86e-03	0.596	62.0	25
4.12e-02	0.637	79.5	25
7.50e-02	0.637	79.5	25
3.93e-02	0.637	79.5	25
4.51e-02	0.626	65.1	25
4.82e-02	0.626	65.1	25

5.36e-02	0.637	79.5	25
6.37e-03	0.757	70.8	25
1.79e-02	0.816	76.3	25

V (mm/s)	K (MPa m)	Krel (%)	Fly ash content (%)
1.49e-02	0.757	70.8	25
2.59e-02	0.746	82.9	25
3.00e-02	0.628	67.5	25
2.13e-02	0.628	67.5	25
2.18e-02	0.628	67.5	25
3.50e-02	0.746	82.9	25
2.39e-02	0.746	82.9	25
4.83e-02	0.628	67.5	25

DATA POINTS FOR FIGURE 7.7

Fly ash content (90 days)

V (mm/s)	K (MPa m)	Krel (%)	Fly ash content (%)
6.22e-02	0.936	84.1	0
3.77e-02	0.936	84.1	0
4.11e-02	0.880	79.1	0
6.11e-02	0.880	79.1	0
2.92e-02	0.880	79.1	0
3.75e-02	0.708	65.1	0
2.16e-02	0.709	69.3	0
6.30e-03	0.708	65.1	0
4.37e-02	0.936	84.1	0
1.74e-02	0.764	70.3	0
3.14e-02	0.880	79.1	0
1.58e-02	0.821	75.5	0
1.75e-02	0.821	75.5	0
1.40e-02	0.821	75.5	0
1.71e-02	0.878	80.8	0
1.58e-02	0.821	75.5	0
2.54e-02	0.823	73.9	0
6.48e-03	0.823	73.9	0
2.18e-02	0.823	73.9	0
2.90e-02	0.878	80.8	0
2.05e-02	0.823	73.9	0
3.65e-02	0.709	69.3	0
4.30e-03	0.992	77.9	0
3.45e-02	1.021	80.2	0
3.51e-01	0.831	70.0	0
1.61e-02	0.964	75.7	0
8.00e-03	0.964	75.7	0
3.06e-03	0.964	75.7	0
8.06e-02	0.891	75.1	0
1.40e-01	0.950	80.0	0
5.64e-02	0.950	80.0	0
2.05e-01	0.831	70.0	0
1.20e-01	0.831	70.0	0
2.08e-01	0.891	75.1	0
5.28e-03	0.749	67.5	0
6.37e-03	0.749	67.5	0
7.98e-03	0.805	72.6	0
2.89e-03	0.694	62.6	0
7.45e-03	0.694	62.6	0
9.97e-04	0.694	62.6	0
2.59e-02	0.851	66.8	0

8.19e-03	0.851	66.8	0

V (mm/s)	K (MPa m)	Krel (%)	Fly ash content (%)
2.88e-02	0.907	71.2	0
3.14e-03	0.805	72.6	0
8.11e-02	0.794	62.4	0
5.97e-03	0.794	62.4	0
2.80e-02	0.796	71.0	0
8.29e-02	0.796	71.0	0
4.75e-02	0.796	71.0	0
2.03e-02	0.816	76.7	0
1.94e-02	0.816	76.7	0
2.18e-02	0.816	76.7	0
2.63e-02	0.891	79.5	0
1.35e-02	0.891	79.5	0
2.14e-02	0.891	79.5	0
1.61e-01	0.859	76.6	0
4.35e-02	0.859	76.6	0
2.37e-02	0.891	79.5	0
3.54e-02	0.742	62.4	0
5.46e-02	0.860	72.3	0
2.75e-02	0.860	72.3	0
1.30e-01	0.950	80.0	0
3.75e-01	1.009	85.0	0
1.50e-01	1.009	85.0	0
4.44e-02	0.920	77.3	0
2.19e-01	0.860	78.5	0
2.12e-02	0.816	76.7	0
1.13e-01	0.920	77.3	0
7.68e-02	0.920	77.3	0
6.53e-02	0.920	77.3	0
1.71e-01	0.914	84.2	25
3.43e-01	0.914	84.2	25
1.21e-01	0.873	86.4	25
2.89e-01	0.873	86.4	25
2.09e-01	0.873	86.4	25
5.13e-02	1.012	81.7	25
6.14e-02	1.012	81.7	25
3.03e-02	0.953	76.9	25
2.27e-01	0.914	84.2	25
1.36e-01	0.893	72.1	25
5.54e-02	0.814	80.6	25
3.40e-02	0.893	67.2	25
3.12e-02	0.893	67.2	25
2.04e-02	0.834	62.8	25
9.02e-02	0.953	71.8	25

1.00e-01	0.953	71.8	25
8.39e-02	0.953	71.8	25
1.00e-01	0.953	71.8	25

V (mm/s)	K (MPa m)	Krel (%)	Fly ash content (%)
1.36e-01	0.873	75.6	25
5.00e-02	0.873	75.6	25
2.05e-01	0.873	75.6	25
5.25e-01	0.873	71.2	25
1.59e-01	0.834	62.8	25
4.47e-02	0.873	71.2	25
1.09e-01	0.873	71.2	25
3.54e-02	0.893	77.3	25
3.28e-02	0.893	77.3	25
2.50e-02	0.834	72.2	25
7.38e-01	0.953	82.5	25
4.72e-02	0.814	80.6	25
5.00e-02	0.814	80.6	25
1.29e-01	0.814	80.6	25
2.30e-01	1.012	76.2	25
3.12e-01	1.012	76.2	25
1.90e-01	1.012	76.2	25
4.63e-01	1.072	80.7	25
1.58e-01	0.814	77.0	25
9.85e-02	0.814	77.0	25
4.84e-02	0.814	77.0	25

DATA POINTS FOR FIGURE 7.8

Fly ash content (180 days)

V (mm/s)	K (MPa m)	Krel (%)	Fly ash content (%)
1.07e-02	0.812	64.1	0
6.47e-03	0.812	64.1	0
1.93e-02	0.812	64.1	0
1.62e-02	0.870	68.7	0
1.76e-01	1.044	82.5	0
5.53e-02	0.986	77.9	0
7.75e-02	0.920	72.7	0
7.36e-03	0.812	64.1	0
1.48e-02	0.737	62.1	0
5.72e-02	0.889	82.7	0
1.44e-01	0.889	82.7	0
5.40e-03	0.737	62.1	0
1.87e-02	0.812	64.1	0
9.83e-03	0.754	59.6	0
8.34e-02	0.754	59.6	0
3.05e-02	0.775	76.1	0
2.65e-03	0.840	70.5	0
1.88e-02	0.840	70.5	0
1.55e-02	0.840	70.5	0
2.35e-02	0.897	75.3	0
3.73e-02	0.765	67.9	0
2.33e-02	0.897	75.3	0
2.32e-02	0.897	75.3	0
2.20e-02	0.840	70.5	0
3.90e-02	0.837	82.1	0
2.86e-02	0.775	76.1	0
3.23e-02	0.775	76.1	0
9.46e-02	0.837	82.1	0
1.35e-02	0.782	65.6	0
3.51e-02	0.782	65.6	0
6.72e-02	0.837	82.1	0
2.63e-02	0.927	82.3	0
1.39e-02	0.927	82.3	0
7.36e-02	0.869	77.2	0
1.92e-02	0.927	82.3	0
5.43e-02	0.985	87.5	0
2.33e-02	0.985	87.5	0
1.81e-02	0.927	82.3	0
5.06e-02	0.869	77.2	0
1.25e-03	0.753	66.9	0
2.82e-03	0.753	66.9	0

2.82e-02	0.753	66.9	0

V (mm/s)	K (MPa m)	Krel (%)	Fly ash content (%)
3.27e-02	0.811	72.0	0
1.60e-02	0.811	72.0	0
7.71e-03	0.811	72.0	0
5.42e-03	0.811	72.0	0
1.83e-02	0.985	87.5	0
2.26e-02	0.868	76.1	0
9.95e-03	0.813	71.3	0
2.73e-02	0.813	71.3	0
8.42e-02	0.972	85.3	0
3.91e-02	0.754	67.0	0
1.18e-02	0.754	67.0	0
1.05e-01	0.754	67.0	0
2.34e-02	0.813	71.3	0
1.18e-02	0.705	61.8	0
4.04e-02	0.705	61.8	0
3.52e-02	0.985	87.5	0
8.26e-03	0.759	66.6	0
2.23e-02	0.813	71.3	0
1.23e-02	0.759	66.6	0
8.93e-03	0.759	66.6	0
1.00e-02	0.834	73.7	25
1.64e-02	0.774	68.4	25
6.30e-02	0.830	75.1	25
3.67e-02	0.834	73.7	25
5.59e-02	0.774	68.4	25
5.43e-02	0.715	63.2	25
6.62e-02	0.765	67.6	25
4.31e-03	0.715	63.2	25
1.70e-02	0.715	63.2	25
3.16e-02	0.830	75.1	25
9.10e-02	0.990	85.8	25
7.20e-02	0.931	80.7	25
2.85e-01	1.056	91.5	25
1.24e-01	1.048	90.8	25
5.04e-02	0.873	75.6	25
1.53e-01	0.853	73.0	25
1.20e-01	0.894	80.9	25
1.63e-02	0.815	70.6	25
8.59e-02	0.815	70.6	25
1.16e-01	0.765	67.6	25
1.91e-02	0.852	67.5	25
8.37e-02	0.852	67.5	25
7.50e-02	0.814	76.7	25

1.14e-01	0.814	76.7	25
2.19e-01	0.852	67.5	25
2.99e-02	0.834	71.7	25

V (mm/s)	K (MPa m)	Krel (%)	Fly ash content (%)
7.22e-02	0.834	71.7	25
4.80e-02	0.834	71.7	25
5.67e-02	0.834	71.7	25
2.26e-02	0.756	71.3	25
1.36e-01	0.829	71.3	25
1.89e-02	0.698	65.8	25
6.67e-03	0.829	71.3	25
7.41e-03	0.829	71.3	25
3.82e-02	0.698	65.8	25
7.14e-02	0.756	71.3	25
4.53e-02	0.756	71.3	25
7.28e-03	0.698	65.8	25
4.21e-02	0.756	71.3	25

DATA POINTS FOR FIGURE 7.9

Sand type

V (mm/s)	K (MPa m)	Krel (%)	Fly ash (%)	Sand
2.90e-02	0.836	75.8	0	Blend
3.97e-02	0.896	81.3	0	Blend
7.04e-02	0.956	86.7	0	Blend
1.51e-01	1.016	92.1	0	Blend
6.17e-03	0.836	75.8	0	Blend
4.09e-03	0.776	70.4	0	Blend
2.98e-02	0.896	81.3	0	Blend
6.87e-03	0.836	75.8	0	Blend
2.41e-01	0.836	86.1	0	Blend
5.78e-02	0.776	80.0	0	Blend
9.71e-02	0.794	85.0	0	Blend
7.64e-02	0.776	80.0	0	Blend
7.28e-03	0.716	73.8	0	Blend
2.89e-02	0.776	80.0	0	Blend
2.55e-01	0.744	92.0	25	Blend
1.45e-01	0.919	89.2	25	Blend
2.98e-02	0.833	94.0	25	Blend
1.39e-01	0.893	100.0	25	Blend
4.53e-02	0.883	86.2	25	Blend
2.09e-02	0.852	83.3	25	Blend
1.91e-02	0.974	84.1	0	Old
5.54e-02	0.893	75.8	0	Old
7.96e+01	1.035	93.8	0	Old
3.52e-02	0.974	84.1	0	Old
8.17e-02	0.956	85.8	0	Old
1.21e-01	0.832	85.0	0	Old
3.04e-02	0.956	85.8	0	Old
3.91e-01	0.935	86.1	0	Old
1.12e-01	0.922		0	Old
1.50e-01	0.913	84.9	0	Old
1.36e-01	0.893	75.8	0	Old
8.47e-01	0.951	93.6	0	Old

DATA POINTS FOR FIGURE 7.10

RH (oven dried)

V (mm/s)	K (MPa m)	Krel (%)	RH (%)
1.40e-02	1.341	80.7	0
8.90e-03	1.341	81.7	0
3.89e-02	1.341	80.7	0
7.49e-02	1.437	87.6	0
1.80e-02	1.437	80.9	0
2.04e-02	1.277	71.9	0
1.14e-01	1.430	86.1	0
2.89e-02	1.184	83.4	1.2
6.66e-02	1.489	95.7	1.9
9.15e-03	1.191	75.7	4.6
2.93e-02	1.306	82.6	10.4
3.41e-02	1.162	93.7	11.4
1.09e-02	1.093	88.1	11.4
7.34e-04	1.173	91.1	14.4
2.34e-02	1.246	96.7	14.4
1.06e-01	1.178	91.9	14.7
1.22e-01	1.152	93.1	16.8
1.25e-02	1.088	80.3	16.1
2.78e-01	1.210		16.6
2.08e-03	1.096	72.4	24.3
1.20e-02	1.314	86.8	24.3
4.92e-03	1.464	84.4	51.9
3.92e-02	1.556	89.7	51.9
3.17e-02	1.509	88.8	57.8
3.60e-02	1.509	89.7	57.9
2.26e-02	1.373	83.1	58.5
5.13e-02	1.373	83.1	58.5
2.25e-03	1.282	77.6	58.5
4.36e-02	1.509	90.5	60.2
7.57e-02	1.556	93.3	60.2
1.90e-01	1.310	81.1	89.3
5.59e-02	1.310	85.0	99
4.73e-02	1.370	88.8	99
6.65e-03	1.250	81.1	99

DATA POINTS FOR FIGURE 7.11

RH (air dried)

V (mm/s)	K (MPa m)	Krel (%)	RH (%)
1.99e-02	1.112	75.7	18.5
6.07e-02	1.171	79.8	18.5
9.75e-03	1.051	74.5	18.5
8.74e-02	0.964	77.8	19.6
2.47e-02	0.913	79.7	20.7
2.74e-02	0.967	84.5	20.7
2.05e-02	1.101	80.1	23.3
5.26e-03	1.041	75.8	23.3
2.46e-02	1.106	75.4	26.9
8.98e-03	0.951	64.8	26.9
4.86e-03	0.951	64.8	26.9
4.72e-02	1.061	72.3	26.9
6.47e-02	1.122	83.9	27.6
3.11e-02	1.099	82.2	27.6
4.32e-02	0.982	82.5	27.9
1.13e-02	0.893	75.0	27.9
6.29e-03	0.836	69.9	28.3
8.26e-04	0.773	69.8	30.6
7.07e-03	0.864	78.0	30.6
2.56e-03	0.914	82.5	30.6
3.06e-03	0.819	73.9	30.6
4.55e-03	0.934	69.8	31.7
9.99e-03	0.893	68.6	33.9
2.84e-02	0.952	73.1	33.9
5.03e-02	0.990	79.5	72.7
9.14e-03	0.990	79.5	72.7
8.86e-03	0.960	76.2	74.7
9.99e-02	1.020	80.9	74.7
1.44e-02	1.050	83.2	74.7
1.98e-01	1.080	89.9	75.9
6.06e-02	0.980	94.6	78.6
1.24e-02	1.070	81.9	78.8
4.62e-03	1.010	74.4	78.8
4.75e-02	1.130	86.5	78.8
2.11e-02	1.000	77.5	80.1
1.35e-03	0.960	73.9	80.1
2.91e-02	1.08	88.3	99
4.53e-02	1.13	84.6	99
3.31e-03	1.08	79.5	99
1.53e-02	1.13	83.9	99
1.07e-02	1.06	82.5	99

4.60e-03	1.12	85.5	99

V (mm/s)	K (MPa m)	Krel (%)	RH (%)
1.19e-01	1.22	92.4	99
1.05e-01	1.25	93.0	99
8.26e-03	1.02	83.5	99
1.29e-01	1.25	92.5	99
3.27e-02	1.19	88.2	99
3.94e-03	1.07	80.0	99

DATA POINTS FOR FIGURE 7.12

RH (gel)

V (mm/s)	K (MPa m)	Krel (%)	RH (%)	Prep
1.33e-02	1.246	89.0	7.1	Gel
2.65e-03	1.184	84.6	7.1	Gel
1.44e-01	1.309	93.5	7.1	Gel
5.06e-02	1.137	94.1	11.5	Gel
8.78e-02	1.219	87.9	12.5	Gel
1.72e-02	1.159	83.6	12.5	Gel
2.18e-01	1.308	95.1	13.2	Gel
6.04e-02	1.221	97.2	17.4	Gel
6.75e-03	1.163	92.6	17.4	Gel
6.93e-02	1.000	81.4	99	Wet
8.23e-02	0.919	84.6	99	Wet
4.67e-02	0.919	84.6	99	Wet
3.65e-02	0.905	80.0	99	Wet
1.13e-02	0.893	75.9	99	Wet
1.15e-02	0.842	75.9	99	Wet
4.91e-03	0.803	73.9	99	Wet
1.69e-02	0.774	69.7	99	Wet

DATA POINTS FOR FIGURE 7.13

Preparation (Low RH)

V (mm/s)	K (MPa m)	Krel (%)	RH (%)	Prep
6.07e-02	1.171	79.8	18.5	Air
1.99e-02	1.112	75.7	18.5	Air
9.75e-03	1.051	74.5	18.5	Air
8.74e-02	0.964	77.8	19.6	Air
2.74e-02	0.967	84.5	20.7	Air
2.47e-02	0.913	79.7	20.7	Air
1.19e-02	0.720		21.8	Air
5.26e-03	1.041	75.8	23.3	Air
2.05e-02	1.101	80.1	23.3	Air
8.98e-03	0.951	64.8	26.9	Air
4.86e-03	0.951	64.8	26.9	Air
4.72e-02	1.061	72.3	26.9	Air
2.46e-02	1.106	75.4	26.9	Air
3.11e-02	1.099	82.2	27.6	Air
6.47e-02	1.122	83.9	27.6	Air
4.32e-02	0.982	82.5	27.9	Air
1.13e-02	0.893	75.0	27.9	Air
6.29e-03	0.836	69.9	28.3	Air
5.12e-03	0.720	68.3	28.5	Air
8.26e-04	0.773	69.8	30.6	Air
7.07e-03	0.864	78.0	30.6	Air
2.56e-03	0.914	82.5	30.6	Air
3.06e-03	0.819	73.9	30.6	Air
4.55e-03	0.934	69.8	31.7	Air
2.84e-02	0.952	73.1	33.9	Air
9.99e-03	0.893	68.6	33.9	Air
2.65e-03	1.184	84.6	7.1	Gel
1.44e-01	1.309	93.5	7.1	Gel
1.33e-02	1.246	89.0	7.1	Gel
5.06e-02	1.137	94.1	11.5	Gel
8.78e-02	1.219	87.9	12.5	Gel
1.72e-02	1.159	83.6	12.5	Gel
2.18e-01	1.308	95.1	13.2	Gel
6.75e-03	1.163	92.6	17.4	Gel
6.04e-02	1.221	97.2	17.4	Gel
1.80e-02	1.437	80.9	0	Oven
1.14e-01	1.430	86.1	0	Oven
1.40e-02	1.341	80.7	0	Oven
8.90e-03	1.341	81.7	0	Oven
3.89e-02	1.341	80.7	0	Oven
2.04e-02	1.277	71.9	0	Oven

7.49e-02	1.437	87.6	0	Oven

V (mm/s)	K (MPa m)	Krel (%)	RH (%)	Prep
2.89e-02	1.184	83.4	1.2	Oven
6.66e-02	1.489	95.7	1.9	Oven
9.15e-03	1.191	75.7	4.6	Oven
3.42e+00	1.190	74.5	4.7	Oven
2.93e-02	1.306	82.6	10.4	Oven
2.60e-01	1.227	98.9	11.4	Oven
1.09e-02	1.093	88.1	11.4	Oven
3.41e-02	1.162	93.7	11.4	Oven
7.34e-04	1.173	91.1	14.4	Oven
2.34e-02	1.246	96.7	14.4	Oven
1.06e-01	1.178	91.9	14.7	Oven
1.22e-01	1.152	93.1	14.8	Oven
1.25e-02	1.088	80.3	16.1	Oven
2.78e-01	1.210		16.6	Oven
1.20e-02	1.314	86.8	24.3	Oven
2.08e-03	1.096	72.4	24.3	Oven

DATA POINTS FOR FIGURE 7.14

Preparation (High RH)

V (mm/s)	K (MPa m)	Krel (%)	RH (%)	Prep
8.86e-03	0.960	76.2	74.7	Air
1.44e-02	1.050	83.2	74.7	Air
1.98e-01	1.080	89.9	75.9	Air
6.06e-02	0.980	94.6	78.6	Air
1.24e-02	1.070	81.9	78.8	Air
4.75e-02	1.130	86.5	78.8	Air
4.62e-03	1.010	74.4	78.8	Air
1.35e-03	0.960	73.9	80.1	Air
3.31e-03	1.080	79.5	99	Air
1.53e-02	1.130	83.9	99	Air
3.27e-02	1.190	88.2	99	Air
4.60e-03	1.120	85.5	99	Air
1.19e-01	1.220	92.4	99	Air
1.07e-02	1.060	82.5	99	Air
3.94e-03	1.070	80.0	99	Air
2.91e-02	1.080	88.3	99	Air
4.53e-02	1.130	84.6	99	Air
8.26e-03	1.020	83.5	99	Air
1.29e-01	1.250	92.5	99	Air
1.05e-01	1.250	93.0	99	Air
1.69e-02	0.774	69.7	99	Wet
4.91e-03	0.803	73.9	99	Wet
1.15e-02	0.842	75.9	99	Wet
1.13e-02	0.893	75.9	99	Wet
8.23e-02	0.919	84.6	99	Wet
4.67e-02	0.919	84.6	99	Wet
3.65e-02	0.905	80.0	99	Wet
6.93e-02	1.000	81.4	99	Wet
1.90e-01	1.310	81.1	89.3	Oven
5.59e-02	1.310	85.0	99	Oven
6.65e-03	1.250	81.1	99	Oven
4.73e-02	1.370	88.8	99	Oven

DATA POINTS FOR FIGURE 7.15

Water

V (mm/s)	K (MPa m)	Krel (%)	Temp (°C)	RH (%)	Prep
5.35e-02	0.89	83.2	4		Wet
1.89e-01	0.95	88.7	4		Wet
3.74e-01	0.90	89.7	4		Wet
1.87e-01	0.97	81.9	4		Wet
4.62e-02	0.94	83.6	4		Wet
4.94e-02	0.95	89.8	4		Wet
6.07e-02	0.90	76.6	4		Wet
5.00e-03	0.82	72.8	4		Wet
3.49e-02	0.88	78.2	4		Wet
1.67e-01	0.90	84.2	20		Wet
2.43e-01	0.90	88.0	20		Wet
8.40e-02	0.85	80.8	20		Wet
6.51e-02	0.81	78.5	20		Wet
4.57e-02	0.84	82.3	20		Wet
2.17e-02	0.76	72.1	20		Wet
8.13e-02	0.84	78.4	20		Wet
7.77e-02	0.82	81.9	40		Wet
1.51e-02	0.81	79.0	40		Wet
4.78e-02	0.78	77.3	40		Wet
4.78e-02	0.85	88.4	40		Wet
1.09e-01	0.88	83.4	40		Wet
3.46e-02	0.84	82.1	40		Wet
4.52e-02	0.84	82.1	40		Wet
4.28e-02	0.83	81.3	60		Wet
1.17e-01	0.82	81.7	60		Wet
4.17e-01	0.95	92.9	60		Wet
1.51e-01	0.84	84.6	60		Wet
2.09e-01	0.88	87.8	60		Wet
9.90e-02	0.89	87.1	60		Wet
1.46e-01	0.81	83.2	60		Wet
6.89e-02	0.84	86.4	60		Wet
3.83e-02	0.80	79.3	60		Wet
2.86e-01	0.85	86.3	60		Wet
9.96e-02	0.79	80.2	60		Wet
2.63e-03	0.73	74.0	60		Wet
6.93e-02	1.000	81.4		99%	Wet
8.23e-02	0.919	84.6		99%	Wet
4.67e-02	0.919	84.6		99%	Wet
3.65e-02	0.905	80.0		99%	Wet

V (mm/s)	K (MPa m)	Krel (%)	Temp (°C)	RH (%)	Prep
1.13e-02	0.893	75.9		99%	Wet
1.15e-02	0.842	75.9		99%	Wet
4.91e-03	0.803	73.9		99%	Wet
1.69e-02	0.774	69.7		99%	Wet

DATA POINTS FOR FIGURE 7.16

Alcohol

V (mm/s)	K (MPa m)	Krel (%)	Fluid (%)	Prep
1.14e-01	1.111	88.9	Alcohol	Air
3.40e-01	0.951	87.3	Alcohol	Air
1.04e-02	0.811	65.1	Alcohol	Air
1.49e-02	0.871	69.8	Alcohol	Air
6.60e-02	1.001	83.5	Alcohol	Air
7.05e-02	0.981	72.8	Alcohol	Air
1.94e+00	0.981	89.3	Alcohol	Air
1.23e-01	1.051	83.2	Alcohol	Air
3.84e-01	0.941	78.4	Alcohol	Air
1.92e-02	0.931	74.7	Alcohol	Air
1.91e+00	0.891		Alcohol	Air
6.29e-02	0.991	79.1	Alcohol	Air
3.57e-02	0.891	66.2	Alcohol	Air
1.49e-02	0.880	70.2	Alcohol	Air
5.68e-02	0.967	76.9	Alcohol	Air
6.72e-02	0.924	73.5	Alcohol	Air
9.13e-01	1.154	100.0	Alcohol	Air
4.06e-01	1.247	88.2	Alcohol	Oven
3.78e-02	1.097	81.1	Alcohol	Oven
4.18e-02	1.337	98.1	Alcohol	Oven
1.38e-02	1.157	73.1	Alcohol	Oven
7.91e-02	1.237	91.6	Alcohol	Oven
1.75e-01	1.157	85.5	Alcohol	Oven
4.78e-02	1.298	91.8	Alcohol	Oven
3.96e-02	1.270	89.8	Alcohol	Oven
1.37e-01	1.241	96.7	Alcohol	Oven
6.16e-01	1.355	95.8	Alcohol	Oven
1.25e-01	1.155	87.9	Alcohol	Oven
9.85e-02	1.298	91.8	Alcohol	Oven
2.37e-02	1.270	92.7	Alcohol	Oven
1.99e-02	1.112	75.7	99% RH	Air
6.07e-02	1.171	79.8	99% RH	Air
9.75e-03	1.051	74.5	99% RH	Air
8.74e-02	0.964	77.8	99% RH	Air
2.47e-02	0.913	79.7	99% RH	Air
2.74e-02	0.967	84.5	99% RH	Air
2.05e-02	1.101	80.1	99% RH	Air
5.26e-03	1.041	75.8	99% RH	Air
2.46e-02	1.106	75.4	99% RH	Air
8.98e-03	0.951	64.8	99% RH	Air
4.86e-03	0.951	64.8	99% RH	Air

4.72e-02	1.061	72.3	99% RH	Air

V (mm/s)	K (MPa m)	Krel (%)	Fluid (%)	Prep
6.47e-02	1.122	83.9	99% RH	Air
3.11e-02	1.099	82.2	99% RH	Air
4.32e-02	0.982	82.5	99% RH	Air
1.13e-02	0.893	75.0	99% RH	Air
6.29e-03	0.836	69.9	99% RH	Air
8.26e-04	0.773	69.8	99% RH	Air
7.07e-03	0.864	78.0	99% RH	Air
2.56e-03	0.914	82.5	99% RH	Air
3.06e-03	0.819	73.9	99% RH	Air
4.55e-03	0.934	69.8	99% RH	Air
9.99e-03	0.893	68.6	99% RH	Air
2.84e-02	0.952	73.1	99% RH	Air
5.03e-02	0.990	79.5	99% RH	Air
9.14e-03	0.990	79.5	99% RH	Air
8.86e-03	0.960	76.2	99% RH	Air
9.99e-02	1.020	80.9	99% RH	Air
1.44e-02	1.050	83.2	99% RH	Air
1.98e-01	1.080	89.9	99% RH	Air
6.06e-02	0.980	94.6	99% RH	Air
1.24e-02	1.070	81.9	99% RH	Air
4.62e-03	1.010	74.4	99% RH	Air
4.75e-02	1.130	86.5	99% RH	Air
2.11e-02	1.000	77.5	99% RH	Air
1.35e-03	0.960	73.9	99% RH	Air
2.91e-02	1.080	88.3	99% RH	Air
4.53e-02	1.130	84.6	99% RH	Air
3.31e-03	1.080	79.5	99% RH	Air
1.53e-02	1.130	83.9	99% RH	Air
1.07e-02	1.060	82.5	99% RH	Air
4.60e-03	1.120	85.5	99% RH	Air
1.19e-01	1.220	92.4	99% RH	Air
1.05e-01	1.250	93.0	99% RH	Air
8.26e-03	1.020	83.5	99% RH	Air
1.29e-01	1.250	92.5	99% RH	Air
3.27e-02	1.190	88.2	99% RH	Air
3.94e-03	1.070	80.0	99% RH	Air

APPENDIX B - STATIC AND CYCLIC FATIGUE

Evans and Fuller[9.22] (E&F) have published an equation that can be used to predict cyclic fatigue behaviour from known static fatigue crack growth rates. Their Equation 30 for cyclic fatigue is:

$$V_c = \frac{dA}{dN} = \lambda\ g\ A\ K_{ave}^{n} \quad \ldots\ldots\ldots \quad (1)$$

and Equation 1 for static fatigue is:

$$V_s = \frac{dA}{dt} = A\ K_{peak}^{n} \quad \ldots\ldots\ldots \quad (2)$$

where

V_c = Cyclic crack velocity
V_s = Static crack velocity
λ = cycle period
g = a factor calculated from E&F Eqn 16
K_{ave} = mean of applied stress intensity cycle
K_{amp} = amplitude of applied stress intensity cycle
K_{peak} = peak of applied stress intensity cycle
n = slope of the line through a set of data on a log log V-K plot

By definition

$$\text{Frequency} = \frac{1}{\lambda} = \frac{dN}{dt}$$

therefore

$$\frac{da}{dN}\frac{1}{\lambda} = \frac{da}{dt}$$

which can be substituted into Eqn. 1

$$V_c = \frac{dA}{dt} = g\ A\ K_{ave}^{n} \quad \ldots\ldots\ldots \quad (3)$$

By definition (ex E&F)

$$\zeta = \frac{K_{amp}}{K_{ave}}$$

therefore

$$K_{peak} = K_{ave} + K_{amp} = K_{ave} + \zeta\ K_{ave} = K_{ave}\ (1 + \zeta) \quad \ldots\ldots\ldots\ldots\ldots\ldots \quad (4)$$

Combine Eqns 2 and 4:

$$V_s = A\ K_{ave}^{n}\ (1 + \zeta)^n \quad \ldots\ldots\ldots\ldots\ldots\ldots\ldots\ldots\ldots\ldots\ldots\ldots\ldots\ldots \quad (5)$$

Combine Eqns 3 and 5:

$$V_s = \frac{V_c}{g}\ (1 + \zeta)^n \quad \ldots\ldots\ldots\ldots\ldots\ldots\ldots\ldots\ldots\ldots\ldots\ldots\ldots\ldots\ldots\ldots \quad (6)$$

If $K_{peak} = 1$, $K_{min} = 0.1$ and n= 18 then the following can be calculated:

R = 0,1
K_{amp} = 0,45
K_{ave} = 0,55
zeta = 0,82
g = 6689

Therefore

$V_s = 7{,}18\ V_c$ (when expressed in terms of K_{peak}) ..... (A)

and

$V_s = 1/g\ V_c = 1{,}5E\text{-}4\ V_c$ (when expressed in terms of K_{ave}) ..... (B)

To examine the predicted effect of changing amplitude consider two cases:

K_{max}	= 90	K_{max}	= 90
K_{min}	= 10	K_{min}	= 22,5
K_{ave}	= 50	K_{ave}	= 56,3
K_{amp}	= 40	K_{amp}	= 33,3
ζ	= 0,8	ζ	= 0,6
g	= 5521	g	= 723
V_s	$= \frac{1{,}8^{18}}{5205}\ V_c$	V_s	$= \frac{1{,}6^{18}}{714}\ V_c$
	$= 7{,}1\ V_c$		$= 6{,}5\ V_c$
or V_c	$= 0{,}14\ V_s$	V_c	$= 0{,}15\ V_s$

Therefore decreasing amplitude implies a slightly increased cyclic crack growth velocity.